Plains CO_2 Reduction (PCOR) Partnership

Energy & Environmental Research Center (EERC)

PRESSURE INTERFERENCE EVALUATION TO SUPPORT STORAGE RESOURCE PLANNING IN THE PLAINS CO_2 REDUCTION (PCOR) PARTNERSHIP REGION

White Paper

Prepared for:

Joshua Hull

U.S. Department of Energy
National Energy Technology Laboratory
3610 Collins Ferry Road
Morgantown, WV 26505

DOE Cooperative Agreement No. DE-FE0031838

Prepared by:

Matthew E. Burton-Kelly
Nicholas A. Azzolina
Wesley D. Peck
David V. Nakles
Kevin C. Connors

Energy & Environmental Research Center
University of North Dakota
15 North 23rd Street, Stop 9018
Grand Forks, ND 58202-9018

2022-EERC-08-06

June 2022
Revised August 2022

EERC DISCLAIMER

LEGAL NOTICE This research report was prepared by the Energy & Environmental Research Center (EERC), an agency of the University of North Dakota, as an account of work sponsored by the U.S. Department of Energy (DOE) National Energy Technology Laboratory (NETL). Because of the research nature of the work performed, neither the EERC nor any of its employees makes any warranty, express or implied, or assumes any legal liability or responsibility for the accuracy, completeness, or usefulness of any information, apparatus, product, or process disclosed or represents that its use would not infringe privately owned rights. Reference herein to any specific commercial product, process, or service by trade name, trademark, manufacturer, or otherwise does not necessarily constitute or imply its endorsement or recommendation by the EERC.

ACKNOWLEDGMENT

This material is based upon work supported by DOE NETL under Award No. DE-FE0031838. and the North Dakota Industrial Commission (NDIC) under Contract Nos. FY20-XCI-226 and G-050-96.

DOE DISCLAIMER

This report was prepared as an account of work sponsored by an agency of the United States Government. Neither the United States Government, nor any agency thereof, nor any of their employees, makes any warranty, express or implied, or assumes any legal liability or responsibility for the accuracy, completeness, or usefulness of any information, apparatus, product, or process disclosed, or represents that its use would not infringe privately owned rights. Reference herein to any specific commercial product, process, or service by trade name, trademark, manufacturer, or otherwise does not necessarily constitute or imply its endorsement, recommendation, or favoring by the United States Government or any agency thereof. The views and opinions of authors expressed herein do not necessarily state or reflect those of the United States Government or any agency thereof.

TABLE OF CONTENTS

LIST OF FIGURES

Continued . . .

LIST OF FIGURES (continued)

LIST OF TABLES

PRESSURE INTERFERENCE EVALUATION TO SUPPORT STORAGE RESOURCE PLANNING IN THE PLAINS CO_2 REDUCTION (PCOR) PARTNERSHIP REGION

EXECUTIVE SUMMARY

The U.S. Department of Energy (DOE) supports carbon capture and storage (CCS) as one approach in a portfolio of strategies to reduce the release of carbon dioxide (CO_2) emissions to the atmosphere from large stationary sources. As part of this support, the DOE's National Energy Technology Laboratory has been working with Regional Carbon Sequestration Partnership initiatives through the Carbon Transport and Storage Program to identify prospective sites within the United States for the geologic storage of CO_2.

Over the past 15 years, numerous studies have published methods to estimate CO_2 storage resource in deep saline formations with the goal of providing reliable estimates of the overall CO_2 storage resource potential at local, regional, and national levels. These methods are useful for rapidly estimating the CO_2 storage resource for broad geographic areas; however, they do not account for change in reservoir pressure over time, instead using an assumed maximum final pressure below the fracture gradient of the reservoir and/or confining unit as the primary injection constraint. A key technical constraint on the achievable storage capacity when considering multiple wells injecting into the same reservoir, from one or several CCS projects, is the pressure interaction among the injection wells. Stated differently, pressure buildup in the storage unit in response to CO_2 injection into one or more wells will extend beyond the CO_2 plumes, such that two or more storage projects may have interfering pressure buildup areas even if they do not have overlapping CO_2 plumes. Consequently, for more detailed planning and permitting of multiple storage projects within the same region, further investigation into pressure interference is warranted to quantify how these interferences may affect the CO_2 storage capacity. Pressure interference has the potential to decrease the storage capacity of a geologic unit because increased pressure buildup reduces the ability of the formation to store CO_2.

This work uses simplified analytical and semianalytical models to examine the nature and extent of pressure interference between two or more storage projects using parameters describing a representative storage complex in North Dakota. The tools and methods presented support the development of easy-to-convey project spacing rules for a given storage complex stratigraphy, providing a common understanding among storage operators and regulators to use the identified CO_2 storage resource more effectively. As an example of the method, the analytical and semianalytical models are used to demonstrate the amount of pressure interference that may occur in a simplified stratigraphy within two, three, four, or five concurrent storage projects, each injecting between 0.2 and 4 $MtCO_2$/year, with spacing between sites ranging from 10 to 25 mi, and a lag of 0, 2, or 5 years between the start of injection at the first site and additional sites.

Results of this work illustrate that the magnitude of pressure interference among storage sites depend on the injection rate, spacing, and number of sites, in addition to the pressure-increase threshold used to define "interference." All these factors should, therefore, be considered prior to developing spacing rules for a particular region. Potential pressure interference among sites can be reduced by i) reducing the injection rate at each site, ii) reducing the number of sites within a given area, iii) increasing the spacing between sites, iv) installing producing wells at points/areas of expected or monitored pressure interference (active reservoir management [ARM]), or v) employing a combination of these factors. Two simplified methods are introduced to heuristically estimate pressure interference among sites. Because the results show measurable pressure interference among sites in at least some scenarios, organized, collaborative development of CO_2 storage resource is proposed.

Recommendations for future work are focused on describing the relationship between the magnitude of pressure interference and the resulting impact on CO_2 storage capacity. The pressure-increase threshold used to define "interference" can then be chosen to represent the smallest substantial impact on storage capacity among multiple injection projects.

PRESSURE INTERFERENCE EVALUATION TO SUPPORT STORAGE RESOURCE PLANNING IN THE PLAINS CO_2 REDUCTION (PCOR) PARTNERSHIP REGION

INTRODUCTION

Background

The Plains CO_2 Reduction (PCOR) Partnership Initiative is one of four projects operating under the U.S. Department of Energy (DOE) National Energy Technology Laboratory (NETL) Regional Initiative to Accelerate CCUS (carbon capture, utilization, and storage). The PCOR Partnership region encompasses ten U.S. states and four Canadian provinces in the upper Great Plains and northwestern regions of North America. The PCOR Partnership Initiative is led by the Energy & Environmental Research Center (EERC) with support from the University of Wyoming and the University of Alaska Fairbanks and includes stakeholders from the public and private sectors. The goal of this joint government–industry effort is to identify and address regional capture, transport, use, and storage challenges facing commercial deployment of CCUS throughout the PCOR Partnership region.

DOE continues to support carbon capture and storage (CCS) as one approach in a portfolio of strategies to reduce the release of carbon dioxide (CO_2) emissions to the atmosphere from large stationary sources. The CCS process comprises the separation and capture of CO_2 from industrial processes followed by the safe, permanent storage of the captured CO_2 in deep underground storage complexes (geologic storage). As part of this support, DOE NETL has been working with Regional Carbon Sequestration Partnership initiatives through the Carbon Transport and Storage Program to identify prospective sites within the United States for the geologic storage of CO_2 (U.S. Department of Energy National Energy Technology Laboratory, 2021). Since 2007, DOE NETL has published several assessments of CO_2 storage resource potential in geologic formations and terrestrial sinks in the United States, considering the following geologic formations as viable targets for CO_2 storage: saline formations; coal seams; conventional hydrocarbon reservoirs; basalt formations; and unconventional oil and gas formations, including shales and tight sands (U.S. Department of Energy National Energy Technology Laboratory, 2015).

Resource Estimate

A CO_2 storage resource estimate is the mass of CO_2 that can be stored in a geologic unit (reservoir) after accounting for the fraction of pore volume of porous and permeable sedimentary rocks available for CO_2 storage. CO_2 storage *resource* assessments do not include economic or regulatory constraints and only include those physical constraints that define the accessible part of the subsurface. One such physical constraint when considering multiple injection wells within a

project or among projects in the same region is the potential for pressure interference, i.e., pressure accommodation is considered a finite resource over project timescales (20 years). Economic and regulatory constraints are additionally considered when estimating geologic CO_2 storage *capacity* (Gorecki and others, 2009).

Numerous studies have published methods to estimate CO_2 storage resource in deep saline formations over the past 15 years, with the goal of providing reliable estimates of the overall CO_2 storage resource potential. These formations are generally deeper than 800 meters (m) (2625 feet [ft]), the depth at which pressure and temperature conditions are effective in keeping injected CO_2 in the supercritical state. Qualifying formations also have a salinity greater than 10,000 milligrams per liter (mg/L) total dissolved solids, which is a key metric used to define underground sources of drinking water (USDW) in the U.S. Code of Federal Regulations Underground Injection Control Program (Code of Federal Regulations, 1983). The published methods generally focus on three calculation steps: 1) estimate the bulk pore volume of a storage complex (i.e., [area × height × porosity] of a geologic unit), 2) apply a storage efficiency factor (i.e., the fraction of the pore space that CO_2 can occupy by displacing the original formation fluids during the course of injection), and 3) make further adjustments based on assumed hydrogeologic boundary conditions (i.e., open, closed, or semiclosed) (Bachu and others, 2007; Gorecki and others, 2009; Goodman and others, 2011; U.S. Department of Energy National Energy Technology Laboratory, 2015; Peck and others, 2014; Bachu, 2015; Bosshart and others, 2018). These calculations are useful for rapidly estimating the CO_2 storage resource for broad geographic areas; however, they do not account for change in reservoir pressure over time, instead using an assumed maximum final pressure below the fracture gradient of the reservoir and/or confining units as the primary injection constraint. A key technical constraint on the achievable storage capacity when considering multiple wells injecting into the same reservoir, from one or several CCS projects, is the pressure interaction among the injection wells. Stated differently, pressure buildup in the storage unit in response to CO_2 injection into one or more wells will extend beyond the CO_2 plumes, such that two or more storage projects may have interfering pressure buildup areas even if they do not have overlapping CO_2 plumes. Consequently, for more detailed planning and permitting of multiple storage projects within the same region, further investigation into pressure interference is warranted to quantify how these interferences may affect the CO_2 storage capacity. Pressure interference has the potential to decrease the storage capacity of a geologic unit because increased pressure buildup reduces the ability of the formation to store CO_2 through rock compressibility (pore dilation) (Bachu, 2015). In addition, pressure interference among projects may also affect the area of review (AOR), which is defined as the region surrounding the storage project where USDWs have the potential to be endangered by the injection activity (Code of Federal Regulations, 2013; North Dakota Administrative Code, 2010). The AOR extent is proportional to the pressure buildup in the storage reservoir and dictates the geographic area that requires monitoring during storage operations and postclosure phases (U.S. Environmental Protection Agency, 2013).

The work presented in this report uses simplified analytical and semianalytical models to examine the nature and extent of pressure interference between two or more storage projects as a planning tool. The results of these efforts may be used to support the development of easy-to-convey project spacing rules for a given storage complex stratigraphy, providing a common understanding among storage operators and regulators to use the identified CO_2 storage resource more effectively. To present the proposed method, this work used a simplified version of Broom

Creek stratigraphy. The results presented here cannot be directly applied to other more detailed geologic models of the Broom Creek that have been, or may be in the future, used for project permitting. Potential pressure interference for geologic scenarios that differ from the scenarios described in this report may be substantially different. Therefore, these general conclusions about spacing should not be extrapolated to more detailed models of the Broom Creek, to other geologic formations, or to other basins.

Future additional work is required to quantify the effects of pressure interference on storage capacity, which requires detailed numerical reservoir simulations.

METHODS

Estimating Pressure Buildup in the Storage Unit from CO_2 Injection

Figure 1 shows the reference geologic stratigraphy (storage complex) used for this pressure interference study and illustrates key geologic terms needed for understanding the subsequent equations and discussions. Individual geologic members are grouped to simplify the stratigraphy into hydrostratigraphic units. In the context of this study, a hydrostratigraphic unit is a geologic formation or group of formations that are hydraulically connected and exhibit similar characteristics with respect to the transmission of fluids. The reference geologic stratigraphy is based on a section of the Williston Basin of North Dakota. In this example, the geologic storage unit is the Broom Creek Formation, a deep saline formation (Aquifer 1) approximately 1445 m (4740 ft) deep and 71 m (233 ft) thick. The primary confining unit (Aquitard 1) is the interval from the top of the Broom Creek Formation to the top of the Swift Formation, a series of shales approximately 267 m (876 ft) thick. The remaining overburden of geologic units above the primary confining unit includes another saline aquifer (Inyan Kara Formation – Aquifer 2), a secondary set of confining units (interval from the top of the Inyan Kara Formation to the top of the Pierre Formation – Aquitard 2), and a freshwater USDW aquifer (Fox Hills Formation – Aquifer 3). This set of geologic units comprises the storage complex; however, this pressure interference study focuses solely on the Broom Creek Formation.

CO_2 injection into a storage unit will cause pressure buildup above native (preinjection) conditions, resulting in a pressure buildup area that expands outward from the injection well(s). Building a geologic model using a commercial-grade software platform like Schlumberger Petrel (Schlumberger, 2021) and running fluid flow simulations using numerical reservoir simulation in a commercial-grade software platform like Computer Modelling Group's compositional simulator, GEM (CMG GEM), provides an industry standard approach for estimating pressure buildup in response to CO_2 injection. For example, Petrel can accommodate detailed geologic heterogeneity, and CMG GEM can handle the multiphase flow for a formation fluid-CO_2 system. These commercial-grade tools also have multiple input settings, which provide a broader set of parameters that can be tested for their influence on pressure interference. However, building and executing a set of geologic models and numerical simulations at a scale large enough to examine the pressure buildup resulting from multiple storage projects over a large area is computationally burdensome and could take hundreds of hours to execute. For example, exploring a set of storage

EERC MBK61295.AI

Depth (m [ft])	Aquifer/Aquitard	ASLMA Unit No.	Formation Name	Formation Thickness (m [ft])
350 [1148]	Aquifer	03	Fox Hills	126 [413]
	Aquitard	02	Pierre–Inyan Kara	773 [2536]
1123 [3684]				
1178 [3865]	Aquifer	02	Inyan Kara	55 [180]
	Aquitard	01	Swift–Broom Creek	267 [876]
1445 [4741]				
1516 [4974]	Aquifer	01	Broom Creek	71 [233]

Figure 1. Reference stratigraphy used for the pressure interference study.

projects separated by 40 km (25 mi) would require a model extent of at least 1600 km^2 (625 mi^2). Therefore, analytical or semianalytical solutions that make simplifying assumptions can accelerate the process and provide initial answers that can be further explored using a smaller set of targeted numerical simulations.

Analytical expressions for estimating the pressure drawdown (or buildup) in a reservoir due to extracting (or injecting) fluids have been well understood for nearly a century. For example, De Glee (1930) developed the following solution (as expressed by Kruseman and DeRidder, 2000) for the steady-state drawdown due to extracting fluids from a reservoir with pressure dissipation from an aquitard proportional to the hydraulic gradient across the aquitard:

$$s_m = \frac{Q}{2\pi KD} K_0\left(\frac{r}{L}\right) \qquad \text{[Eq. 1]}$$

Where:

s_m = steady-state (stabilized) drawdown in a piezometer at distance r from the well (m)
Q = volumetric discharge of the well (m^3/d)
K = hydraulic conductivity of the reservoir (m/d)
D = thickness of the reservoir (m)

r = radial distance from the well (m)

L = $\sqrt{KDc}$: leakage factor (m)

c = $\frac{D'}{K'}$: hydraulic resistance of the aquitard (days)

D′ = saturated thickness of the aquitard (m)

K′ = hydraulic conductivity of the aquitard for vertical flow (m/d)

$K_0(x)$ = modified Bessel function of the second kind and of zero order (Hankel function)

r = radial distance from the well (m)

In the context of geologic carbon storage, Q is the volumetric injection rate (not discharge), which results in a pressure buildup (positive s_m) in the reservoir rather than a pressure drawdown when steady-state conditions are reached. Several adaptations of Equation 1 have been presented in the literature, which make slightly different assumptions about the solution constraints and, therefore, have different applications. In addition, transient (time-series) solutions also exist for estimating buildup as a function of time since injection. However, the important aspects of these solutions for this study is that pressure buildup in the reservoir in response to injection is predominantly a function of Q, the hydrogeologic properties of the reservoir (K and D) and aquitard (K′ and D′), and the radial distance from the well (r). The pressure buildup resulting from multiple storage can be superimposed in space and time by solving the equation for each project and then adding the results together (notwithstanding any small reduction in pressure buildup because of increased mobility within the CO_2 plumes, as noted by De Simone and others [2019]). Therefore, analytical solutions like Equation 1 provide a rapid, screening-level approach for estimating the pressure interference effects from multiple storage projects using a relatively simple set of input parameters.

Equation 1 and similar derivations rely on multiple simplifying assumptions, namely:

- The reservoir is semiconfined (meaning that pressure can dissipate from the storage unit through the overlying aquitard).
- The reservoir and the aquitard have a seemingly infinite areal extent.
- The reservoir and the aquitard are homogeneous, isotropic, and of uniform thickness.
- Prior to injection, the piezometric surface is horizontal over the area that will be influenced by the injection.
- The injection into the reservoir is done at a constant injection rate.
- The injection well penetrates the entire thickness of the reservoir and, thus, induces horizontal flow.
- The flow in the aquitard is vertical.

- The buildup in the overlying aquifer (or in the aquitard, if there is no overlying aquifer) is negligible.

- The system represents steady-state conditions, i.e., does not account for injection time.

In addition to these simplifying assumptions, Equation 1 requires a volumetric injection rate that assumes a single-phase fluid and does not account for the greater compressibility and resulting change in density of the injected CO_2. However, there are extensive examples in the literature that show that multiphase processes inside the CO_2 plume may be assumed negligible for the prediction of far-field pressure buildup, making the accuracy of analytical solutions sufficient for this type of investigation (Birkholzer and others, 2009; Cihan and others, 2011, 2012). Therefore, despite these simplifying assumptions, analytical solutions yield useful solutions to questions about pressure interference that provide generalized injection rate–distance relationships and a starting point for additional investigation of the impacts of pressure interference.

This study also used a reduced order model for simulating reservoir injection and pressure buildup that was developed by Lawrence Berkeley National Laboratory called the "analytical solution for leakage in multilayered aquifers" (ASLMA) (hereafter "ASLMA model"). The ASLMA model has been extensively described in Cihan and others (2011, 2012); a brief overview of the solution approach used here is given in Burton-Kelly and others (2021). The semianalytical solution assumes single-phase flow in a multilayered system of aquifers and aquitards, which has been shown to be applicable for far-field pressure changes beyond the CO_2 plume (Cihan and others, 2011, 2012; Nicot, 2008; Birkholzer and others, 2009; Bandilla and others, 2012). Because the ASLMA model is a single-phase model, multiphase processes are not incorporated into the solution. However, the ASLMA model results for injection of a single-phase fluid (brine) with an equivalent volume of CO_2 compared well with the numerical model, TOUGH2-ECO_2N, and provided accurate results for pressures beyond the CO_2 plume and brine leakage zone (Cihan and others, 2011, 2012; Birkholzer and others, 2009). The ASLMA model version used in the current study accounts for diffuse brine leakage (i.e., flux through aquitards). The ASLMA model assumptions are like those for Equation 1. For example, all aquifers and aquitards are assumed to be homogeneous, with uniform thickness and infinite radial extent. Fluid flow is horizontal in the aquifers and vertical in the aquitards. The equations of horizontal groundwater flow in the aquifers are coupled to the vertical-flow equations in the aquitards. The ASLMA model is necessarily more complex because it incorporates temporal change in pressure.

Both the De Glee and ASLMA pressure solutions lack feedback loops, used by more advanced semianalytical or numerical methods, to modify injection rates as injection wellhead or bottomhole pressure change over the injection period. In practice, this means that buildup in reservoir pressure caused by injection is unconstrained by physical limits like the fracture pressure of the reservoir or confining units. Therefore, results comparing the change in reservoir pressure among model cases are expressed relative to a base case, rather than as absolute measures of differences in injectivity, storage resource, or related metrics. The current work uses a concept referred to as the "pressure inventory," or the sum of the pressure buildup above hydrostatic pressure within a specified areal extent. The pressure inventory for a storage project with no neighboring storage projects is then compared against alternative scenarios with one or more neighboring storage projects to quantify the change in pressure inventory. While the loss of

pressure inventory does not directly translate to a loss of CO_2 storage capacity, comparing changes in pressure inventories across cases provides insights into the timing and magnitude of pressure interferences among storage projects under different development scenarios.

The remainder of this document describes the methods used to apply analytical and semianalytical solutions to investigate the nature and extent of pressure interference among storage projects and summarizes the results and interpretations. The objectives of this work are to i) investigate the pressure interference induced on a storage project as additional storage projects emerge nearby and ii) evaluate the sensitivity of the pressure interference to the number of neighboring storage projects, CO_2 mass injection rates of the storage projects, distances between storage projects, and development schedules (start dates) of the storage projects. Future modeling-based research efforts will extend the current work by using numerical reservoir simulations to quantify how pressure interference may affect estimated CO_2 injection rates and storage resources, thereby moving beyond pressure interference to injectivity interference.

Hydrogeologic Properties

The solutions used in the current work required inputs of hydrogeologic properties for the storage unit and overlying formations. For each geologic unit shown in Figure 1, pressure, temperature, porosity, permeability, and salinity were used to derive two key inputs: hydraulic conductivity (K) and specific storage (SS). The derivations of these properties are described in Appendix A, and Attachment A includes a macro-enabled Microsoft Excel workbook with built-in Visual Basic for Applications (VBA) functions to estimate the formation fluid density and viscosity from the aquifer or aquitard pressure, temperature, and salinity inputs, which were then used to estimate the K and S_S. Table 1 shows the average hydrogeologic properties of each geologic unit from the reference stratigraphy, which provided inputs to the analytical and semianalytical approaches.

Study Design Matrix

Pressure buildup was evaluated in the storage unit for a base case where the storage project of interest (Site A), comprising one or more injection wells, proceeded with no neighboring sites for a 20-year injection period. The pressure interference effects on Site A were then examined when adding storage projects to the west (Site B), north (Site C), east (Site D), and south (Site E). Figure 2 shows the spatial arrangement of the storage projects on a Cartesian grid of points at which pressure buildup was measured at a spacing of 1609.34 m (1 mi) from (x, y) locations (−40233.50, −40233.50) to (40233.50, 40233.50). The design matrix for the study varied the following inputs:

- Number of concurrent storage projects from one (Site A) to five (Sites A–E): A (base case); A and B; A, B, and D; A, B, C, and D; and A, B, C, D, and E.

- Four CO_2 mass injection rates from 0.2 million metric tons (Mt) CO_2 per year to 4 $MtCO_2$/year: 0.2, 1, 2, and 4 $MtCO_2$/year.

- Four distances of neighboring storage projects to Site A from 40.2 km (25 mi) to 16.1 km (10 mi): 25, 20, 15, and 10 mi.

- Three start dates from 0 (all sites starting at the same time) to 5 years, i.e., all of the neighboring storage projects do not begin injecting CO_2 until 5 years after Site A begins injecting CO_2 (0, 2, and 5 years).

The total combination of 240 unique cases (five concurrent projects, four mass injection rates, four distances from Site A, and three different start dates for the neighboring sites) were generated from this design matrix.

Table 1. Average Hydrogeologic Properties for the Reference Stratigraphy

Hydrostratigraphic Unit	Depth, m	Thickness, m	Pressure, MPa	Temperature, °C	Porosity, %	Permeability, m^2	Salinity, ppm	Hydraulic Conductivity, m/d	Specific Storage, m^{-1}
Overlying Units to Ground Surface	0	224							
Aquifer 3 – USDW (Fox Hills Fm.)	224	126	2.92	14.5	34.4	2.76×10^{-13}	1800	2.03×10^{-1}	5.57×10^{-6}
Aquitard 2 – Additional Seals (Pierre–Inyan Kara Fms.)	351	773	7.34	27.6	10	9.87×10^{-17}	5800	9.90×10^{-5}	9.20×10^{-6}
Aquifer 2 – Thief Zone (Inyan Kara Fm.)	1123	55	10.78	48.1	13.3	3.59×10^{-14}	3365	5.31×10^{-2}	4.89×10^{-6}
Aquitard 1 – Primary Seal or Cap Rock (Swift–Broom Creek Fms.)	1178	267	12.90	44.4	10	9.87×10^{-17}	40,000	1.31×10^{-4}	9.38×10^{-6}
Aquifer 1 – Storage Reservoir (Broom Creek Fm.)	1445	71	16.41	57.4	14.5	2.17×10^{-13}	49,350	3.50×10^{-1}	5.07×10^{-6}

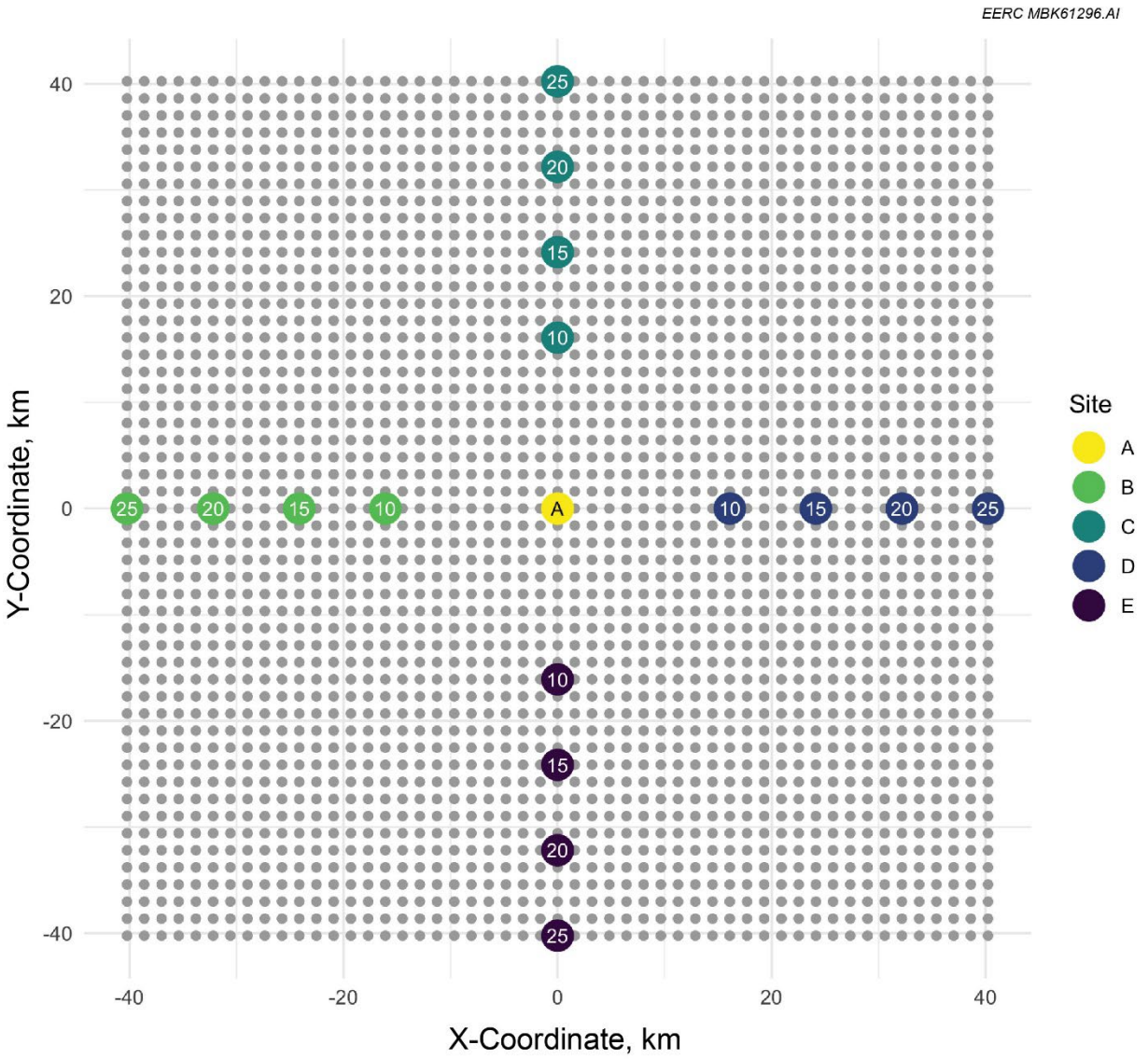

Figure 2. Cartesian grid layout for investigating ASLMA model pressure interferences showing the prime storage project in the middle of the domain (Site A) and four additional storage projects located at varying distances west (Site B), north (Site C), east (Site D), and south (Site E). Gray points represent locations where pressure buildup was measured. Numbers represent distance (in miles) from each site to Site A.

This study used two complementary approaches to investigate pressure interference. The first approach used the ASLMA model to investigate the full design matrix of sites, injection rates, distances, and start dates. The second approach used a simple analytical solution (Equation 1) to estimate the pressure buildup at the end of the 20-year injection period for the base case (Site A) and Site A and B scenarios, with each storage project injecting 4 $MtCO_2$/year, located 15 mi from Site A, and starting at the same time. These analytical solutions were a subset of the full design matrix. A comparison of the ASLMA model and Equation 1 results for the same grid coordinates were made to assess the accuracy of the latter for estimating the long-term pressure buildup.

ASLMA Modeling (semianalytical solution)

Inputs

Storage Complex Stratigraphy and Properties

Figure 1 and Table 1 illustrate the stratigraphy and average properties used to represent the storage complex in this study. These properties were averaged from available wireline log and drill core data from regional oil and gas wells and project-specific characterization wells. The storage project example model is based on a scenario in which CO_2 is injected into the Broom Creek Formation of North Dakota. The Broom Creek Formation consists of coastal eolian dunes overlain by high-energy, shallow marine beach or offshore bar deposits and has been identified as a primary CO_2 storage target with high porosity and permeability (Kringstad, 2007; Sorensen and others, 2009; Peck and others, 2014, 2019). Individual geologic members were grouped to simplify the stratigraphy into hydrostratigraphic units with similar hydrologic characteristics related to fluid flow. The resultant stratigraphy (Figure 1, Table 1) consists of a deep saline formation storage reservoir, an overlying aquitard that serves as the primary seal or cap, an intermediate saline aquifer, a second set of aquitards that act as additional seals, and a shallow USDW. The average properties for each hydrostratigraphic unit define the reference case for the ASLMA model.

Aquifer- and Aquitard-Derived Properties

For each unit shown in Figure 1, pressure, temperature, porosity, permeability, and salinity were used to derive two key inputs for the ASLMA model: K and SS (Table 1). VBA functions included in the Attachment A Excel workbook were used to estimate the formation fluid density and viscosity from the aquifer or aquitard pressure, temperature, and salinity inputs, which were then used to estimate the K and SS. Details regarding the K and SS derivations are provided in Appendix A.

CO_2 injection parameters

Like the Equation 1 analytical solution, the ASLMA model requires the CO_2 injection rate to be converted into an equivalent volume injection of formation fluid in units of cubic meters per day. VBA functions included in the Attachment A Excel workbook were used to estimate the CO_2 density from the storage reservoir pressure and temperature, which resulted in an estimated density of 677 kg/m^3. The CO_2 mass injection rate and CO_2 density were then used to derive the daily equivalent volume injection rate for 0.2, 1, 2, and 4 $MtCO_2$/year: approximately 809, 4047, 8093, and 16,186 m^3 per day, respectively. Details of these calculations are provided in Appendix A. Changes in CO_2 density as the storage reservoir evolves from initial pressure conditions to maximum pressure conditions were ignored, which mildly underestimated the CO_2 density over the injection period (by less than 10%) and, therefore, overestimated pressure buildup.

R Token Methodology and Saving Outputs

Custom code functions written in the software environment, R (R Core Team), were developed to automate multiple runs of the ASLMA model using given ranges for one or more

input parameters (Burton-Kelly and others, 2021). The input text file for the ASLMA model was modified to include an "@R-variable-name" token for the inputs that are varied across model runs.

The custom R wrapper consists of two parts: 1) an R package containing the ASLMA model FORTRAN code and R functions to read tokenized input files, replace tokens with given parameter values, write new input files, call the ASLMA model executable, and capture the resulting "CONTOUR" output files as R data frames and 2) a script that calls the functions in the R package and handles parameter preprocessing and output data postprocessing. Inputs to the R script are the tokenized ASLMA model input file, parameter token names, and values with which to replace those token names in the input file.

Postprocessing

Pressure buildup results for the Broom Creek (AQ1) from the ASLMA model runs were grouped by i) number of storage projects, ii) CO_2 mass injection rate, iii) distance(s) of neighboring storage project(s) to Site A, and iv) start date(s) of neighboring storage project(s). Each pressure buildup result group included the timestep at which buildup was calculated (d), (x, y) location of buildup calculation (m), amount of buildup in total head (m), and buildup conversion from total head in meters to pressure (psi). Detailed result comparisons were generated by joining results from alternative cases (cases with multiple storage projects) to the base case (Site A) results to compare buildup/pressure at each (x, y) location for each timestep. Summary result comparisons were generated from the detailed result comparisons using the following summary statistics for pressure values of each group and each of the base and alternative cases: pressure inventory (sum of defined pressure values), minimum, mean, standard deviation, and maximum.

Data Analysis

Visual Assessment

The pressure interference among storage projects was visually assessed by plotting maps showing the change in pressure buildup in the storage unit between the base case (Site A only) and alternative cases with multiple storage projects (e.g., Sites A and B; Sites A, B, and C; etc.) for each combination of sites, injection rates, distances, and start dates.

The area influenced by Site A injection ("base case pressure buildup area") was delineated at each timestep by including all points where the storage reservoir experienced pressure buildup of at least 6.9 kPa (1 psi). The base case pressure buildup areas at each timestep were subtracted from the alternative cases to calculate the net effect of additional sites on Site A relative to the base case scenario.

Pressure Metric

In addition to the visual assessments, a metric called pressure inventory was calculated as the sum of pressure buildup within the base case (Site A) pressure buildup area at each timestep. The pressure inventory was delineated by including all points within the base case pressure buildup area. Like the visual assessment, the absolute value of pressure buildup was used to derive a change

in pressure inventory between the base case and the alternative cases. The change in pressure inventory provided a coarse measure of how the neighboring storage project affected the pressure buildup for Site A. All results are presented to show the comparative effect of other sites on the pressure inventory of Site A operating alone. A two-site case, for example, only accounts for the additional pressure of the second site when it increases the pressure inventory of Site A.

The change in pressure inventory between the base case and each alternative case was expressed as a percentage change using the following formula:

$$\% \text{ Change} = \left(\frac{P_{Case\ X} - P_{Base\ Case}}{P_{Base\ Case}}\right) \times 100 \qquad \text{[Eq. 2]}$$

Where:

$P_{Case\ X}$ = pressure metric for Case X (injection at Site A plus injection at one or more additional neighboring sites)

$P_{Base\ Case}$ = pressure metric for the Base Case (injection at Site A alone).

The % change for each timestep was then plotted for the different combination of storage projects, injection rates, distances, and start dates to illustrate the pressure interferences for each condition.

Contour Plots

The ASLMA change in pressure inventory outputs for all cases were compiled into a single file and summarized to create contour maps showing the estimated pressure interference as a function of injection rate (0.2, 1, 2, or 4 $MtCO_2$/year), spacing (distance between Site A and neighboring storage projects of 10, 15, 20, or 25 mi), number of sites (2 = Case A and B, 3 = Case A, B, C, and D, 4 = Case A, B, C, and D, or 5 = Case A, B, C, D, and E), and start date (0 = all sites start at the same time, 2 = other sites start 2 years after Site A, or 5 = other sites start 5 years after Site A). The response variable used as a proxy for pressure interference was the percentage change in pressure inventory at the end of 20 years of injection at Site A, which ranged from less than 1% to 370%. Contour plots were produced of the percentage change in pressure inventory as a function of spacing and injection rate for each of the discrete number of sites and each of the discrete number of start dates (i.e., 12 separate contour plots).

De Glee (1930) Analytical Solution

A detailed description of Equation 1 is included in Appendix B and the Excel-based model used to solve it is provided as Attachment B. A summary of the solution follows here. As described earlier, Equation 1 provides the steady-state solution, meaning the long-term pressure buildup after many years of CO_2 injection, assumed to represent the end of the 20-year injection period. In the Excel-based model, each of the input parameters were derived from the Table 1 properties and Appendix A calculations. Solutions for pressure buildup were generated for the scenario described above for each point in the Cartesian grid in Figure 2. These solutions were then compared against the ASLMA model solutions for the same grid coordinates to assess the accuracy of the Equation 1 approach for estimating the long-term pressure buildup.

RESULTS

ASLMA Model Solutions

The ASLMA model results are grouped by the number of concurrent storage projects, beginning with the base case (Site A) followed by successively more concurrent storage projects: the two-site case (Sites A and B), three-site case (Sites A, B, and D), four-site case (Sites A, B, C, and D) and, finally, the five-site case (Sites A, B, C, D, and E).

Base Case – Single Storage Project (Site A)

Figure 3 shows the ASLMA model results for the base case (Site A only) and shows the areal evolution of reservoir pressure over time (Figure 3 shows results for 4 million tonnes per annum (Mtpa) injection rate; see Appendix C for maps of other injection rates). For each timestep, pressure buildup is greatest closest to the injection well and decreases radially away from the injection well (Site A) to the edge of the pressure buildup. In successive timesteps (i.e., from Year 1 to Year 2, Year 2 to Year 3, etc.), the areal extent of pressure buildup expands. At the end of 1 year of CO_2 injection at 4 Mtpa (upper left-hand panel in Figure 3), the pressure buildup area encompasses an area of 355 km^2 (137 mi^2), with a range of pressure from 6.9 to 10,508 kPa (1 to 1524 psi). At the end of 20 years of CO_2 injection, the pressure buildup area encompasses 2582 km^2 (997 mi^2), with a range of pressure from 6.9 to 11,425 kPa (1 to 1657 psi) (Table 2). Higher injection rates cause more rapid pressure buildup that results in larger areal extents. The pressure buildup areas at 20 years for the 0.2, 1, and 2 Mtpa injection rates were 572, 1494, and 2012 km^2 (221, 577, and 777 mi^2), respectively (see Appendix C). Twenty years of injection at rates of 0.2, 1, 2, and 4 Mtpa result in pressure buildup radii of 13.5, 21.9, 25.3, and 28.7 km (8.4, 13.6, 15.7, and 17.8 mi), respectively (Table 3; Figure 4).

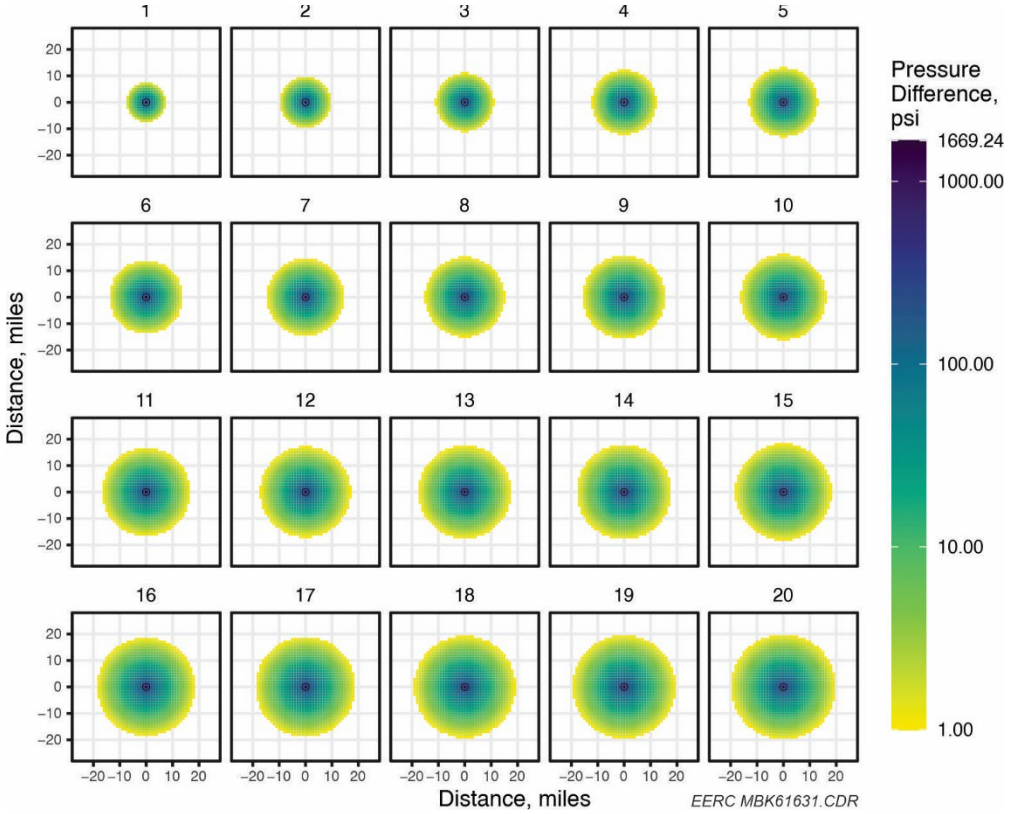

Figure 3. Base-case Site A pressure buildup (6.9-kPa [1-psi] threshold) for Years 1, 2, …, 20, while injecting a constant rate of 4 Mt CO_2/yr. Site A is marked by a small circle in each panel.

Table 2. Summary of the Pressure Buildup Areas and Radii Using a 6.9-kPa (1-psi) Pressure Buildup Threshold for the Base Case (Site A only) at 5, 10, 15, and 20 years of Injection (ASLMA model, Figure 5) and Steady State (analytical model) for Injection Rates of 0.2, 1, 2, and 4 Mtpa

	Pressure Buildup Area After, km^2 (mi^2)				
	ASLMA Model				Analytical Model
Injection Rate, Mtpa	5 years	10 years	15 years	20 years	Steady State
0.2	313 (121)	479 (185)	603 (233)	588 (227)	558 (215)
1.0	821 (317)	1246 (481)	1536 (593)	1857 (717)	1662 (642)
2.0	1090 (421)	1660 (641)	2085 (805)	2520 (973)	2359 (911)
4.0	1412 (545)	2147 (829)	2717 (1049)	3204 (1237)	3177 (1227)
	Pressure Buildup Radius After, km (mi)				
	ASLMA Model				Analytical Model
Injection Rate, Mtpa	5 years	10 years	15 years	20 years	Steady State
0.2	10.0 (6.2)	12.4 (7.7)	13.8 (8.6)	15.1 (9.4)	13.3 (8.3)
1.0	16.1 (10.0)	20.0 (12.4)	22.0 (13.7)	24.3 (15.1)	23.0 (14.3)
2.0	18.7 (11.6)	23.0 (14.3)	25.7 (16.0)	28.3 (17.6)	27.4 (17.0)
4.0	21.2 (13.2)	26.1 (16.2)	29.5 (18.3)	31.9 (19.8)	31.8 (19.8)

Table 3. Summary of the Pressure Buildup Areas and Radii Using a 70-kPa (10-psi) Pressure Buildup Threshold for the Base Case (Site A only) at 5, 10, 15, and 20 years of Injection (ASLMA model) and Steady State (analytical model) for Injection Rates of 0.2, 1, 2, and 4 Mtpa

	Pressure Buildup Area After, km² (mi²)				
	ASLMA Model				Analytical Model
Injection Rate, Mtpa	5 years	10 years	15 years	20 years	Steady State
0.2	13.0 (5)	13.0 (5)	13.0 (9)	23.3 (9)	15.2 (5.87)
1.0	179 (69)	251 (97)	313 (121)	376 (145)	284 (110)
2.0	313 (121)	479(185)	603 (233)	717 (277)	556 (215)
4.0	500 (193)	758 (293)	966 (373)	1132 (437)	951 (367)
	Pressure Buildup Radius After, km (mi)				
	ASLMA Model				Analytical Model
Injection Rate, Mtpa	5 years	10 years	15 years	20 years	Steady State
0.2	2.0 (1.3)	2.0 (1.3)	2.0 (1.7)	2.7 (1.7)	2.2 (1.4)
1.0	7.6 (4.7)	9.0 (5.6)	9.1 (6.2)	10.9 (6.8)	9.5 (5.9)
2.0	10.0 (6.2)	12.4 (7.7)	12.3 (8.6)	15.1 (9.4)	13.3 (8.3)
4.0	11.7 (7.3)	15.6 (9.7)	15.5 (10.9)	19.0 (11.8)	17.4 (10.8)

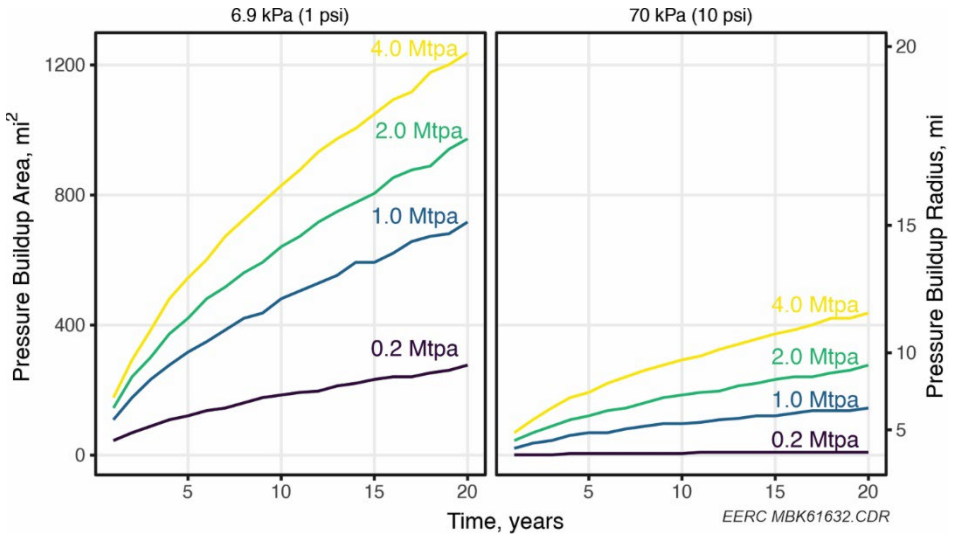

Figure 4. Base-case Site A pressure buildup area (left *y*-axis, mi²) and pressure buildup radius (right *y*-axis, mi) over time for each injection rate (Tables 2 and 3). The pressure buildup area is defined by the pressure inventory and includes locations where more than 6.9 kPa (1 psi, left-hand panel) or 70 kPa (10 psi, right-hand panel) of pressure increase is observed in the ASLMA model.

Two-Storage Project (Sites A and B)

Analysis of the two-site case begins with the primary site (Site A) and a second site located to the west (Site B). In cases with two or more injection sites, the effect of additional sites on Site A was measured by the difference in pressure inventory (hereafter "pressure difference") within the base case (Site A only) pressure buildup area, holding the injection rate equal among the base case and the alternative case. Figure 5 illustrates one of the two-site examples and shows the pressure difference with the addition of Site B, where Site B is located 15 mi west of Site A, and where both Sites A and B begin injection at the same time and inject 4 Mtpa. Additional two-site examples (with 10-, 20-, and 25-mi site spacing) are provided in Appendix C. The pressure differences between the Site A and B case and the base case form a north–south trending ellipsoid, which shows the intersection of the pressure buildup areas caused by Site A and Site B. Stated differently, while Sites A and B each generate their own pressure buildup areas, Figure 5 illustrates only the intersection of the two areas for each timestep for the given case. A threshold of 6.9 kPa (1 psi) of pressure difference is used to delineate the ellipsoids shown in the figures, which represent the base case pressure buildup area for all comparisons between cases.

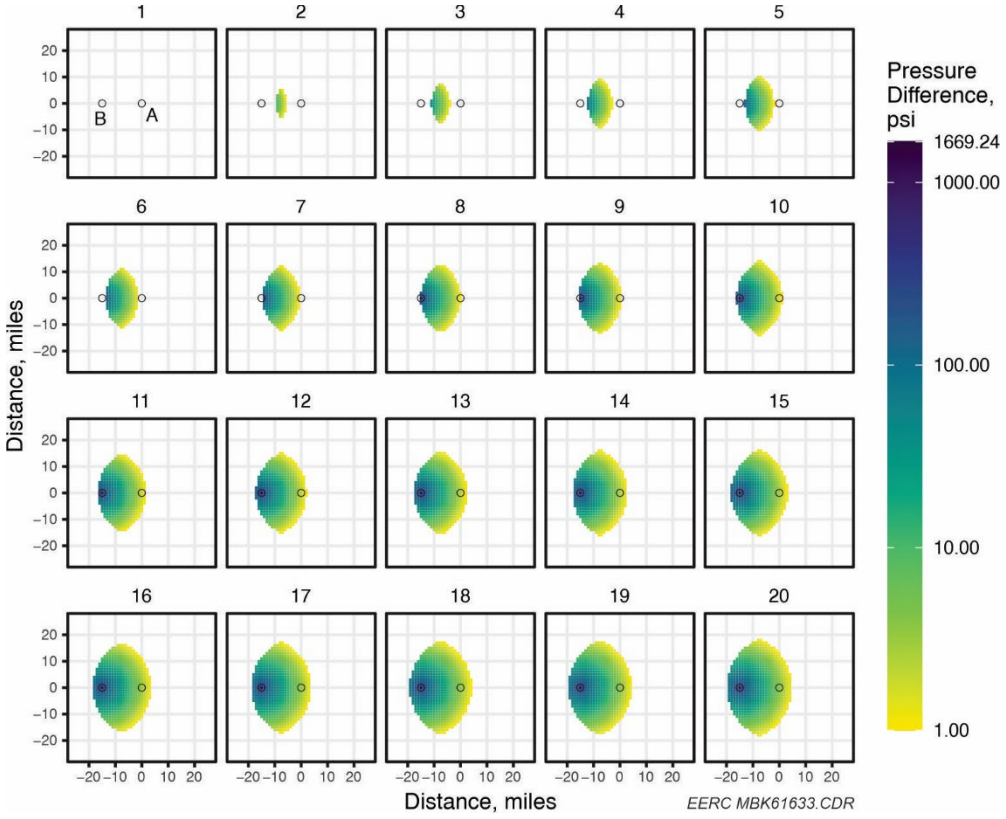

Figure 5. One of the two-site (Sites A and B) examples showing the pressure difference over time caused by Site B injection, relative to the base case (Site A only) within the base case pressure buildup area while injecting 4 Mt CO_2/yr into both Site A and B. Injection sites (A and B) are marked by small circles in each panel; Site B is located 15 mi west of Site A in this case. Additional two-project cases (with 10-, 20-, and 25-mi site spacing) are shown in Appendix C.

The greatest pressure difference between the Site A and B case and the base case occurs near the Site B location because this region of the model had no injection well under the base case and then injected 4 Mtpa under the two-site case. As shown in the figure, the arrival of a pressure difference effect within the Site A pressure buildup area occurs in Year 2, with a small region appearing approximately 7 mi west of Site A. As time progresses, the pressure difference effect expands. In Figure 5, the pressure difference area reaches the Site A location at approximately Year 8, but this does not occur for all comparisons (see Appendix C).

Figure 6 shows the pressure inventory comparison of the Site A and B case against the base case (Site A only), expressed as percentage change from the base case pressure inventory. As shown in the figure, the magnitude and timing of the percentage change depends on the injection rates of Sites A and B (columns in Figure 6: 0.2, 1, 2, or 4 Mtpa), start time of the Site B injection relative to the Site A injection (rows in Figure 6: 0 = both sites start at the same time; 2 = Site B began injecting 2 years after Site A; and 5 = Site B began injection 5 years after Site A), and distance between Sites A and B (line colors and types in Figure 6: 10, 15, 20, or 25 mi between Sites A and B). For example, when both sites are injecting 4 Mtpa and start at the same time (upper right-hand panel), the percentage changes in pressure inventory increase from about 10% under the 25-mi distance case (purple dashed line) to nearly 100% under the 10-mi distance case (red solid line). Within the top row where both sites start at the same time, the percentage changes on the pressure inventory increase as the injection rates increase from 0.2 to 4 Mtpa (moving left to right). Finally, delaying the start of Site B relative to Site A delays the arrival time of the effect on Site A. For example, in the 10-mi case in the upper right-hand panel, the percentage change in pressure inventory induced by Site B occurs almost immediately. In contrast, when Site B does not begin injecting until 5 years after Site A (bottom right-hand panel), the percentage change in pressure inventory under the 10-mi case is delayed until Year 5. This two-site example illustrates the simplest case of a second storage project, Site B, affecting Site A and the interrelationships among injection rates, distances between sites, and injection start dates of the two sites on the magnitude and timing of the pressure interference imposed by Site B onto Site A.

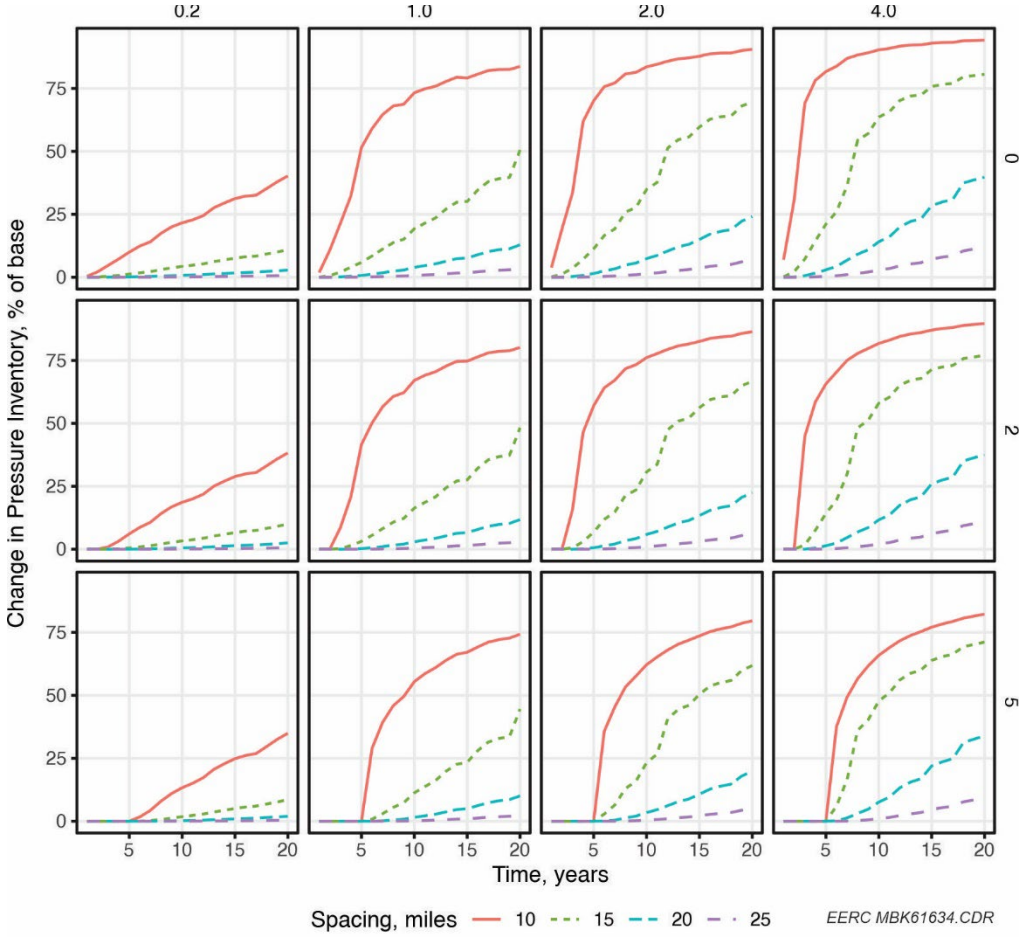

Figure 6. Percentage change in pressure inventory over time between the base case and Site A and B case. Each row (right *y*-axis label) shows the same delay between the start of Site A injection and the start of Site B injection in years (0 = both sites start at the same time; 2 = Site B began injecting 2 years after Site A; and 5 = Site B began injection 5 years after Site A). Each column (top *x*-axis label) shows the same injection rate (Site A = Site B) in Mtpa. Curves with the same color and style represent the same distance between Site A and Site B (10, 15, 20, or 25 mi).

Three-Storage Project (Sites A, B, and D)

The three-site case begins with the primary site (Site A), a second site located to the west (Site B), and a third site located to the east (Site D), such that Site A is straddled by two injection sites.

Figure 7 illustrates one of the three-site examples and shows the pressure difference with the addition of Sites B and D, where Site B is located 15 mi west of Site A; Site D is located 15 mi east of Site A; and Sites A, B, and D begin injection at the same time, injecting 4 Mtpa (additional three-site examples with 10-, 20-, and 25-mi site spacing are provided in

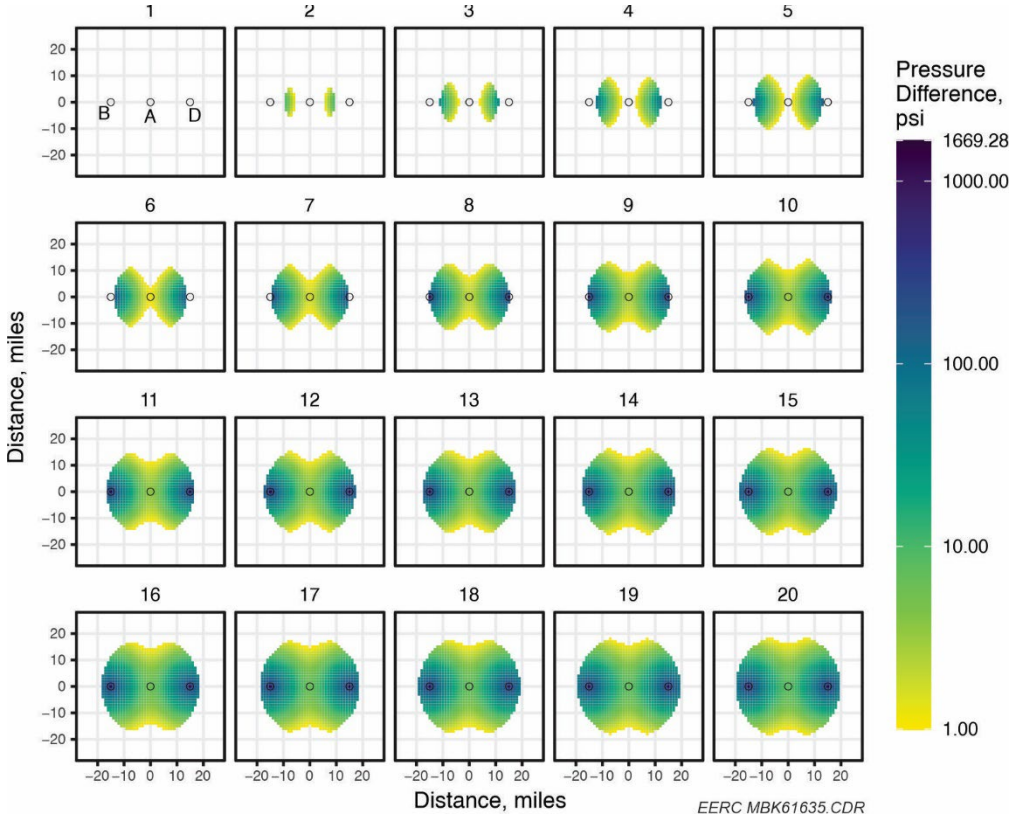

Figure 7. One of the three-site (Sites A, B, and D) examples showing the pressure difference over time caused by Site B and D injection, relative to the base case (Site A only) within the base case pressure buildup area while injecting 4 Mt CO_2/yr into each of Sites A, B, and D. Injection sites (A, B, and D) are marked by small circles in each panel; Site B is located 15 mi west of Site A; and Site D is located 15 mi east of Site A in this case. Additional three-project cases with 10-, 20-, and 25-mi site spacing are shown in Appendix C.

Appendix C). The pressure differences between the Site A, B, and D case and the base case form two north–south trending ellipsoids, which show the intersection of the pressure buildup areas caused by Site A and Site B (west ellipsoid) and by Site A and Site D (east ellipsoid). At approximately Year 5 or 6, the two ellipsoids begin to intersect as the pressure buildup areas for all three sites converge. At 20 years of injection, nearly the entire pressure buildup area for Site A shows effects from Sites B and D.

Figure 8 shows the pressure inventory comparison of the Site A, B, and D case against the base case (Site A only), expressed as percentage change from the base case pressure inventory. Like the previous figure for the two-site case (Figure 6), the magnitude and timing of the percentage change depends on the injection rates of Sites A, B, and D (columns in Figure 8: 0.2, 1, 2, or 4 Mtpa), injection start times of Sites B and D relative to Site A (rows in Figure 8: 0 = all sites start at the same time; 2 = Sites B and D began injecting 2 years after Site A; and 5 = Sites B and D began injection 5 years after Site A), and distance between Site A and Sites B and D (line colors and types in Figure 8: 10, 15, 20, or 25 mi between Site A and Sites B and D).

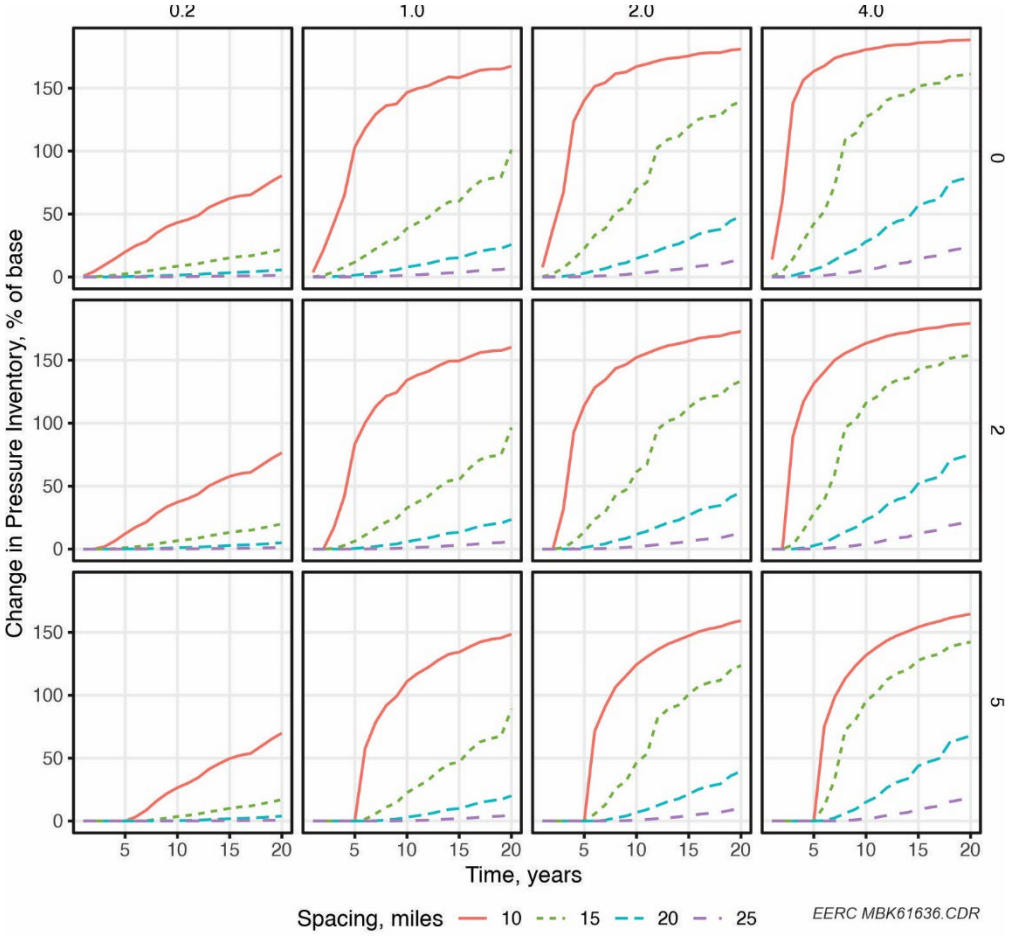

Figure 8. Percentage change in pressure inventory over time between the base case and Site A, B, and D case. Each row (right *y*-axis label) shows the same delay between the start of Site A injection and the start of injection at Sites B and D in years (0 = all sites start at the same time; 2 = Sites B and D began injecting 2 years after Site A; and 5 = Sites B and D began injection 5 years after Site A). Each column (top *x*-axis label) shows the injection rate for all the sites (Site A = Site B = Site D) in Mtpa. Curves with the same color and style represent the same distance between Site A and Sites B and D (10, 15, 20, or 25 mi).

However, the additional site (three versus two) essentially doubles the effects observed in the two-site case. For example, when all three sites are injecting 4 Mtpa and start at the same time (upper right-hand panel), the percentage changes in pressure inventory increase for the 15-mi case at the end of 20 years was nearly 150%, which is essentially twice the effect observed for the same scenario under the two-site case (75%, Figure 6). Thus the three-site example extends the lessons from the two-site example and further illustrates the interrelationships among injection rates, distances between three sites, and injection start dates of Sites B and D on the magnitude and timing of the pressure interference imposed by Sites B and D onto Site A.

Four-Storage Project (Sites A, B, C, and D)

The four-site case begins with the primary site (Site A), a second site located to the west (Site B), a third site located to the north (Site C), and a fourth site located to the east (Site D), such that Site A is surrounded by other injection sites on three sides.

Figure 9 illustrates one of the four-site examples and shows the pressure difference with the addition of Sites B, C, and D, where Site B is located 15 mi west of Site A; Site C is located 15 mi north of Site A; Site D is located 15 mi east of Site A; and where Sites A, B, C, and D begin injection at the same time and inject 4 Mtpa (additional three-site examples with 10-, 20-, and 25-mi site spacing are provided in Appendix C). The pressure difference between the Site A, B, C, and D case and the base case is an arc showing the intersection of the pressure buildup areas of Site A and the other sites. Pressure buildup areas for all four sites begin to converge at Year 3. At 20 years of injection, nearly the entire pressure buildup area for Site A shows effects from Sites B, C, and D.

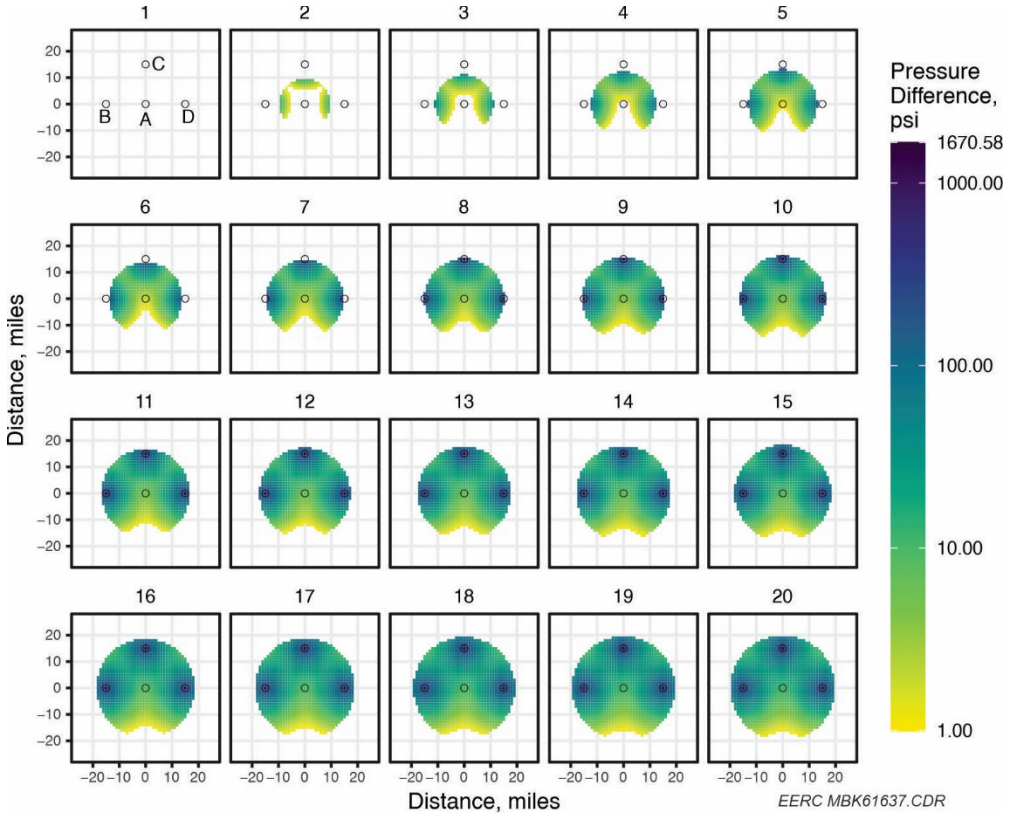

Figure 9. One of the four-site (Sites A, B, C, and D) examples showing the pressure difference over time caused by injection at Sites B, C, and D, relative to the base case (Site A only) within the base case pressure buildup area while injecting 4 Mt CO_2/yr into each of Sites A, B, C, and D. Injection sites (A, B, C, and D) are marked by small circles in each panel; Site B is located 15 mi west of Site A; Site C is located 15 mi north of Site A, and Site D is located 15 mi east of Site A in this case. Additional three-project cases with 10-, 20-, and 25-mi site spacing are shown in Appendix C.

Figure 10 shows the pressure inventory comparison of the Site A, B, C, and D case against the base case, expressed as percentage change from the base case pressure inventory. Like the previous figures for the two- and three- site cases (Figures 6 and 8, respectively), the magnitude and timing of the percentage change depends on the injection rates of Sites A, B, C, and D (columns in Figure 10: 0.2, 1, 2, or 4 Mtpa); injection start times of Sites B, C, and D relative to Site A (rows in Figure 10: 0 = all sites start at the same time; 2 = Sites B, C, and D began injecting 2 years after Site A; and 5 = Sites B, C, and D began injection 5 years after Site A); and distance between Site A and Sites B, C, and D (line colors and types in Figure 10: 10, 15, 20, or 25 mi between Site A and Sites B, C, and D). The additional site (four versus three) increases the effects observed in the three-site case.

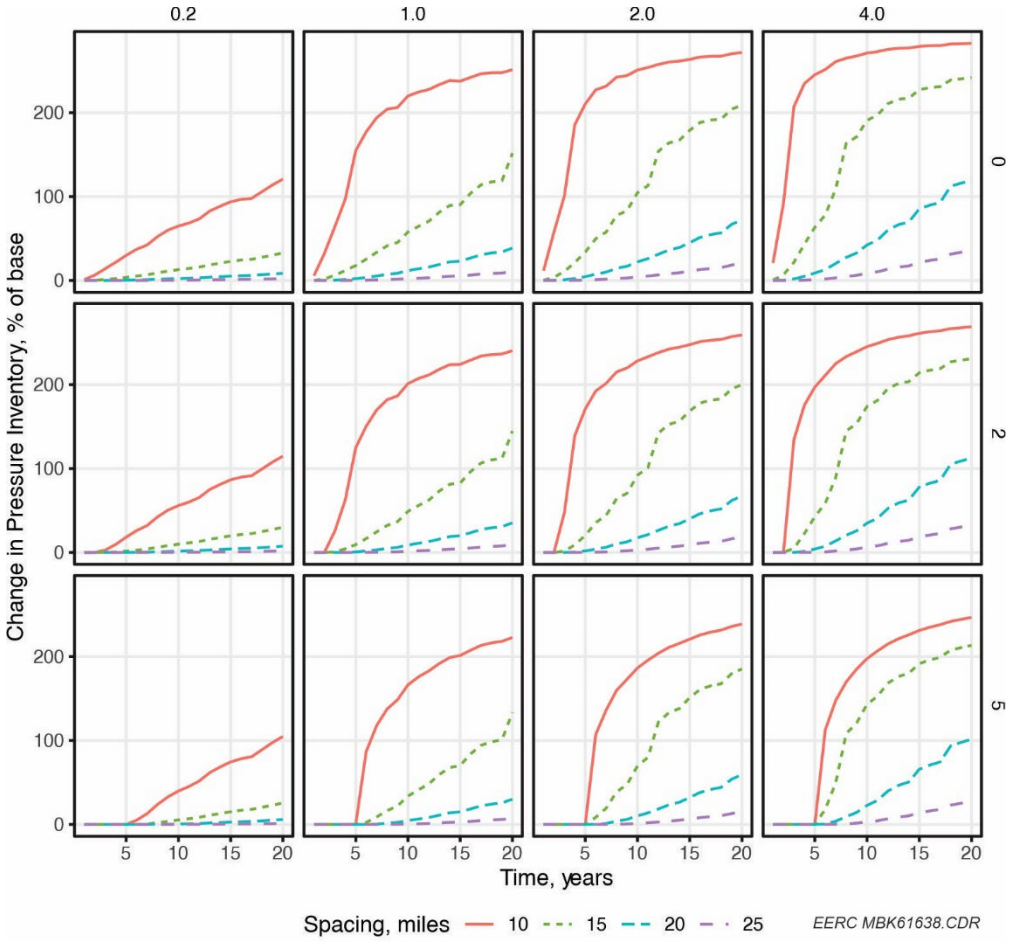

Figure 10. Percentage change in pressure inventory over time between the base case and Site A, B, C, D case. Each row (right *y*-axis label) shows the delay between the start of injection at Site A and the start of injection at Sites B, C, and D in years (0 = all sites start at the same time; 2 = Sites B, C, and D began injecting 2 years after Site A; and 5 = Sites B, C, and D began injection 5 years after Site A). Each column (top *x*-axis label) shows the injection rate at all the sites (Site A = Site B = Site C = Site D) in Mtpa. Curves with the same color and style represent the same distance between Site A and Sites B, C, and D (10, 15, 20, or 25 mi).

Five-Storage Project (Sites A, B, C, D, and E)

The five-site case comprises the primary site (Site A), a second site located to the west (Site B), a third site located to the north (Site C), a fourth site located to the east (Site D), and a fifth site located to the south (Site E), such that Site A is surrounded by other injection sites on four sides. The areal distribution of pressure difference and pressure inventory continue along trends established in the two-, three-, and four-site cases (Figures 11 and 12).

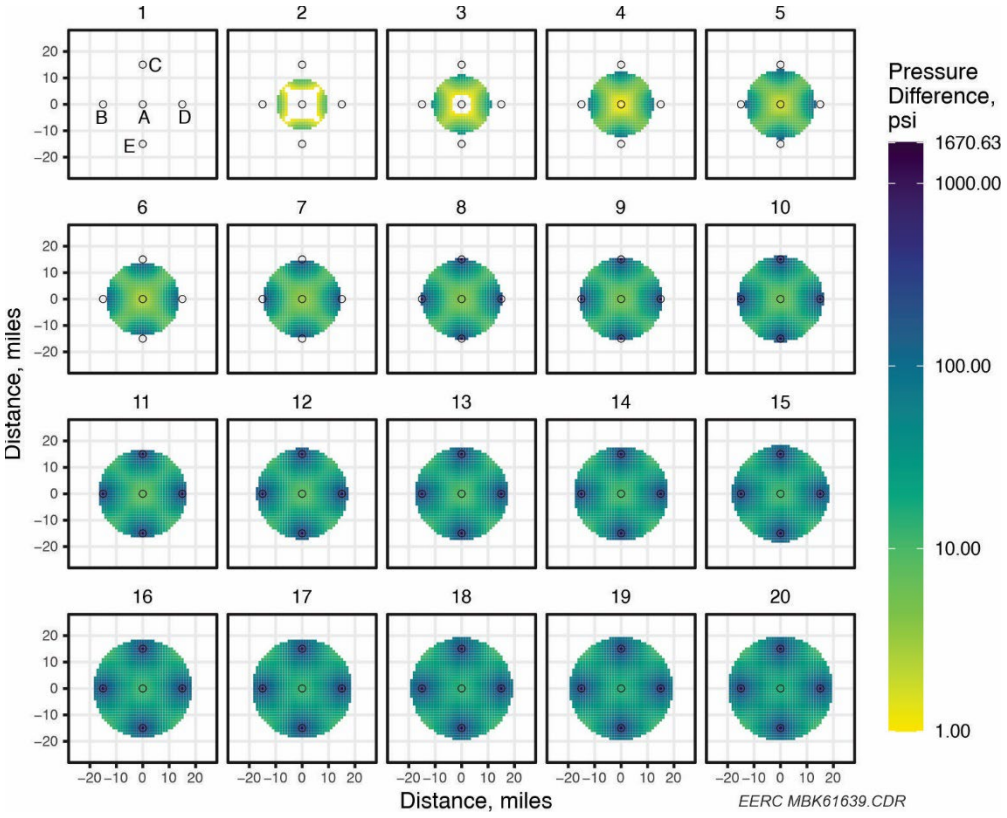

Figure 11. The five-site (Sites A, B, C, D, and E) example showing the pressure difference over time caused by injection at Sites B, C, D, and E, relative to the base case (Site A only) within the base case pressure buildup area while injecting 4 Mt CO_2/yr into each of Sites A, B, C, D, and E. Injection sites (A, B, C, D, and E) are marked by small circles in each panel; Site B is located 15 mi west of Site A; Site C is located 15 mi north of Site A, Site D is located 15 mi east of Site A, and Site E is located 15 mi south of Site A in this case. Additional five-project cases with 10-, 20-, and 25-mi site spacing are shown in Appendix C.

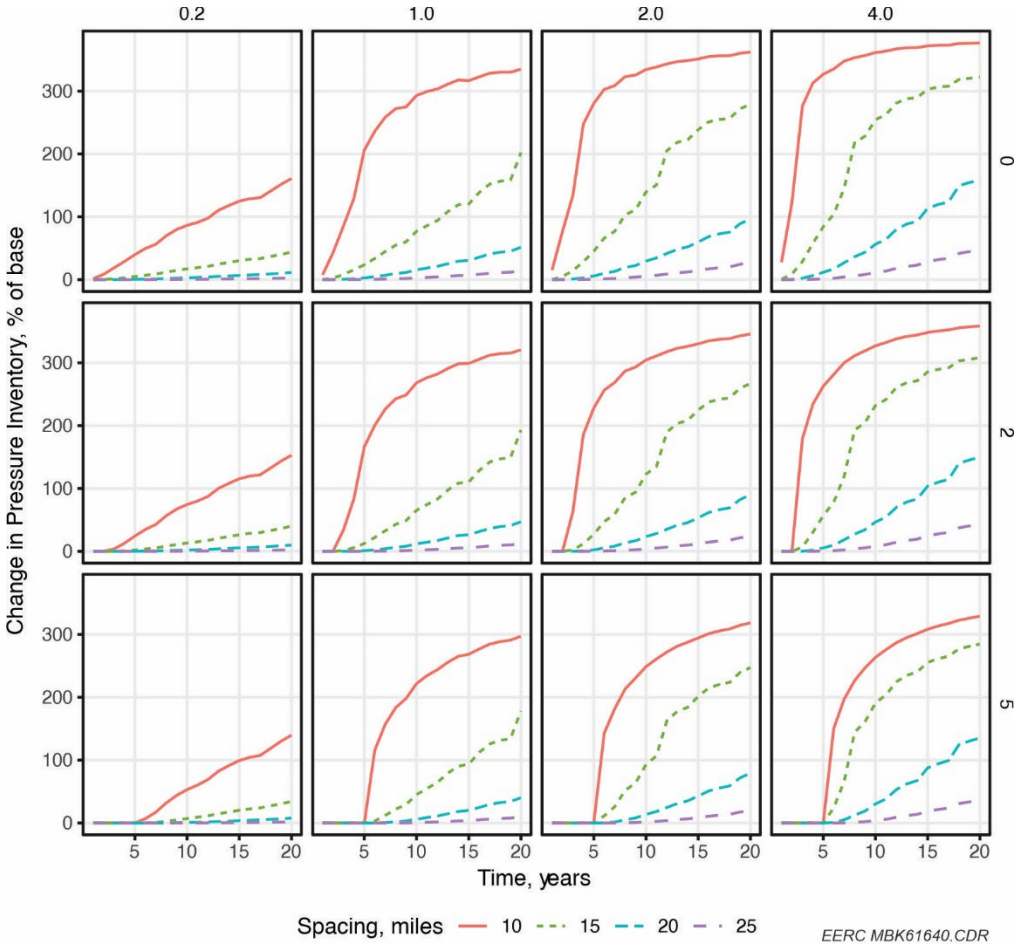

Figure 12. Percentage change in pressure inventory over time between the base case and five-site example (Sites A, B, C, D, and E) case. Each row (right *y*-axis label) shows the delay between the start of Site A injection and the start of injection at Sites B, C, D, and E in years (0 = all sites start at the same time; 2 = Sites B, C, D, and E began injecting 2 years after Site A; and 5 = Sites B, C, D, and E began injection 5 years after Site A). Each column (top *x*-axis label) shows the injection rate for all the sites (Site A = Site B = Site C = Site D = Site E) in Mtpa. Curves with the same color and style represent the same distance between Site A and Sites B, C, D, and E (10, 15, 20, or 25 mi).

Analytical Solutions

Figure 13a shows pressure buildup maps using the Equation 1 analytical solution for the base case (Site A only, left-hand side) and a two-site case (Sites A and B with 15-mi spacing, right-hand side). The Equation 1 analytical solution compares very well to the ASLMA model solution at the end of 20 years of CO_2 injection. For example, for the base case (Site A only), the difference between the Equation 1 analytical solution and the ASLMA model solution at 20 years is a maximum of 96 kPa (14 psi) (Figure 13b, left), which equates to less than a 5% change, defined as (Equation 1 – ASLMA model)/ASLMA model (Figure 13c, left). Similarly, for a two-site case, the difference between the Equation 1 analytical solution and the ASLMA model solution at 20 years is a maximum of 96 kPa (14 psi) (Figure 13b, right), which equates to less than a 5% change (Figure 13c, right). The De Glee (1930) solution depends solely on the CO_2 volumetric injection rate (Q), the hydrogeologic properties of the storage reservoir (aquifer, K and D) and primary seal (aquitard, K' and D'), and the radial distance (r) from the injection well for each storage project. This agreement between the De Glee solution and the ASLMA model solution suggests that Q, K, D, K', and D' can be reasonably used to generate "proximity rules" for multiple storage projects within a region.

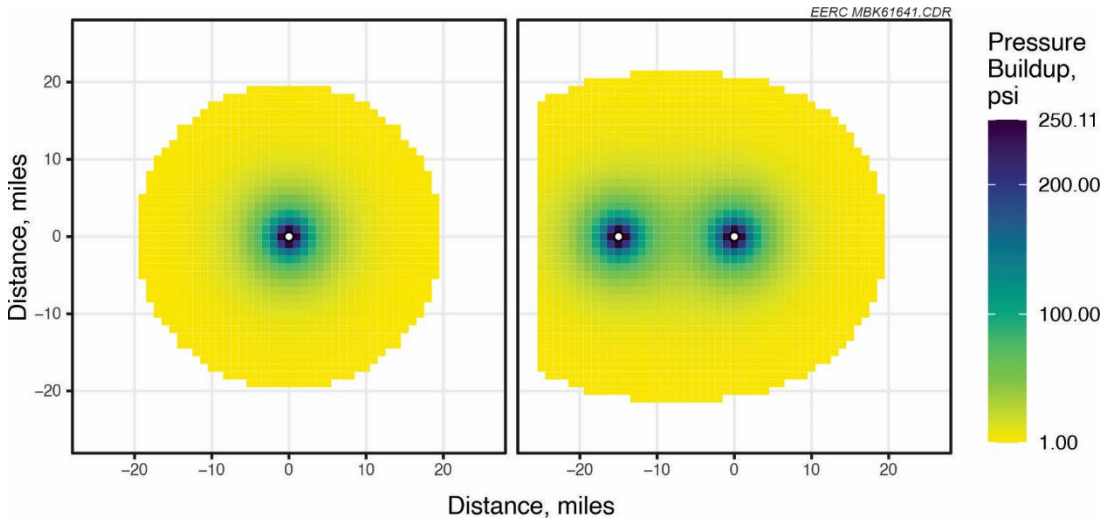

Figure 13a. Pressure buildup greater than 6.9 kPa (1 psi) using the Equation 1 analytical solution for the base case (Site A only, left-hand side) and a two-site case (Sites A and B with 15-mi spacing, right-hand side). Injection sites are marked by white circles.

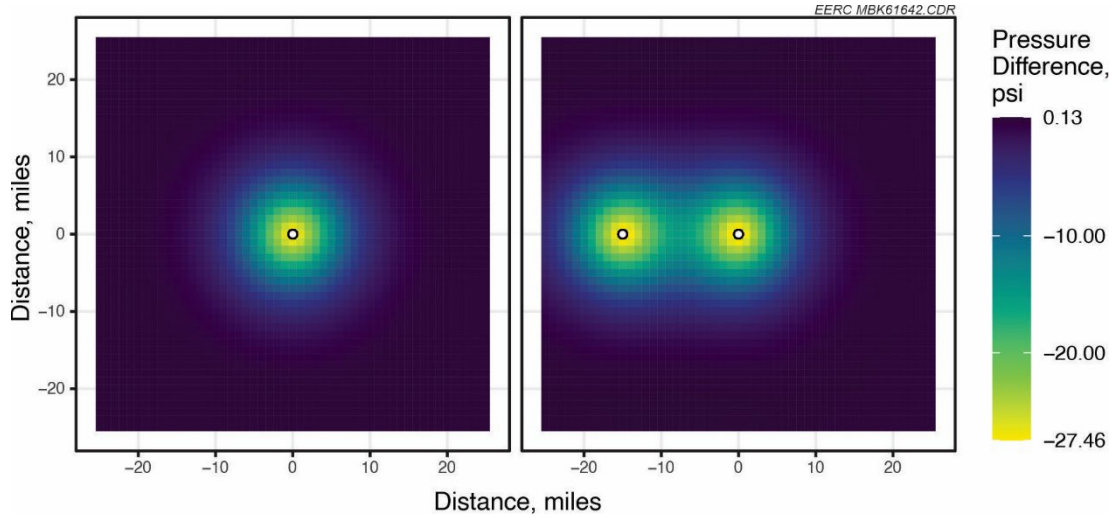

Figure 13b. Absolute pressure difference between the steady-state Equation 1 analytical solution and the ASLMA solution at the end of 20 years of CO_2 injection for the base case (Site A only, left-hand side) and a two-site case (Sites A and B with 15-mi spacing, right-hand side). Injection sites are marked by white circles in each panel.

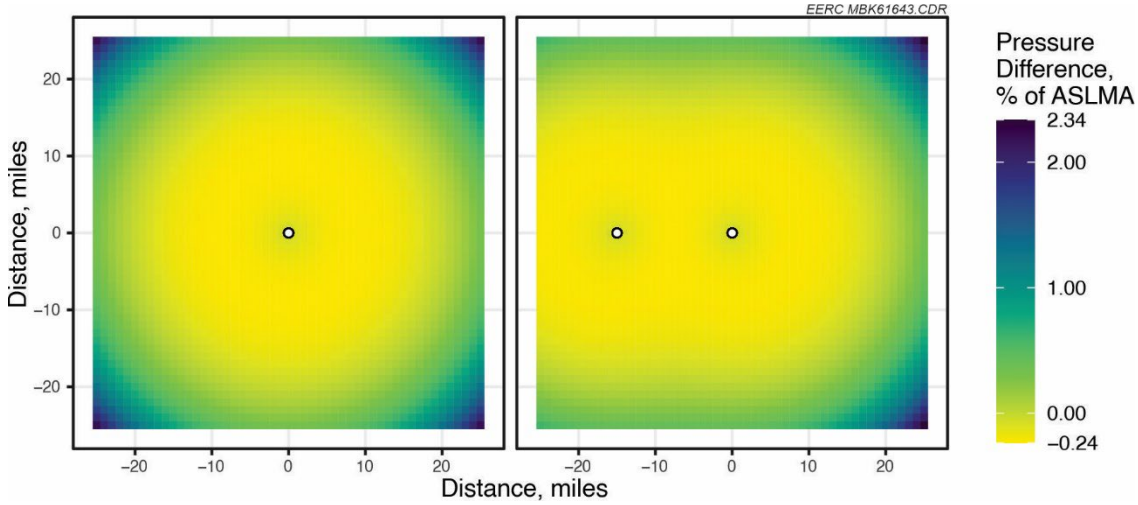

Figure 13c. Comparison between the steady-state Equation 1 analytical solution and the ASLMA solution at the end of 20 years of CO_2 injection for the base case (Site A only) and a two-site case (Sites A and B with 15-mi spacing) as percent pressure difference, defined as (Equation 1 – ASLMA model)/ASLMA model). Injection sites are marked by white circles in each panel.

DISCUSSION

Preliminary Proximity Rules Using Equation 1 and ASLMA Model

Table 2 showed the pressure buildup radii (greater than 6.9 kPa [1 psi] pressure buildup in response to CO_2 injection) determined by the ASLMA model for a single storage site (base case) using 0.2-, 1-, 2-, and 4-$MtCO_2$/year injection rates and minimum pressure threshold to be 15.1, 24.3, 28.3, and 31.9 km (9.4, 15.1, 17.6, 19.8 mi), respectively, after 20 years in injection. Also shown for the base case are the steady-state pressure buildup radii of 13.3, 23.0, 27.4, and 31.8 km (8.3, 14.3, 17.0, and 19.8 mi), respectively, which were determined by solving Equation 1 for the same injection rates and pressure buildup threshold. These results are within 12% of the ASLMA results, with the difference decreasing as injection rate increases. Using the ASLMA results, two or more storage projects injecting at these rates would need to be separated by twice the respective radius to avoid pressure interference, i.e., 30.2, 48.6, 56.6, and 63.8 km (18.8, 30.2, 35.2, and 39.6 mi), respectively. Storage projects operating concurrently inside these distances will exert pressure interference on one another, i.e., their pressure buildup areas will overlap. A 6.9 kPa (1 psi) threshold is extremely low, and therefore, these distances represent the most conservative rules for essentially a no-interference threshold, i.e., the largest distance between sites to ensure no pressure interference above the stated threshold.

Increasing the pressure buildup threshold to a higher value, for example, 70 kPa (10 psi), significantly reduces the radii. The pressure buildup radii greater than 70 kPa (10 psi) pressure buildup in response to CO_2 injection solving Equation 1 for 0.2-, 1, 2-, and 4-$MtCO_2$/year injection rates are 2.7, 10.9, 15.1, and 19.0 km (1.7, 6.8, and 9.4, 11.8 mi), respectively (see Table 3). Therefore, two or more storage projects injecting at these rates would need to be separated by twice the radii to avoid pressure interference, i.e., 5.4, 21.8, 30.2, and 38 km (3.3, 13.5, 18.8, and 23.6 mi), respectively. The smaller distances under the 70 kPa (10 psi) threshold are 82%, 55%, 47%, and 40% smaller, respectively, than the 6.9 kPa (1 psi) threshold distances. Again, these Equation 1 results reasonably align with ASLMA model results after 20 years of injection.

These preliminary proximity rules illustrate the significant effects of injection rate and threshold pressure on the estimated radii for pressure interference and show how a simple analytical equation with inputs of Q, K, D, K', and D' can be used to rapidly estimate the radii and show relatively close alignment with a more complex model. The remainder of the results and interpretations use the ASLMA model outputs, which provide more robust outputs across the model domain and support more detailed visual and quantitative assessments of pressure interference as a function of the number of storage projects, injection rates, distances, and start dates of the storage projects.

Contour Plots

The ASLMA model outputs summarized in Figures 6, 8, 10, and 12 were compiled into a single file and used to create contour plots, interpolating the estimated pressure interference as a function of injection rate and spacing for the discrete number of sites and injection start dates. The contoured variable used as a proxy for pressure interference was the percentage change in pressure inventory at the end of 20 years of injection at Site A, which ranged from less than 1% to 370%. Figures 14–16 show the contoured data for injection start dates of 0, 2, and 5 years, respectively.

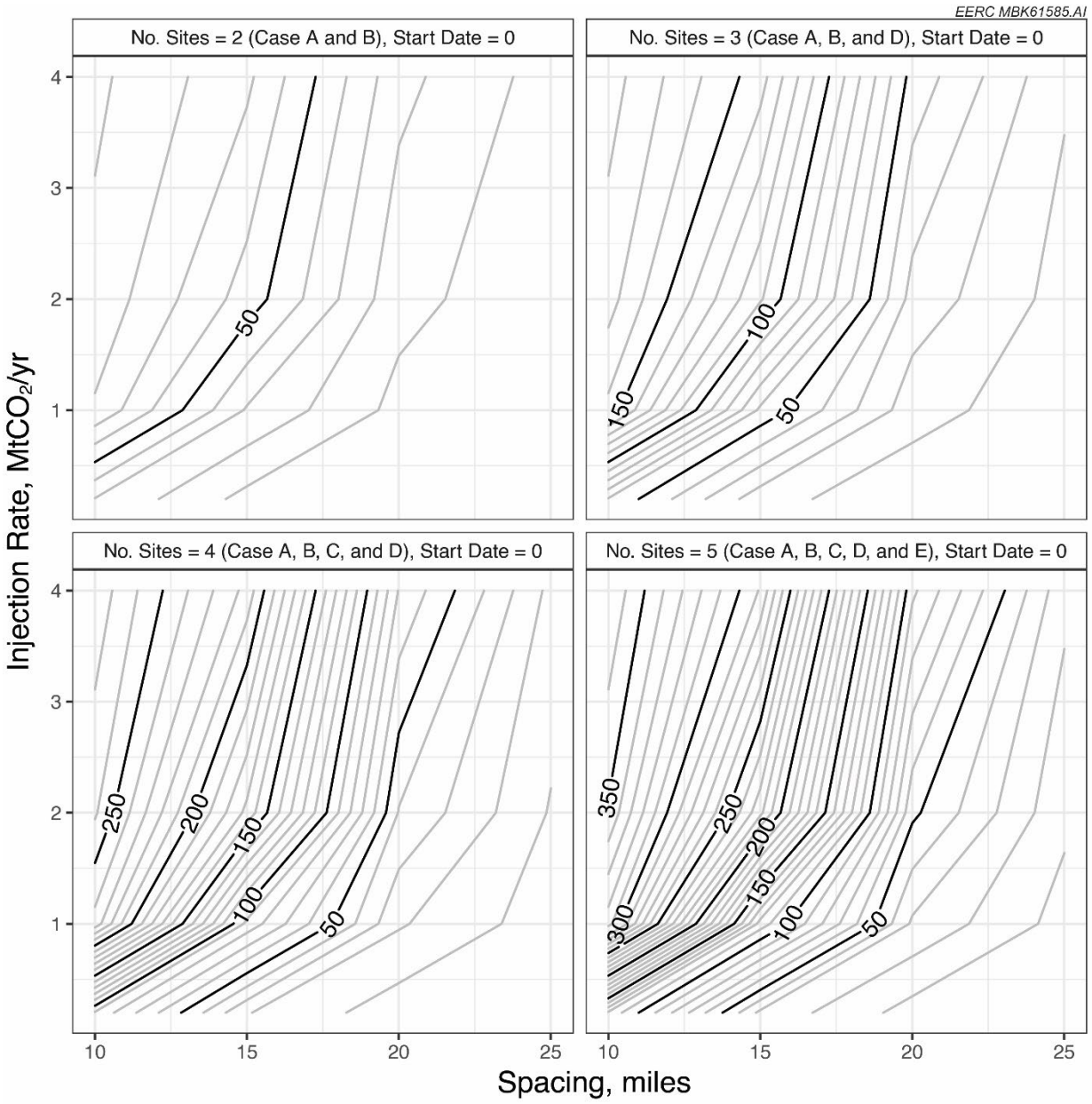

Figure 14. Contoured data for injection start date = 0 (sites injecting simultaneously) showing the percentage change in pressure inventory above 10% for Site A at the end of 20 years of injection as a function of spacing between sites (x-axis) and injection rate (y-axis) and the number of sites equal to two (Case A and B, upper left-hand panel), three (Case A, B, and D; upper right-hand panel), four (Case A, B, C, and D; lower left-hand panel), or five (Case A, B, C, D, and E; lower right-hand panel). Contour interval 10%.

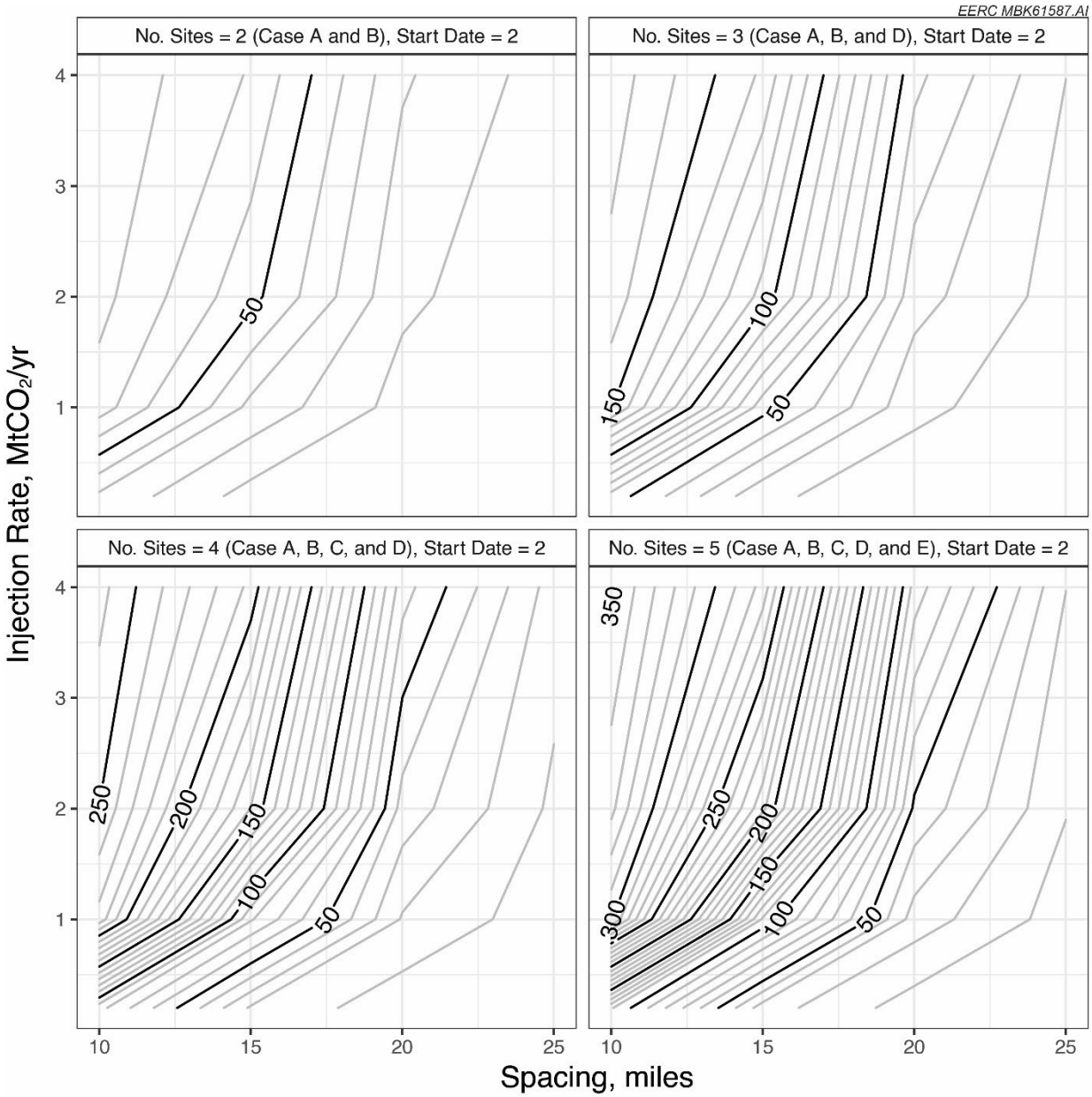

Figure 15. Contoured data for injection start date = 2 (the other sites began injecting 2 years after Site A) showing the percentage change in pressure inventory above 10% for Site A at the end of 20 years of injection as a function of spacing between sites (x-axis) and injection rate (y-axis) and the number of sites equal to two (Case A and B, upper left-hand panel), three (Case A, B, D; upper right-hand panel), four (Case A, B, C, and D; lower left-hand panel), or five (Case A, B, C, D, and E; lower right-hand panel). Contour interval 10%.

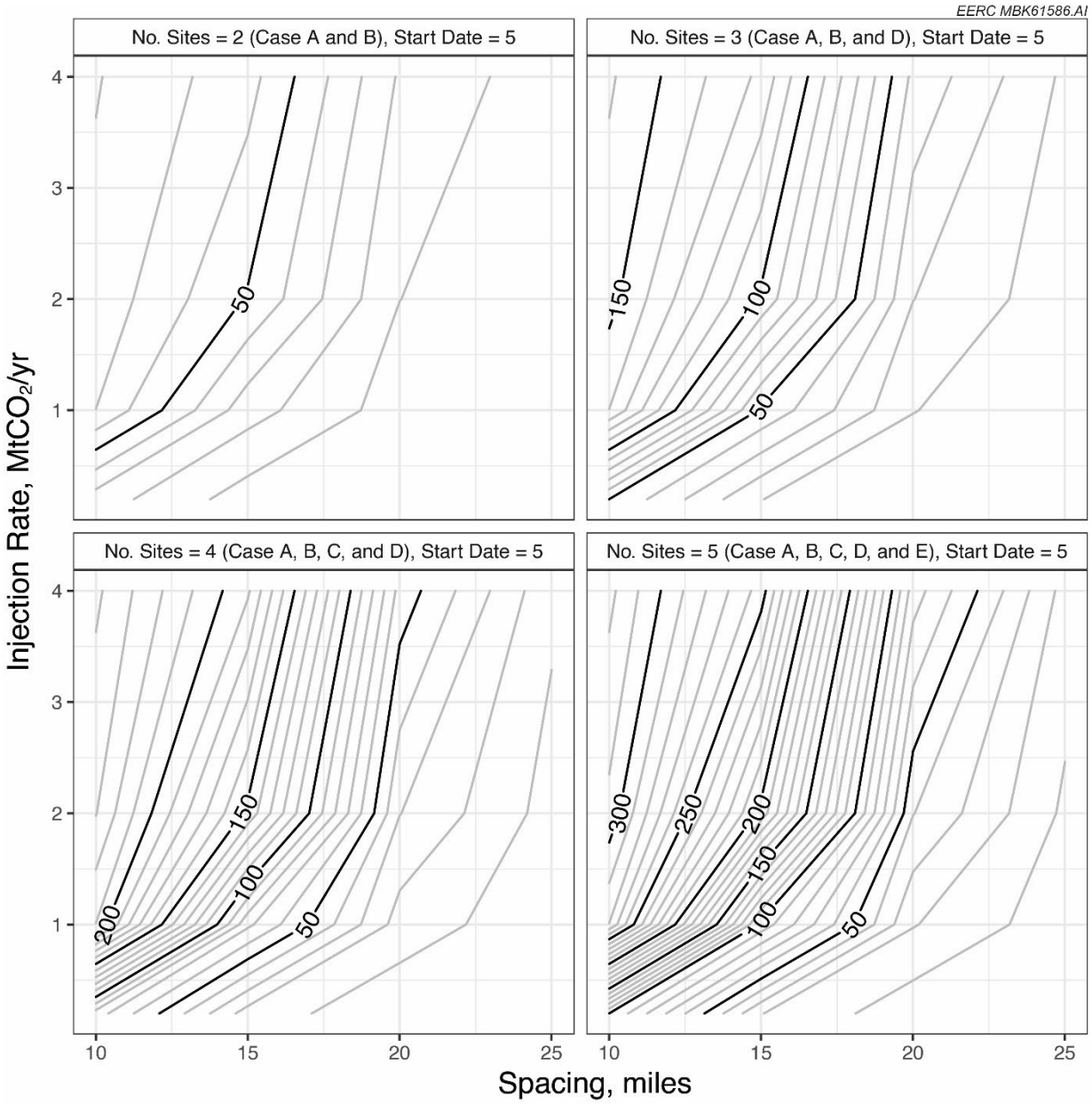

Figure 16. Contoured data for injection start date = 5 (the other sites began injecting 5 years after Site A) showing the percentage change in pressure inventory above 10% for Site A at the end of 20 years of injection as a function of spacing between sites (x-axis) and injection rate (y-axis) and the number of sites equal to two (Case A and B, upper left-hand panel), three (Case A, B, and D; upper right-hand panel), four (Case A, B, C, and D; lower left-hand panel), or five (Case A, B, C, D, and E; lower right-hand panel). Contour interval 10%.

As shown in the figures, the delay in start date from 0 (all sites start at the same time) to 5 (all other sites start 5 years after Site A) results in a time-offset of the pressure interference contours. In other words, the magnitude of the pressure interference is greatest for the scenario where all sites start at the same time (Figure 14) and then decreases as the start date delays by 2 years (Figure 15) and 5 years (Figure 16). If the delayed start date scenarios were evaluated over a longer time frame equivalent to the delay, for example, at 22 and 25 years instead of 20 years, then the contoured data would be like the scenario where all sites start at the same time. Therefore, the remaining interpretations are based on Figure 14.

The 7-kPa (1-psi) and 70-kPa (10-psi) thresholds used to develop the pressure buildup areas in the preceding figures were intended to illustrate the potentially lowest detectable pressure interference (7 kPa [1 psi]) and then an order-of-magnitude increase from that threshold (70 kPa [10psi]). However, small pressure increases of these magnitudes may not have any measurable impact on the ability to operate a storage project, i.e., no effect on the ability to inject and store the target mass of CO_2. As previously discussed, the De Glee and ASLMA pressure solutions lack feedback loops, used by more advanced semianalytical or numerical methods, to modify injection rates as injection wellhead or bottomhole pressure change over the injection period. In practice, this means that buildup in reservoir pressure caused by injection is unconstrained by physical limits like the fracture pressure of the reservoir or confining units. The percentage change in pressure inventory from a base case (Site A only), rather than an absolute measure of differences in injectivity, may therefore overestimate the interferences as they relate to storage project performance. For example, if a set of storage projects plan to use 90% of the available pressure space, defined as the difference between hydrostatic pressure and maximum allowable pressure, then a 10% threshold may adversely impact the storage projects. However, if the storage reservoir provides ample pressure space such that the storage projects plan to use only 20% of the available pressure space, then a 10% threshold may be inconsequential. Therefore, the contour plots in Figures 14–16 should be viewed as providing information about the relative timing and magnitude of pressure interferences among storage projects under different development scenarios, which do not necessarily translate directly to operational impacts.

The interactions between the number of sites, injection rates, and spacing between sites all factor into the pressure interference with Site A caused by additional sites. For the two-site scenario (Case A and B), the pressure interference ranges from 10%, when the two sites are approximately 20 mi apart and have an injection rate ~1 $MtCO_2$/yr, to 90%, when the two sites are within approximately 12 mi of each other and have injection rates exceeding 3 $MtCO_2$/year (upper left-hand panel of Figure 14). The contoured value for pressure interference increases with each additional site. For scenarios with three, four, and five sites operating within 15 mi of each other and with injection rates exceeding 3 $MtCO_2$/year, the pressure interference is estimated to be ≥130%, ≥190%, or ≥250%, respectively. When the distance increases to 25 mi and the injection rate decreases to 1 $MtCO_2$/year, then the pressure interference is estimated to be <10%. Therefore, proximity rules for storage projects must account for the number of sites, injection rates, and spacing between sites.

The five-site case (Case A, B, C, D, and E) likely represents the most useful contoured data set for planning purposes, since the contours reflect the scenario where each adjacent land parcel direction surrounding Site A (north, east, south, and west) contains a storage project and is,

therefore, representative of a more regional development plan. As shown in the bottom right-hand corner of Figure 14, under the five-site scenario, when the sites are spaced closer than approximately 18 mi apart and injection rates are greater than 1 $MtCO_2$/year, there is substantial pressure interference.

SUMMARY OF KEY FINDINGS

- Reservoir pressure increase caused by injection of CO_2 into the same reservoir at multiple sites can result in intersecting pressure buildup areas, which this document refers to as "pressure interference."

- This work used simplified analytical and semianalytical models to examine the nature of pressure interference between two or more storage projects as a function of injection rate (0.2, 1, 2, or 4 $MtCO_2$/year), spacing (distance between storage projects of 10, 15, 20, or 25 mi), number of sites (two = Case A and B; three = Case A, B, and D; four = Case A, B, C, and D; or five = Case A, B, C, D, and E), and injection start date (0 = all sites start at the same time, 2 = other sites start 2 years after Site A, or 5 = other sites start 5 years after Site A).

- The timing of the pressure interference among storage sites is a function of the delay between the injection at the first storage site and subsequent storage sites, as modeled here using "start date." More time between start dates simply delays the pressure interference between sites; however, the magnitude of the pressure interference is comparable to the scenario where all sites begin injecting CO_2 at the same time.

- The results illustrate that the magnitude of pressure interference among storage sites depends on the injection rate, spacing, and number of sites, in addition to the pressure-increase threshold used to define "interference," all of which must, therefore, be considered prior to developing spacing rules for a particular region. Under the cases considered here, which included a maximum CO_2 injection rate of 4 $MtCO_2$/year and a maximum number of five concurrent sites, pressure interference above 70 kPa (10 psi) did not occur at spacings greater than approximately 20 mi. However, results indicate larger injection rates, above 4 $MtCO_2$/year, would require larger spacing to avoid pressure interference.

- The pressure-increase threshold used to define "interference" significantly affects the estimated minimum spacing. For example, the minimum spacing to avoid pressure interference using a 6.9 kPa (1 psi) threshold was significantly greater than the minimum spacing to avoid pressure interference using a 70 kPa (10 psi) threshold. Agreed-upon pressure interference thresholds are required to determine whether a potential storage project will interfere with an existing storage project above the stated threshold.

- Potential pressure interference among sites can be reduced by i) reducing the injection rate at each site, ii) reducing the number of sites, iii) increasing the spacing between sites, iv) installing producing wells at points/areas of expected or monitored pressure interference (ARM), or v) employing a combination of these factors. The contour plots provided in this document provide a screening-level basis for considering potential spacing requirements as a function of

these three factors. Alternatively, storage project developers may use simplified analytical solutions such as the De Glee (1930) method illustrated here or the semianalytical model, ASLMA, to estimate pressure interference among sites.

- This work used a simplified version of Broom Creek stratigraphy with no lateral continuity constraints (laterally homogeneous). The results presented here cannot be directly applied to other formations or more detailed geologic models of the Broom Creek that have been, or may be in the future, used for project permitting. Potential pressure interference for geologic scenarios that differ from the scenarios described in this report may be substantially different. Therefore, these general conclusions about spacing should not be extrapolated to more detailed models of the Broom Creek, to other geologic formations, or to other basins.

- Even without considerations of asymmetric plume expansion due to lateral formation barriers and baffles, pressure interference among neighboring projects has been identified as a potential challenge to wide-scale commercial deployment of carbon storage. Regulatory bodies and project developers should be aware of pressure interference among neighboring projects competing for subsurface pore and pressure space. To maximize the use of a jurisdiction's potential storage resource, state and provincial governments may want to consider policies that promote the orderly development and optimal use of pore space as a resource. For example, Alberta, Canada, has a program to "ensure that [CCS] will be deployed in a responsible, safe, and strategic manner [and] avoid challenges associated with numerous, and potentially overlapping" projects (Alberta, 2022). From a project development standpoint, the application of storage optimization strategies that optimize the use of the pore space resource will not only reduce pressure impacts to surrounding areas but can also reduce the areal footprint of the CO_2 plume, thereby reducing the amount of land within which pore space must be leased.

- Although this effort represents one building block, additional work needs to be done to better understand pressure interference among neighboring projects in relation to commercial storage. Modeling- and simulation-based studies based on documented 3D models incorporating geophysical surveys would be useful, if not necessary, for evaluating different pressure management strategies under a variety of project development scenarios.

FUTURE WORK

The analytical method illustrated in this study provides a potential simplification of the more complicated ASLMA model (semianalytical model); however, further investigation would be needed to better understand 1) the applicability of the analytical method beyond the geologic and operational parameter space described in this work and 2) the amount of uncertainty surrounding the conditions under which a steady-state assumption is valid. Although the ASLMA model results at 20 years for the described scenarios show the system is near enough to steady state to be approximated by the analytical model, other systems may approach steady state earlier or later. Therefore, the primary interpretations of proximity rules should consider using the ASLMA model outputs, which provide more robust outputs across the model domain and support more detailed visual and quantitiatve assessments of pressure interference among the storage projects.

In regions without active CO_2 storage operations, a minimum-distance development strategy based on the simplified axisymmetric pressure buildup radius may be sufficient to prevent substantial pressure interference among storage sites. However, where multiple commercial-scale projects in a single flow unit are expected to be near enough for pressure interaction, contour plots derived from the ASLMA model results provide more accurate proximity evaluations to determine guidelines for the allowable distances between storage sites to avoid substantial pressure interference. These ASLMA model results would then guide more comprehensive evaluations using full-scale geologic modeling and reservoir simulation.

A major simplifying assumption in the current work is that both the reservoir and confining formations are homogeneous and isotropic, meaning that the petrophysical properties are uniform through the entire geologic unit and identical in all directions (horizontally and vertically). Oil industry experience with waterflooding and CO_2 flooding illustrates that homogeneous and isotropic reservoir conditions do not exist. Modeling using a heterogeneous, geocellular geologic model based on 3D reservoir data to capture heterogeneity across the geologic unit, coupled with compositional reservoir simulation of a subset of the ASLMA model scenarios, would provide calibration against the pressure interference results derived from the simplified models presented here. Additionally, reservoir simulation of heterogeneous models will be able to directly relate the magnitude of pressure interference to the potential for loss of CO_2 injectivity and, therefore, better link pressure interference to storage capacity.

The design matrix presented here used a static set of geologic parameters and varied operational parameters (injection rate, site spacing, and time between projects). The described methods could be expanded to determine the sensitivity of the pressure interference results to 3D survey-based geologic parameters (e.g., geologic unit thickness, porosity, and permeability), and be compared against the pressure results of reservoir simulation of geologic models with varying structure (e.g., thickness or porosity trends within the pressure buildup area). Brine extraction wells might be used for ARM to ameliorate reservoir pressure buildup.

REFERENCES

Alberta, 2022, Carbon Sequestration Tenure Management: www.alberta.ca/carbon-sequestration-tenure-management.aspx (accessed February 2022).

Bachu, S., Bonijoly, D., Bradshaw, J., Burruss, R., Holloway, S., Christensen, N.P., and Mathiassen, O.M., 2007, CO_2 storage capacity estimation—methodology and gaps: International Journal of Greenhouse Gas Control, v. 1, p. 430–443.

Bachu, S., 2015, Review of CO_2 storage efficiency in deep saline aquifers: International Journal of Greenhouse Gas Control, v. 40, p. 188–202.

Bandilla, K.W., Kraemer, S.R., and Birkholzer, J.T., 2012, Using semianalytic solutions to approximate the area of potential impact for carbon dioxide injection: International Journal of Greenhouse Control, v. 8, p. 196–204.

Birkholzer, J.T., Zhou, Q., and Tsang, C.F., 2009, Large-scale impact of CO_2 storage in deep saline aquifers—a sensitivity study on the pressure response in stratified systems: International Journal of Greenhouse Control, v. 3, no 2, p. 181–194.

Bosshart, N.W., Azzolina, N.A., Ayash, S.C., Peck, W.D., Gorecki, C.D., Ge, J., Jiang, T., and Dotzenrod, N.W., 2018, Quantifying the effects of depositional environment on deep saline formation CO_2 storage efficiency and rate: International Journal of Greenhouse Gas Control, v. 69, p. 8–19. DOI: 10.1016/j.ijggc.2017.12.006.

Burton-Kelly, M.E., Azzolina, N.A., Connors, K.C., Peck, W.D., Nakles, D.V. and Jiang, T., 2021, Risk-based area of review estimation in overpressured reservoirs to support injection well storage facility permit requirements for CO_2 storage projects: Greenhouse Gas Science Technology, v. 11, no. 5, p. 887–906. DOI: https://doi.org/10.1002/ghg.2098.

Cihan, A., Zhou, Q., and Birkholzer, J.T., 2011, Analytical solutions for pressure perturbation and fluid leakage through aquitards and wells in multilayered aquifer systems: Water Resources Research, v. 47, no. 10. DOI:10.1029/2011WR010721.

Cihan, A., Birkholzer, J.T., and Zhou, Q., 2012, Pressure buildup and brine migration during CO_2 storage in multilayered aquifers: Ground Water, v. 51, no. 2, p. 252–267. DOI:10.1111/j.1745-6584.2012.00972.x.

Code of Federal Regulations, 1983, Underground injection control program: Title 40, Section 144.3.

Code of Federal Regulations, 2013, Underground injection control program—criteria and standards: Title 40, Section 146.84.

De Glee, G.J. 1930. Over grondwaterstromingen bij wateronttrekking door middel van putten [Ph.D. thesis]: Delft, p. 175. https://repository.tudelft.nl/islandora/object/uuid:c3e13209-4626-41b9-9038-c223d61e35c4?collection=research (accessed November 2021).

De Simone, S., Jackson, S.J., and Krevor, S., 2019, The error in using superposition to estimate pressure during multisite subsurface CO_2 storage: Geophysical Research Letters, v. 46, p. 6525–6533. DOI: 10.1029/2019GL082738.

Goodman, A., Hakala, A., Bromhal, G., Deel, D., Rodosta, T., Frailey, S., Small, M., Allen, D., Romanova, V., Fazio, J., Huerta, N., McIntyre, D., Kutchko, B., and Guthrie, G., 2011, U.S. DOE methodology for the development of geologic storage potential for carbon dioxide at the national and regional scale: International Journal of Greenhouse Gas Control, v. 5, no. 4, p. 952–965.

Gorecki, C.D., Sorensen, J.A., Bremer, J.M., Ayash, S.C., Knudsen, D.J., Holubnyak, Y.I., Smith, S.A., Steadman, E.N., and Harju, J.A., 2009, Development of storage coefficients for carbon dioxide storage in deep saline formation: report for U.S. Department of Energy Cooperative Agreement. Energy & Environmental Research Center, Grand Forks, North Dakota, p. 61.

Kringstad J.J., 2007, Reservoir characterization of the Broom Creek Formation for carbon dioxide sequestration [Ph.D. thesis]: University of North Dakota. https://commons.und.edu/senior-projects/92.

Kruseman, G.P., and de Ridder, N.A., 2000, Analysis and evaluation of pumping test data: Wageningen, the Netherlands, Bulletins of the International Institute for Land Reclamation and Improvement (ILRI), 372 p.

Minitab, 2021, Minitab 20 Statistical Software, [Computer software]. State College, Pennsylvania, Minitab, Inc. www.minitab.com (accessed November 2021).

Nicot, J.P., 2008, Evaluation of large-scale CO_2 storage on freshwater sections of aquifers—an example from the Texas Gulf Coast Basin: International Journal of Greenhouse Gas Control, v. 2, no. 4, p. 582–593.

North Dakota Administrative Code, 2010, Geologic storage of carbon dioxide—section 43-05-01-05.1. Area of review and corrective action, p. 11–12.

Peck, W.D., Ayash, S.C., Klapperich, R.J., and Gorecki, C.D., 2019, The North Dakota integrated carbon storage complex feasibility study: International Journal of Greenhouse Gas Control, v. 84, p. 47–53. DOI: 10.1016/j.ijggc.2019.03.001.

Peck, W.D., Glazewski, K.A., Klenner, R.C.L., Gorecki, C.D., Steadman, E.N., and Harju, J.A., 2014, A workflow to determine CO_2 storage potential in deep saline formations: Energy Procedia, v. 63, p. 5231–5238.

R Core Team, 2020, R—A language and environment for statistical computing: R Foundation for Statistical Computing. www.R-project.org/ (accessed November 2021).

Schlumberger, 2021, Petrel E&P Software Platform. https://www.software.slb.com/products/petrel (accessed October 2021).

Sorensen, J.A., Smith, S.A., Dobroskok, A.A., Peck, W.D., Belobraydic, M.L., Kringstad, J.J., and Zeng, Z., 2009, Carbon dioxide storage potential of the Broom Creek Formation in North Dakota—a case study in site characterization for large-scale sequestration, *in* Grobe, M., Pashin, J.C., and Dodge, R.L., eds., Carbon dioxide sequestration in geological media—state of the science: AAPG Studies in Geology 59, Tulsa, OK, American Association of Petroleum Geologists, p. 279–296.

U.S. Department of Energy National Energy Technology Laboratory, 2015, The 2015 United States carbon utilization and storage atlas (5th ed.).

U.S. Department of Energy National Energy Technology Laboratory, 2021, About the carbon storage program. https://netl.doe.gov/coal/carbon-storage/about-the-carbon-storage-program (accessed July 2021).

U.S. Environmental Protection Agency, 2013, Geologic sequestration of carbon dioxide—underground injection control (UIC) program Class VI well area of review evaluation and corrective action guidance: EPA 816-R-13-005.

APPENDIX A

DERIVATION OF HYDROGEOLOGIC PROPERTIES

DERIVATION OF HYDROGEOLOGIC PROPERTIES

A macro-enabled Microsoft Excel workbook with built-in Visual Basic for Applications (VBA) functions is included as Attachment A that provides the calculations needed to execute the analytical solution for leakage in multilayered aquifers (ASLMA) model (Attachment A workbook). The remainder of this supporting information describes the calculations included in the Attachment A workbook.

Aquifer and Aquitard Properties

Hydraulic Conductivity (HCON)

HCON is a function of fluid density, fluid viscosity, and the reservoir permeability, as shown in Equation A-1:

$$k = \kappa \frac{\rho g}{\mu} \qquad \text{[Eq. A-1]}$$

Where:

k is hydraulic conductivity (m/d).
κ is permeability (m^2).
ρ is the fluid density (kg/m^3).
g is the acceleration due to gravity (9.81 m/s^2).
μ is the fluid viscosity (kg/m-s).

The fluid density and viscosity are a function of pressure, temperature, and salinity.

To estimate the brine density, the Attachment A workbook utilizes a VBA function, *BrineDen*, which uses inputs of temperature (T in units of °C), pressure (P in units of Pa), and salinity (XS as a dimensionless salt mass fraction). The *BrineDen* function was developed by Bandilla (2016a) based on the brine density solutions described in Haas (1976) and Battistelli and others (1997).

To estimate brine viscosity, the Attachment A workbook utilizes a VBA function, *BrineVisc*, which also uses inputs of temperature (T in units of °C), pressure (P in units of Pa), and salinity (XS as a dimensionless salt mass fraction). The *BrineVisc* function was developed by Bandilla (2016b) based on the brine viscosity solutions described in Phillips and others (1981).

The formation-specific pressure, temperature, and salinity values provide the inputs needed to estimate brine density via *BrineDen* and brine viscosity via *BrineVisc*, which, along with the formation-specific permeability, provide the inputs for estimating HCON for each unit via Equation A-1. For example, the pressure, temperature, and salinity for Aquifer 1 (Broom Creek Formation) are 16.41 MPa (2380 psi), 57.4°C (135.3°F), and 49,350 ppm, respectively. These inputs result in an estimated brine density and viscosity of 1024 kg/m^3 and 5.38E-04 kg/m-s, respectively. The average permeability for Aquifer 1 is 2.17E-13 m^2 (220 mD), which results in a HCON of 3.50E-01 m/d.

Specific Storage (SS)

SS is a function of fluid density, gravity, formation porosity, fluid compressibility, and pore compressibility, as shown in Equation A-2:

$$SS = \rho g(\alpha + \phi\beta) \quad \text{[Eq. A-2]}$$

Where:

ρ is the fluid density (kg/m^3).
g is the acceleration due to gravity (9.81 m/s^2).
ϕ is porosity (unitless).
α is the pore compressibility (1/Pa).
β is the brine compressibility (1/Pa).

Similar to the process for estimating HCON, the formation-specific pressure, temperature, and salinity values provide the inputs needed to estimate brine density via *BrineDen* and brine viscosity via *BrineVisc*, which, along with the formation-specific porosity, brine compressibility, and pore compressibility, provide the inputs for estimating SS for each unit via Equation A-2. The pore compressibility is assumed to be 4.5E-10 (1/Pa) for aquifers and 9.0E-10 (1/Pa) for aquitards, which is consistent with values used in Birkholzer and others (2009) and representative of the site-specific lithology for the storage project. Users may change these inputs to reflect their site-specific values. An additional function is used to estimate pore compressibility. To estimate the brine compressibility, the Attachment A workbook utilizes a VBA function, *BrineComp*, which uses inputs of temperature (T in units of °C), pressure (P in units of Pa), and salinity (XS as a dimensionless salt mass fraction). The *BrineVisc* function was developed by Morgan (2016).

For example, the pressure, temperature, and salinity for Aquifer 1 (Broom Creek Formation) noted above result in an estimated brine compressibility of 3.79E-10 (1/Pa) and the pore compressibility is assumed to be 4.5E-10 (1/Pa). Therefore, the estimated SS for Aquifer 1 is 5.07E-06 (1/m).

CO_2 EQUIVALENT-VOLUME INJECTION OF BRINE

The target CO_2 injection rate for the storage project is one of 0.2, 1, 2, or 4 million metric tons CO_2 per year for 20 years. The ASLMA model (Cihan and others, 2011) requires the CO_2 injection rate to be converted into an equivalent-volume injection of brine in units of cubic meters per day. For estimating the CO_2 density, the Attachment A workbook utilizes a macro function, *CO2Den* (Burton-Kelly and Bosshart, 2020), which uses inputs of temperature (T in units of °C) and pressure (P in units of psi) of to estimate CO_2 density in the reservoir from correlations described in Ouyang (2011). The estimated CO_2 density is 677 kg/m^3, which results in daily equivalent-volume injection rates of approximately 809, 4047, 8093, or 16186 m^3 per day, respectively, for 0.2-, 1-, 2-, and 4-MtCO_2/year injection rates.

As CO_2 injection progresses throughout the 20-year operating period, the pressure in the storage reservoir will increase. Consequently, the CO_2 density will also increase, resulting in a lower equivalent-volume injection rate over time if the CO_2 mass injection rate is held constant at

the surface. The current approach uses a constant equivalent-volume injection rate throughout the entire operational period, which results in overestimating pressure buildup in the storage reservoir over time. However, the ASLMA model outputs are used to create a relationship between pressure buildup in the storage reservoir and the incremental total cumulative leakage that occurs because of the injection, not to delineate a distance–leakage relationship.

REFERENCES

Bandilla, D.J., 2016a, BrineDen—an Excel Visual Basic for Applications function for calculating brine density: Princeton University.

Bandilla, D.J., 2016b, BrineVisc—an Excel Visual Basic for Applications function for calculating brine viscosity: Princeton University.

Battistelli, A., Calore, C., and Pruess, K., 1997, The simulator TOUGH2/EWASG for modelling geothermal reservoirs with brines and non-condensible [sic] gas: Geothermics, v. 26, no. 4, p. 437–464.

Birkholzer, J.T., Zhou, Q., and Tsang, C.F., 2009, Large-scale impact of CO_2 storage in deep saline aquifers—a sensitivity study on pressure response in stratified systems: International Journal of Greenhouse Gas Control, v. 3, p. 181–194.

Burton-Kelly, M.E., and Bosshart, N.W., 2020, CO2Den—an Excel Visual Basic for Applications function for calculating CO_2 density: Energy & Environmental Research Center.

Cihan, A., Zhou, Q., and Birkholzer, J.T., 2011, Analytical solutions for pressure perturbation and fluid leakage through aquitards and wells in multilayered aquifer systems: Water Resources Research, v. 47, no. 10. DOI:10.1029/2011WR010721.

Haas, J.L., 1976, Physical properties of the coexisting phases and thermochemical properties of the H_2O component in boiling NaCl solutions: Geological Survey Bulletin, 1421-A, Washington, DC, p. 73.

Morgan, D.J., 2016, BrineComp—an Excel Visual Basic for Applications function for calculating brine compressibility: National Energy Technology Laboratory, U.S. Department of Energy.

Oldenburg, C.M., Cihan, A., Zhou, Q., Fairweather, S., and Spangler, L.J., 2014, Delineating area of review in a system with pre-injection relative overpressure: Energy Procedia, v. 63, p. 3715–3722.

Ouyang, L.B., 2011, New correlations for predicting the density and viscosity of supercritical carbon dioxide under conditions expected in carbon capture and sequestration operations: The Open Petroleum Engineering Journal, v. 4, p. 13–21. DOI: 10.2174/1874834101104010013.

Phillips, S.L., Igbene, A., Fair, J.A., Ozbek, H., and Tavana, M., 1981, A technical databook for geothermal energy utilization: Lawrence Berkeley Laboratory Report LBL-12810.

Weyer, K.U., 1978, Hydraulic forces in permeable media: Mémoires du B.R.G.M., 91, p. 285–297, Orléans, France.

APPENDIX B

DE GLEE (1930) SOLUTION

DE GLEE (1930) SOLUTION

Introduction

This appendix describes the De Glee (1930) analytical solution cited in the main text and walks the user through an accompanying macro-enabled Microsoft Excel file (Attachment B) for executing the calculations (hereafter "De Glee Calculator").

De Glee (1930)

De Glee (1930) developed the following solution for the steady-state drawdown due to extracting fluids from a reservoir with pressure dissipation from an aquitard proportional to the hydraulic gradient across the aquitard:

$$s_m = \frac{Q}{2\pi KD} K_0\left(\frac{r}{L}\right) \qquad \text{[Eq. B-1]}$$

Where:

- s_m = steady-state (stabilized) drawdown in a piezometer at distance r from the well (m)
- Q = volumetric discharge of the well (m^3/d)
- K = hydraulic conductivity of the reservoir (m/d)
- D = thickness of the reservoir (m)
- r = radial distance from the well (m)
- L = $\sqrt{KDc}$: leakage factor (m)
- c = $\frac{D'}{K'}$: hydraulic resistance of the aquitard (days)
- D′ = saturated thickness of the aquitard (m)
- K′ = hydraulic conductivity of the aquitard for vertical flow (m/d)
- $K_0(x)$ = modified Bessel function of the second kind and of zero order (Hankel function)
- r = radial distance from the well (m)

In the context of geologic carbon storage, Q is the volumetric injection rate (not discharge), which results in a pressure buildup (positive s_m) in the reservoir rather than a pressure drawdown when steady-state conditions are reached. Several adaptations of Equation B-1 have been presented in the literature, which make slightly different assumptions about the solution constraints and, therefore, have different applications. In addition, transient (time-series) solutions also exist for estimating buildup as a function of time since injection. However, the important aspects of these solutions is that pressure buildup in the reservoir in response to injection is predominantly a function of Q, the hydrogeologic properties of the reservoir (K and D) and aquitard (K′ and D′), and the radial distance from the well (r). The pressure buildup resulting from multiple storage projects can be superimposed in space and time by solving the equation for each project and then adding the results together (notwithstanding any small reduction in pressure buildup because of increased mobility within the CO_2 plumes, as noted by De Simone and others [2019]). Therefore, analytical solutions like Equation B-1 provide a rapid, screening-level approach for estimating the pressure interference effects from multiple storage projects using a relatively simple set of input parameters.

Equation B-1 and similar derivations make multiple simplifying assumptions, namely:

- The reservoir is semiconfined (meaning that pressure can dissipate from the storage unit through the overlying aquitard).
- The reservoir and the aquitard have a seemingly infinite areal extent.
- The reservoir and the aquitard are homogeneous, isotropic, and of uniform thickness.
- Prior to injection, the piezometric surface is horizontal over the area that will be influenced by the injection.
- The injection into the reservoir is done at a constant injection rate.
- The injection well penetrates the entire thickness of the reservoir and, thus, induces horizontal flow.
- The flow in the aquitard is vertical.
- The buildup in the overlying aquifer (or in the aquitard, if there is no overlying aquifer) is negligible.
- The system represents steady-state conditions, i.e., injection time is not accounted for.

In addition to these simplifying assumptions, Equation B-1 requires a volumetric injection rate assuming a single-phase fluid and does not account for the greater compressibility and, thus, changing density of the injected CO_2. However, there are extensive examples in the literature that show that multiphase processes inside the CO_2 plume may be assumed negligible for prediction of far-field pressure buildup, thus, analytical solutions provide sufficient accuracy for this type of investigation (Birkholzer and others, 2009; Cihan and others, 2011, 2012). Therefore, despite these simplifying assumptions, analytical solutions yield useful solutions to questions about pressure interference that provide generalized injection rate–distance relationships and a starting point for additional investigation.

Inputs

This section describes the inputs in the De Glee Calculator (Attachment B) in the tab "De Glee (1930) Solution."

Design Inputs

Volumetric Injection Rate (Q)

The volumetric injection rate (Q) (cubic meters per day, (m^3/d) is a function of the i) target CO_2 mass injection rate (e.g., 4 million metric tons [tonnes] per year) specified by the storage project injection schedule and ii) reservoir pressure (kilopascals, kPa) and temperature (degrees

Celsius, °C), which determine the CO_2 density (kilograms per cubic meter, kg/m^3). These calculations were described in Appendix A. The example calculations in the De Glee Calculator assume 4 million tonnes per year and a CO_2 density of 677 kg/m^3, resulting in a volumetric injection rate of Q = 16,186 m^3/day.

Radial Distance from the Injection Well (r)

The radial distance from the injection well (r) (meters, m) must be specified by the user. The example calculations in the De Glee Calculator (Attachment B) use 24,140 m (15 mi).

Aquitard (cap rock) Properties

The reference stratigraphy used in the pressure interference study was described in the main text and is repeated below as Figure B-1. In this context, the "aquitard (cap rock)" is a series of shales in the interval from the top of the Broom Creek Formation to the top of the Swift Formation (Aquitard 1). Equation B-1 requires two properties of the cap rock: thickness (D′) and hydraulic conductivity (K′).

Cap Rock Thickness (D')

The example calculations in the De Glee Calculator use 267 m (867 ft) for the cap rock thickness (D′).

Cap Rock Hydraulic Conductivity (K')

The hydraulic conductivity is a function of fluid density (kg/m^3), fluid viscosity (kg/m-s), and the reservoir permeability (m^2). While reservoir permeability is an intrinsic property of the rock matrix, the fluid density and fluid viscosity are a function of reservoir pressure (kPa), temperature (°C), and salinity (salt mass fraction). The derivation of hydraulic conductivity was described in Appendix A. The example calculations in the De Glee Calculator use 1.31E-04 m/d for the hydraulic conductivity of the cap rock (K′).

Storage Reservoir Properties

The "storage reservoir" is the Broom Creek Formation (Aquifer 1) [Figure B-1]. Equation B-1 requires two properties of the storage reservoir: thickness (D) and hydraulic conductivity (K).

Storage Reservoir Thickness

The example calculations in the De Glee Calculator use 71.3 m (234 ft) for the storage reservoir thickness (D).

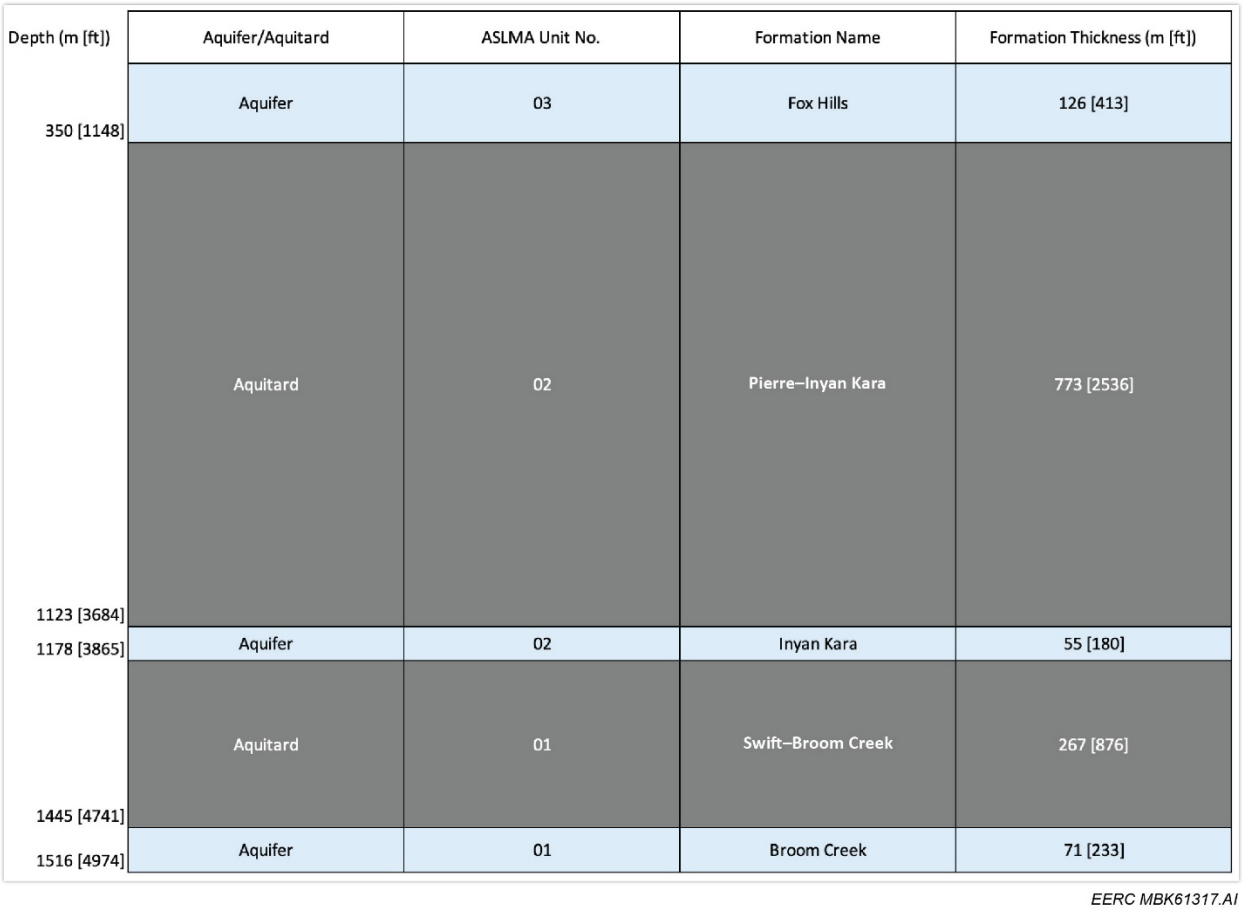

Figure B-1. Reference stratigraphy used for the pressure interference study.

Storage Reservoir Hydraulic Conductivity

The derivation of hydraulic conductivity was described in Appendix A. The example calculations in the De Glee Calculator use 3.50E-01 m/d for the hydraulic conductivity of the storage reservoir (K).

Buildup in the Storage Reservoir

The last set of steps in the De Glee Calculator is to estimate the buildup in the storage reservoir at the specified Q and r values from the design inputs, cap rock properties, and storage reservoir properties.

Hydraulic Resistance of the Aquitard (c)

The hydraulic resistance of the aquitard (c) is the ratio of K′/D′ from the aquitard properties, which results in 2.03E06 days.

Leakage Factor (L)

The leakage factor (L) is the square root of (K × D × c) from the storage reservoir properties and the hydraulic resistance of the aquitard, which results in 7.13E03 m.

Modified Bessel Function of the Second Kind and of Zero Order

The final term uses the built-in function "BESSELK," the inputs of the radial distance from the injection well (r) divided by the leakage factor (L) and specifies N=0 for the order of the function, which results in 0.0222.

Buildup in the Storage Reservoir

Combining the inputs described above and solving Equation B-1 provides the buildup in the storage reservoir in meters of hydraulic head, resulting in 2.3 m. Conversions are included in the De Glee Calculator to express buildup in kPa (23.0 kPa) and psi (3.3 psi).

The solution presented in the De Glee Calculator can be expanded to different Q and r settings. In addition, multiple storage projects can be added together using superposition to generate buildup in the storage reservoir for two or more concurrent storage projects.

References

Birkholzer, J.T., Zhou, Q., and Tsang, C.F., 2009, Large-scale impact of CO_2 storage in deep saline aquifers—a sensitivity study on the pressure response in stratified systems: International Journal of Greenhouse Control, v. 3, no. 2, p. 181–194.

Cihan, A., Zhou, Q., and Birkholzer, J.T., 2011, Analytical solutions for pressure perturbation and fluid leakage through aquitards and wells in multilayered aquifer systems: Water Resources Research, v. 47, no. 10. DOI:10.1029/2011WR010721.

Cihan, A., Birkholzer, J.T., and Zhou, Q., 2012, Pressure buildup and brine migration during CO_2 storage in multilayered aquifers: Ground Water, v. 51, no. 2, p. 252–267. DOI:10.1111/j.1745-6584.2012.00972.x.

De Glee, G.J. 1930. Over grondwaterstromingen bij wateronttrekking door middel van putten [Ph.D. thesis]: Delft, p. 175. https://repository.tudelft.nl/islandora/object/uuid:c3e13209-4626-41b9-9038-c223d61e35c4?collection=research (accessed November 2021).

De Simone, S., Jackson, S.J., and Krevor, S., 2019, The error in using superposition to estimate pressure during multisite subsurface CO_2 storage: Geophysical Research Letters, v. 46, p. 6525–6533. DOI: 10.1029/2019GL082738.

APPENDIX C

ASLMA MODEL RESULTS

ASLMA MODEL RESULTS

Figures show the pressure difference over time caused by injection at other sites (Sites B, C, D, or E), relative to the base case (Site A only) within the base case pressure buildup area defined by 1 psi (6.9 kPa). Each figure caption includes the injection rate (0.2, 1, 2, or 4 Mtpa CO_2), distance from Site A to other sites (10, 15, 20, or 25 mi), and time between the start of Site A injection and start of other injection sites (0, 2, or 5 years).

SITE A (BASE CASE)

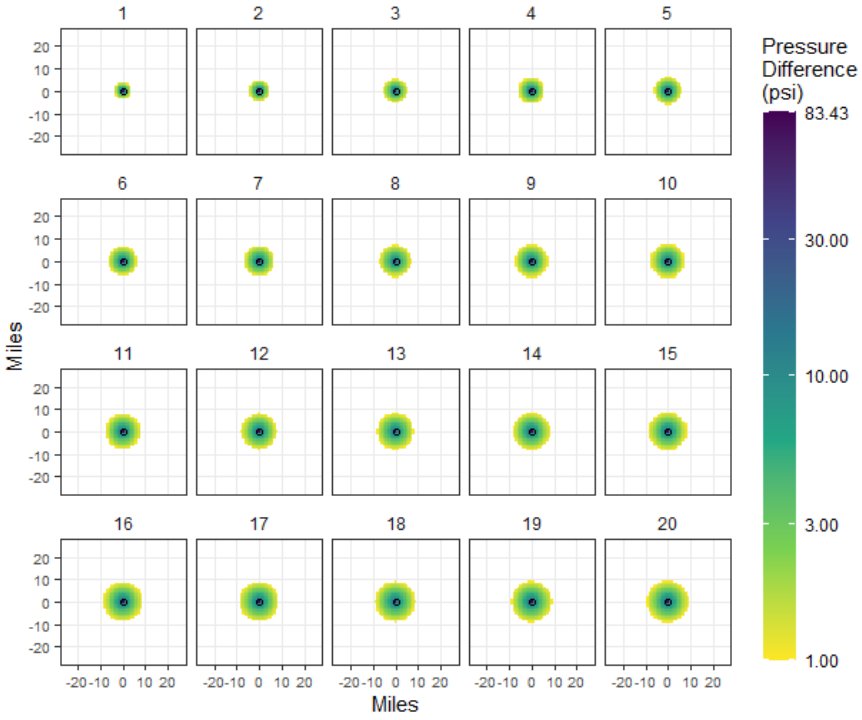

Figure C-1. 0.2 million tonnes per annum (Mtpa).

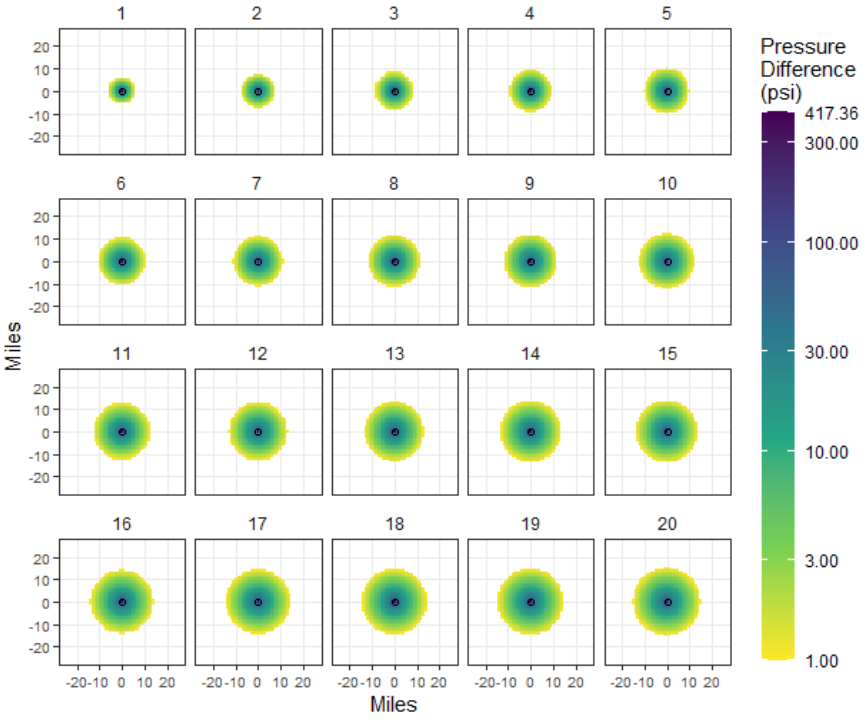

Figure C-2. 1 Mtpa.

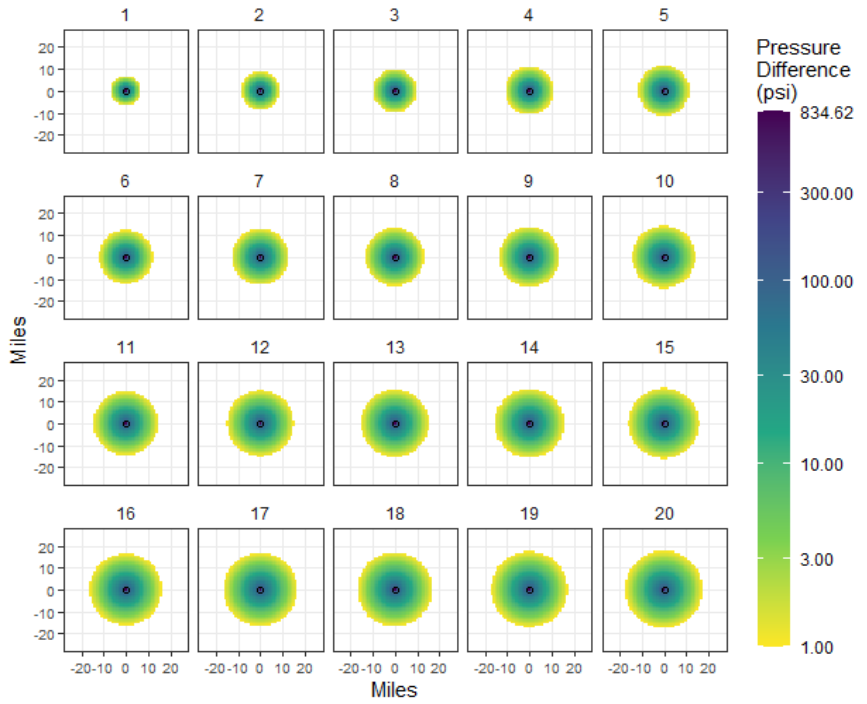

Figure C-3. 2 Mtpa.

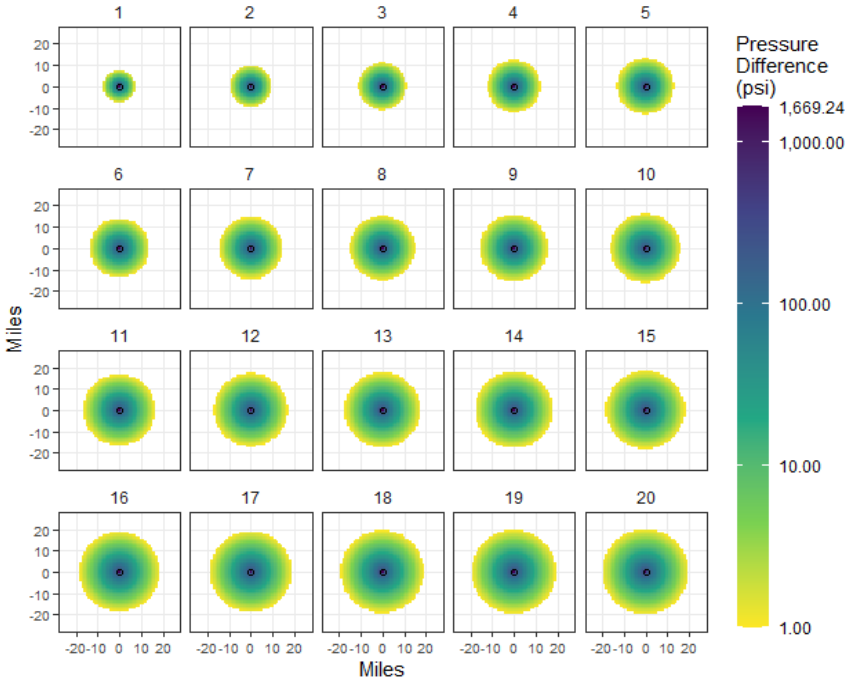

Figure C-4. 4 Mtpa.

SITES A AND B

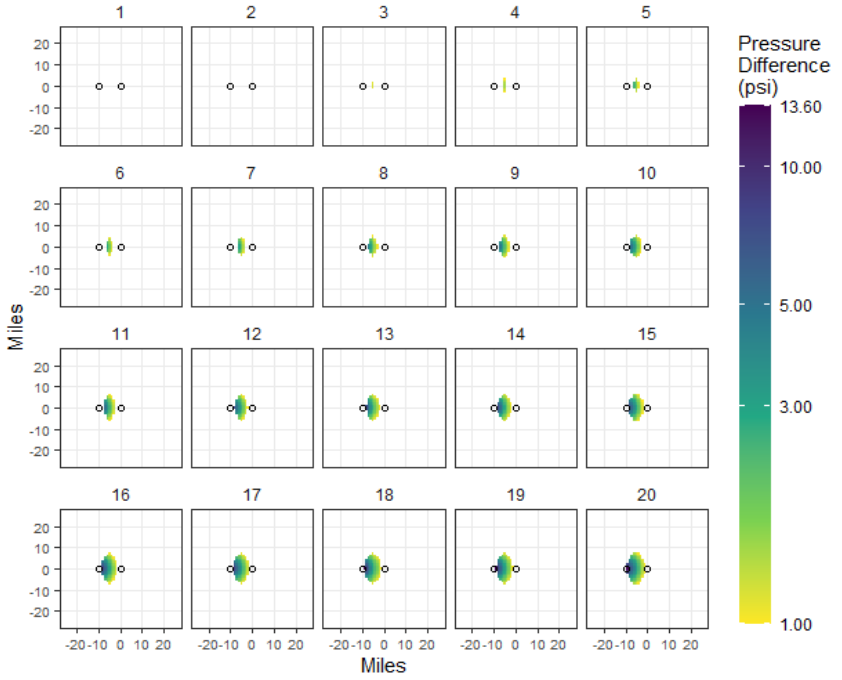

Figure C-5. Zero-year delay, 0.2-Mtpa injection, 10-mi spacing.

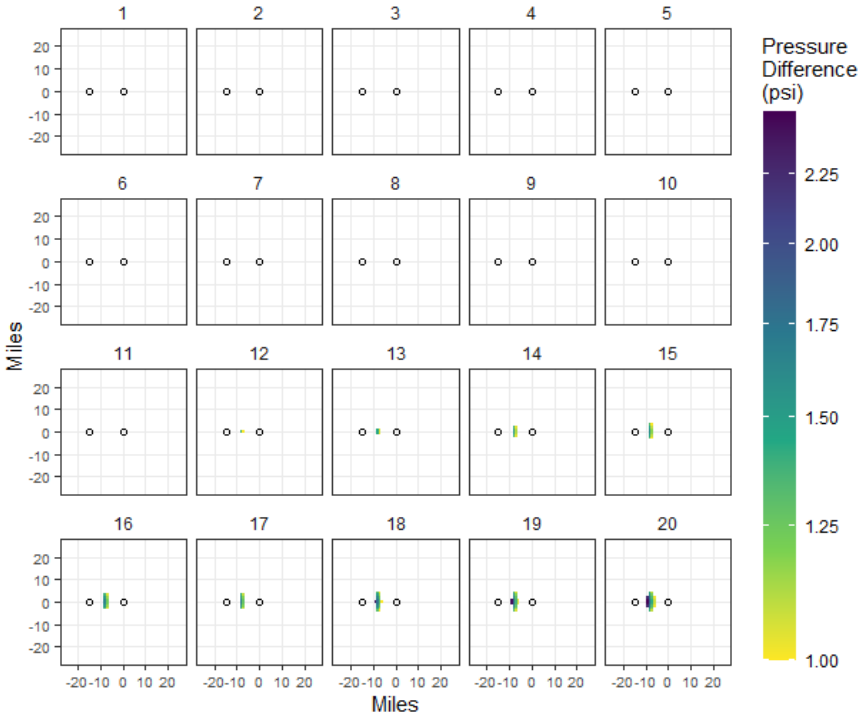

Figure C-6. Zero-year, 0.2-Mtpa injection, 15-mi spacing.

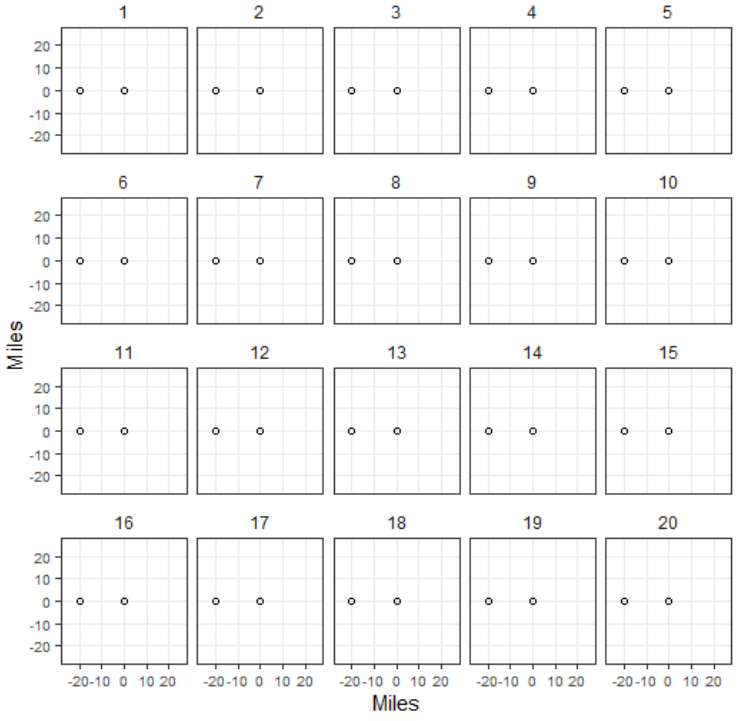

Figure C-7. Zero-year delay, 0.2-Mtpa injection, 20-mi spacing. All values less than 1 psi.

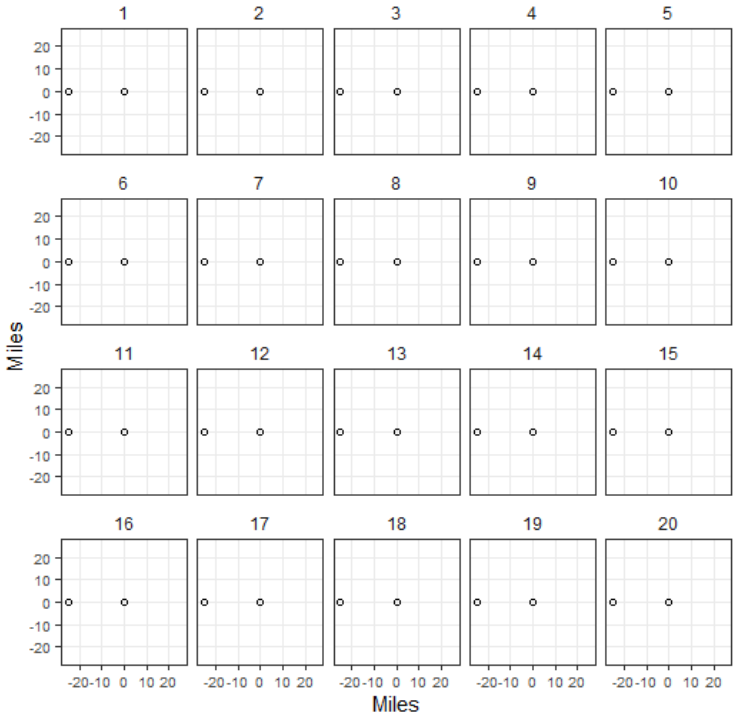

Figure C-8. Zero-year delay, 0.2-Mtpa injection, 25-mi spacing. All values less than 1 psi.

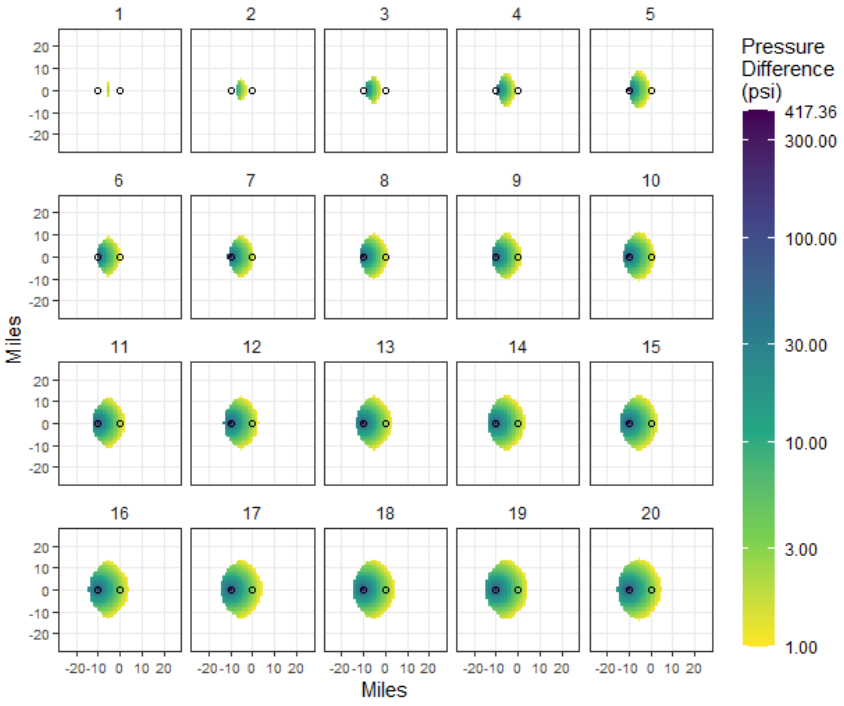

Figure C-9. Zero-year delay, 1-Mtpa injection, 10-mi spacing.

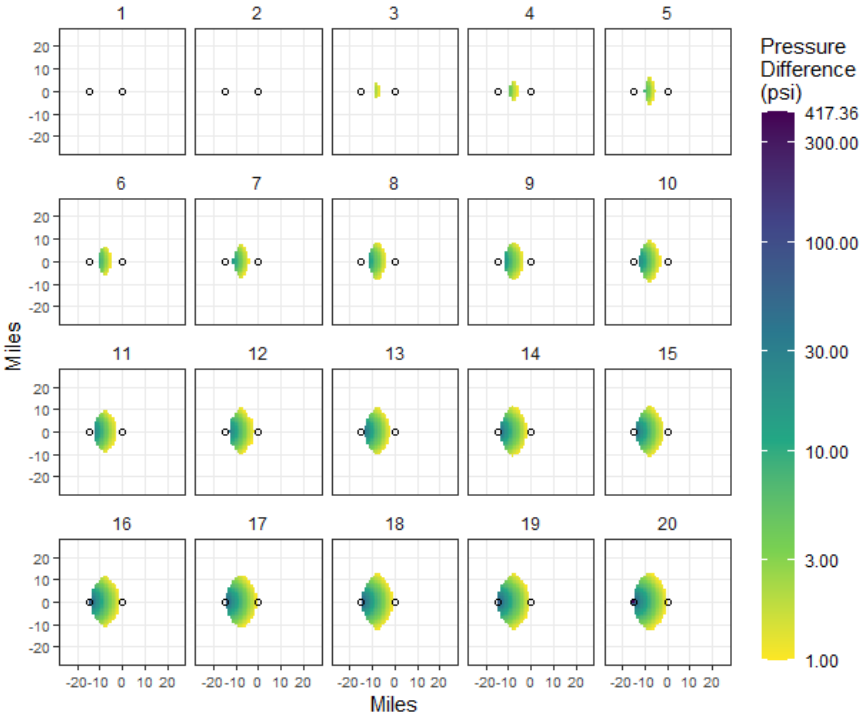

Figure C-10. Zero-year delay, 1-Mtpa injection, 15-mi spacing.

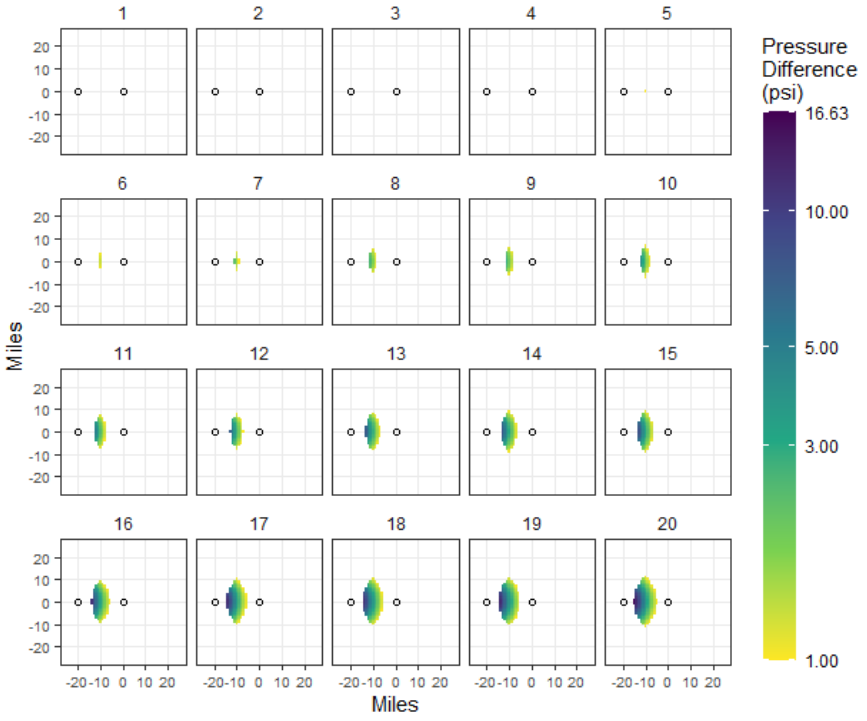

Figure C-11. Zero-year delay, 1-Mtpa injection, 20-mi spacing.

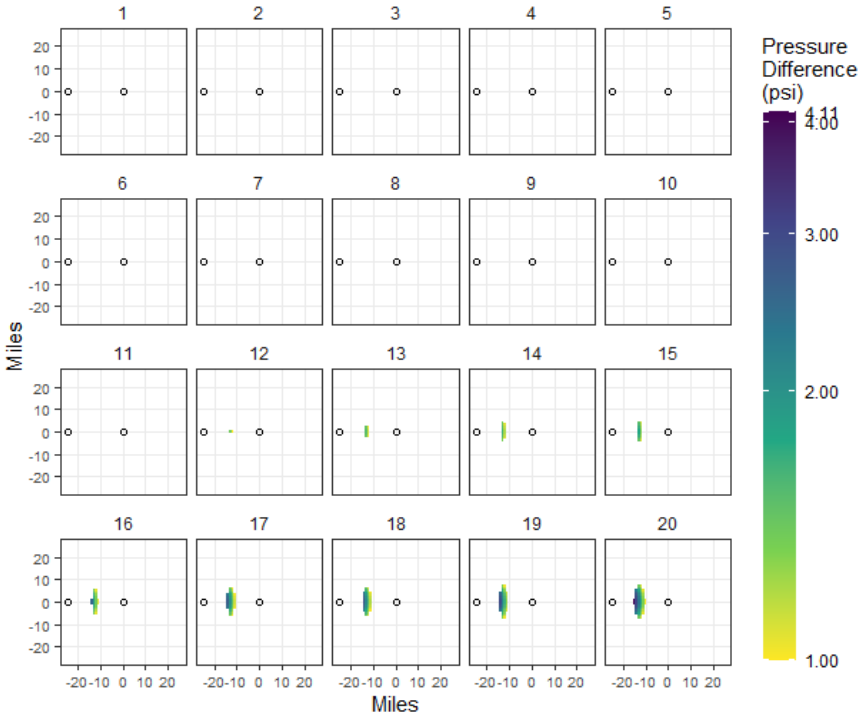

Figure C-12. Zero-year delay, 1-Mtpa injection, 25-mi spacing.

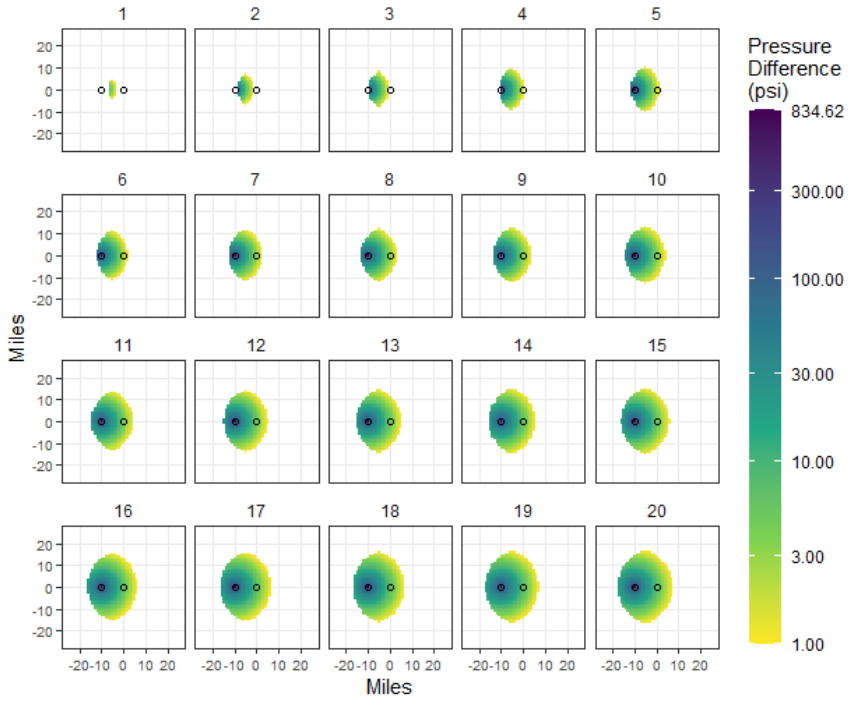

Figure C-13. Zero-year delay, 2-Mtpa injection, 10-mi spacing.

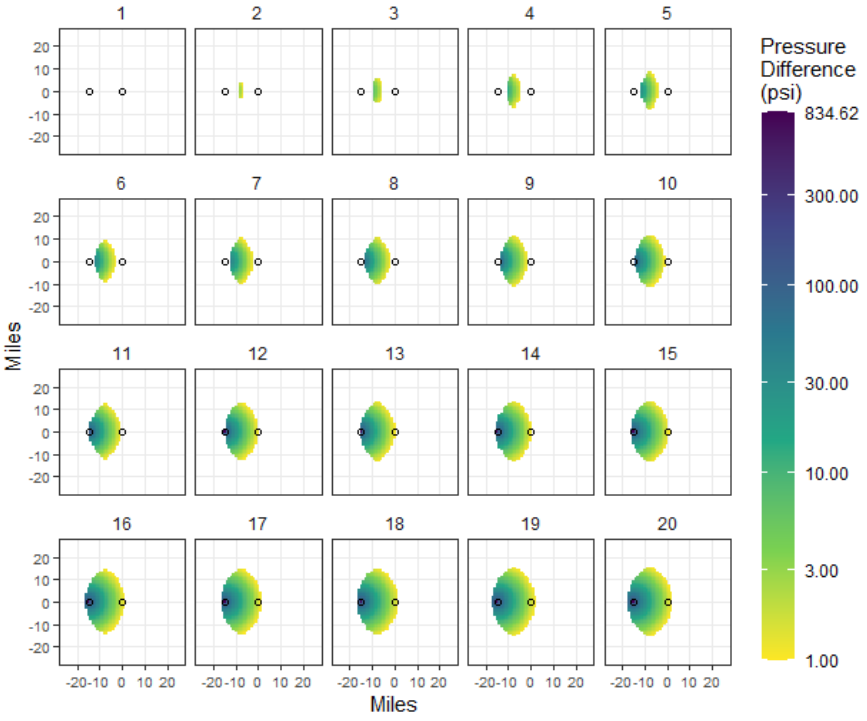

Figure C-14. Zero-year delay, 2-Mtpa injection, 15-mi spacing.

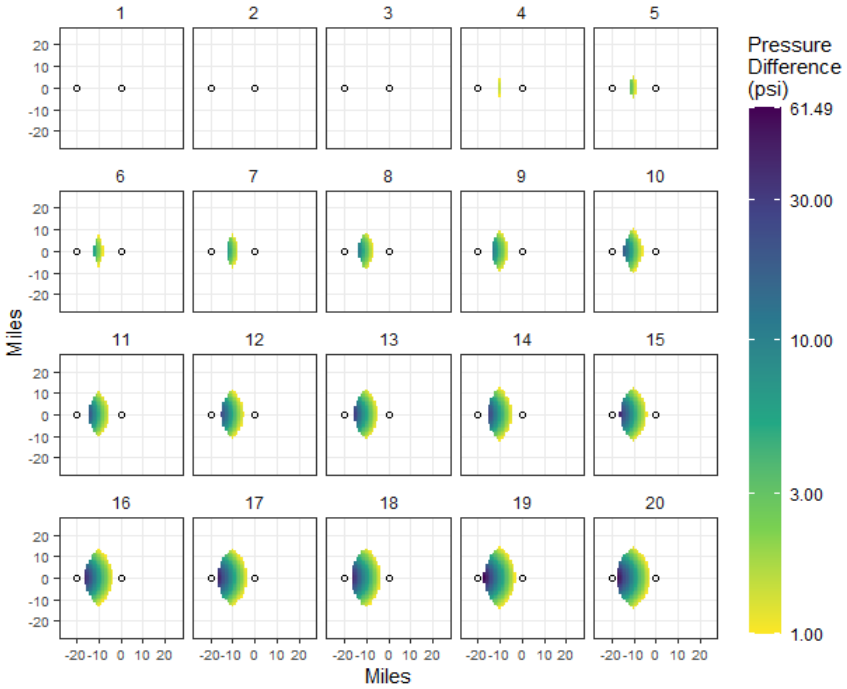

Figure C-15. Zero-year delay, 2-Mtpa injection, 20-mi spacing.

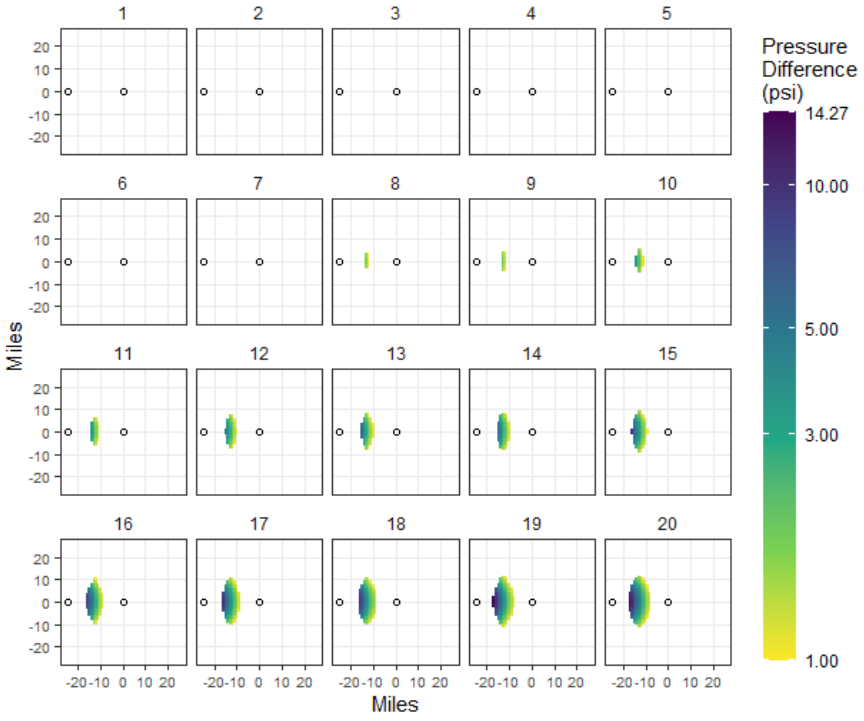

Figure C-16. Zero-year delay, 2-Mtpa injection, 25-mi spacing.

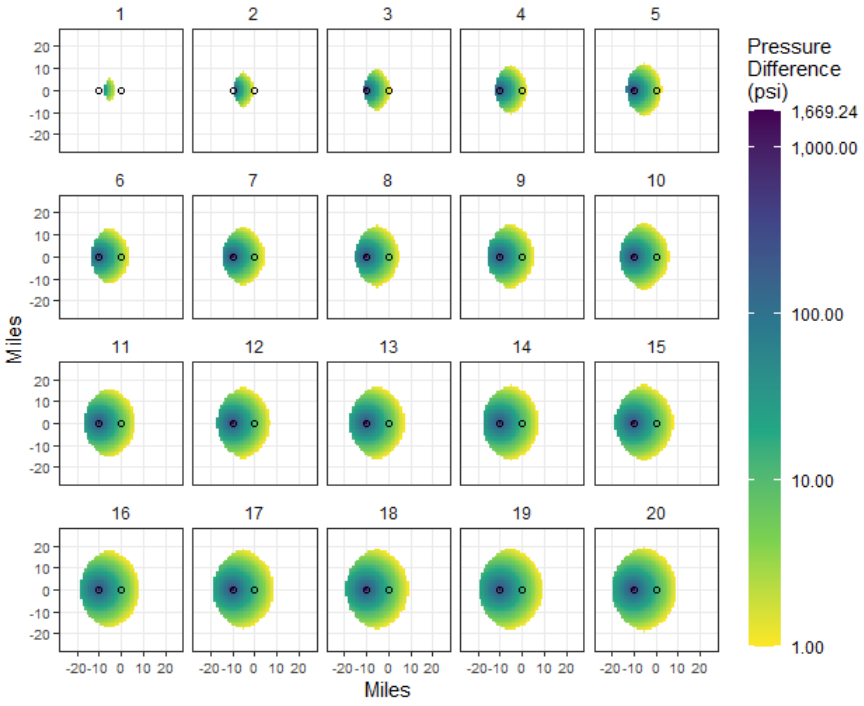

Figure C-17. Zero-year delay, 4-Mtpa injection, 10-mi spacing.

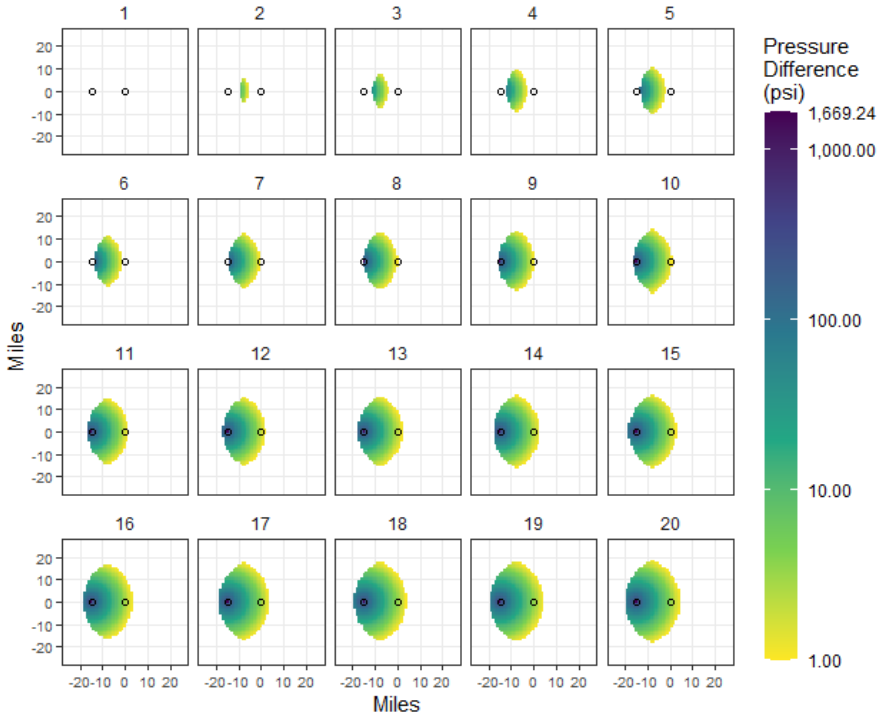

Figure C-18. Zero-year delay, 4-Mtpa injection, 15-mi spacing.

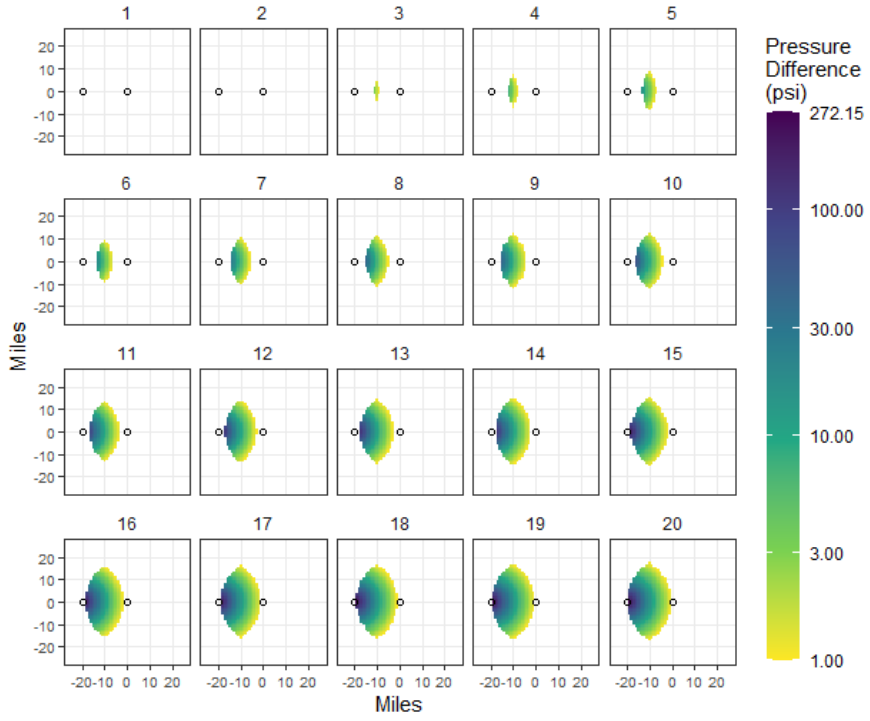

Figure C-19. Zero-year delay, 4-Mtpa injection, 20-mi spacing.

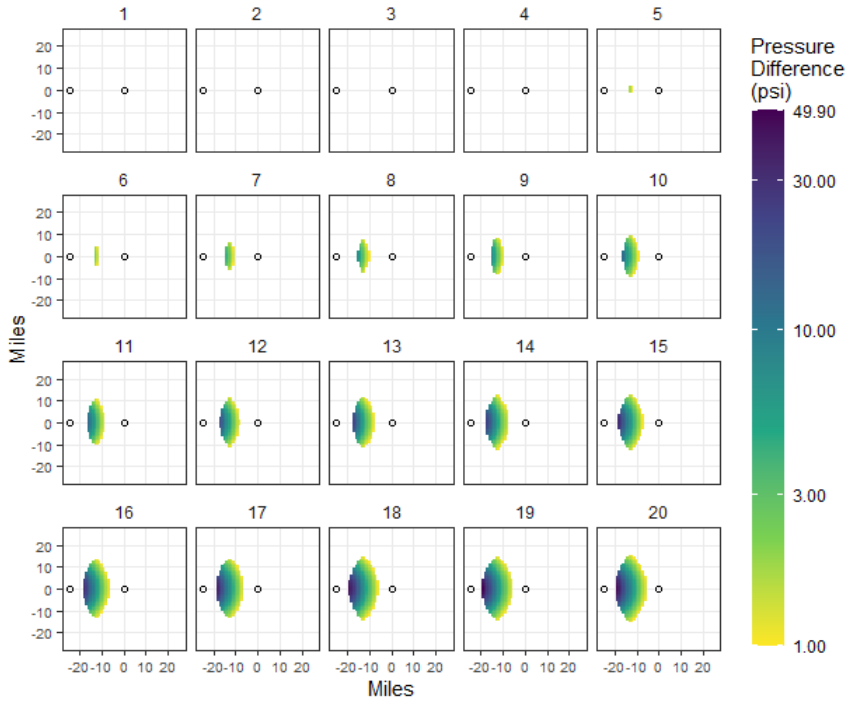

Figure C-20. Zero-year delay, 4-Mtpa injection, 25-mi spacing.

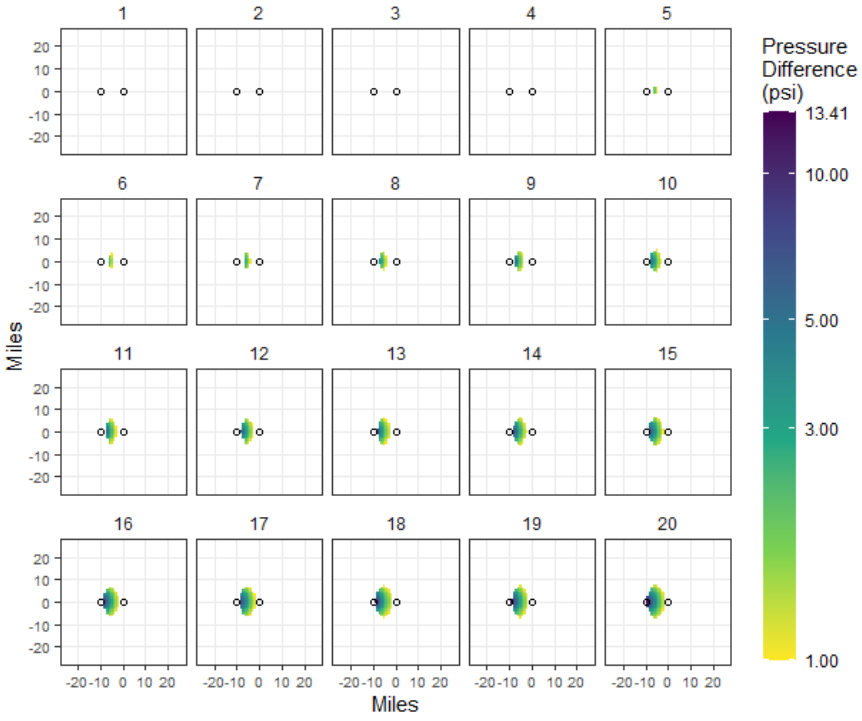

Figure C-21. Two-year delay, 0.2-Mtpa injection, 10-mi spacing.

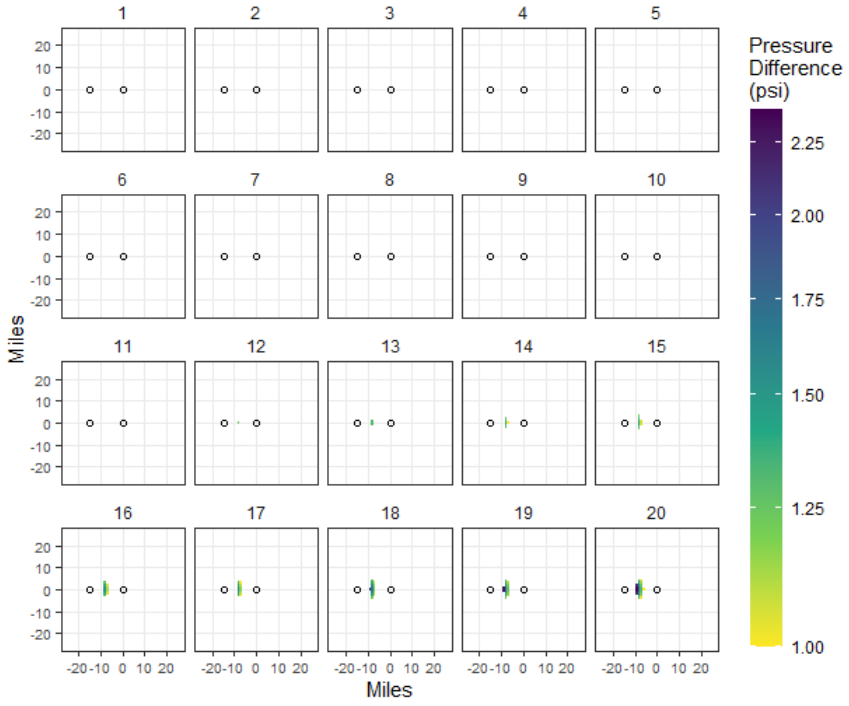

Figure C-22. Two-year delay, 0.2-Mtpa injection, 15-mi spacing.

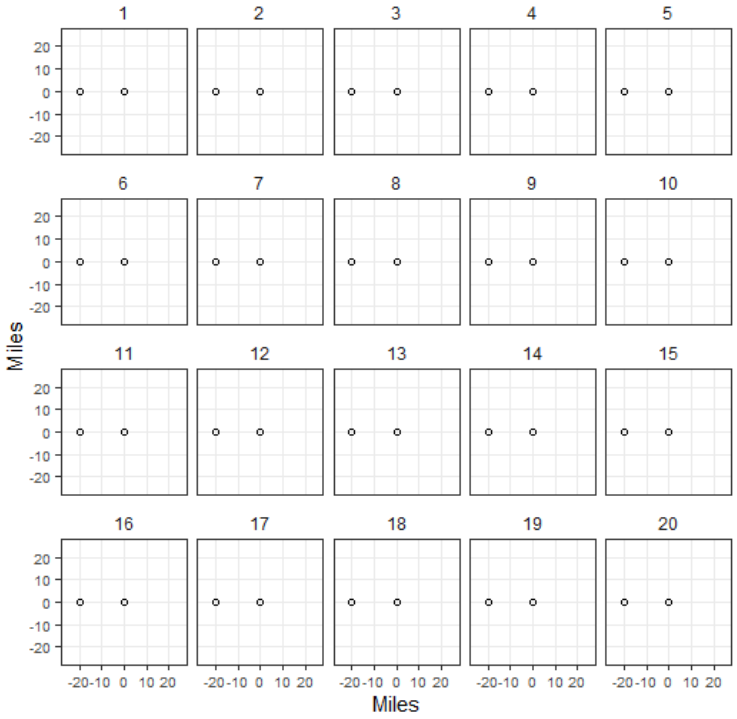

Figure C-23. Two-year delay, 0.2-Mtpa injection, 20-mi spacing. All values less than 1 psi.

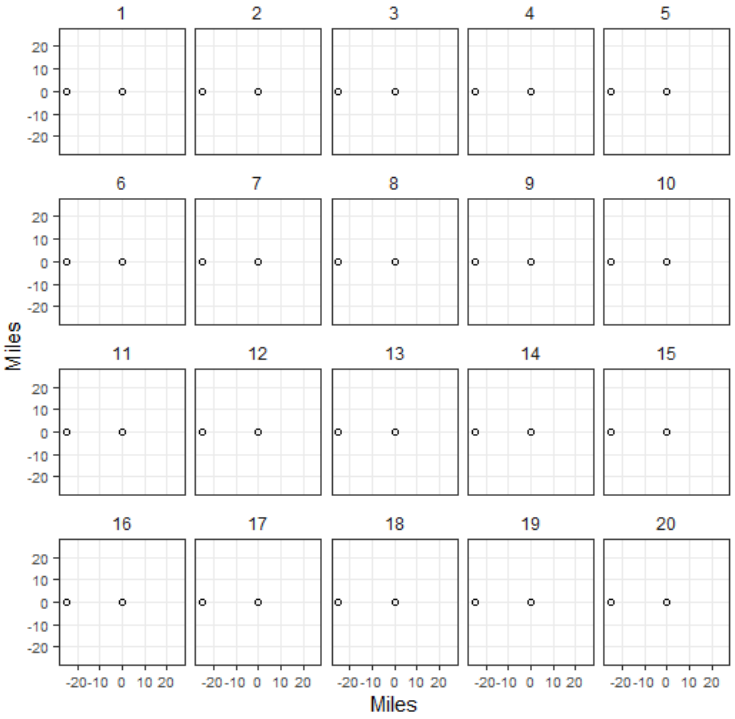

Figure C-24. Two-year delay, 0.2-Mtpa injection, 25-mi spacing. All values less than 1 psi.

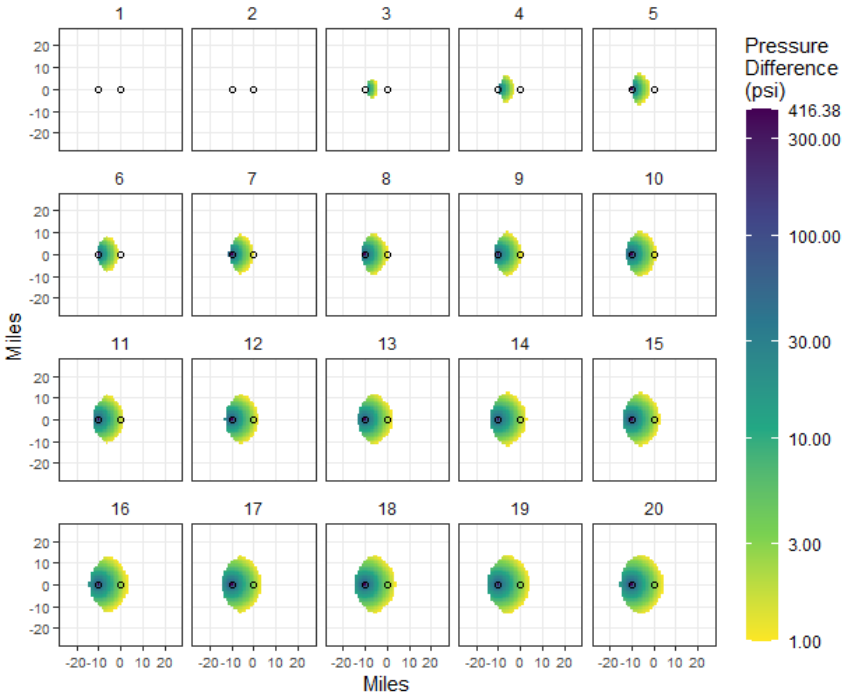

Figure C-25. Two-year delay, 1-Mtpa injection, 10-mi spacing.

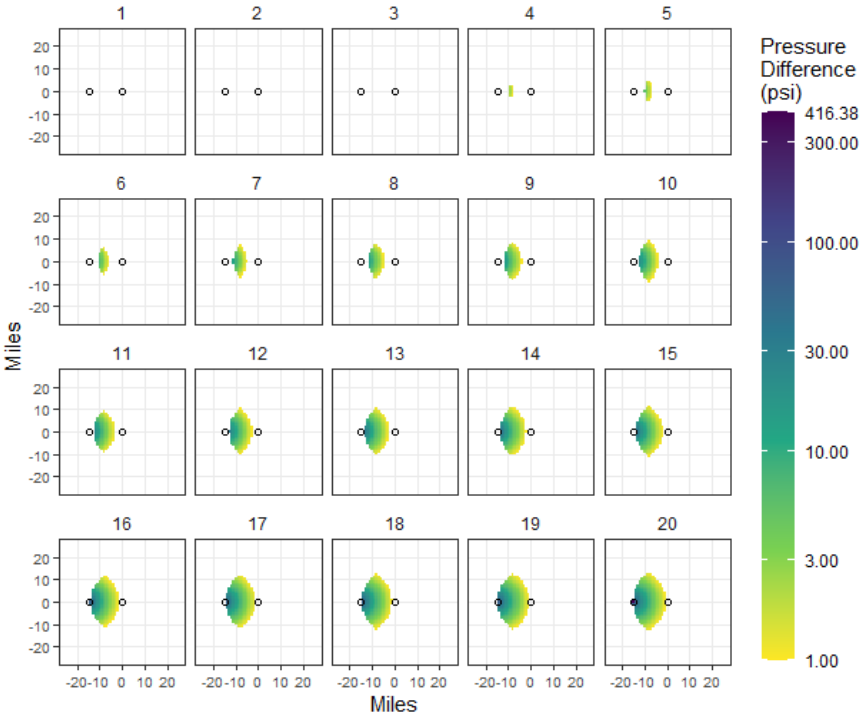

Figure C-26. Two-year delay, 1-Mtpa injection, 15-mi spacing.

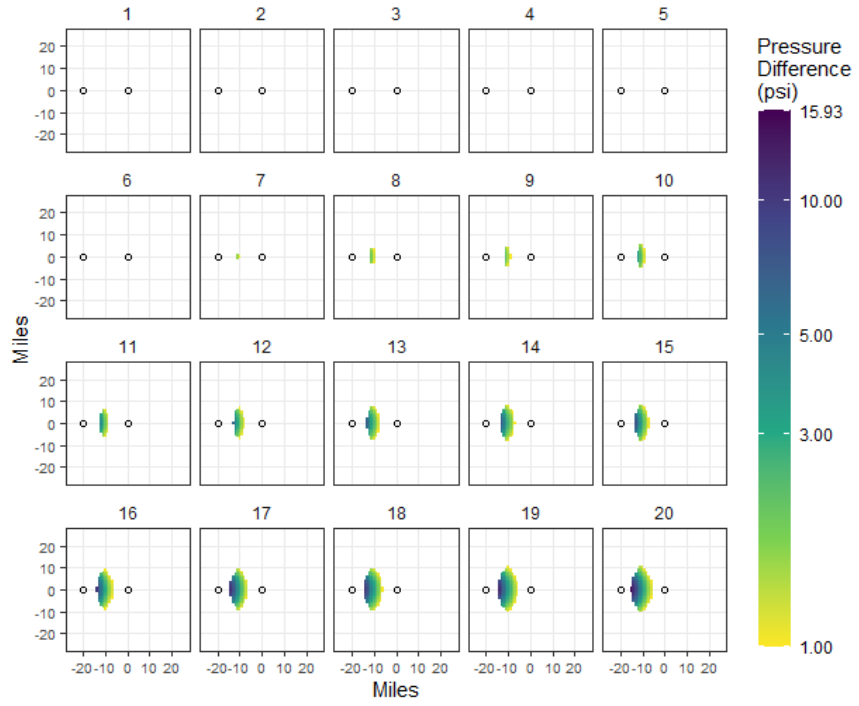

Figure C-27. Two-year delay, 1-Mtpa injection, 20-mi spacing.

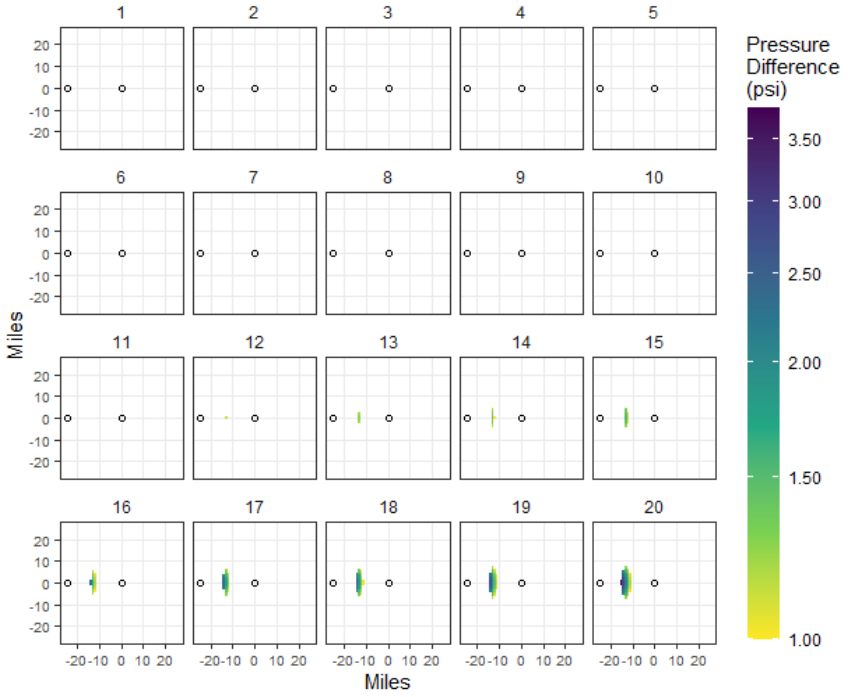

Figure C-28. Two-year delay, 1-Mtpa injection, 25-mi spacing.

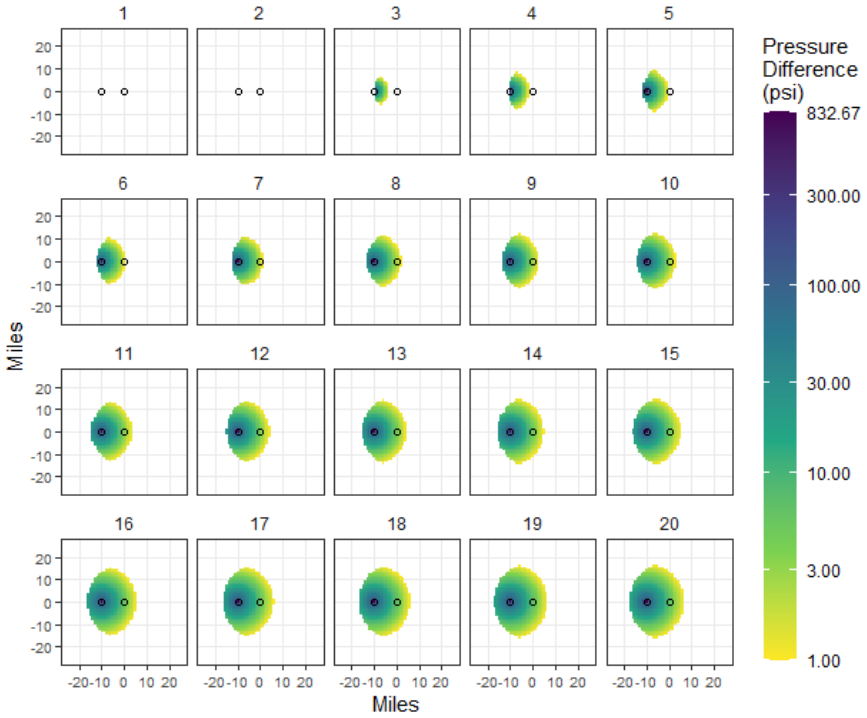

Figure C-29. Two-year delay, 2-Mtpa injection, 10-mi spacing.

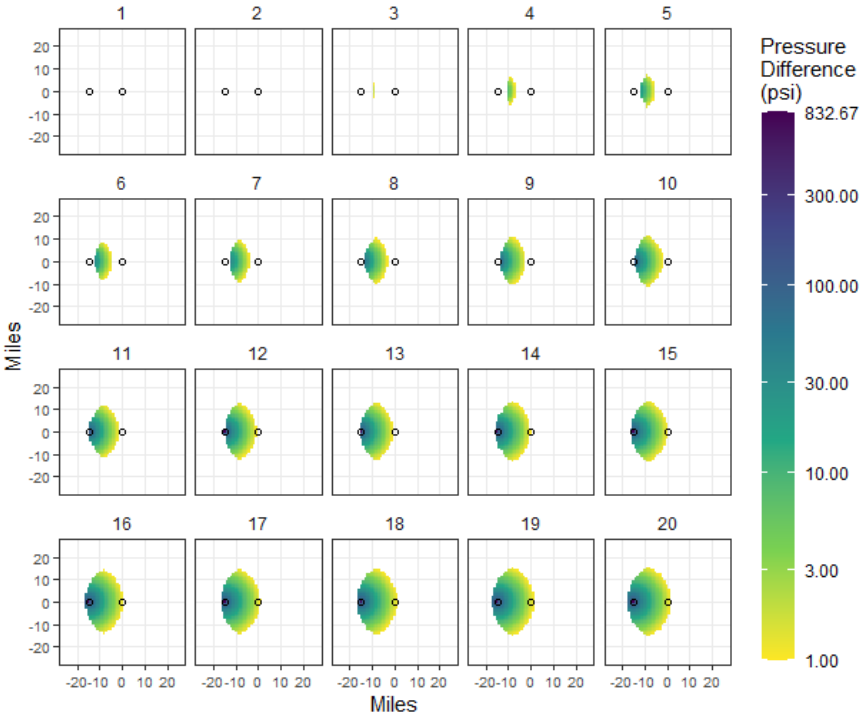

Figure C-30. Two-year delay, 2-Mtpa injection, 15-mi spacing.

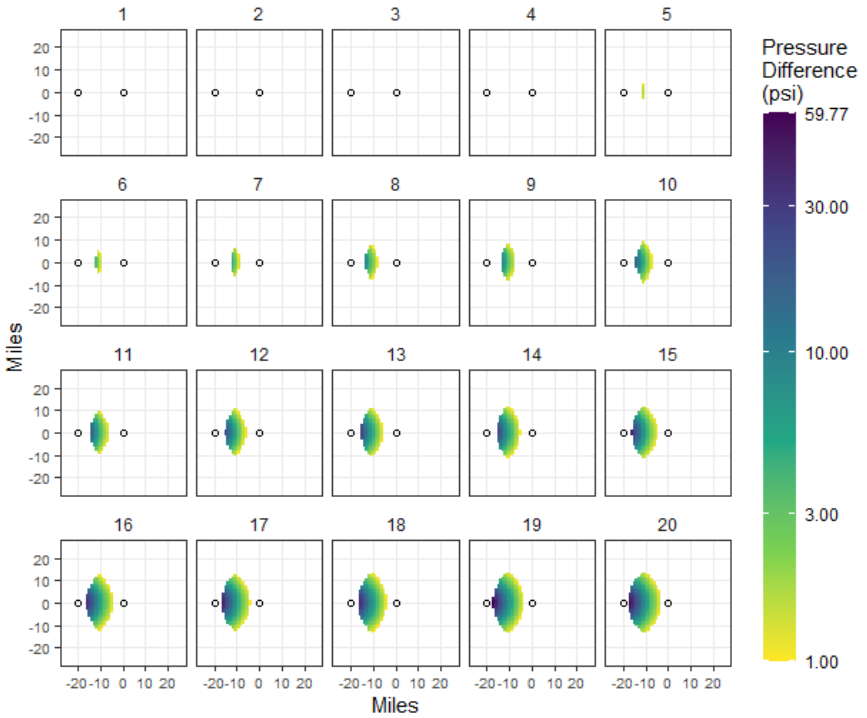

Figure C-31. Two-year delay, 2-Mtpa injection, 20-mi spacing.

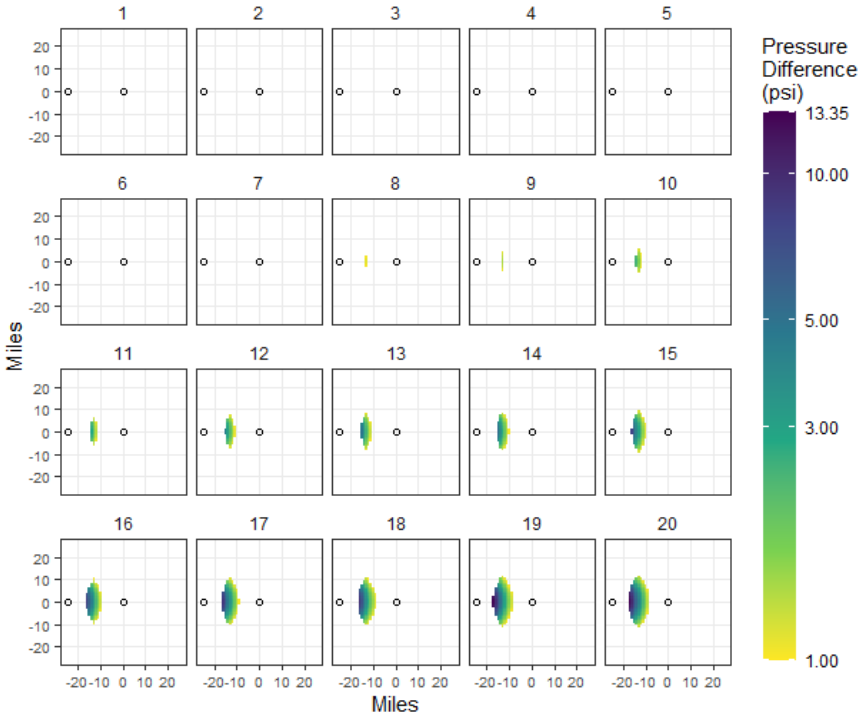

Figure C-32. Two-year delay, 2-Mtpa injection, 25-mi spacing.

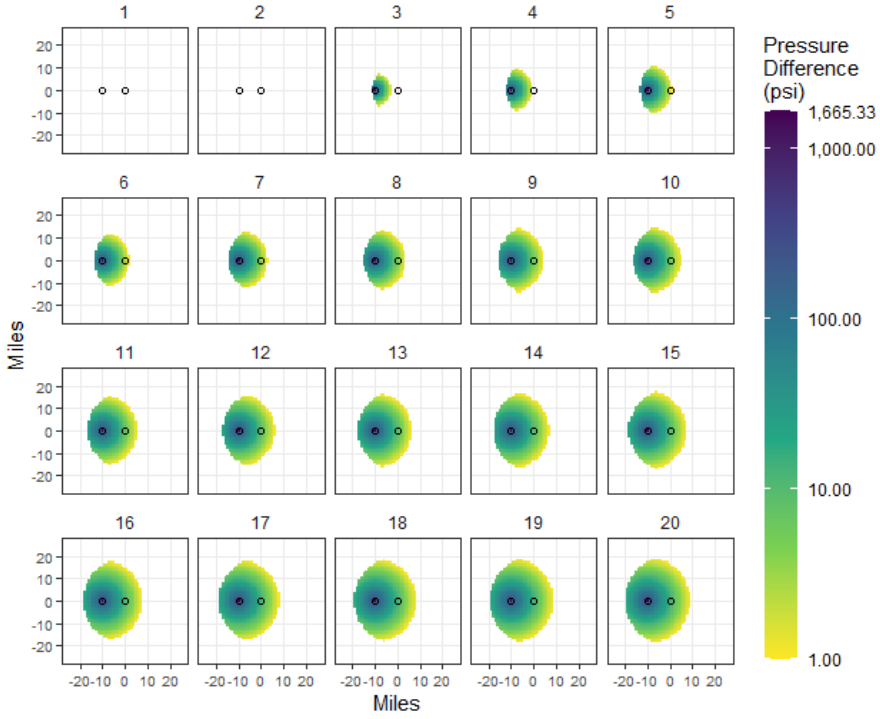

Figure C-33. Two-year delay, 4-Mtpa injection, 10-mi spacing.

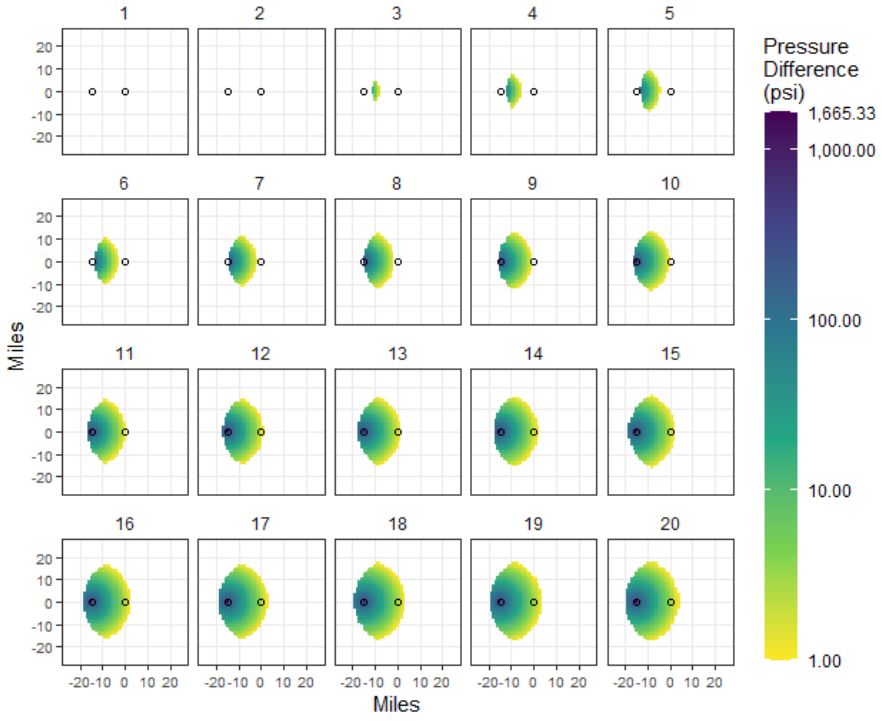

Figure C-34. Two-year delay, 4-Mtpa injection, 15-mi spacing.

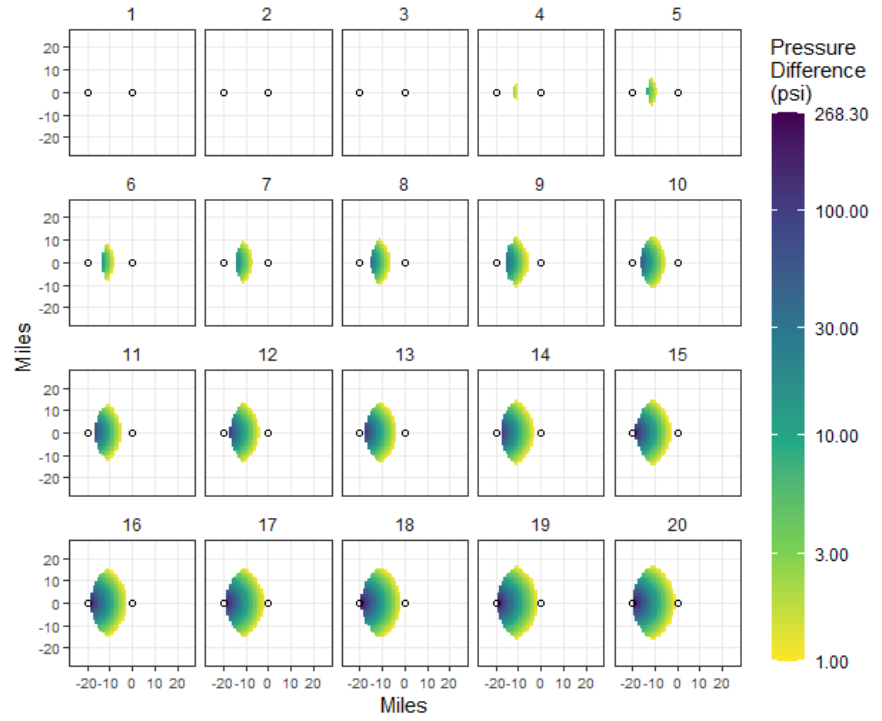

Figure C-35. Two-year delay, 4-Mtpa injection, 20-mi spacing.

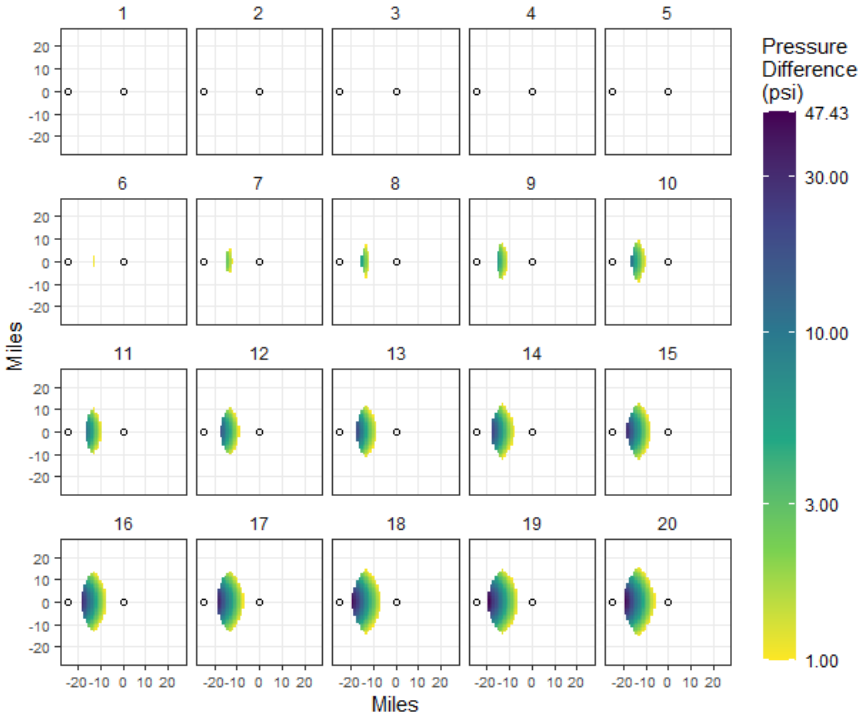

Figure C-36. Two-year delay, 4-Mtpa injection, 25-mi spacing.

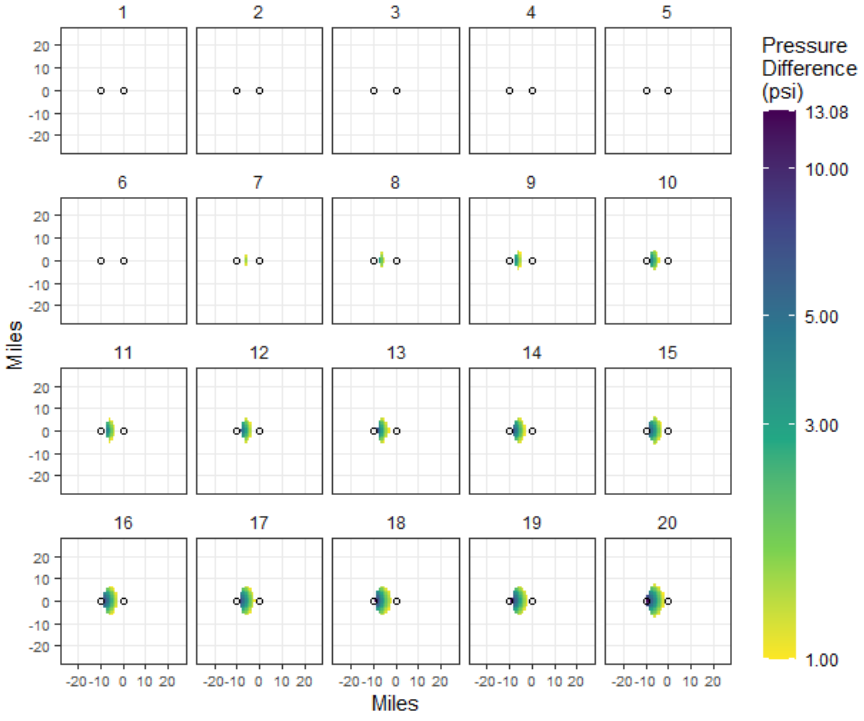

Figure C-37. Five-year delay, 0.2-Mtpa injection, 10-mi spacing.

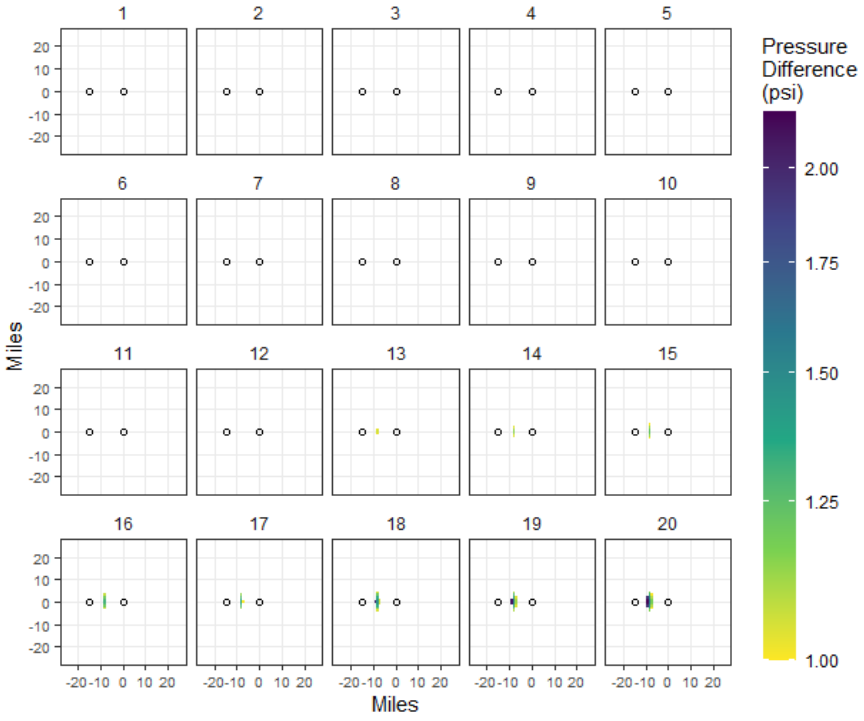

Figure C-38. Five-year delay, 0.2-Mtpa injection, 15-mi spacing.

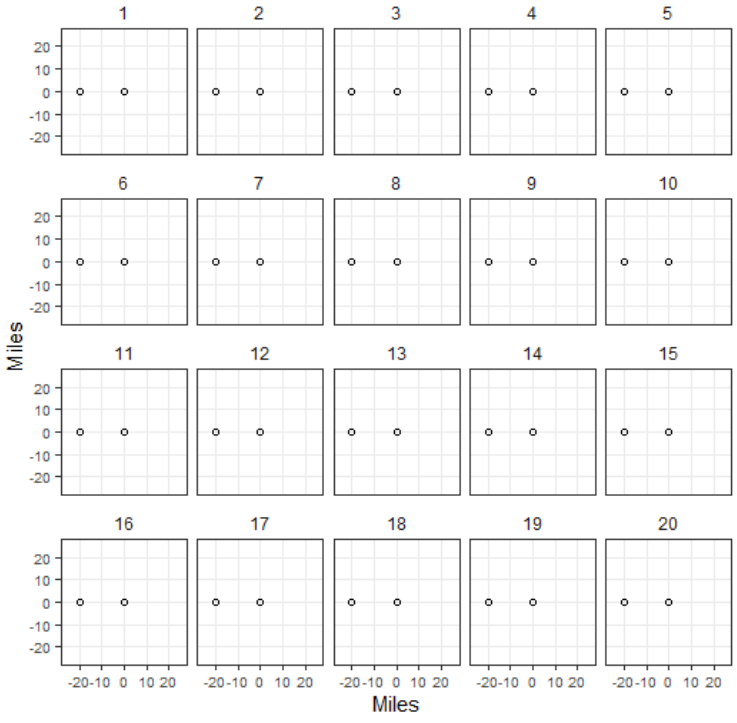

Figure C-39. Five-year delay, 0.2-Mtpa injection, 20-mi spacing. All values less than 1 psi.

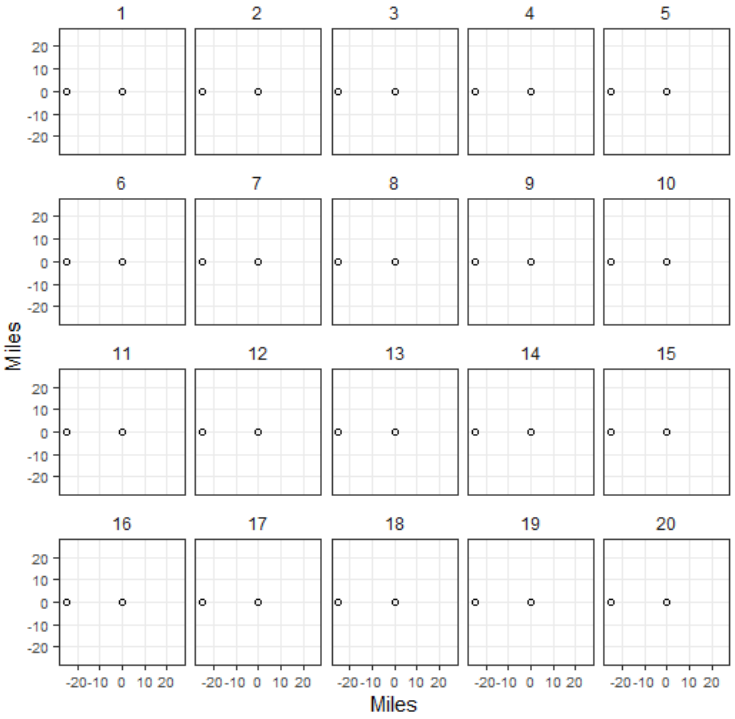

Figure C-40. Five-year delay, 0.2-Mtpa injection, 25-mi spacing. All values less than 1 psi.

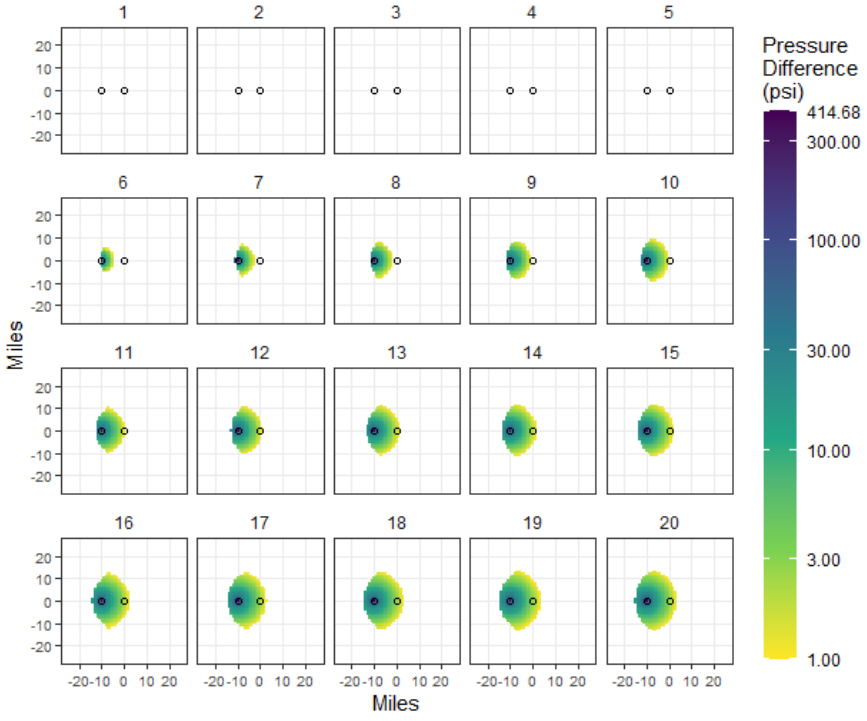

Figure C-41. Five-year delay, 1-Mtpa injection, 10-mi spacing.

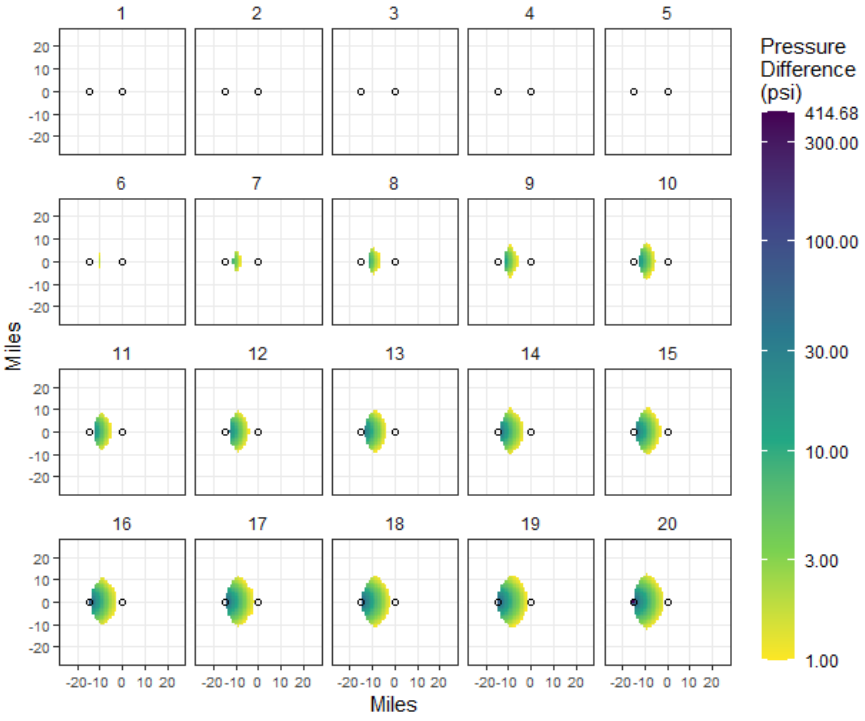

Figure C-42. Five-year delay, 1-Mtpa injection, 15-mi spacing.

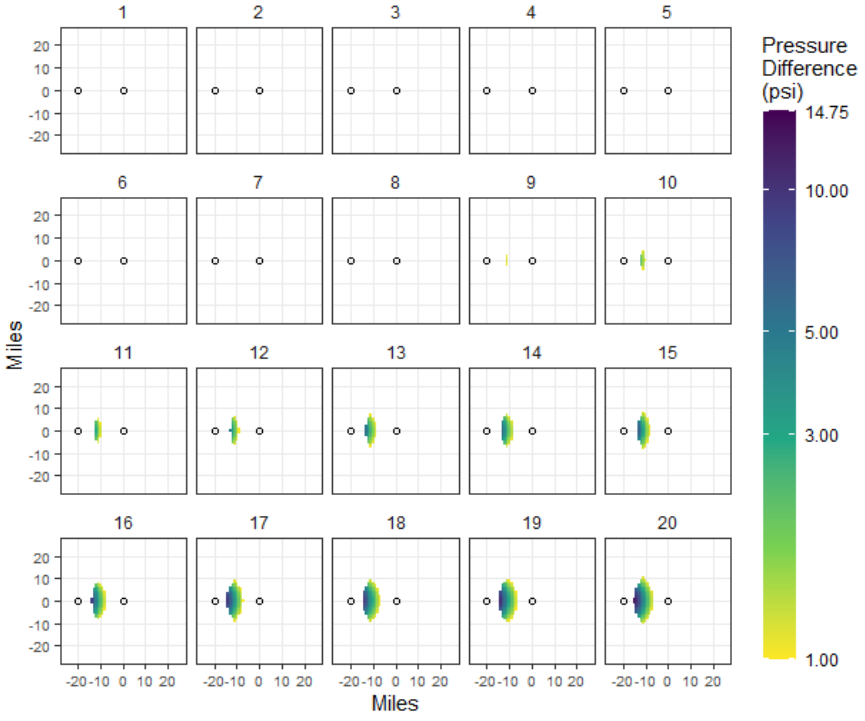

Figure C-43. Five-year delay, 1-Mtpa injection, 20-mi spacing.

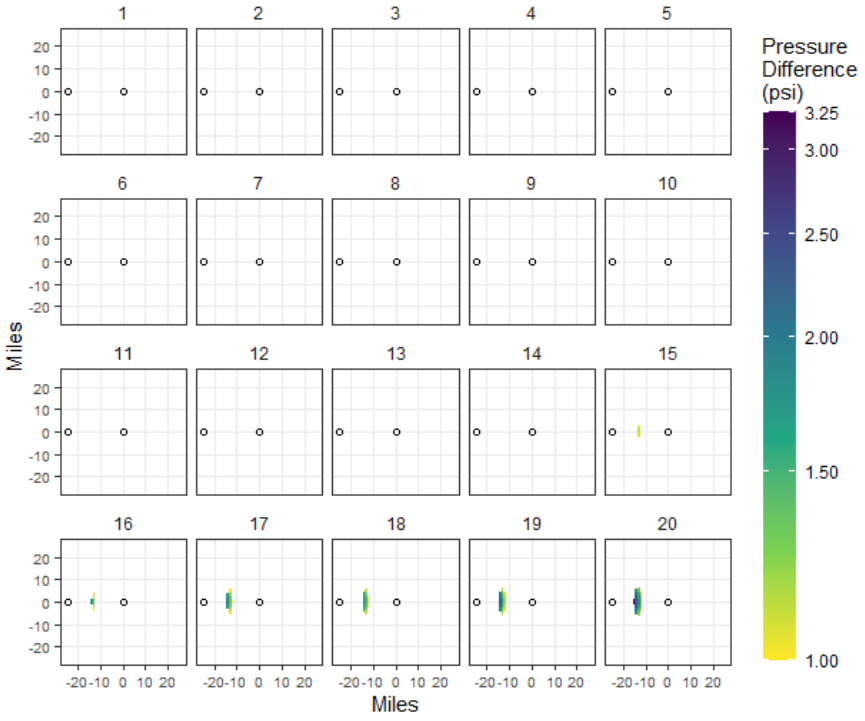

Figure C-44. Five-year delay, 1-Mtpa injection, 25-mi spacing.

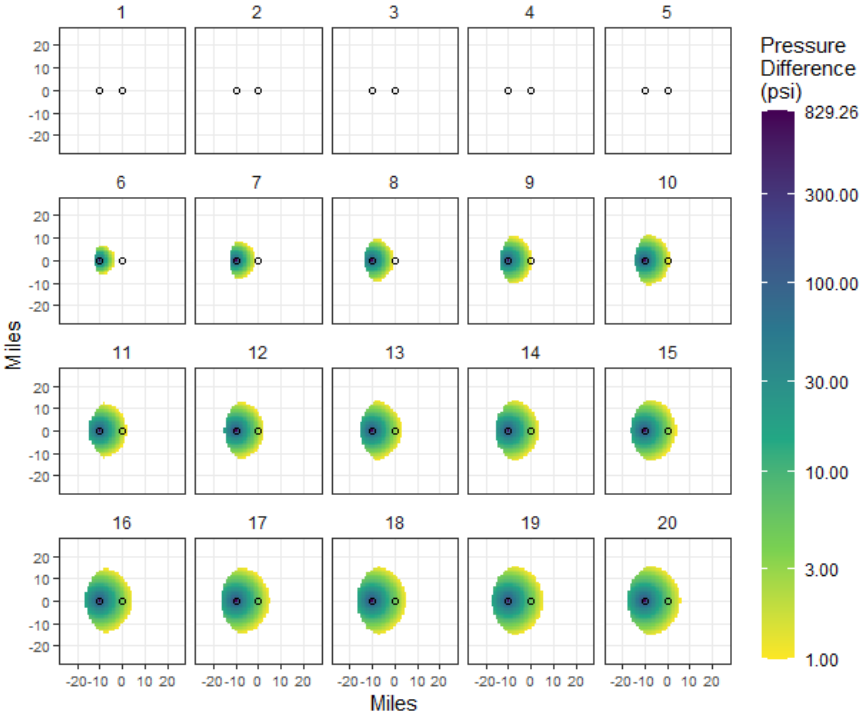

Figure C-45. Five-year delay, 2-Mtpa injection, 10-mi spacing.

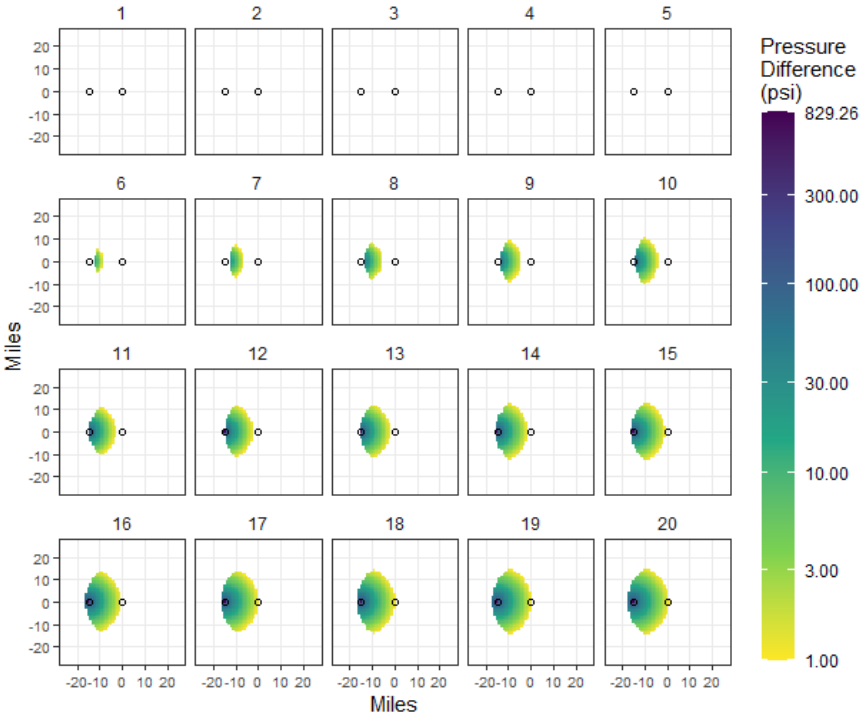

Figure C-46. Five-year delay, 2-Mtpa injection, 15-mi spacing.

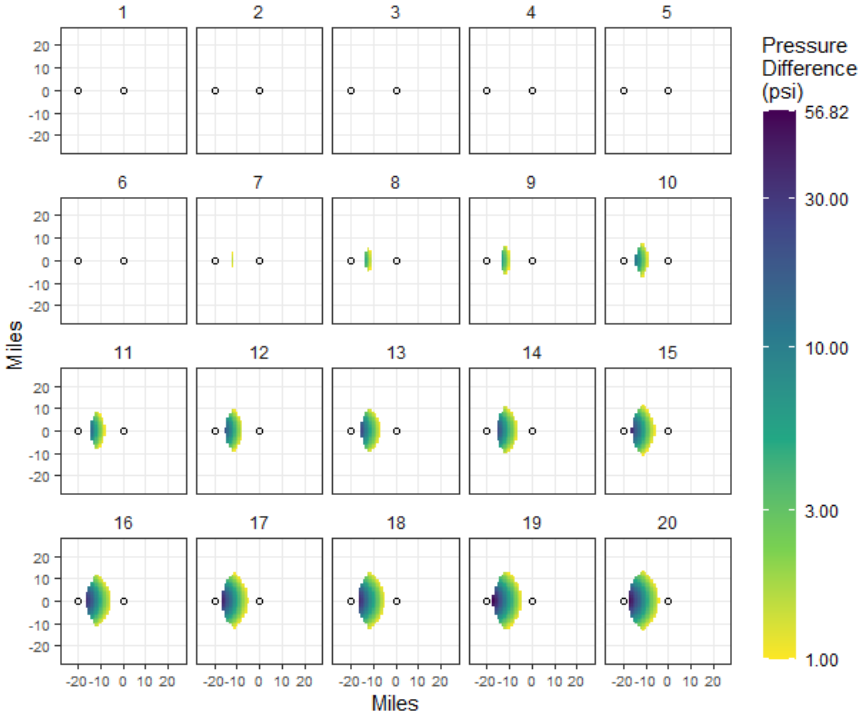

Figure C-47. Five-year delay, 2-Mtpa injection, 20-mi spacing.

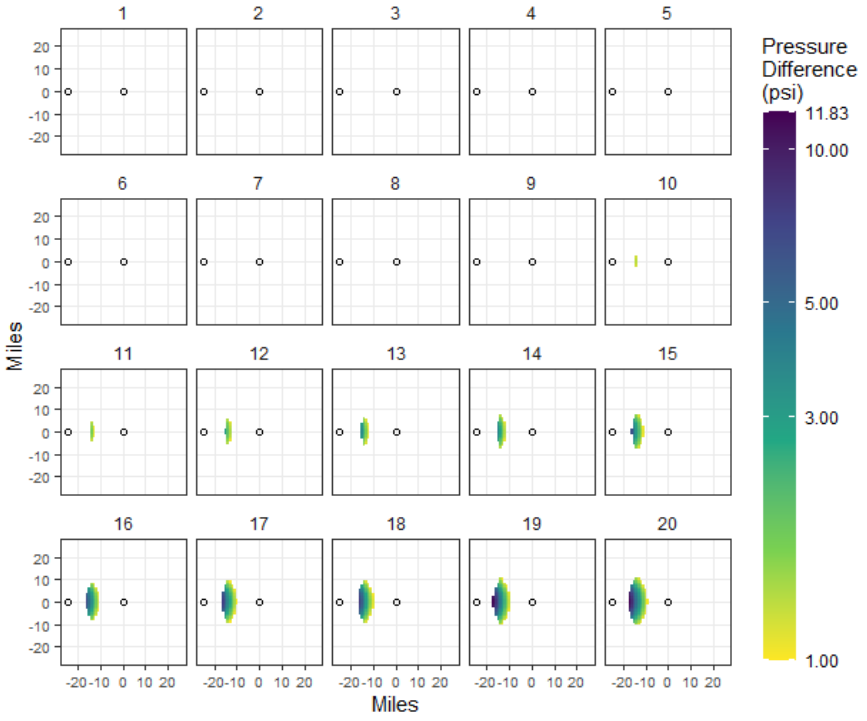

Figure C-48. Five-year delay, 2-Mtpa injection, 25-mi spacing.

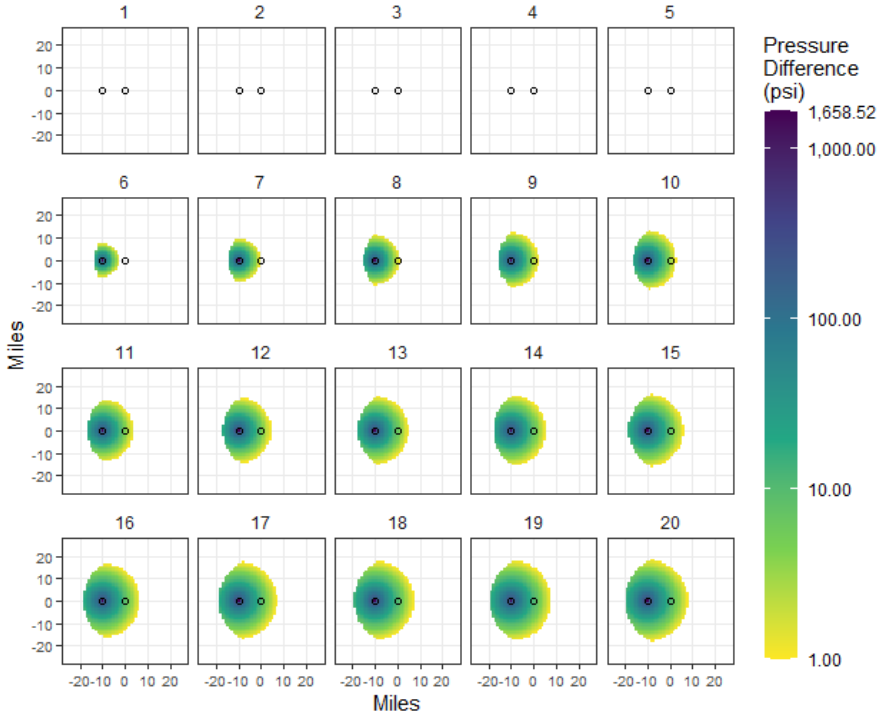

Figure C-49. Five-year delay, 4-Mtpa injection, 10-mi spacing.

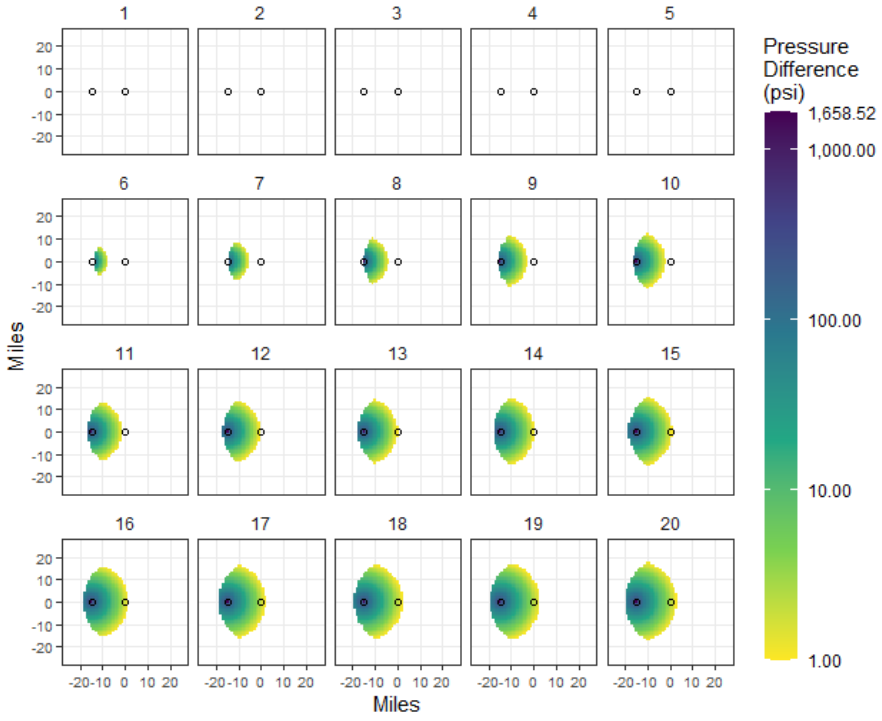

Figure C-50. Five-year delay, 4-Mtpa injection, 15-mi spacing.

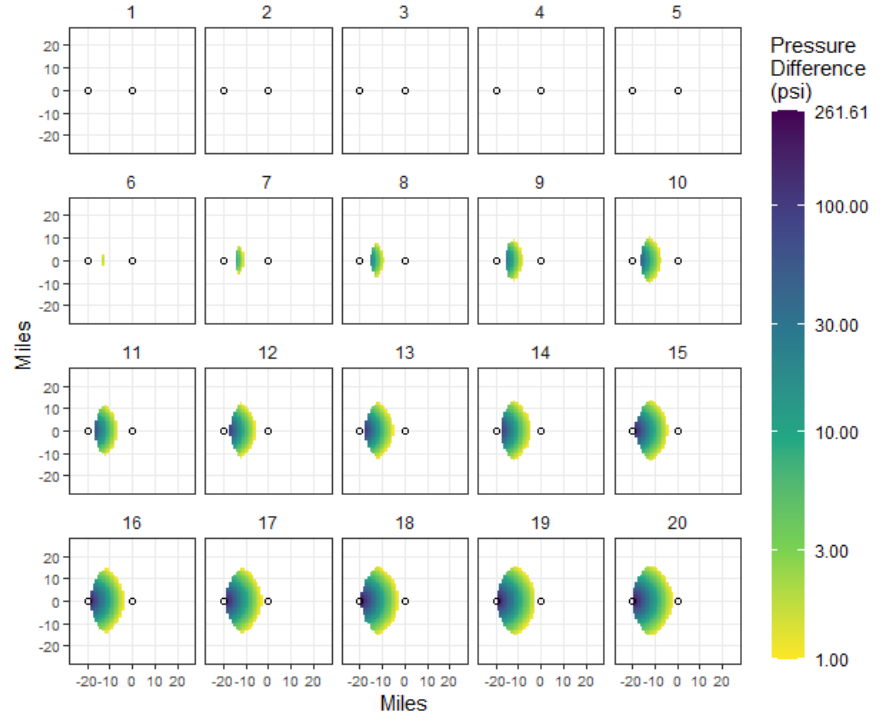

Figure C-51. Five-year delay, 4-Mtpa injection, 20-mi spacing.

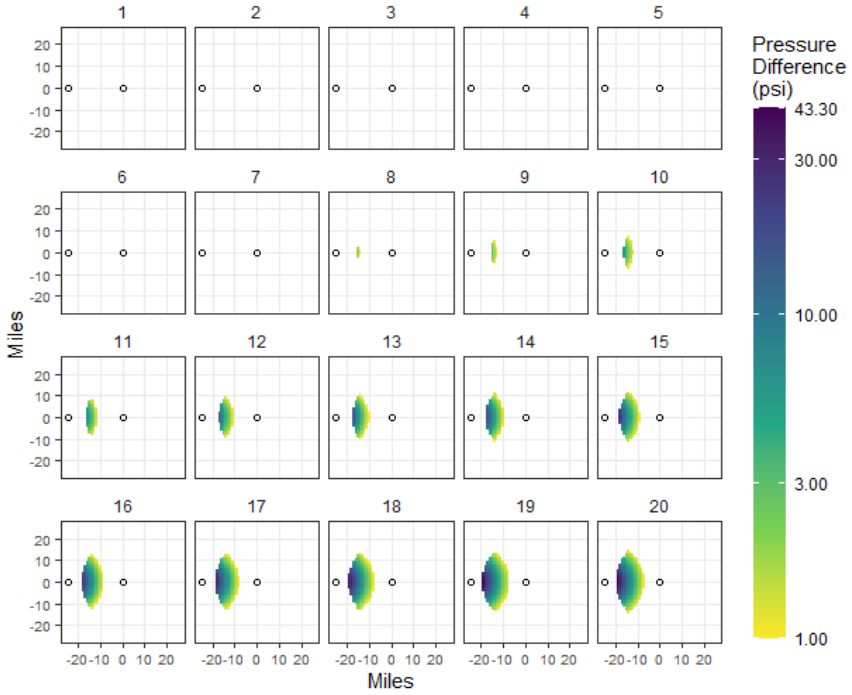

Figure C-52. Five-year delay, 4-Mtpa injection, 25-mi spacing.

SITES A, B, AND D

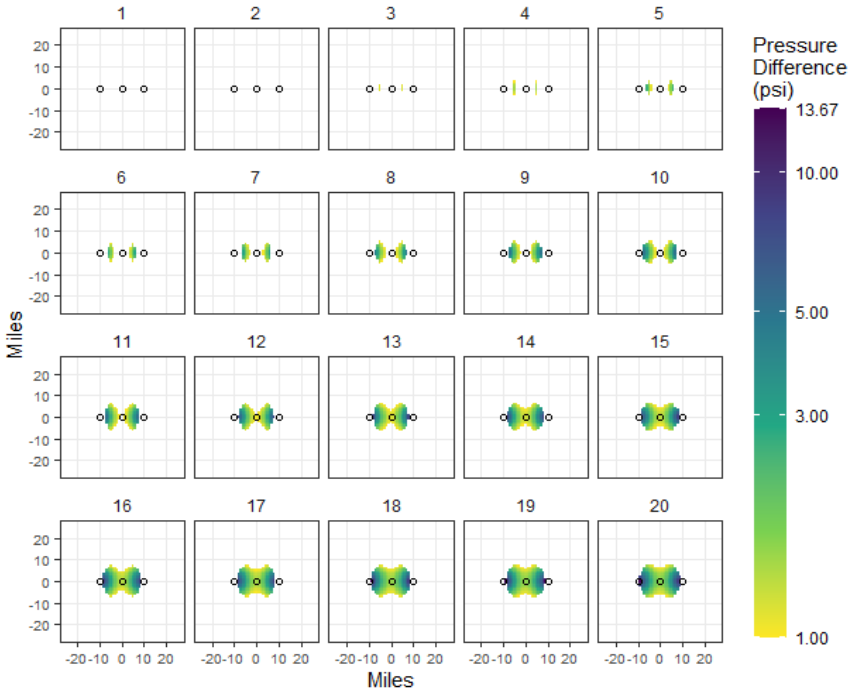

Figure C-53. Zero-year delay, 0.2-Mtpa injection, 10-mi spacing.

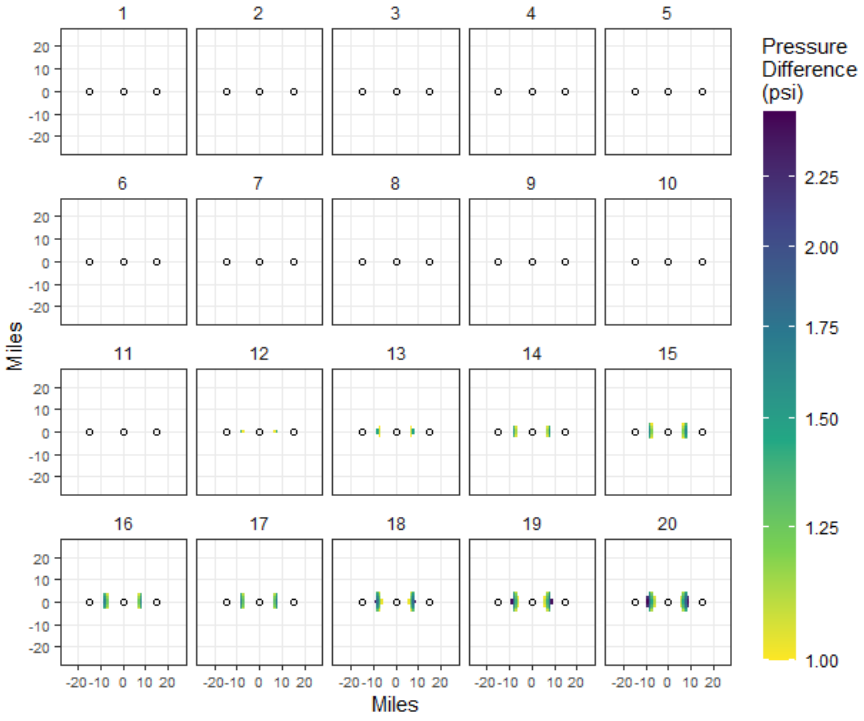

Figure C-54. Zero-year delay, 0.2-Mtpa injection, 15-mi spacing.

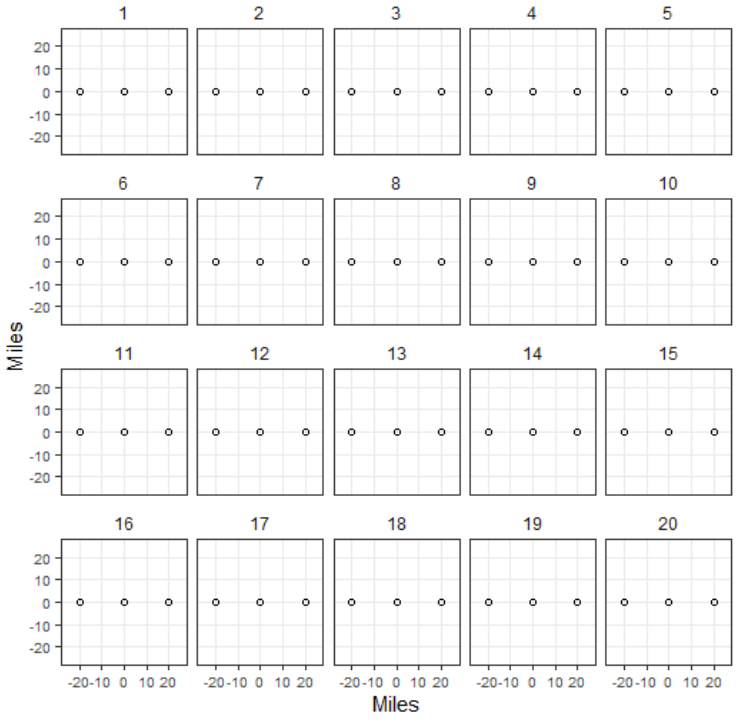

Figure C-55. Zero-year delay, 0.2-Mtpa injection, 20-mi spacing. All values less than 1 psi.

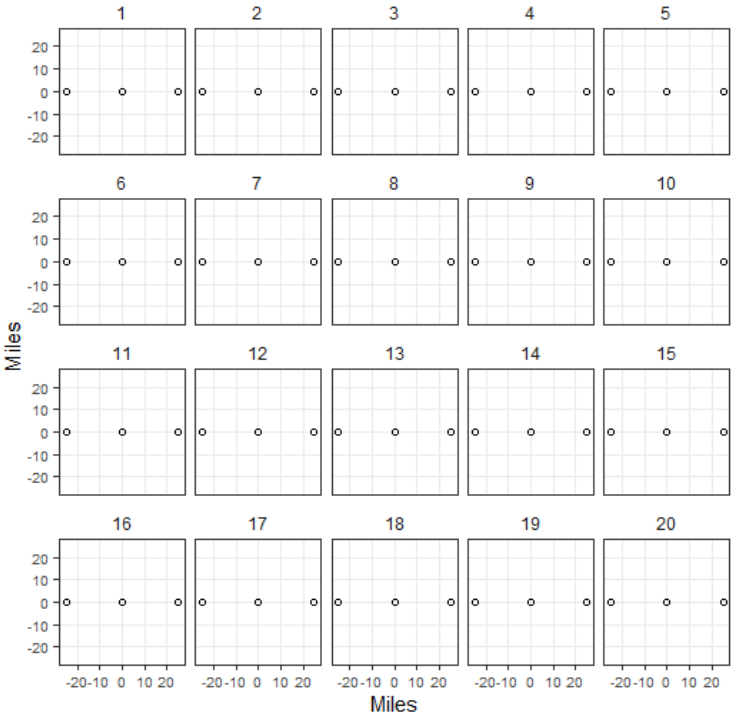

Figure C-56. Zero-year delay, 0.2-Mtpa injection, 25-mi spacing. All values less than 1 psi.

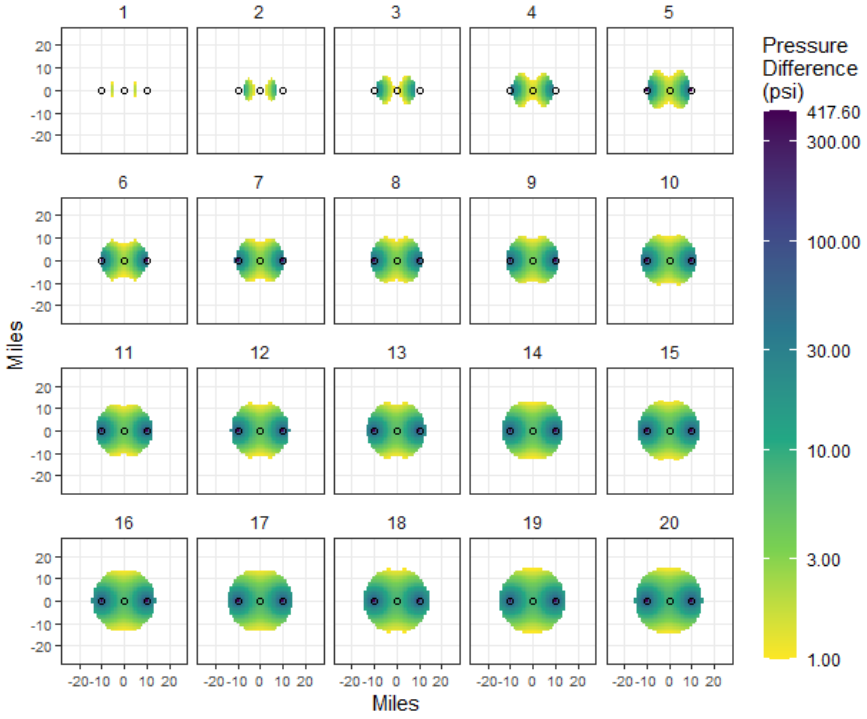

Figure C-57. Zero-year delay, 1-Mtpa injection, 10-mi spacing.

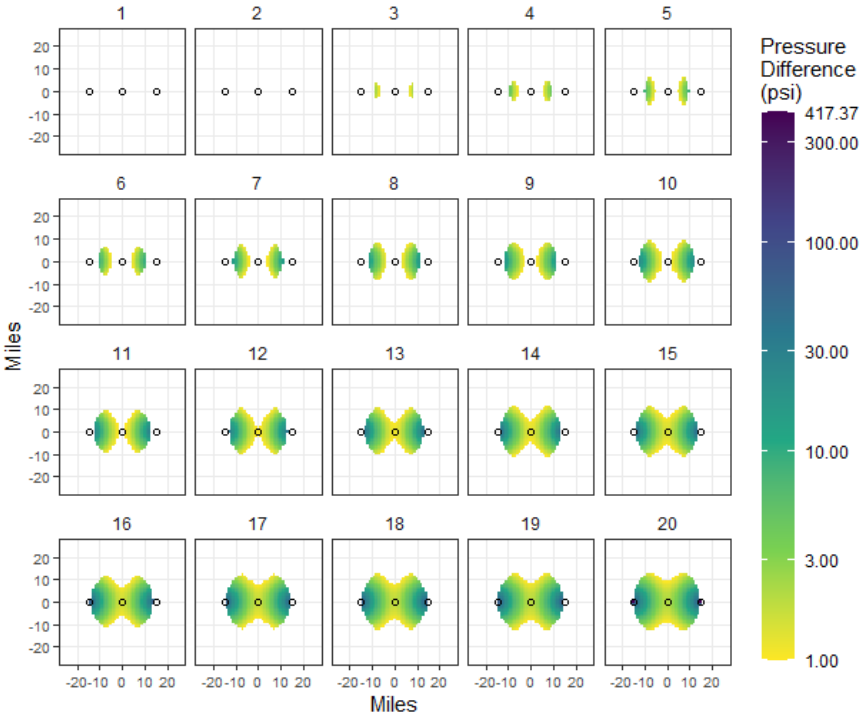

Figure C-58. Zero-year delay, 1-Mtpa injection, 15-mi spacing.

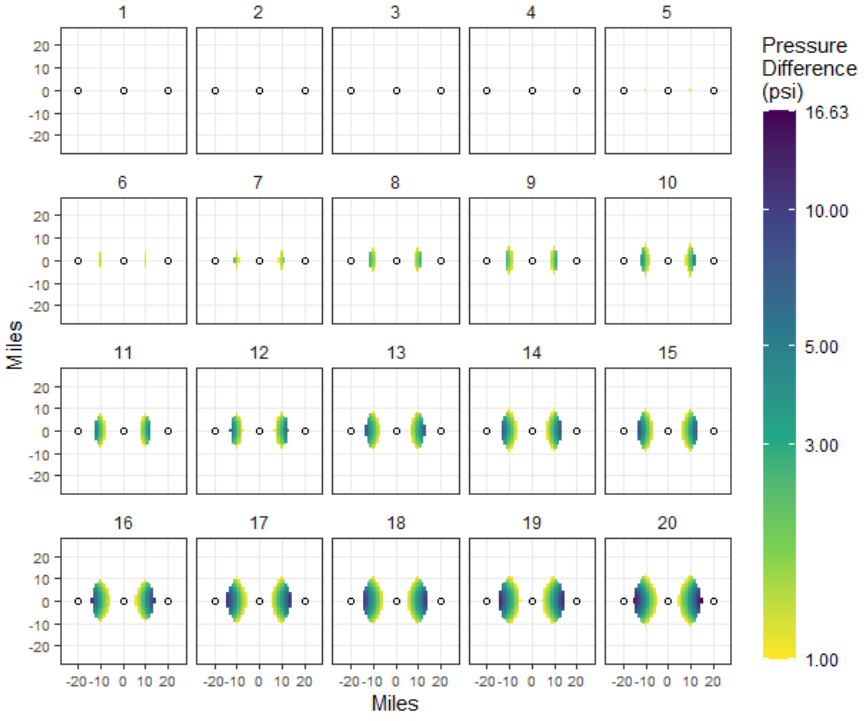

Figure C-59. Zero-year delay, 1-Mtpa injection, 20-mi spacing.

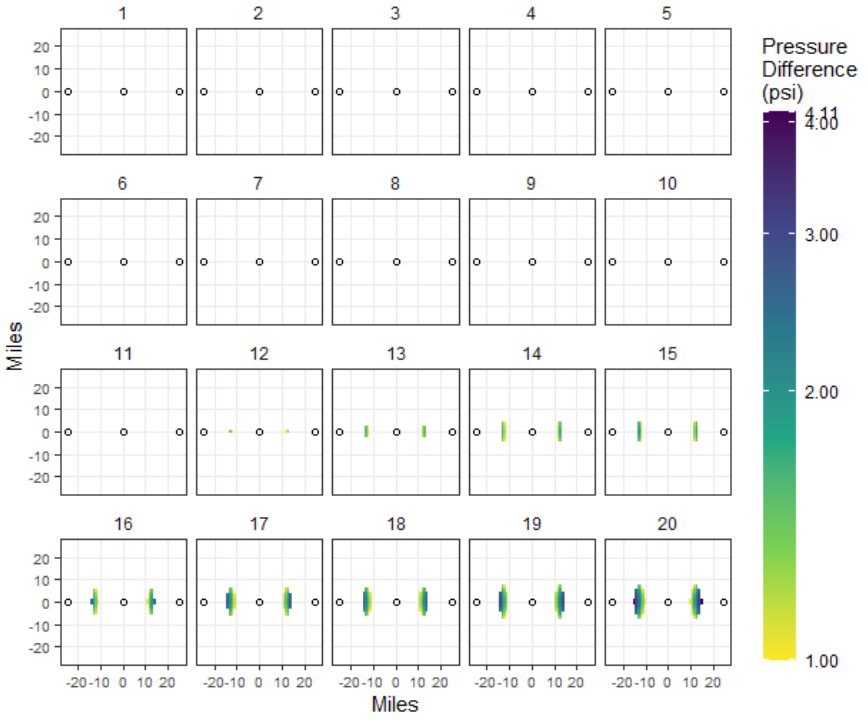

Figure C-60. Zero-year delay, 1-Mtpa injection, 25-mi spacing.

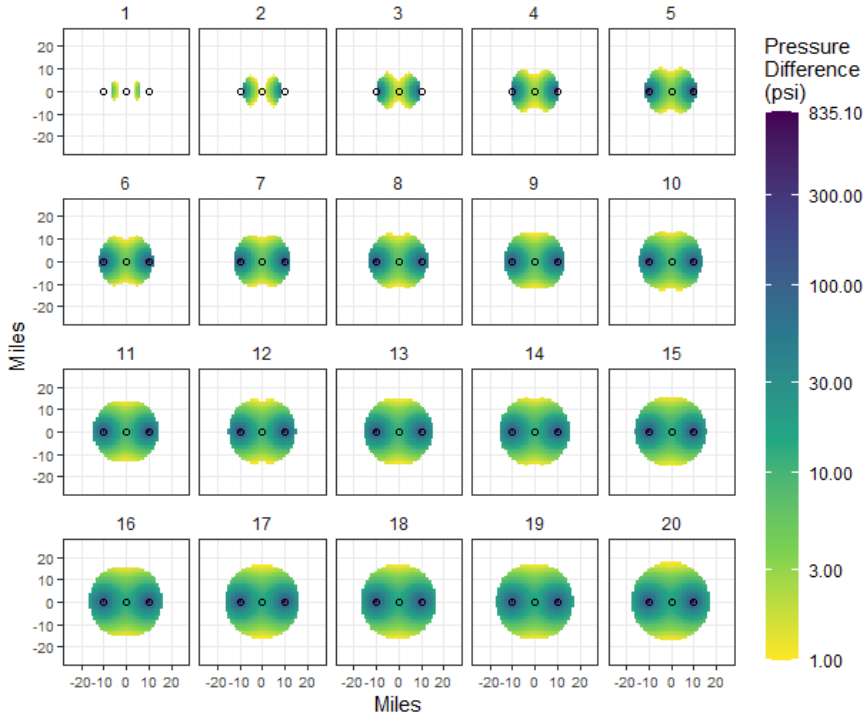

Figure C-61. Zero-year delay, 2-Mtpa injection, 10-mi spacing.

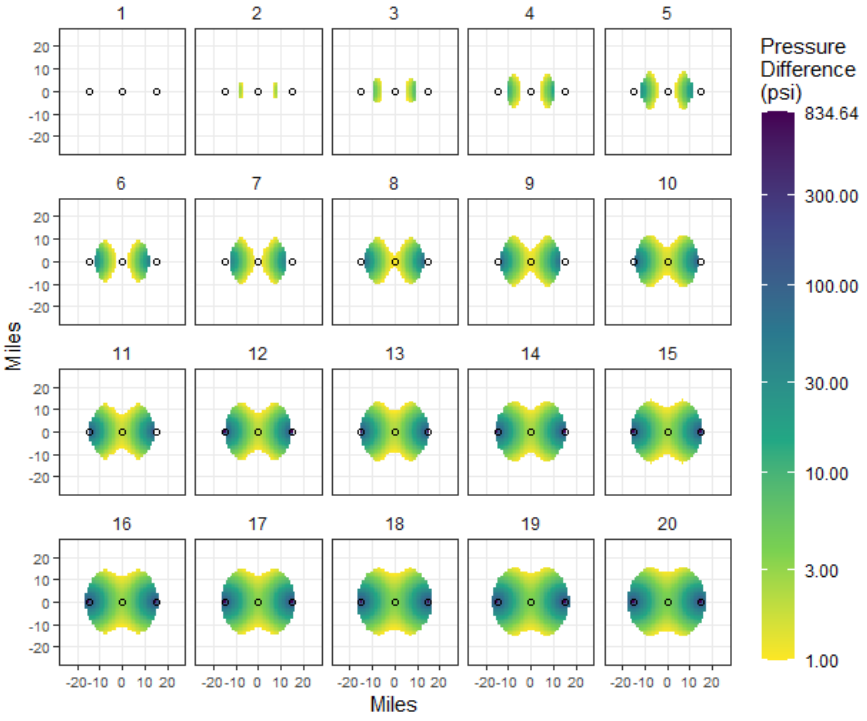

Figure C-62. Zero-year delay, 2-Mtpa injection, 15-mi spacing.

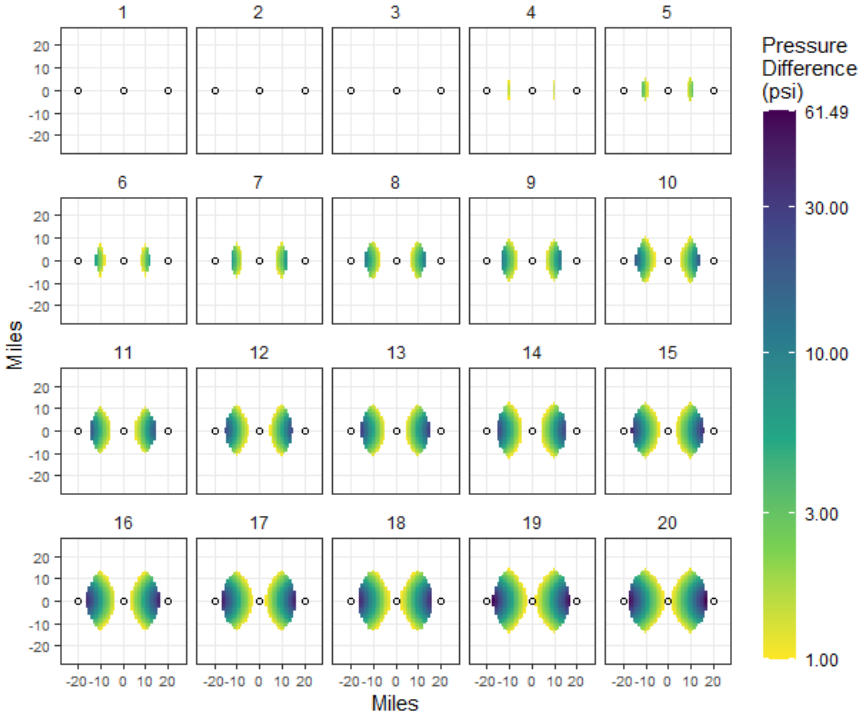

Figure C-63. Zero-year delay, 2-Mtpa injection, 20-mi spacing.

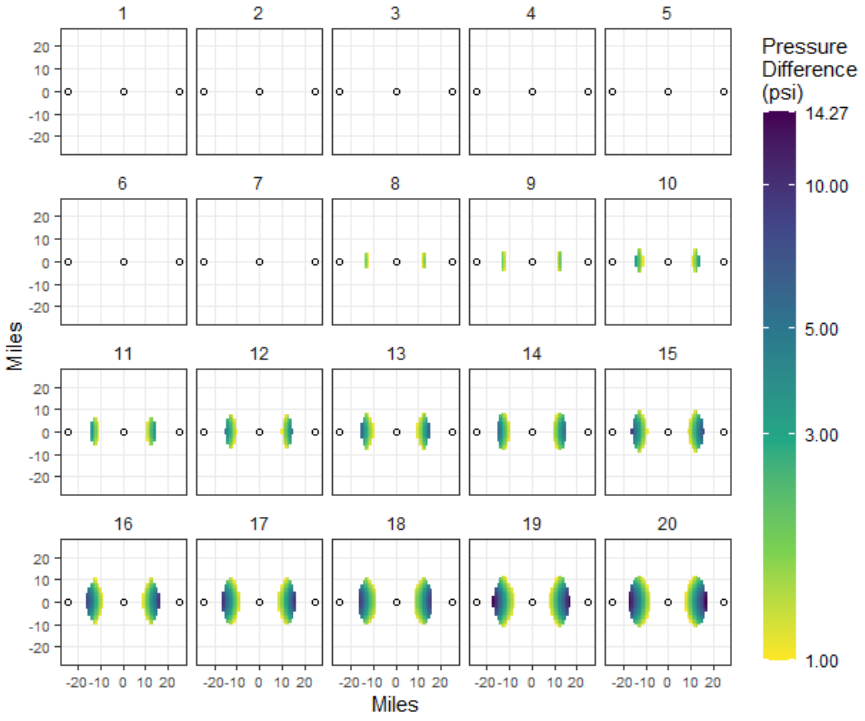

Figure C-64. Zero-year delay, 2-Mtpa injection, 25-mi spacing.

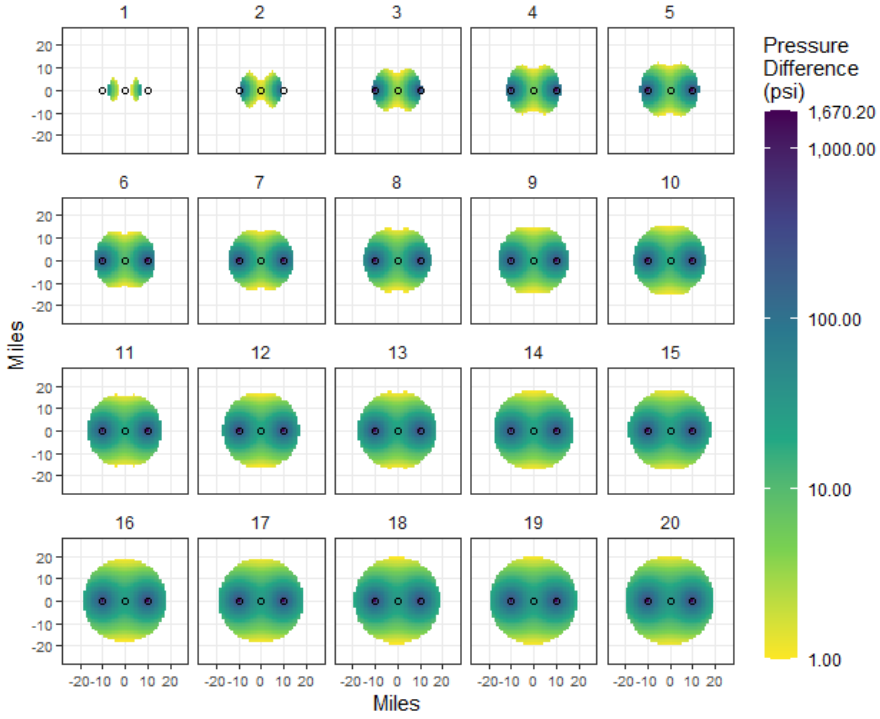

Figure C-65. One-year delay, 4-Mtpa injection, 10-mi spacing.

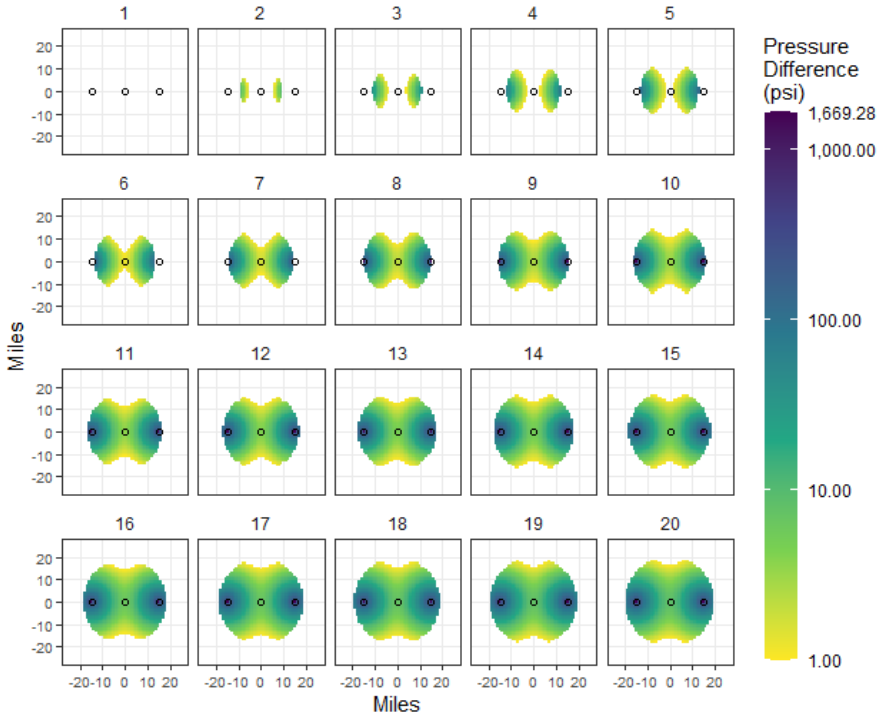

Figure C-66. One-year delay, 4-Mtpa injection, 15-mi spacing.

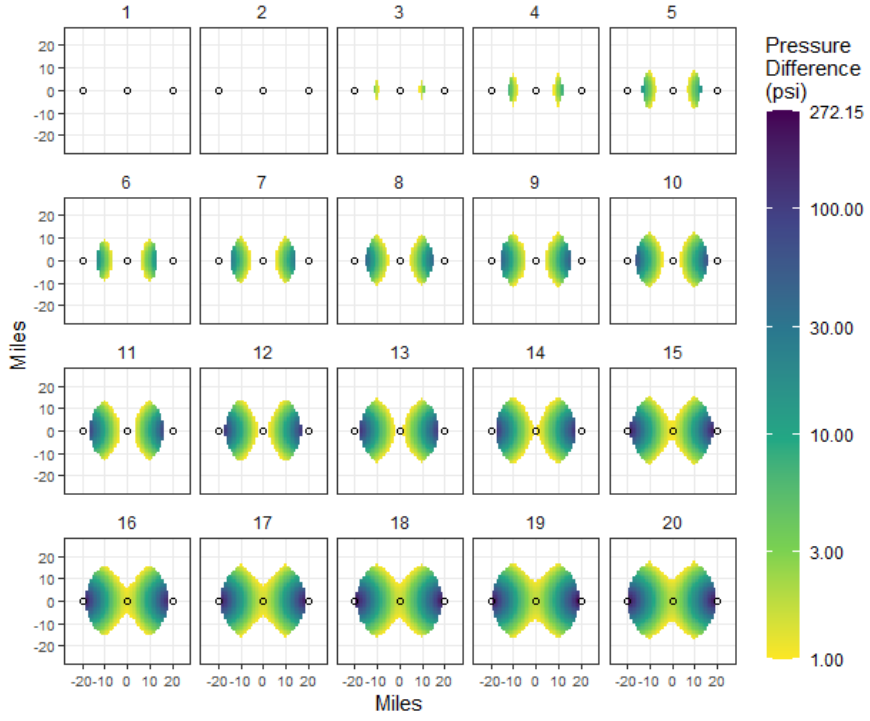

Figure C-67. One-year delay, 4-Mtpa injection, 20-mi spacing.

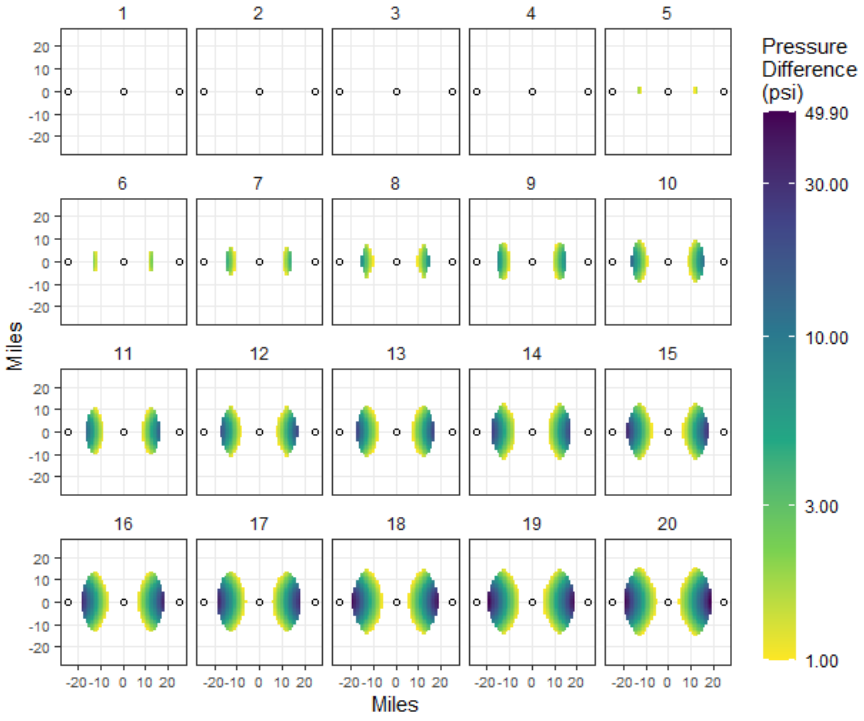

Figure C-68. One-year delay, 4-Mtpa injection, 25-mi spacing.

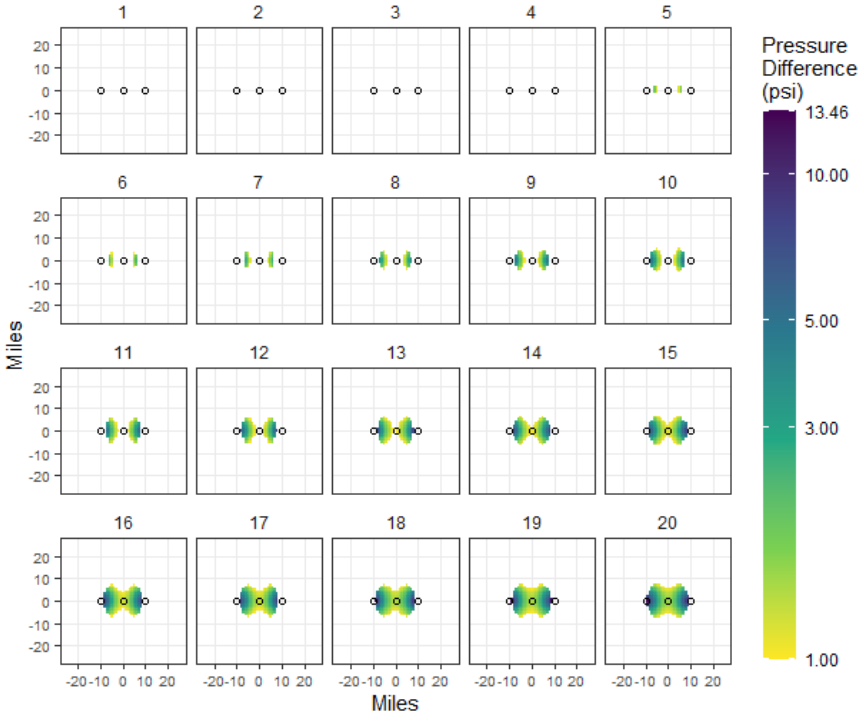

Figure C-69. Two-year delay, 0.2-Mtpa injection, 10-mi spacing.

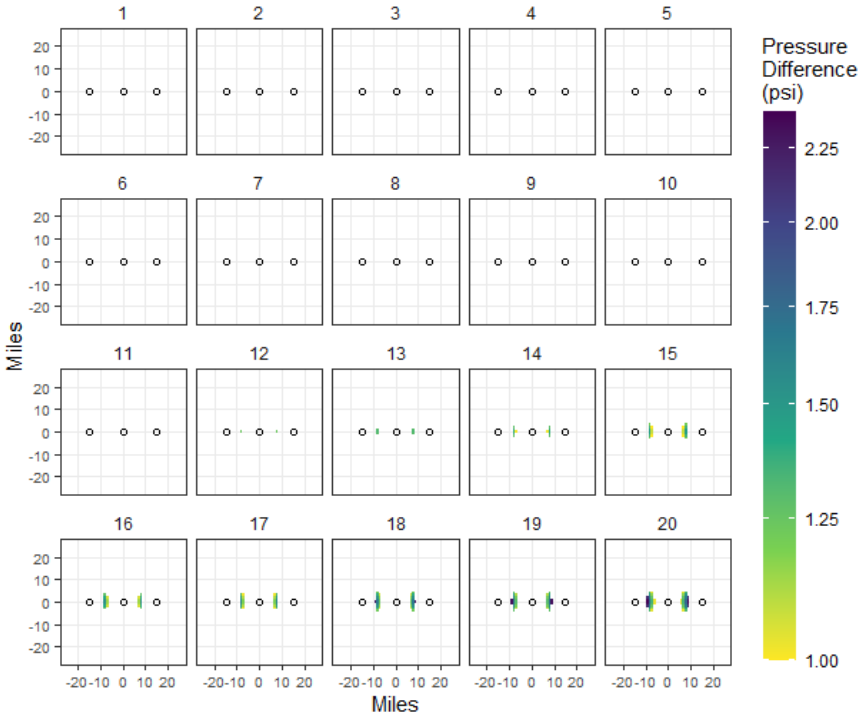

Figure C-70. Two-year delay, 0.2-Mtpa injection, 15-mi spacing.

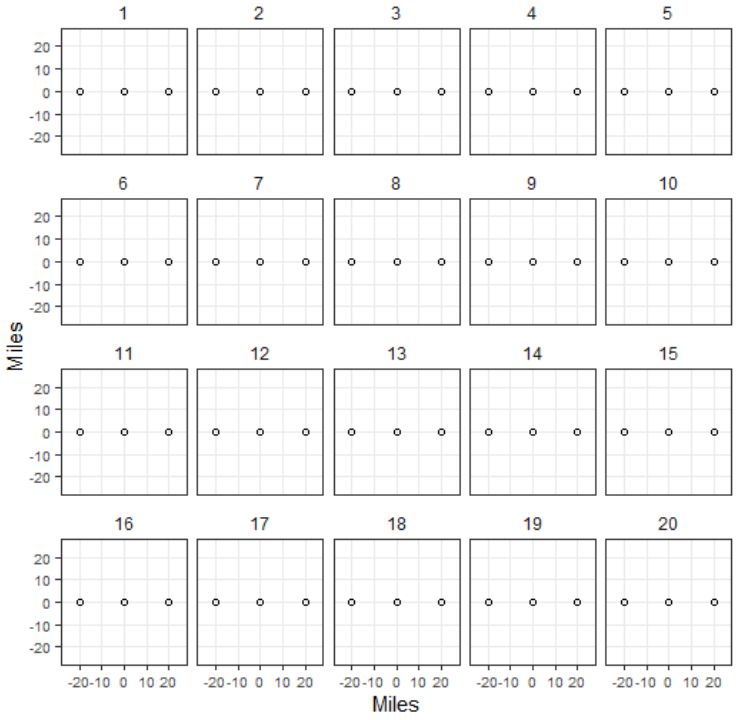

Figure C-71. Two-year delay, 0.2-Mtpa injection, 20-mi spacing. All values less than 1 psi.

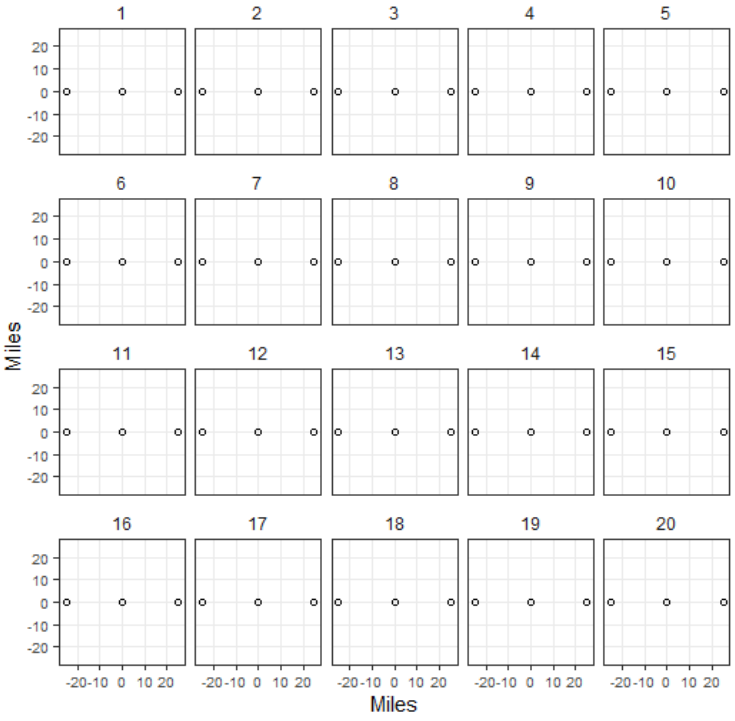

Figure C-72. Two-year delay, 0.2-Mtpa injection, 25-mi spacing. All values less than 1 psi.

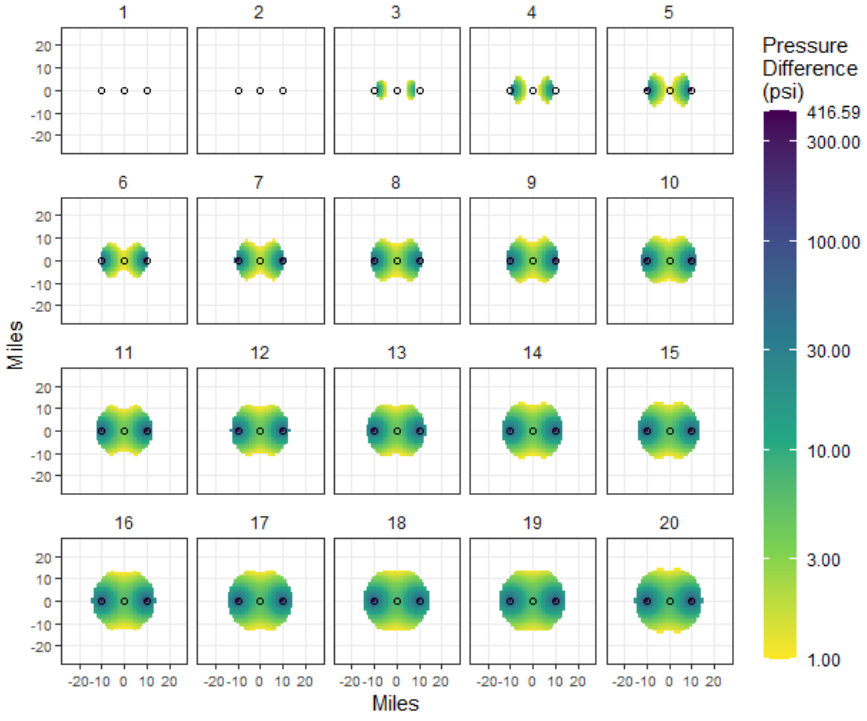

Figure C-73. Two-year delay, 1-Mtpa injection, 10-mi spacing.

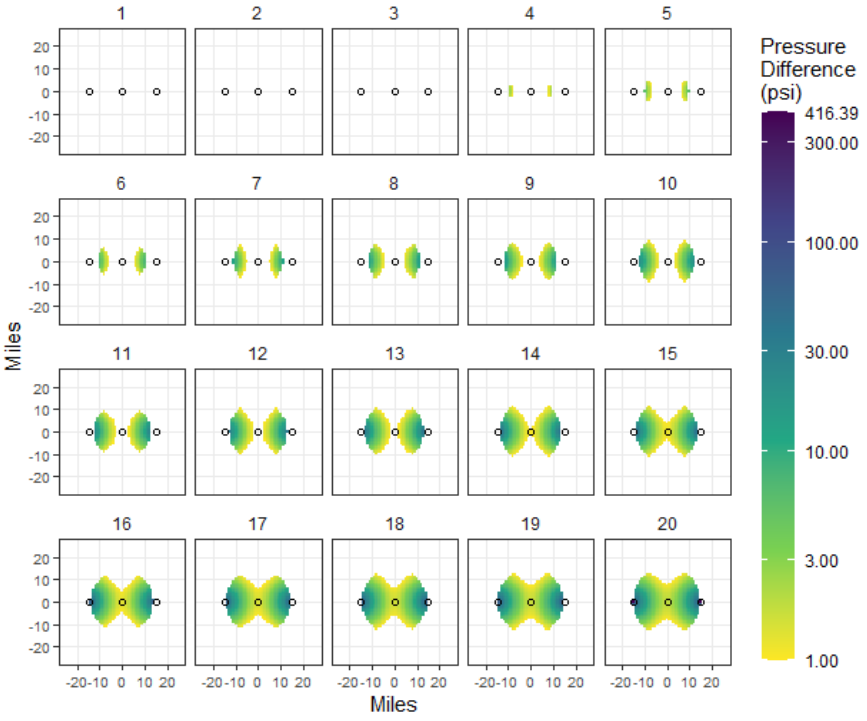

Figure C-74. Two-year delay, 1-Mtpa injection, 15-mi spacing.

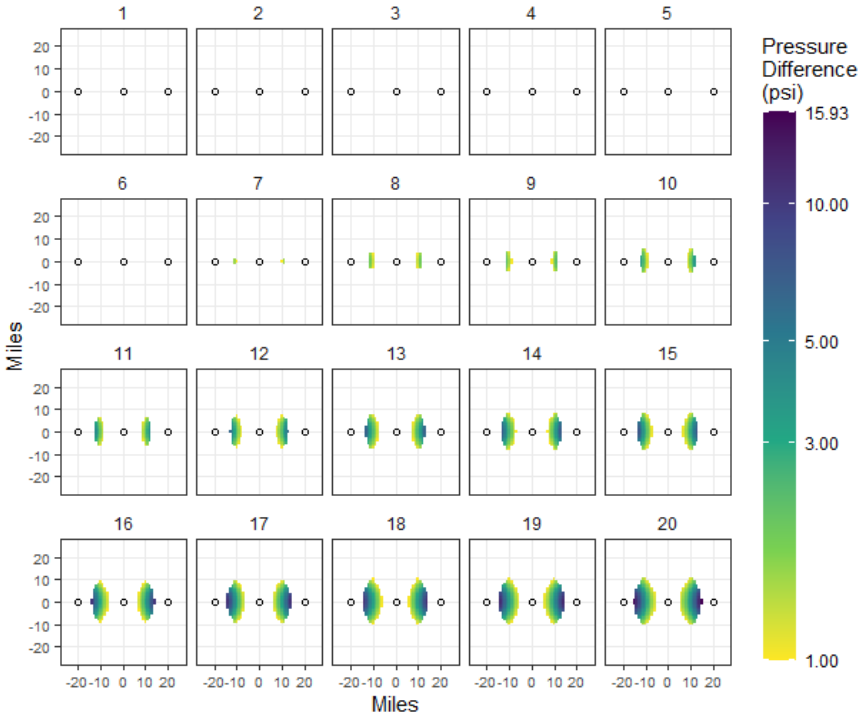

Figure C-75. Two-year delay, 1-Mtpa injection, 20-mi spacing.

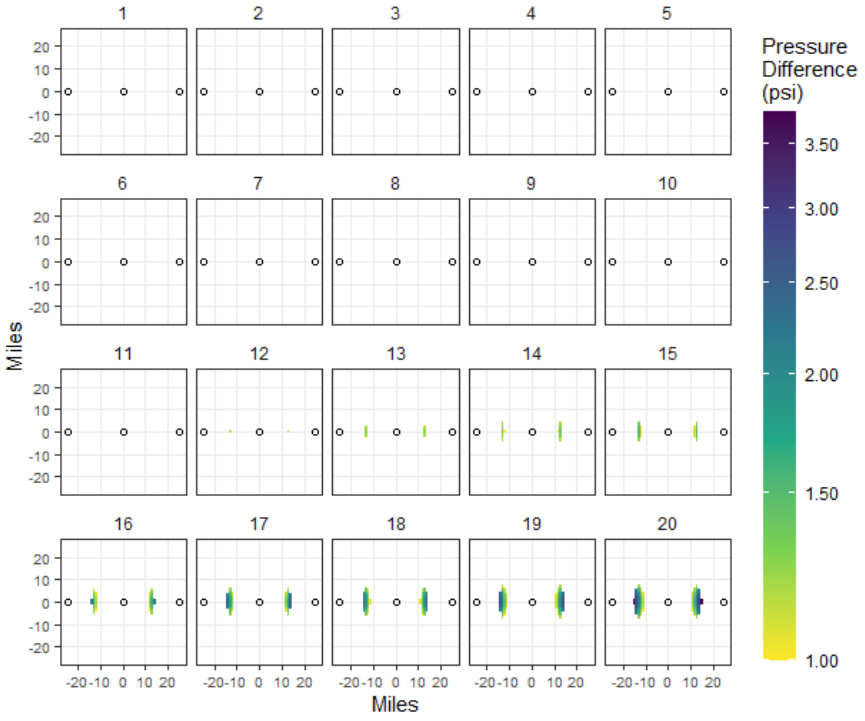

Figure C-76. Two-year delay, 1-Mtpa injection, 25-mi spacing.

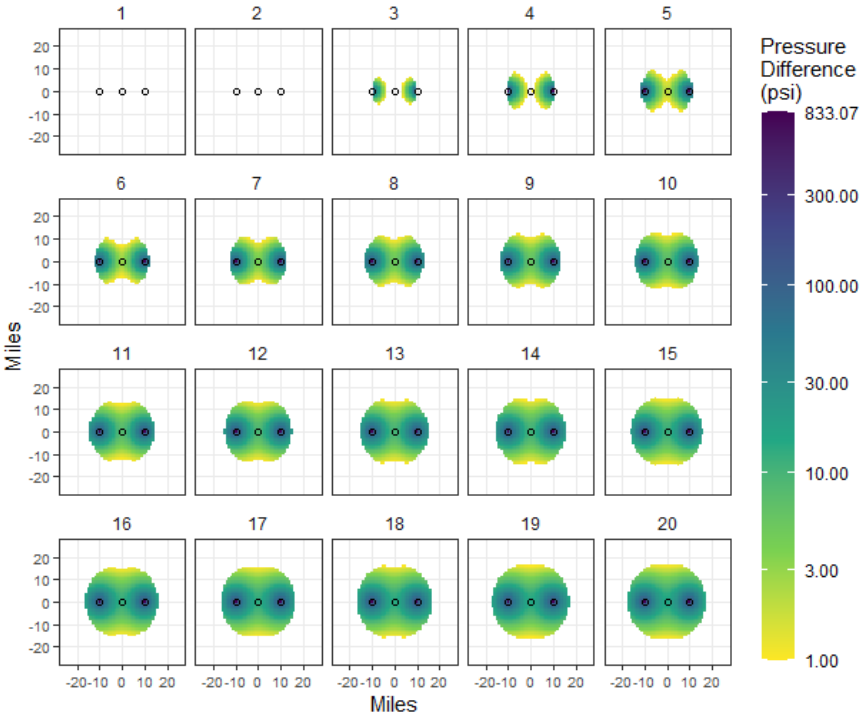

Figure C-77. Two-year delay, 2-Mtpa injection, 10-mi spacing.

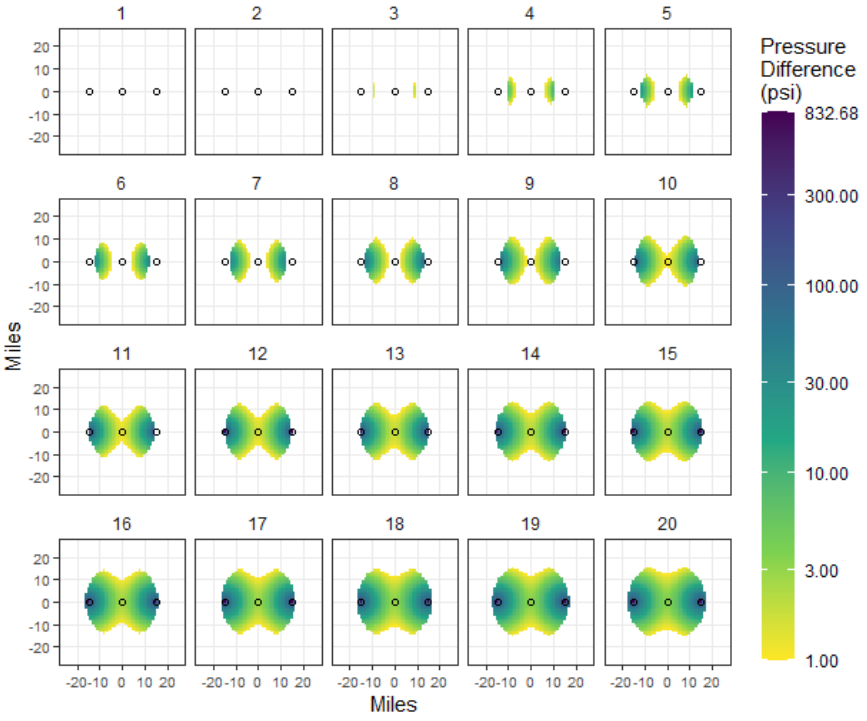

Figure C-78. Two-year delay, 2-Mtpa injection, 15-mi spacing.

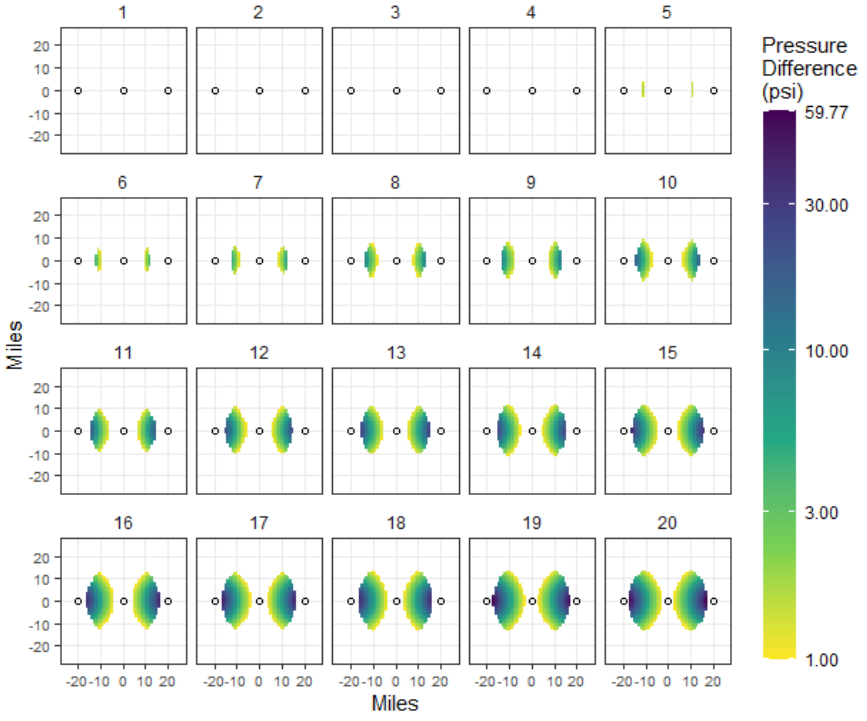

Figure C-79. Two-year delay, 2-Mtpa injection, 20-mi spacing.

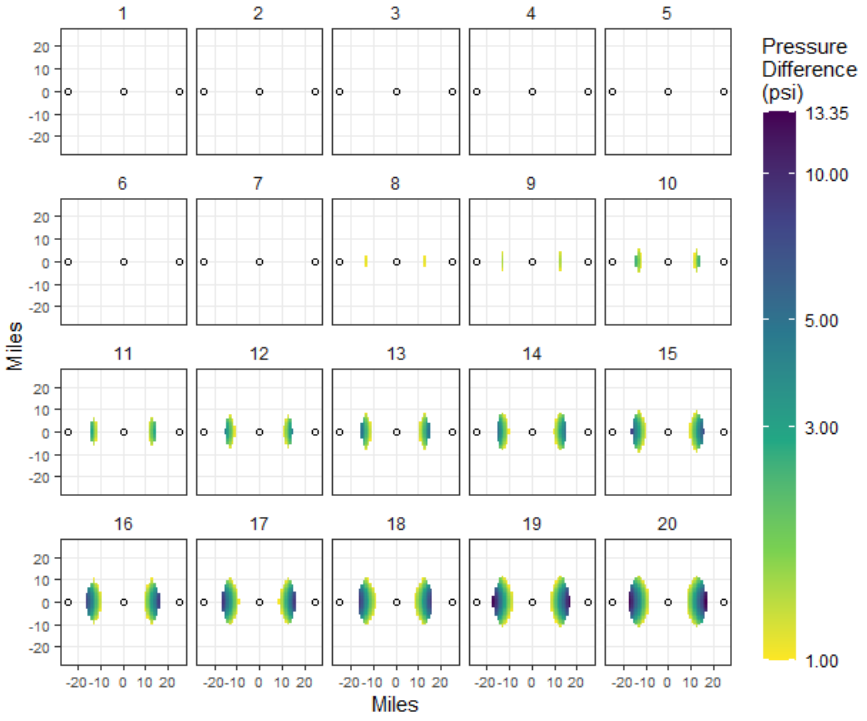

Figure C-80. Two-year delay, 2-Mtpa injection, 25-mi spacing.

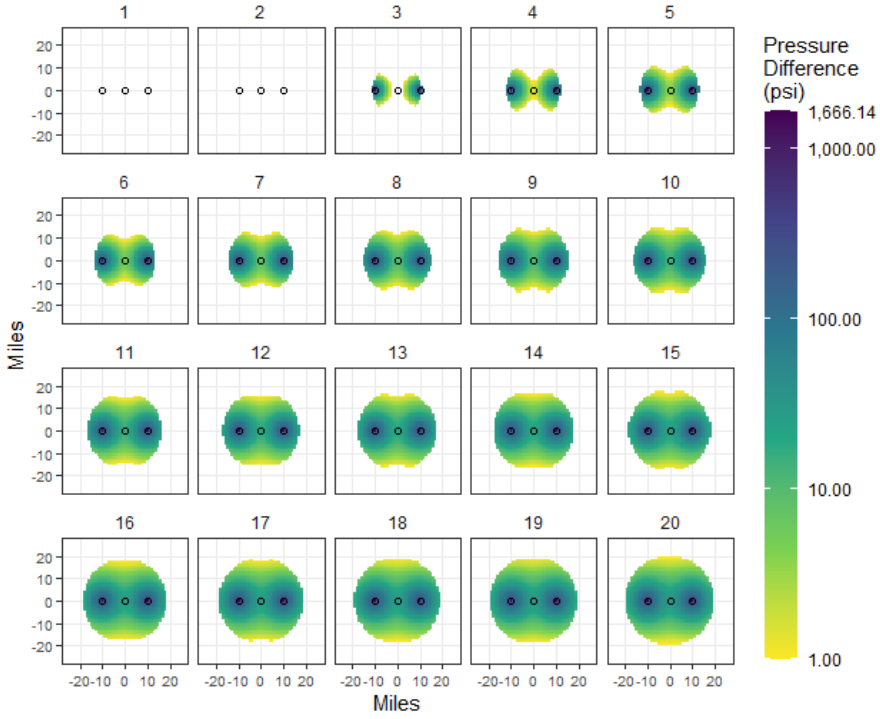

Figure C-81. Two-year delay, 4-Mtpa injection, 10-mi spacing.

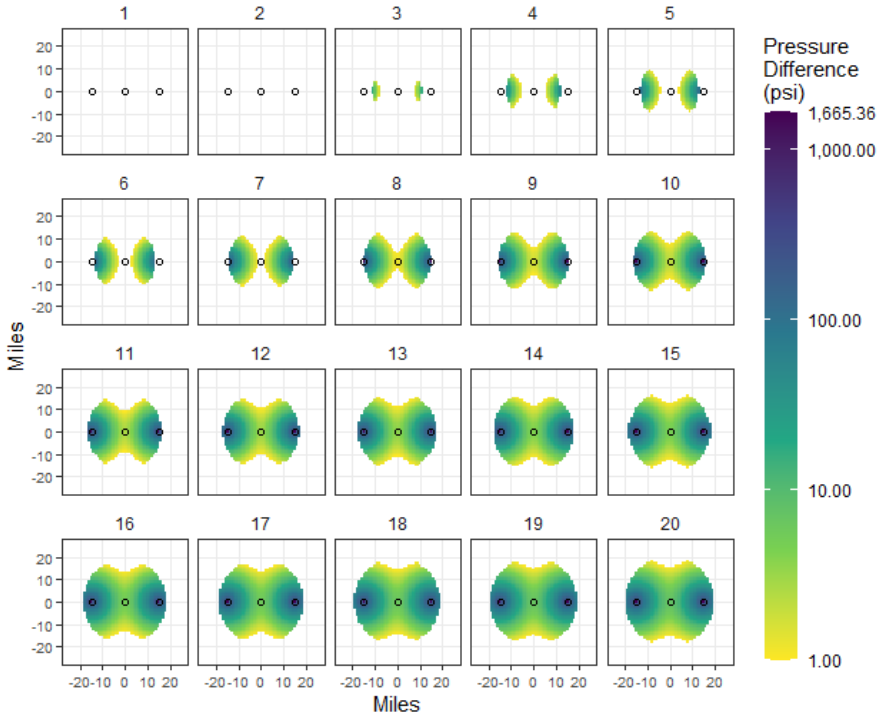

Figure C-82. Two-year delay, 4-Mtpa injection, 15-mi spacing.

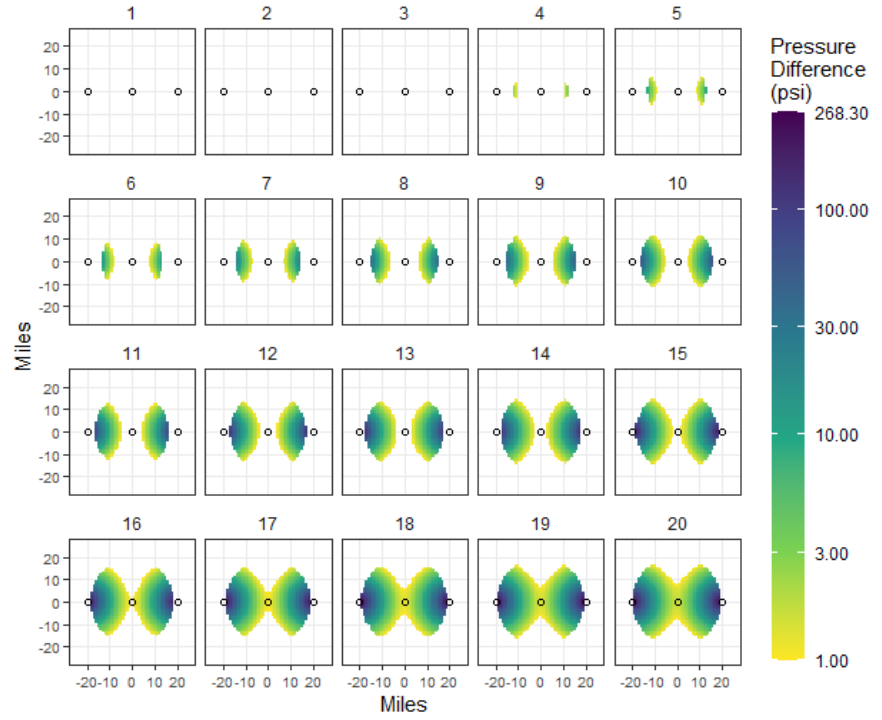

Figure C-83. Two-year delay, 4-Mtpa injection, 20-mi spacing.

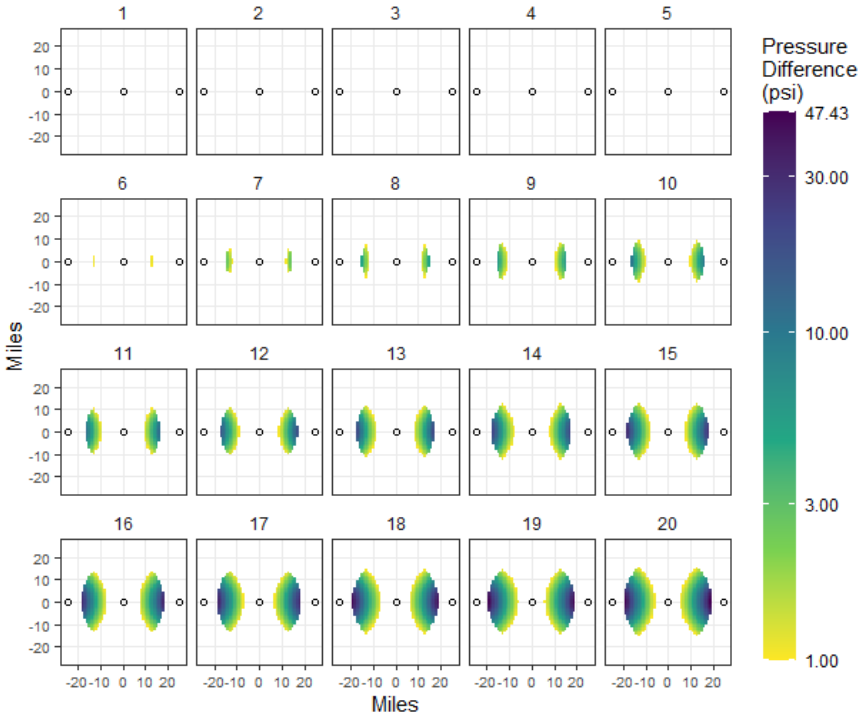

Figure C-84. Two-year delay, 4-Mtpa injection, 25-mi spacing.

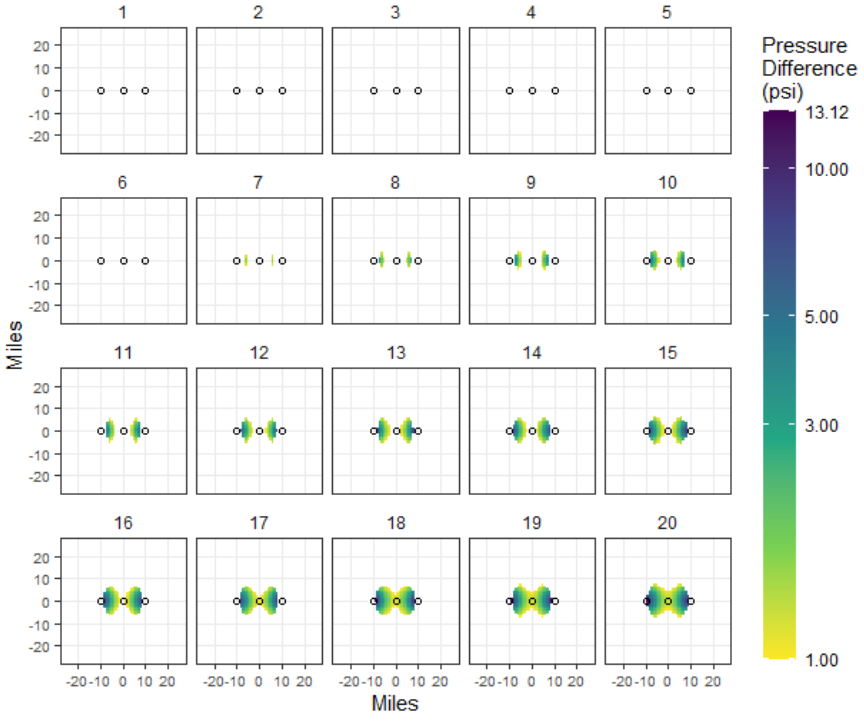

Figure C-85. Five-year delay, 0.2-Mtpa injection, 10-mi spacing.

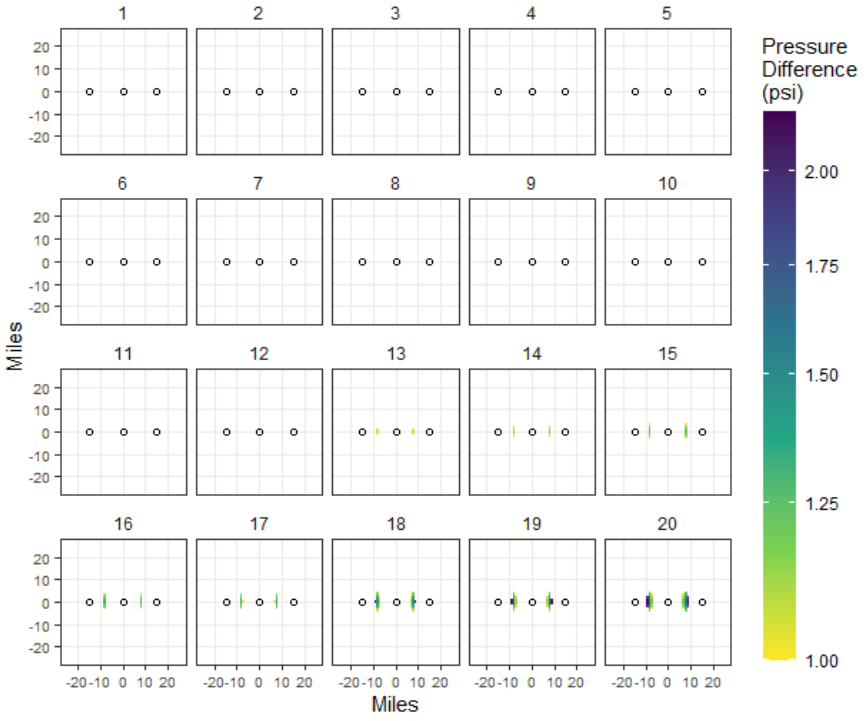

Figure C-86. Five-year delay, 0.2-Mtpa injection, 15-mi spacing.

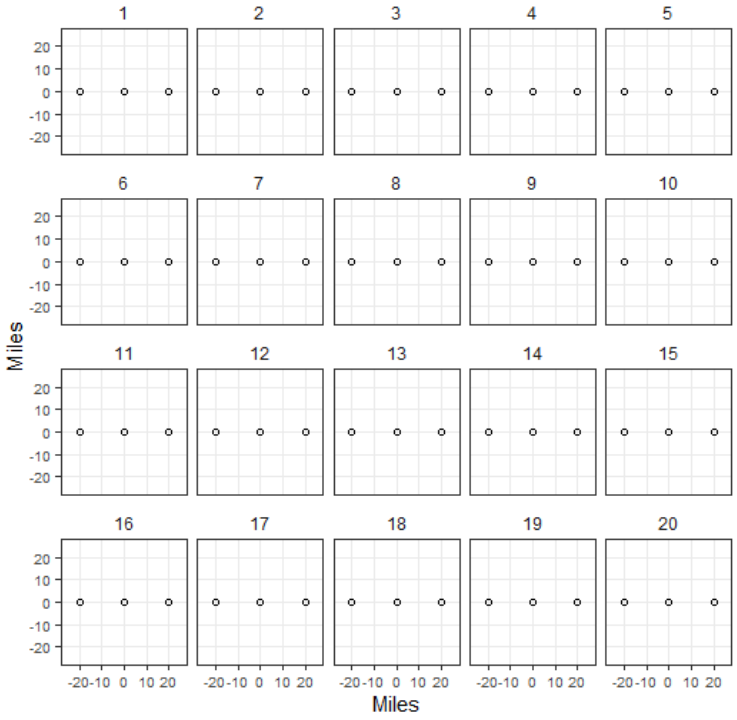

Figure C-87. Five-year delay, 0.2-Mtpa injection, 20-mi spacing. All values less than 1 psi.

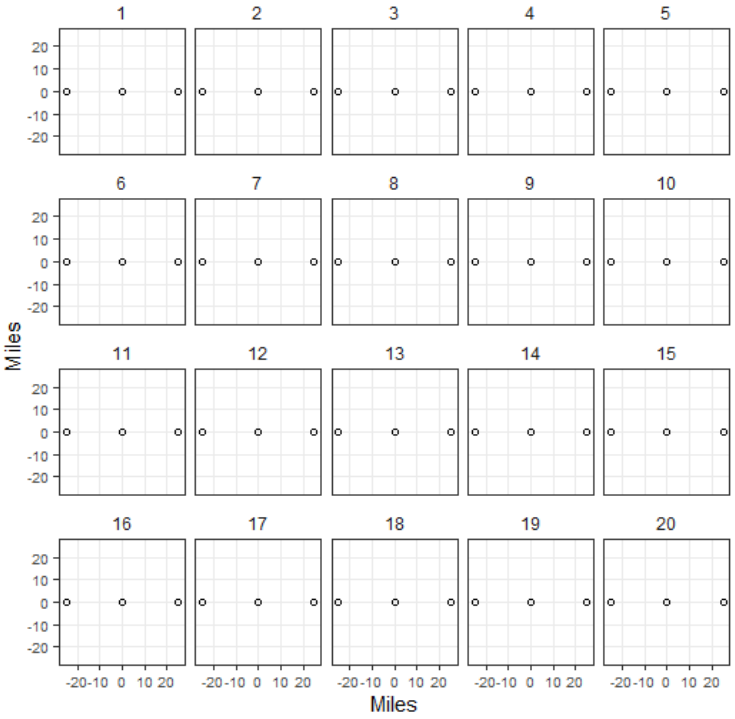

Figure C-88. Five-year delay, 0.2-Mtpa injection, 25-mi spacing. All values less than 1 psi.

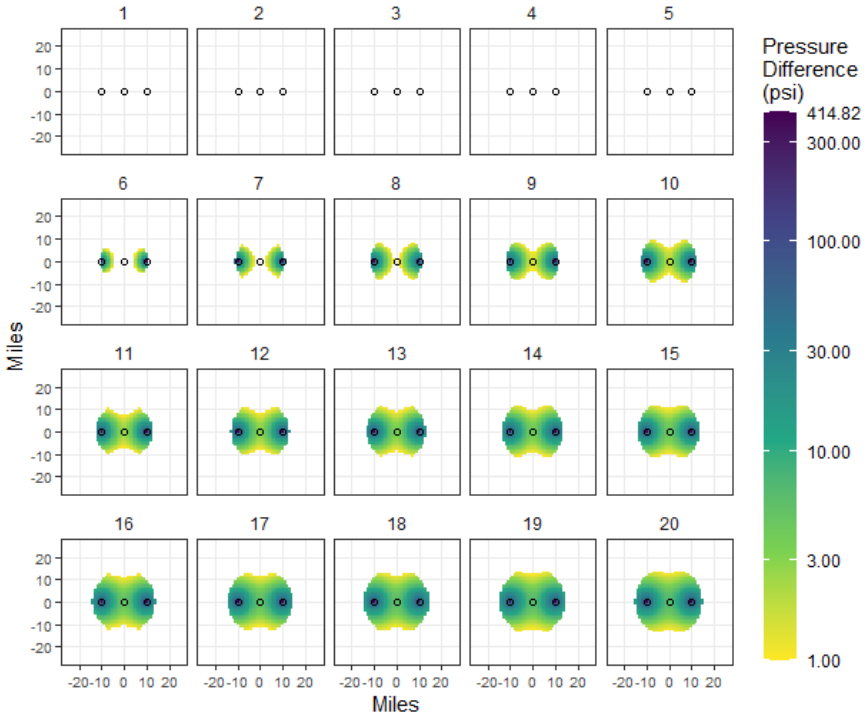

Figure C-89. Five-year delay, 1-Mtpa injection, 10-mi spacing.

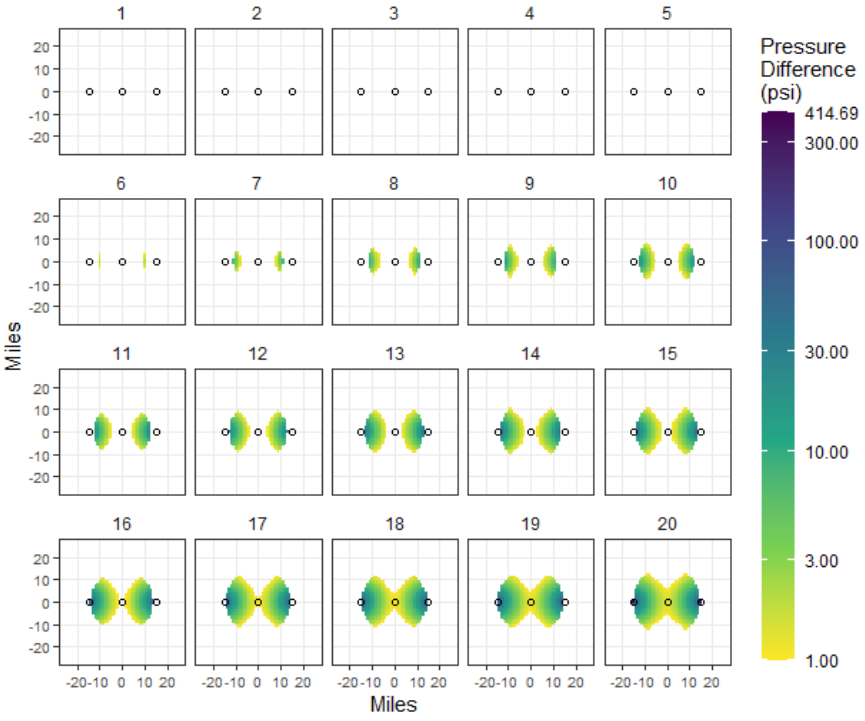

Figure C-90. Five-year delay, 1-Mtpa injection, 15-mi spacing.

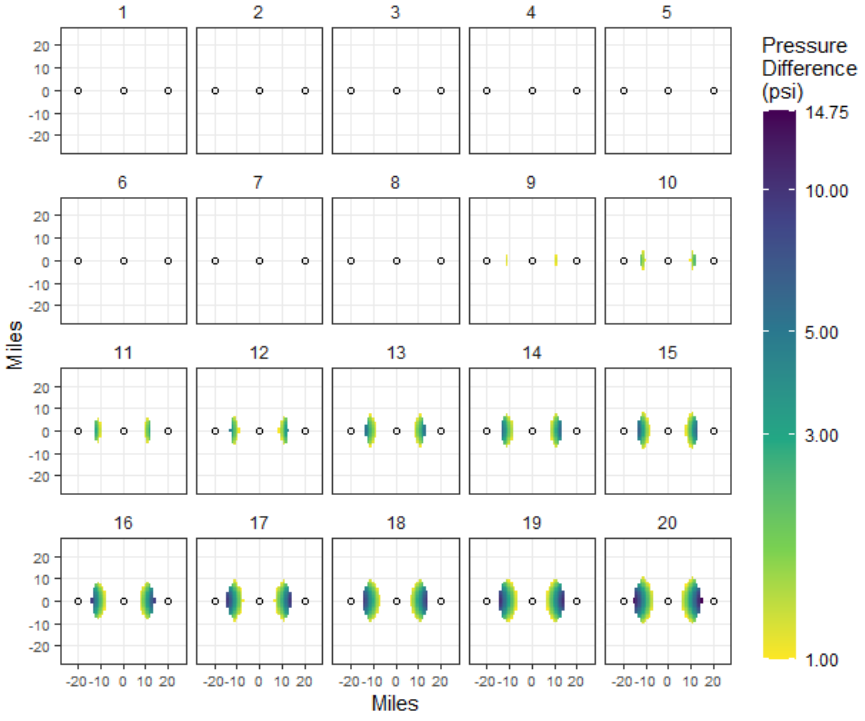

Figure C-91. Five-year delay, 1-Mtpa injection, 20-mi spacing.

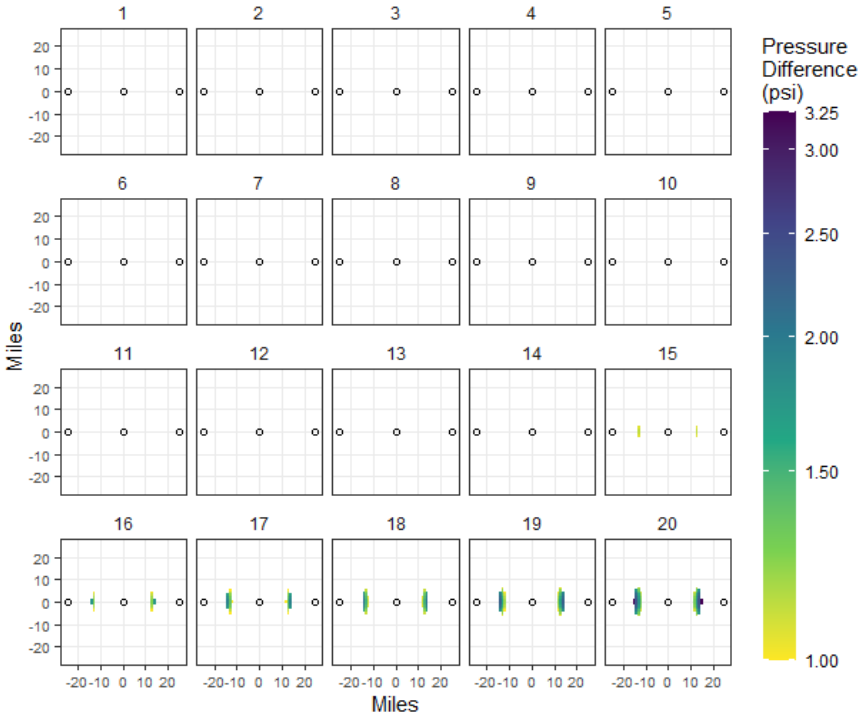

Figure C-92. Five-year delay, 1-Mtpa injection, 25-mi spacing.

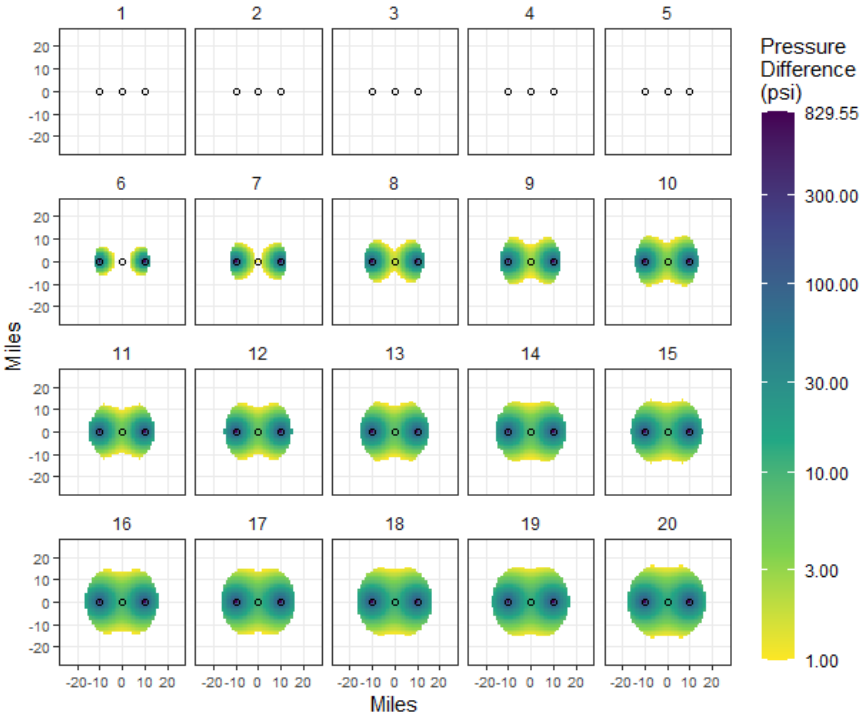

Figure C-93. Five-year delay, 2-Mtpa injection, 10-mi spacing.

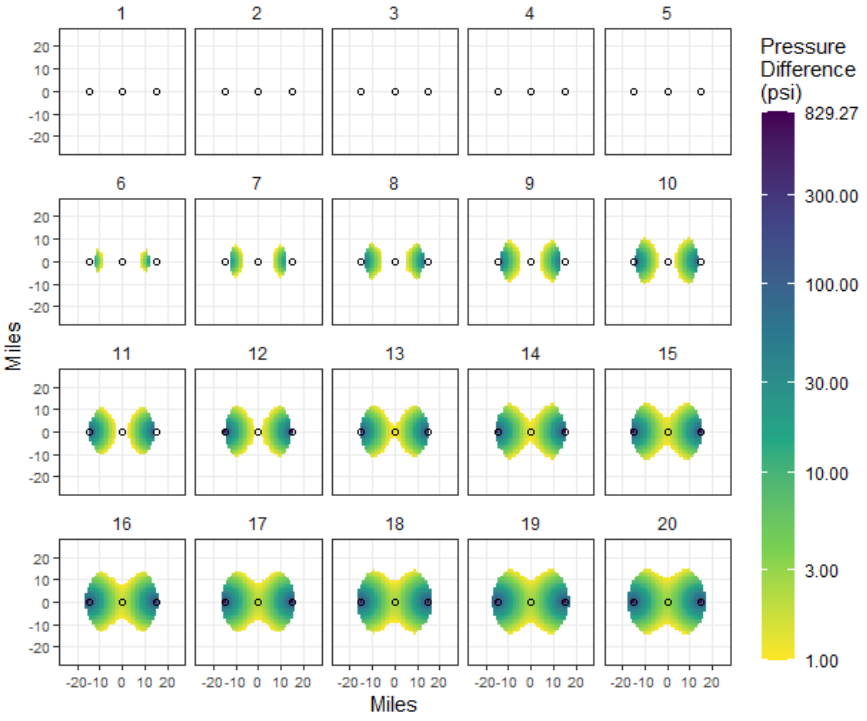

Figure C-94. Five-year delay, 2-Mtpa injection, 15-mi spacing.

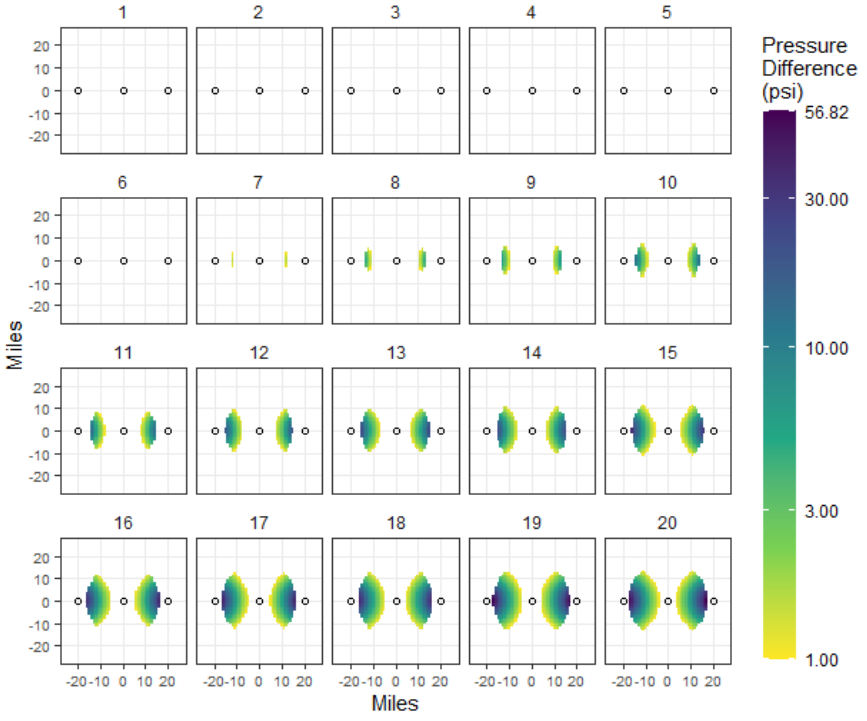

Figure C-95. Five-year delay, 2-Mtpa injection, 20-mi spacing.

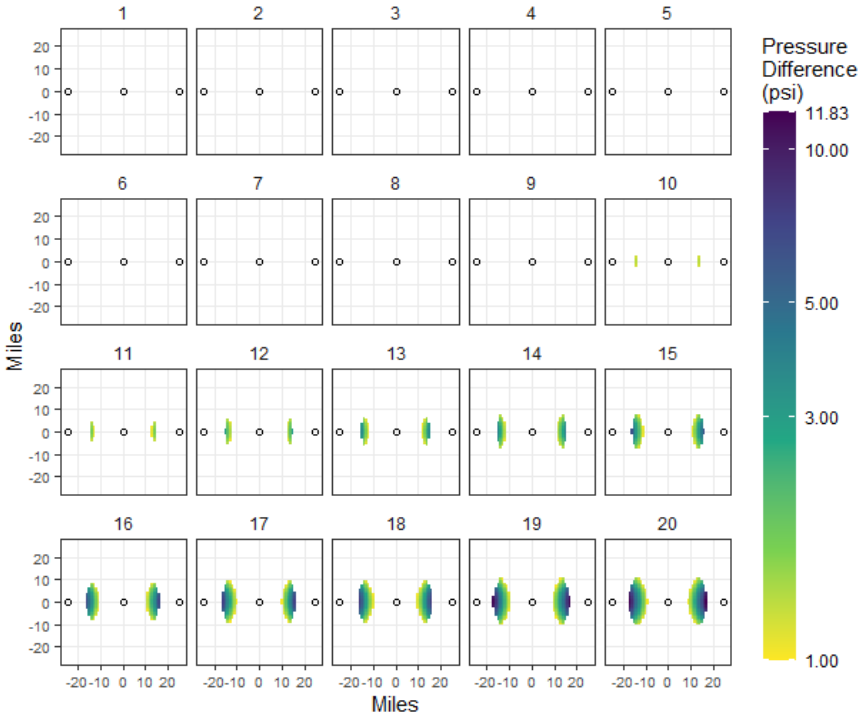

Figure C-96. Five-year delay, 2-Mtpa injection, 25-mi spacing.

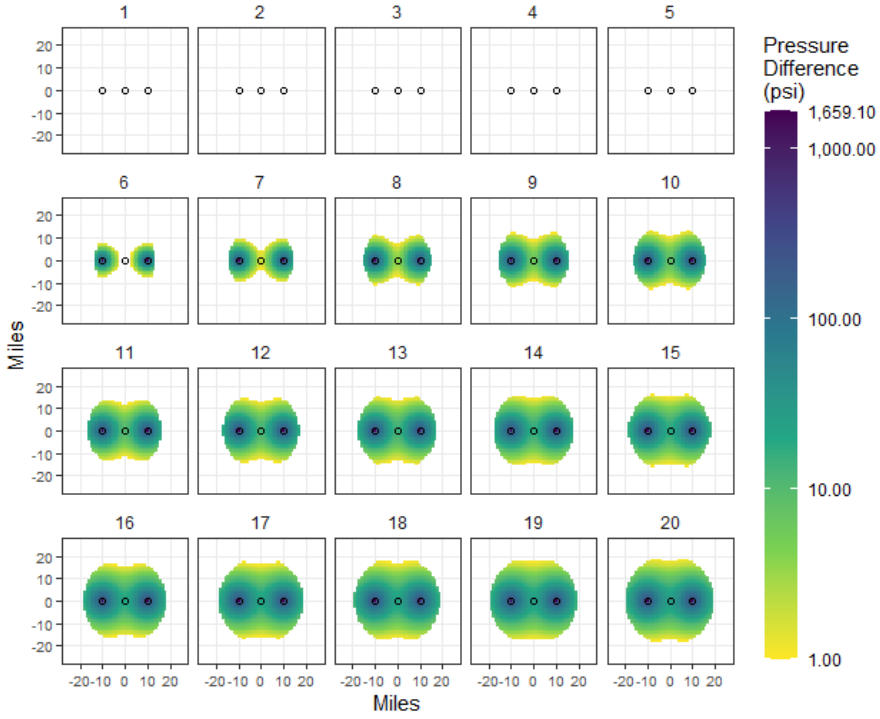

Figure C-97. Five-year delay, 4-Mtpa injection, 10-mi spacing.

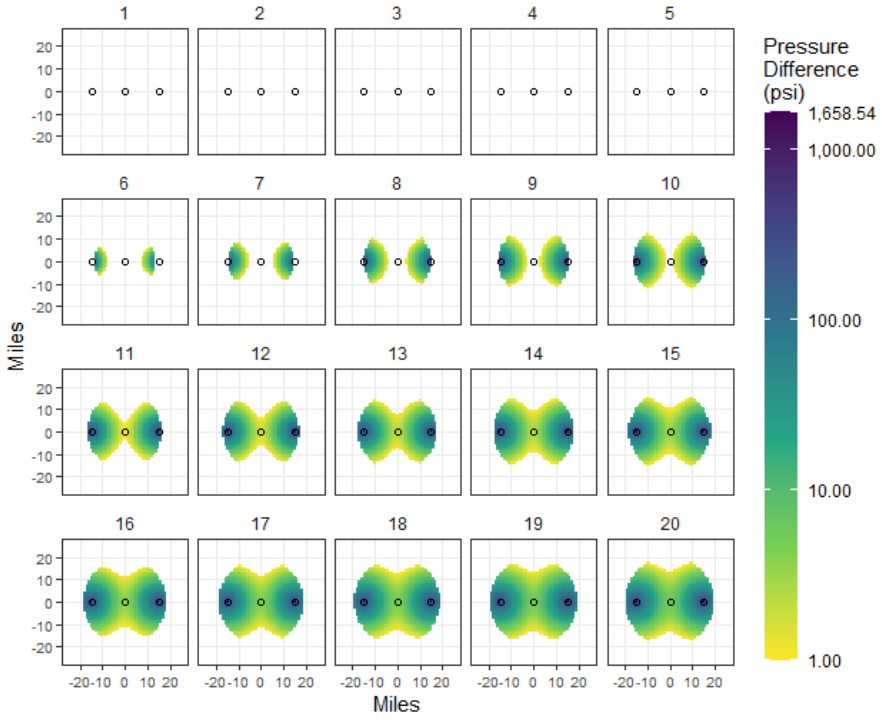

Figure C-98. Five-year delay, 4-Mtpa injection, 15-mi spacing.

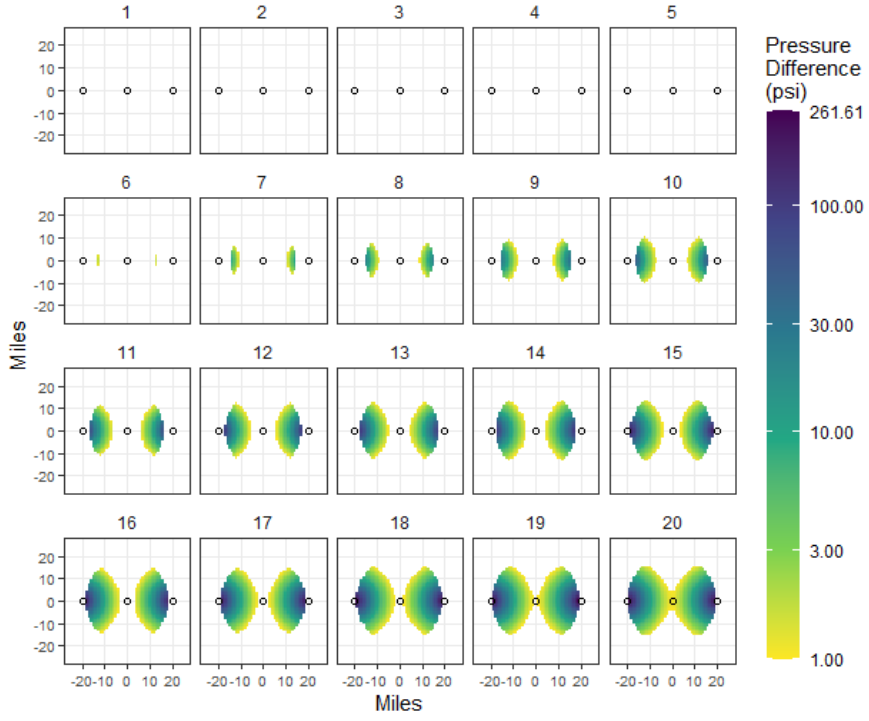

Figure C-99. Five-year delay, 4-Mtpa injection, 20-mi spacing.

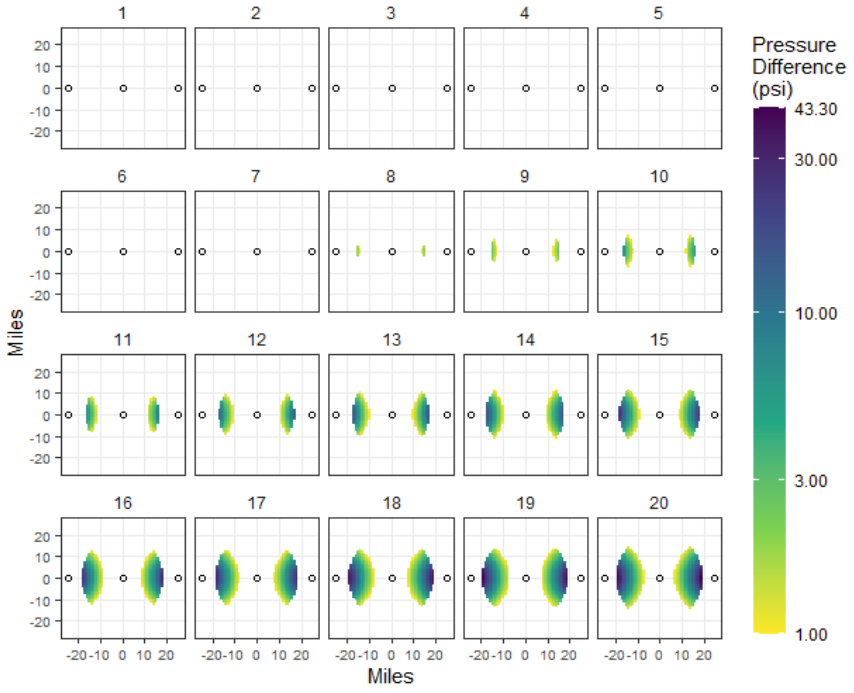

Figure C-100. Five-year delay, 4-Mtpa injection, 25-mi spacing.

SITES A, B, C, AND D

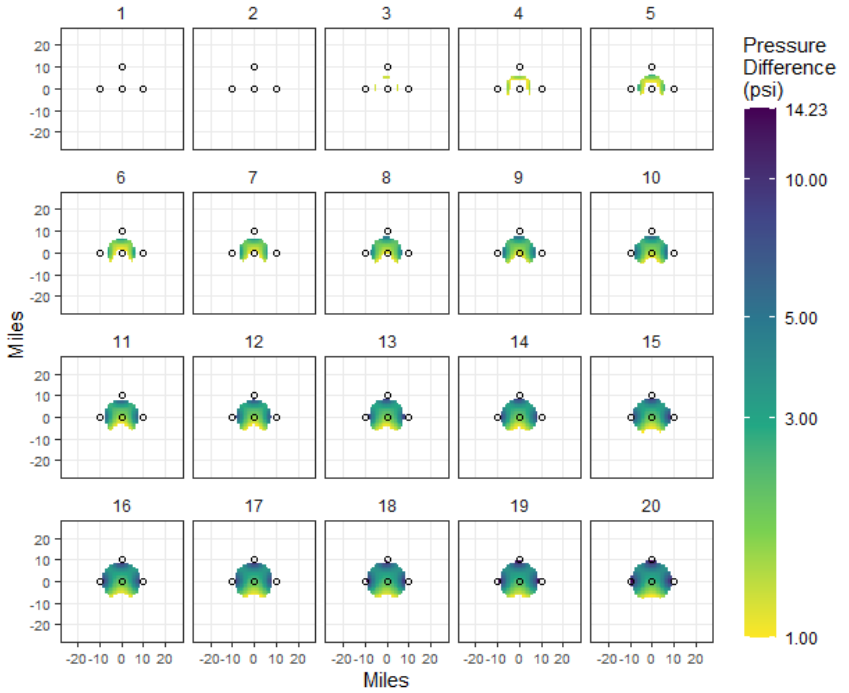

Figure C-101. Zero-year delay, 0.2-Mtpa injection, 10-mi spacing.

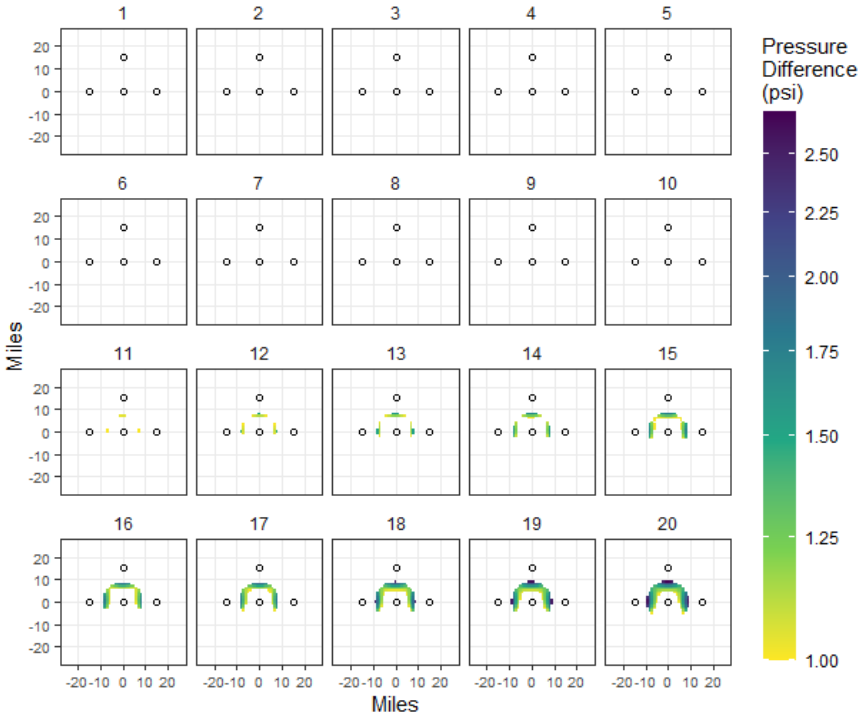

Figure C-102. Zero-year delay, 0.2-Mtpa injection, 15-mi spacing.

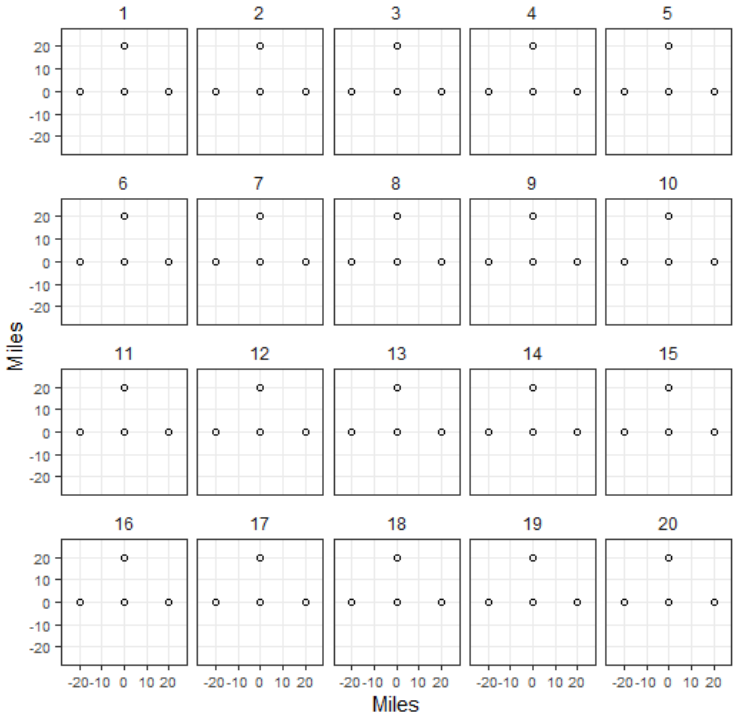

Figure C-103. Zero-year delay, 0.2-Mtpa injection, 20-mi spacing. All values less than 1 psi.

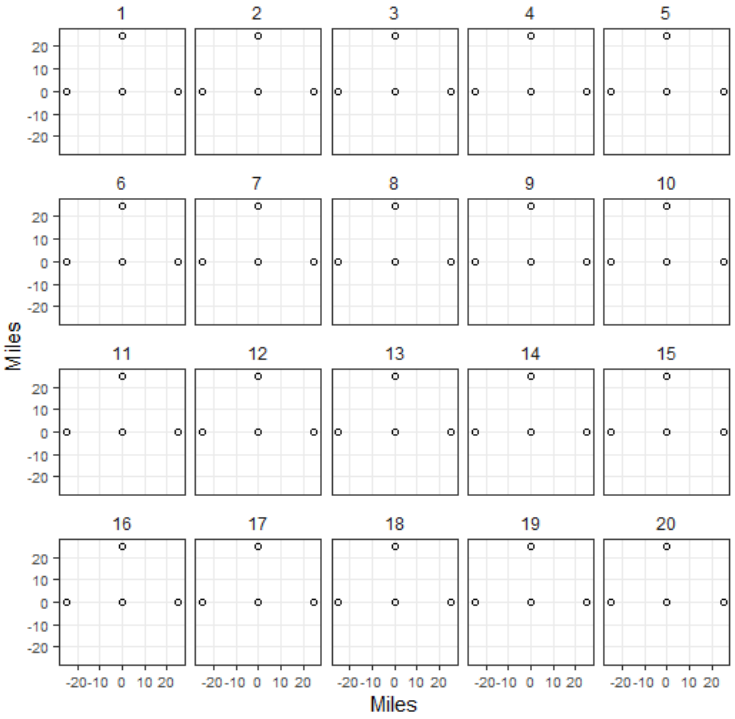

Figure C-104. Zero-year delay, 0.2-Mtpa injection, 25-mi spacing. All values less than 1 psi.

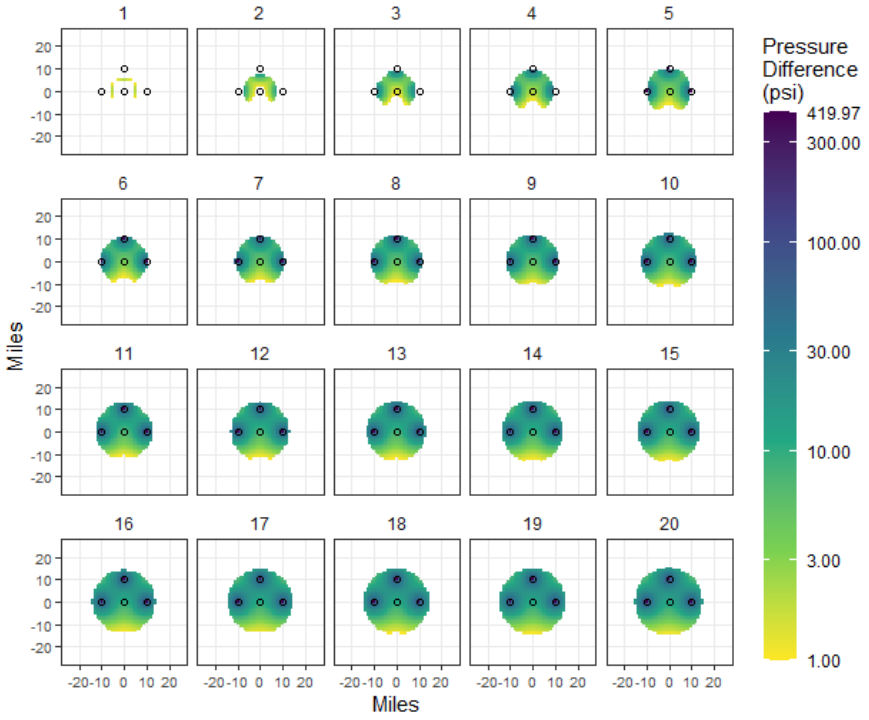

Figure C-105. Zero-year delay, 1-Mtpa injection, 10-mi spacing.

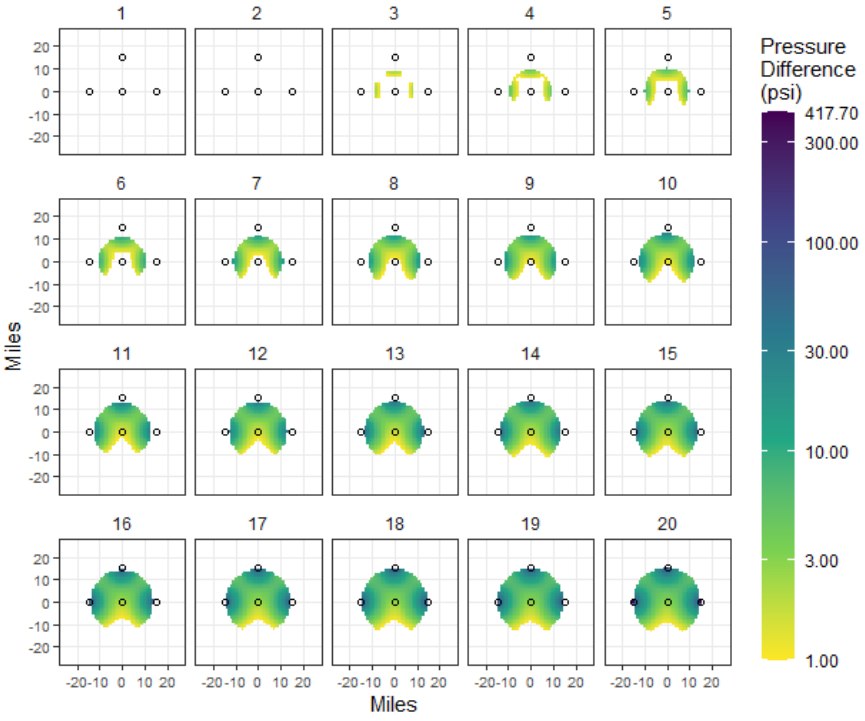

Figure C-106. Zero-year delay, 1-Mtpa injection, 15-mi spacing.

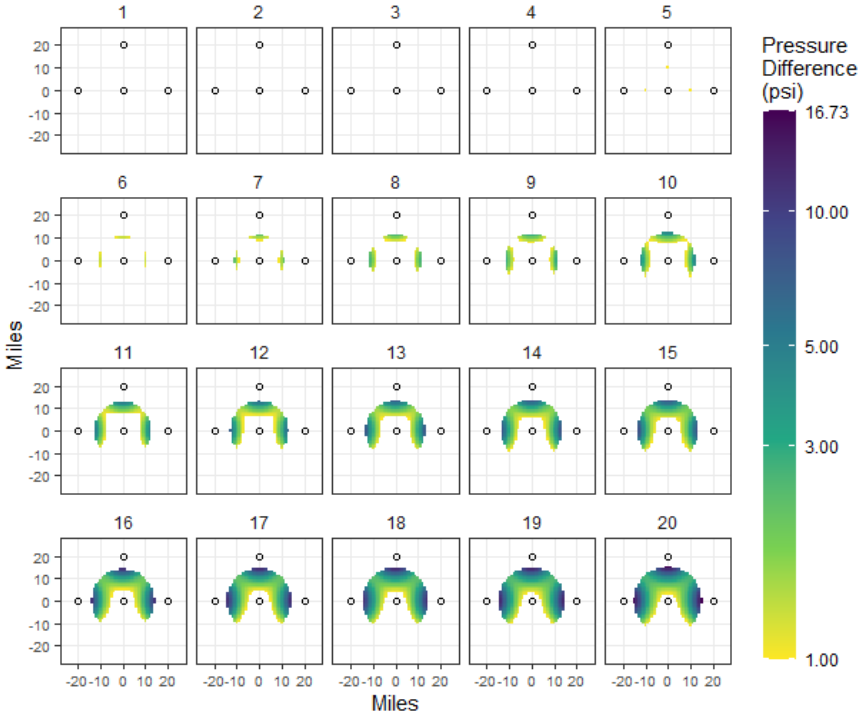

Figure C-107. Zero-year delay, 1-Mtpa injection, 20-mi spacing.

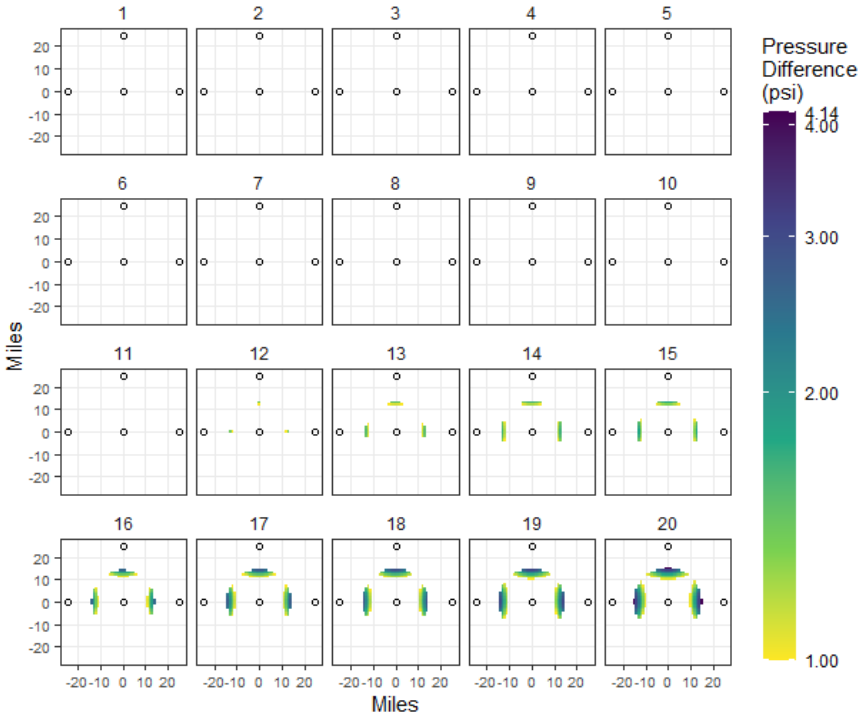

Figure C-108. Zero-year delay, 1-Mtpa injection, 25-mi spacing.

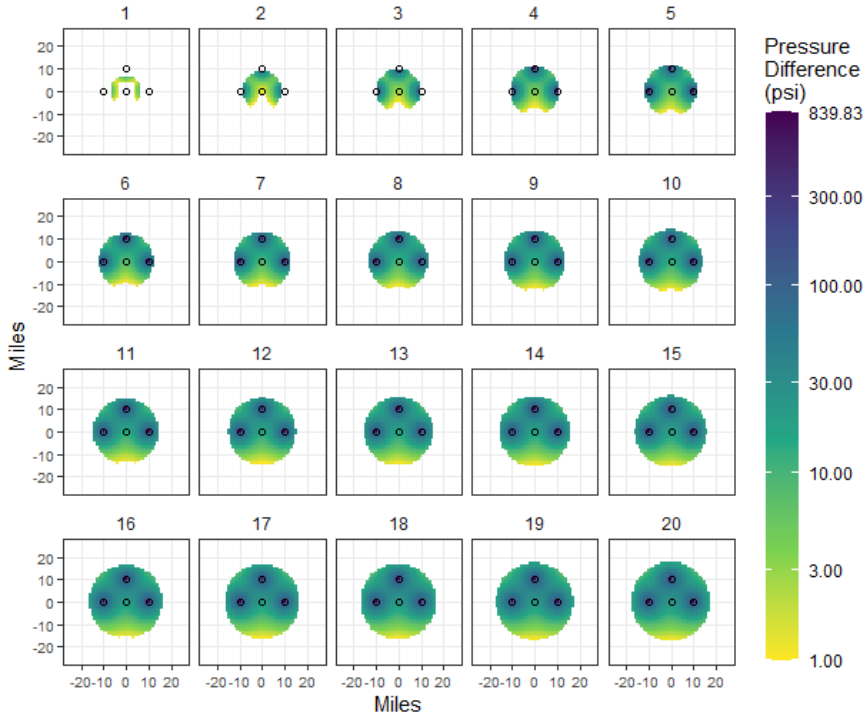

Figure C-109. Zero-year delay, 2-Mtpa injection, 10-mi spacing.

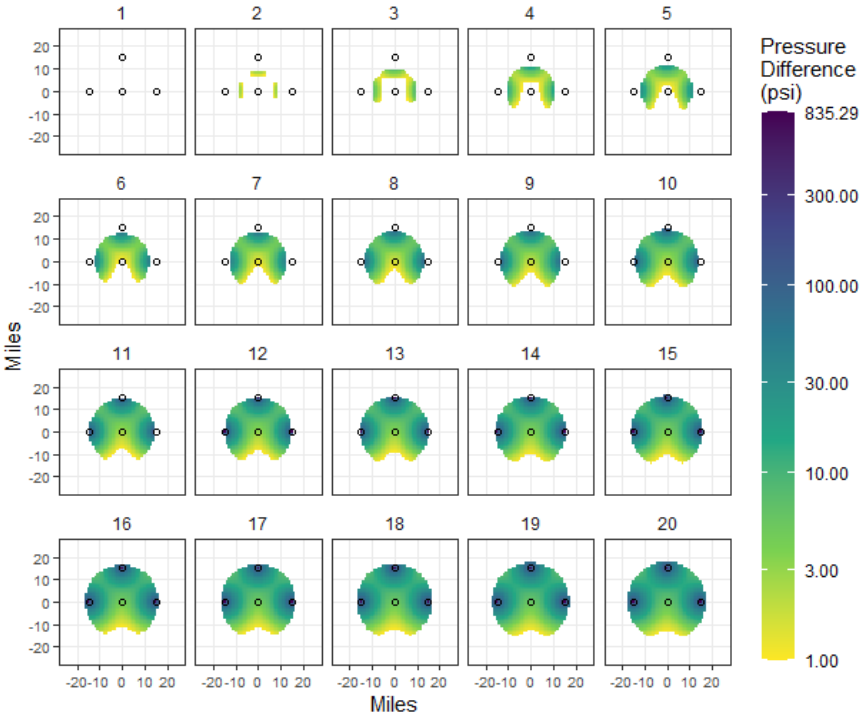

Figure C-110. Zero-year delay, 2-Mtpa injection, 15-mi spacing.

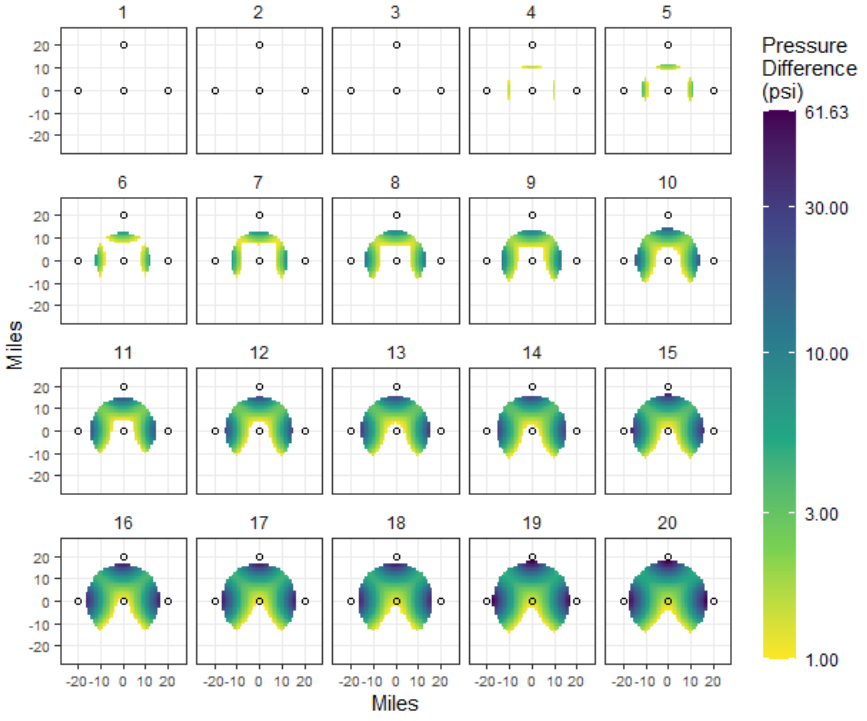

Figure C-111. Zero-year delay, 2-Mtpa injection, 20-mi spacing.

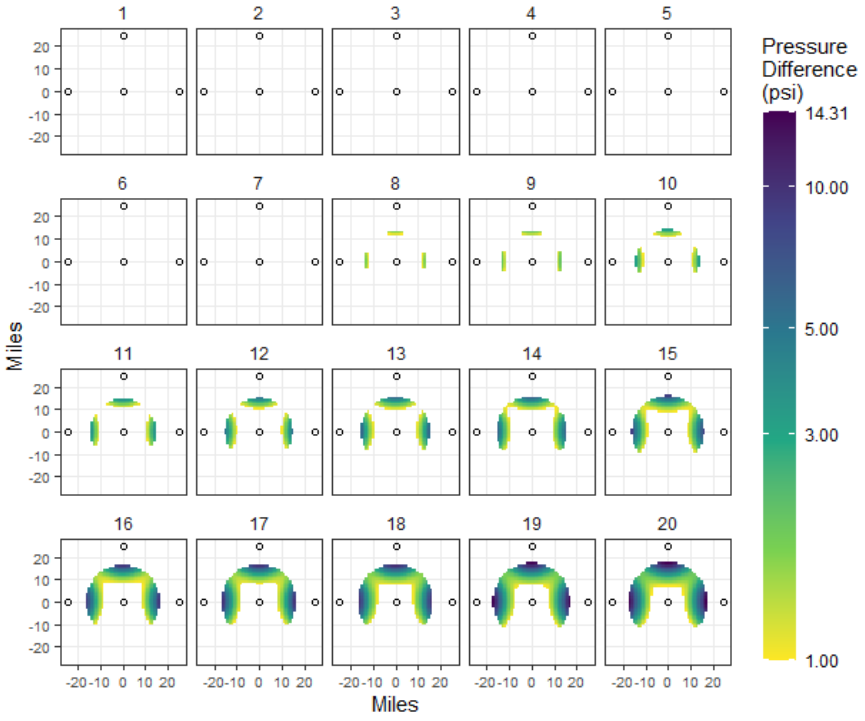

Figure C-112. Zero-year delay, 2-Mtpa injection, 25-mi spacing.

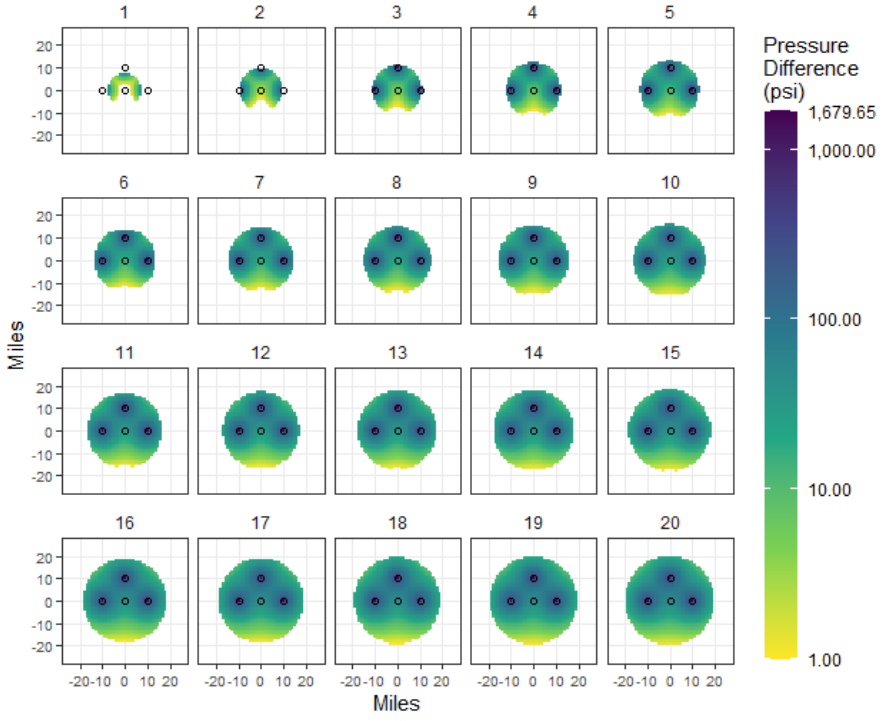

Figure C-113. Zero-year delay, 4-Mtpa injection, 10-mi spacing.

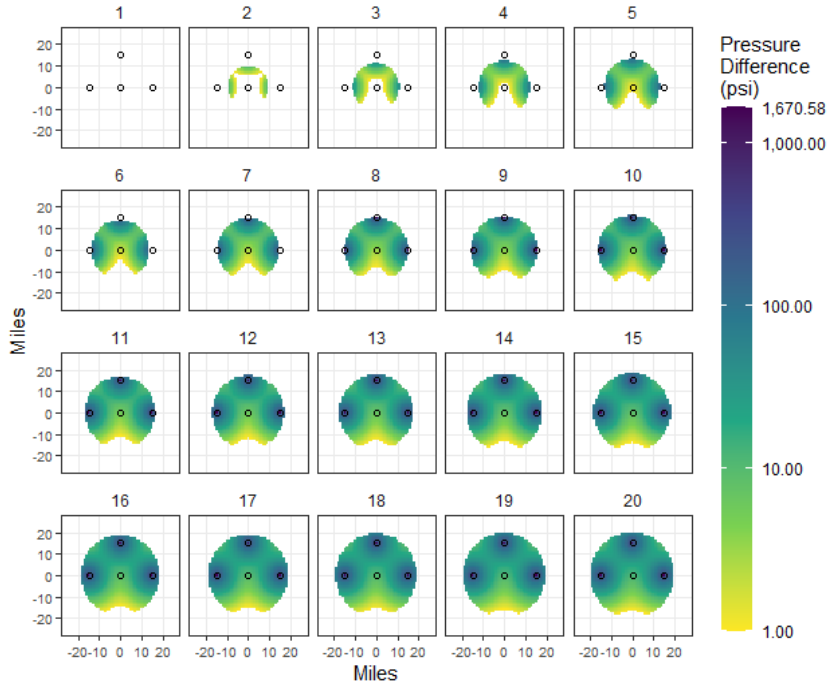

Figure C-114. Zero-year delay, 4-Mtpa injection, 15-mi spacing.

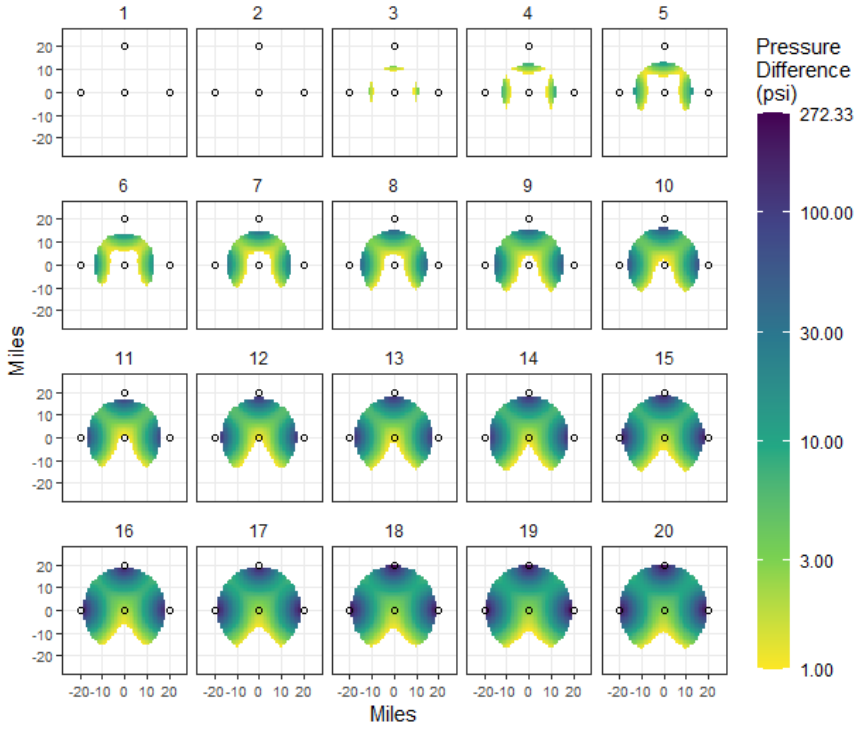

Figure C-115. Zero-year delay, 4-Mtpa injection, 20-mi spacing.

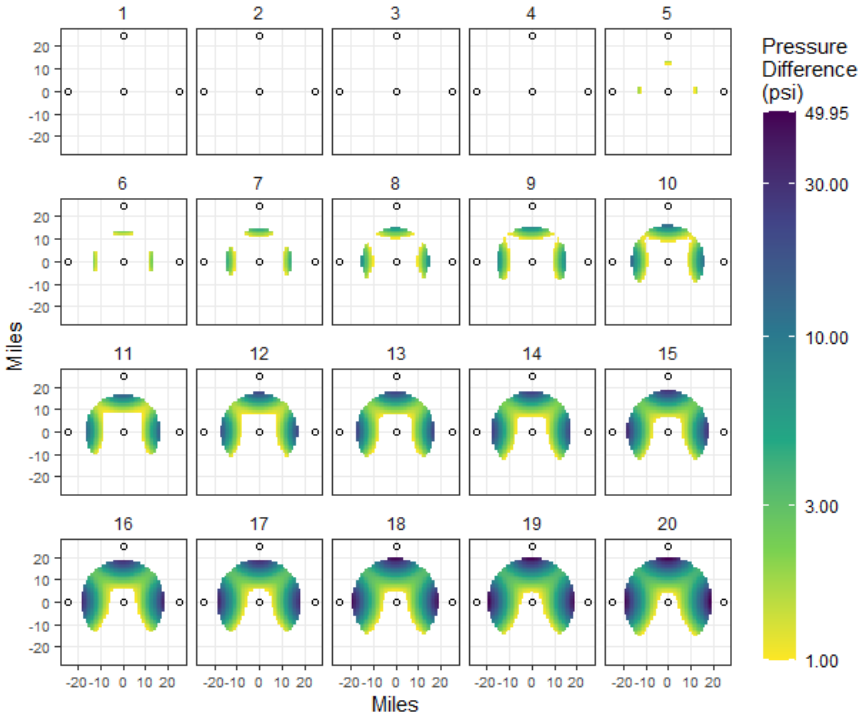

Figure C-116. Zero-year delay, 4-Mtpa injection, 25-mi spacing.

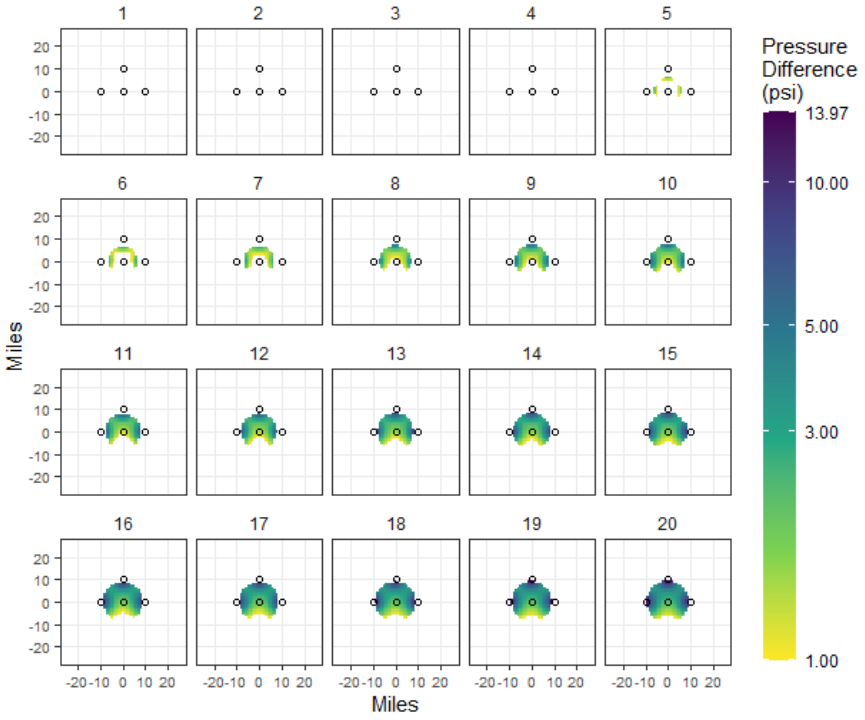

Figure C-117. Two-year delay, 0.2-Mtpa injection, 10-mi spacing.

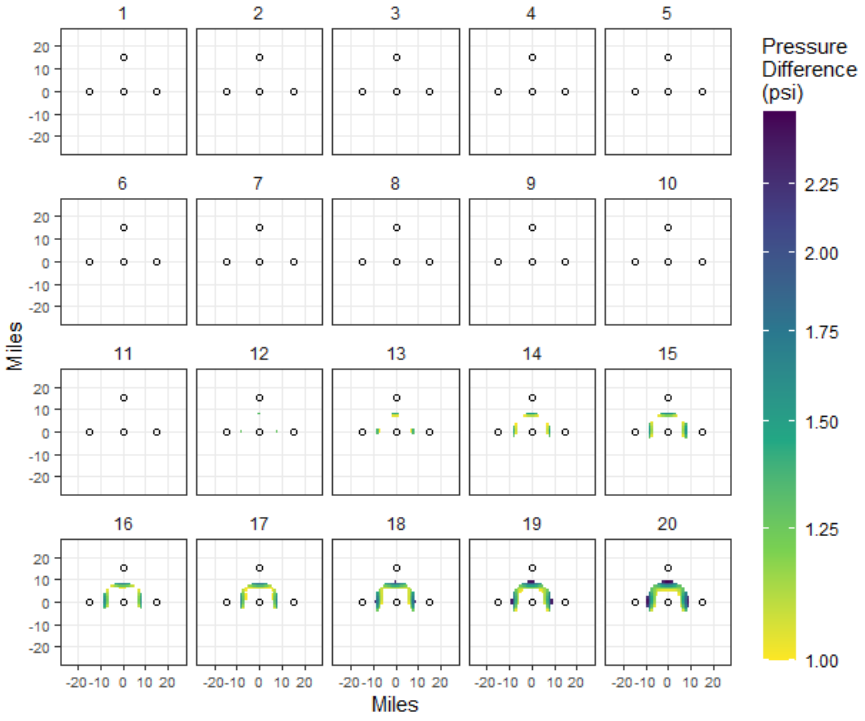

Figure C-118. Two-year delay, 0.2-Mtpa injection, 15-mi spacing.

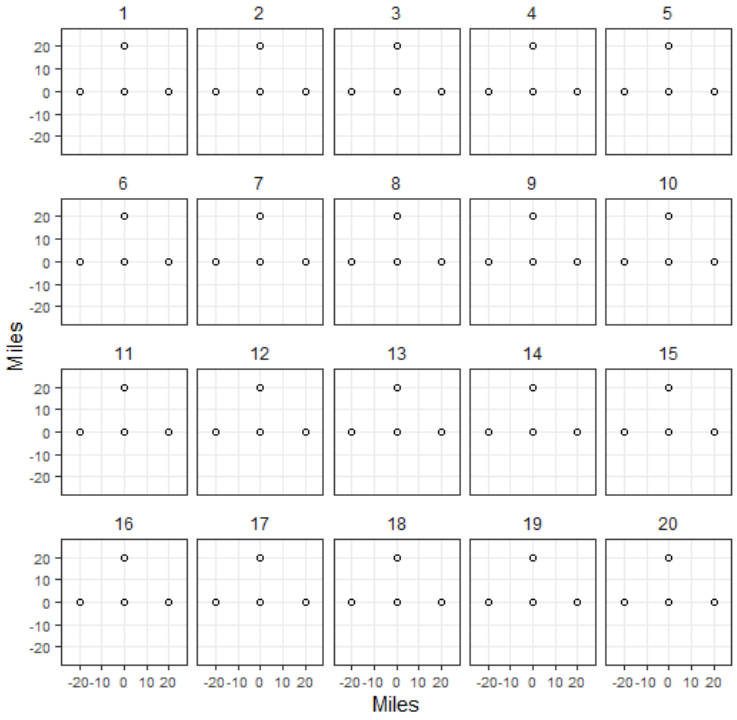

Figure C-119. Two-year delay, 0.2-Mtpa injection, 20-mi spacing. All values less than 1 psi.

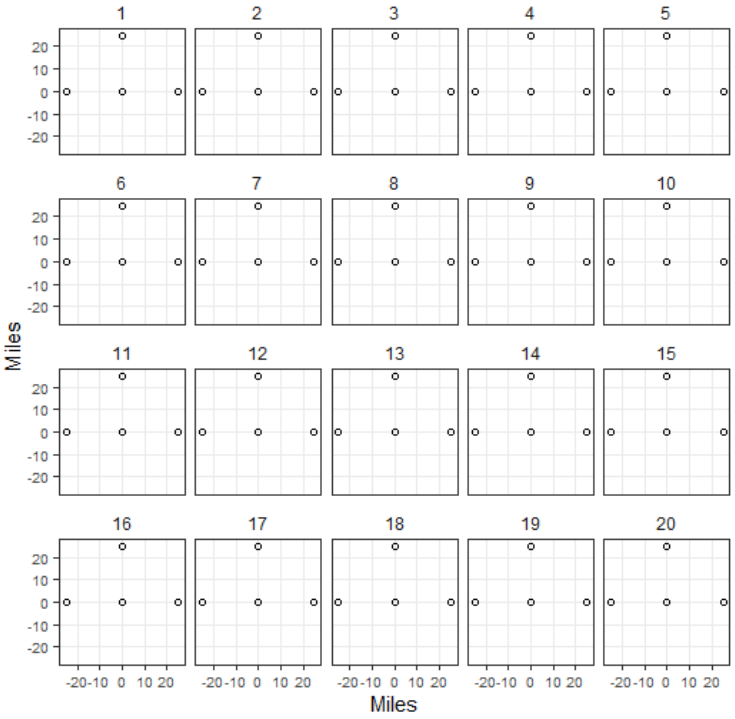

Figure C-120. Two-year delay, 0.2-Mtpa injection, 25-mi spacing. All values less than 1 psi.

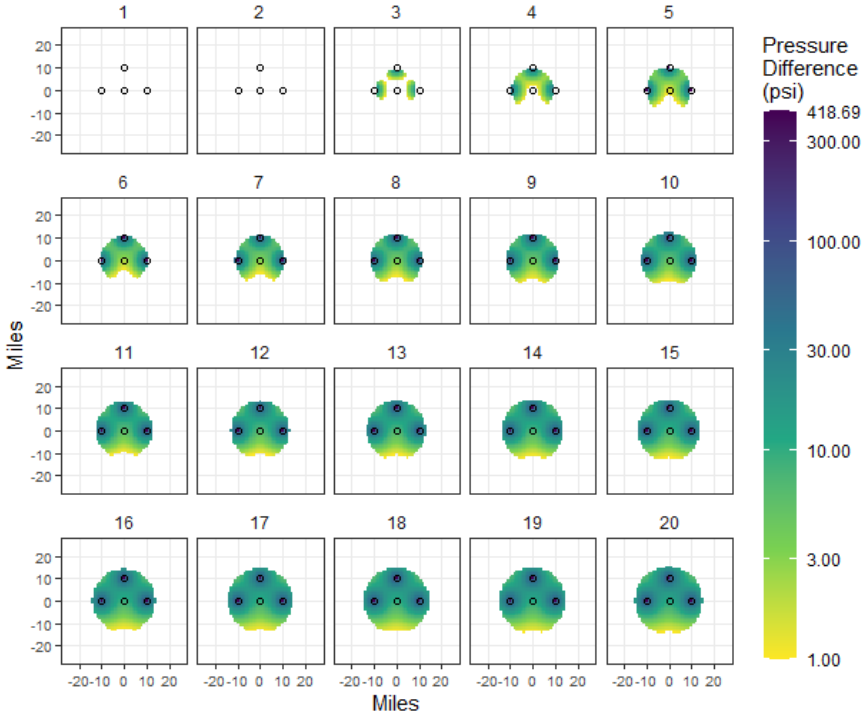

Figure C-121. Two-year delay, 1-Mtpa injection, 10-mi spacing.

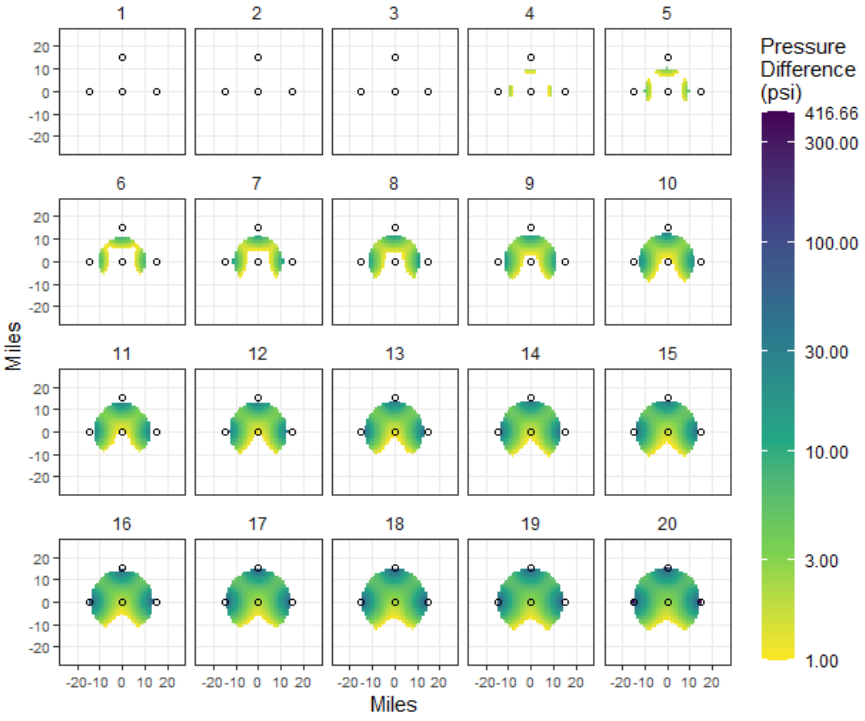

Figure C-122. Two-year delay, 1-Mtpa injection, 15-mi spacing.

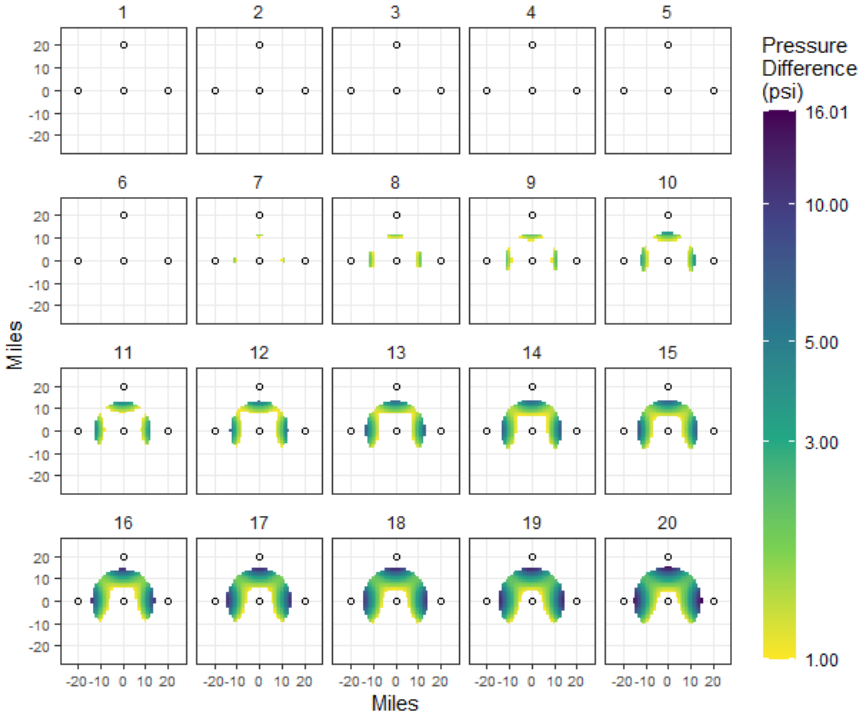

Figure C-123. Two-year delay, 1-Mtpa injection, 20-mi spacing.

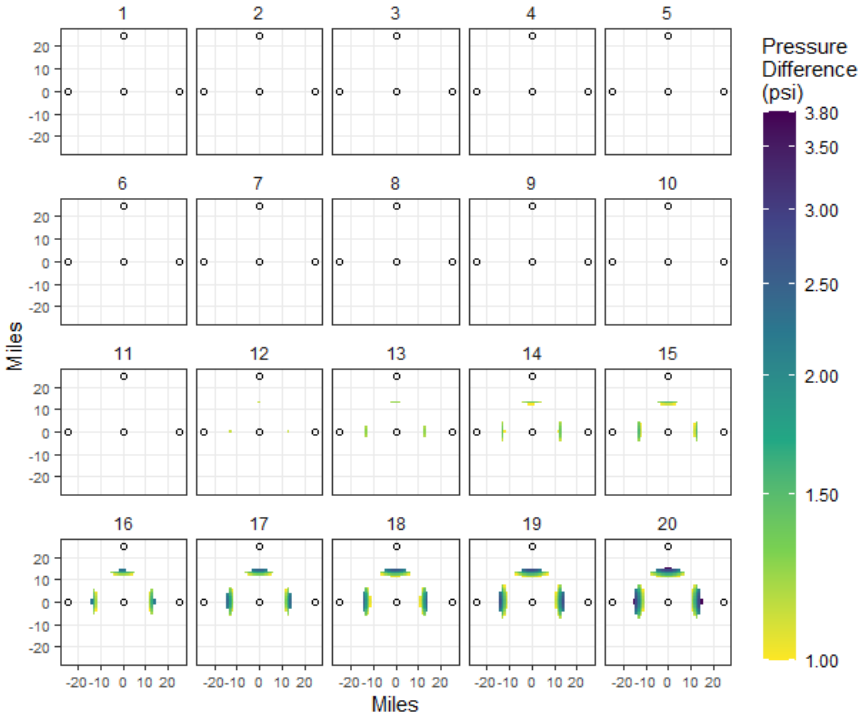

Figure C-124. Two-year delay, 1-Mtpa injection, 25-mi spacing.

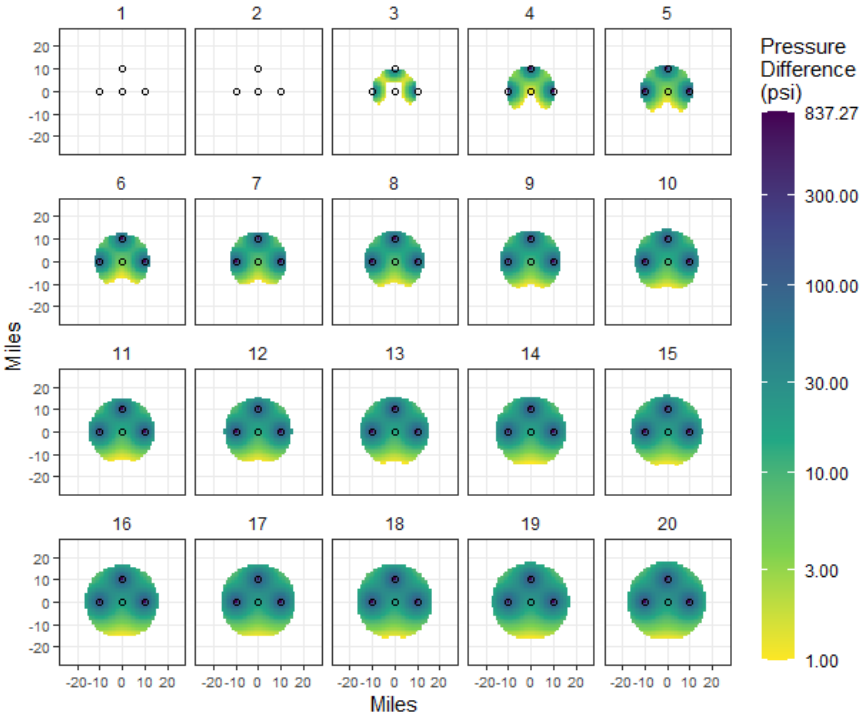

Figure C-125 Two-year delay, 2-Mtpa injection, 10-mi spacing.

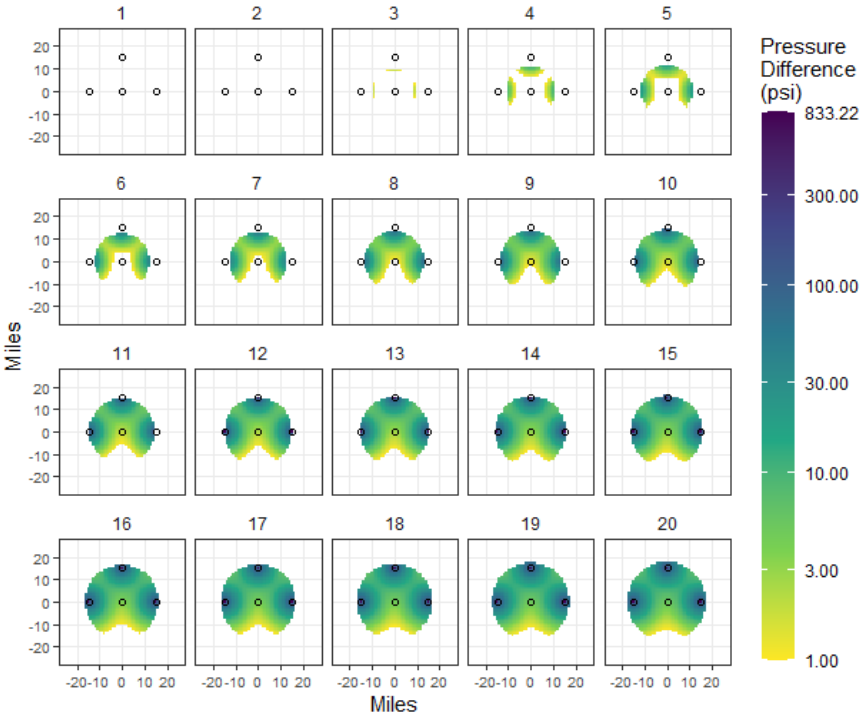

Figure C-126 Two-year delay, 2-Mtpa injection, 15-mi spacing.

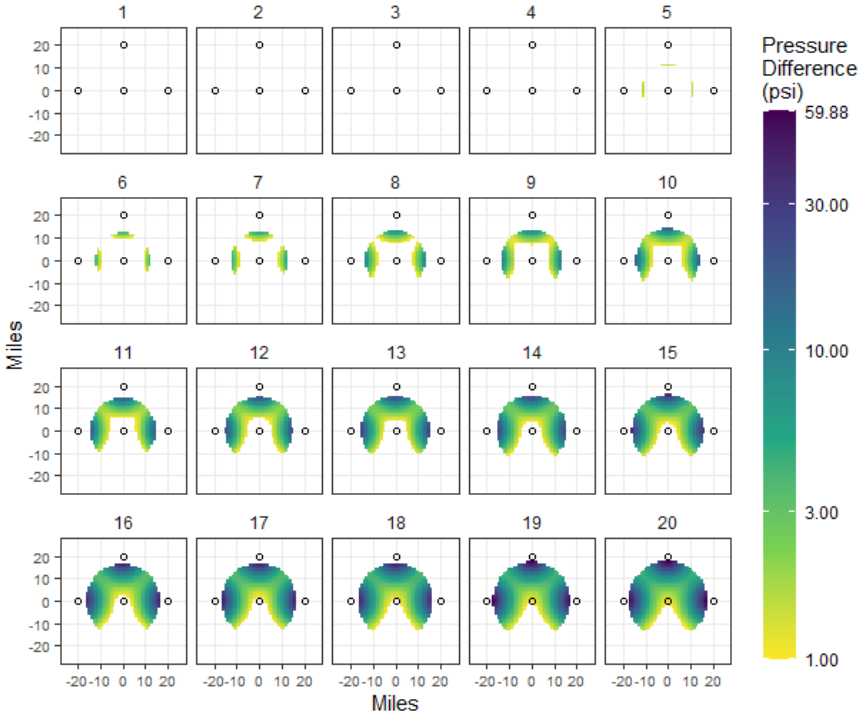

Figure C-127. Two-year delay, 2-Mtpa injection, 20-mi spacing.

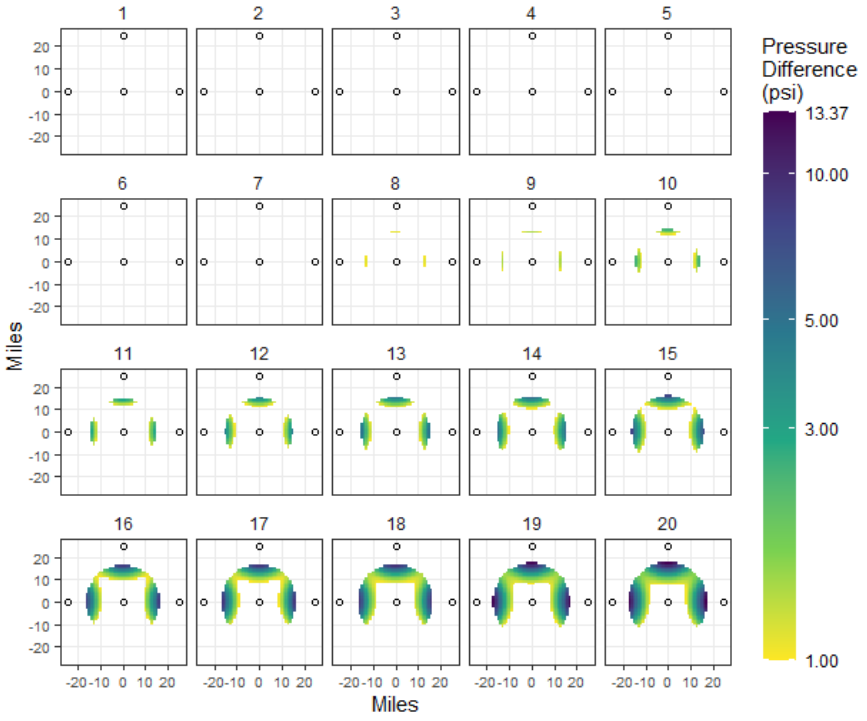

Figure C-128. Two-year delay, 2-Mtpa injection, 25-mi spacing.

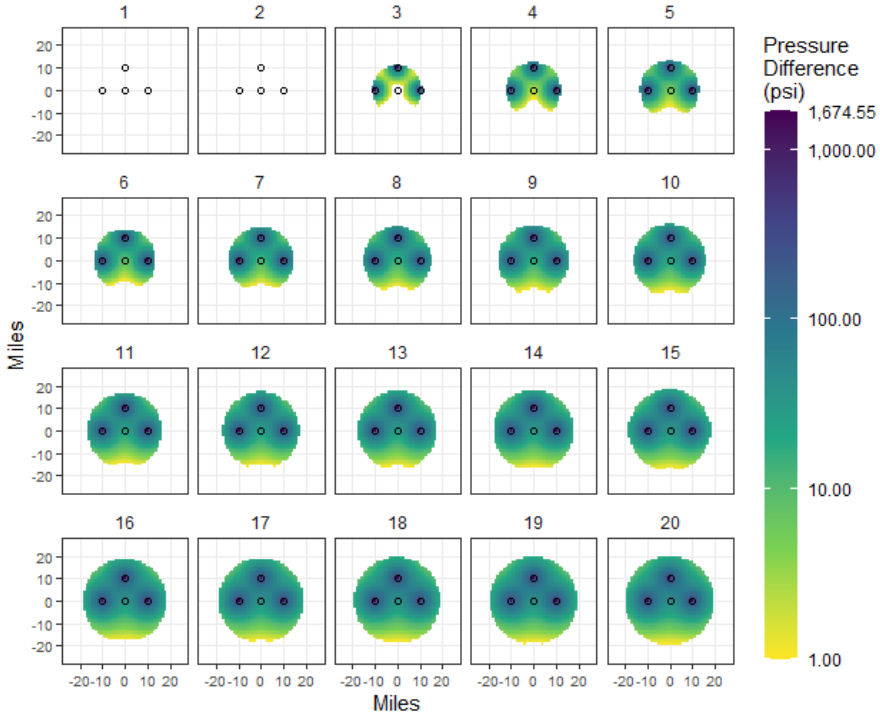

Figure C-129. Two-year delay, 4-Mtpa injection, 10-mi spacing.

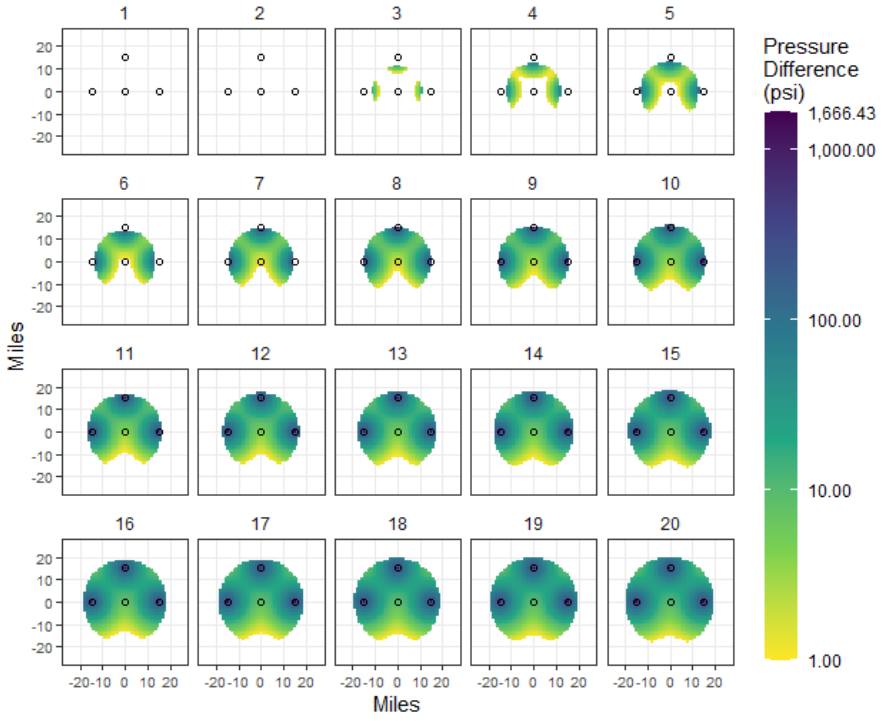

Figure C-130. Two-year delay, 4-Mtpa injection, 15-mi spacing.

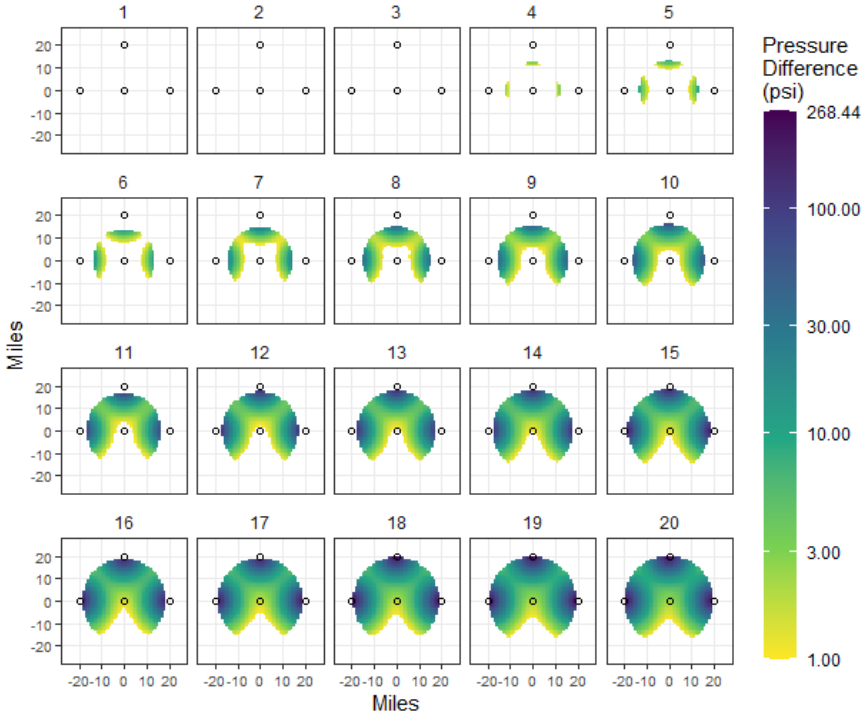

Figure C-131. Two-year delay, 4-Mtpa injection, 20-mi spacing.

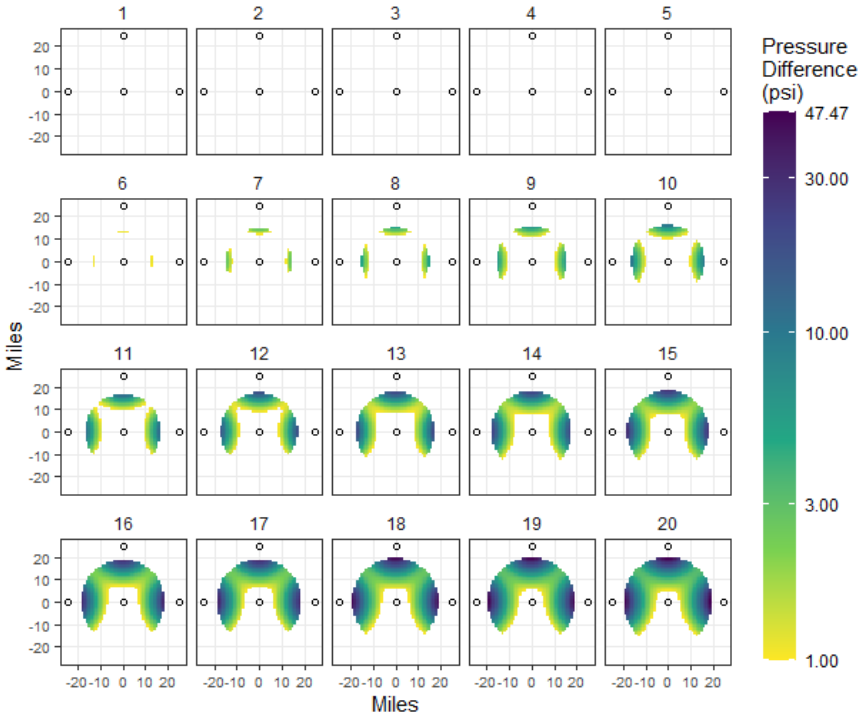

Figure C-132. Two-year delay, 4-Mtpa injection, 25-mi spacing.

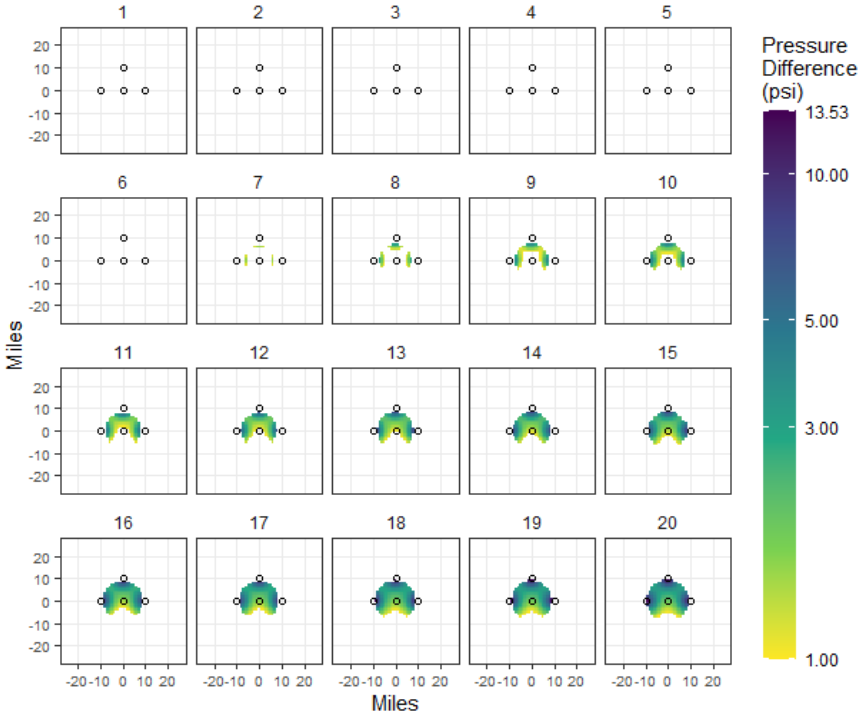

Figure C-133. Five-year delay, 0.2-Mtpa injection, 10-mi spacing.

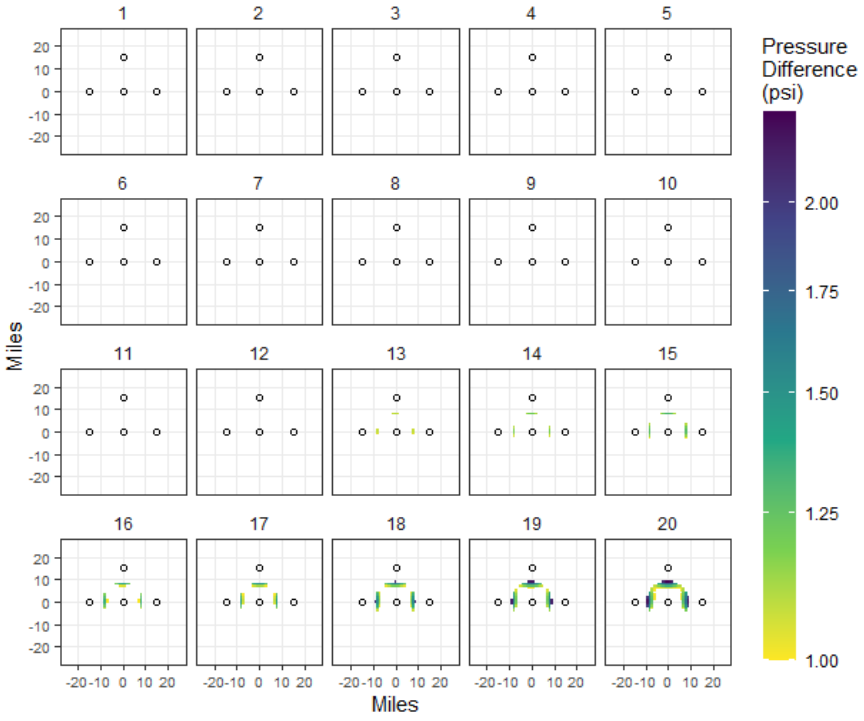

Figure C-134. Five-year delay, 0.2-Mtpa injection, 15-mi spacing.

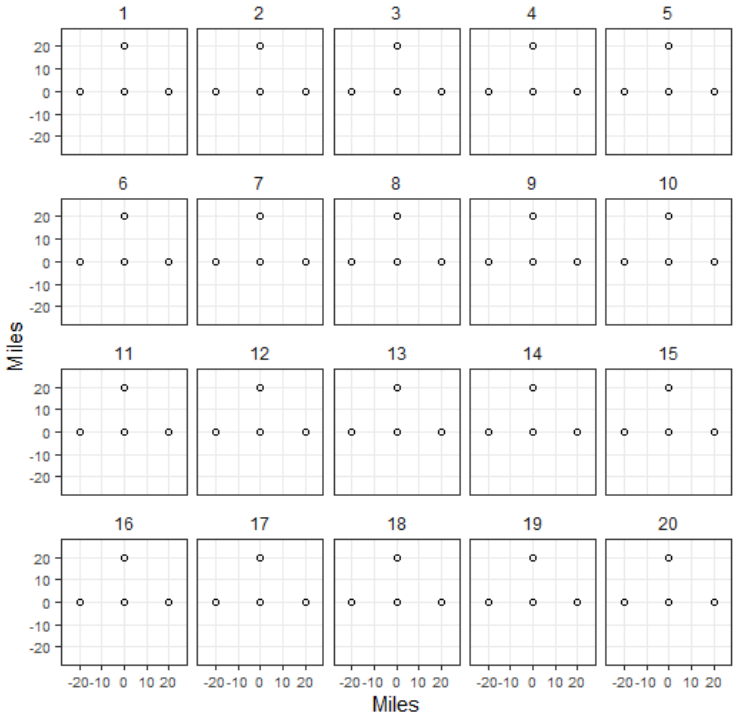

Figure C-135. Five-year delay, 0.2-Mtpa injection, 20-mi spacing. All values less than 1 psi.

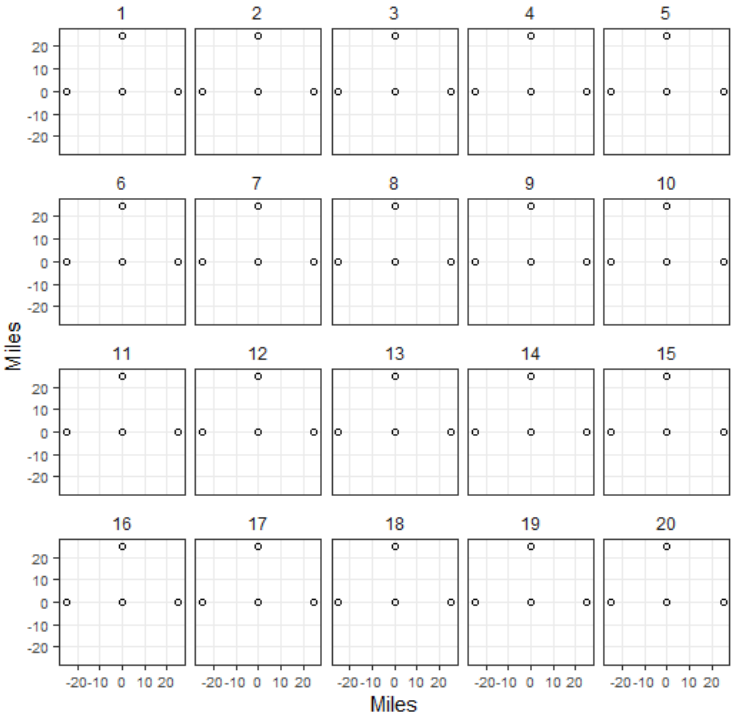

Figure C-136. Five-year delay, 0.2-Mtpa injection, 25-mi spacing. All values less than 1 psi.

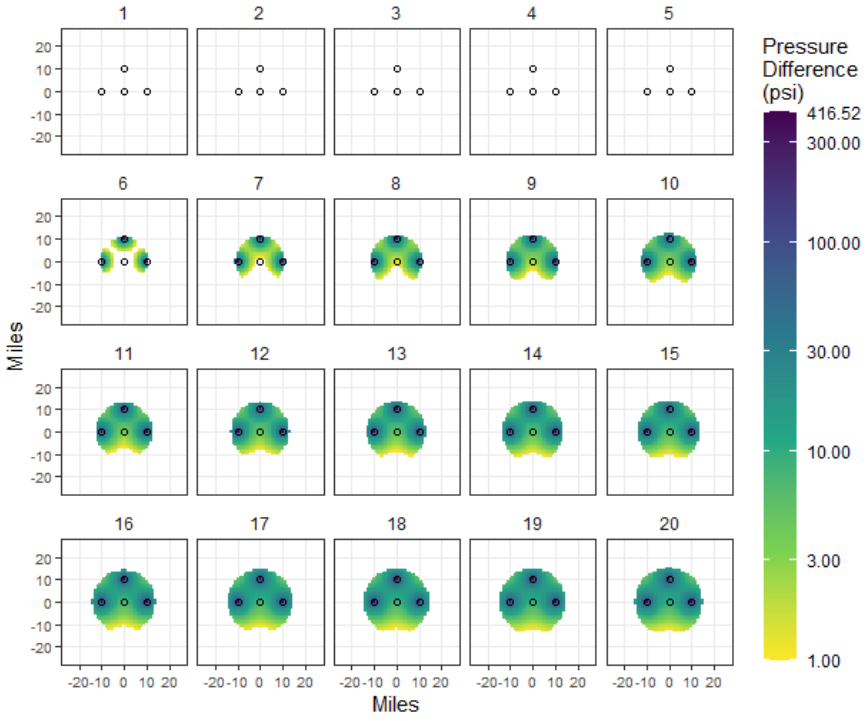

Figure C-137. Five-year delay, 1-Mtpa injection, 10-mi spacing.

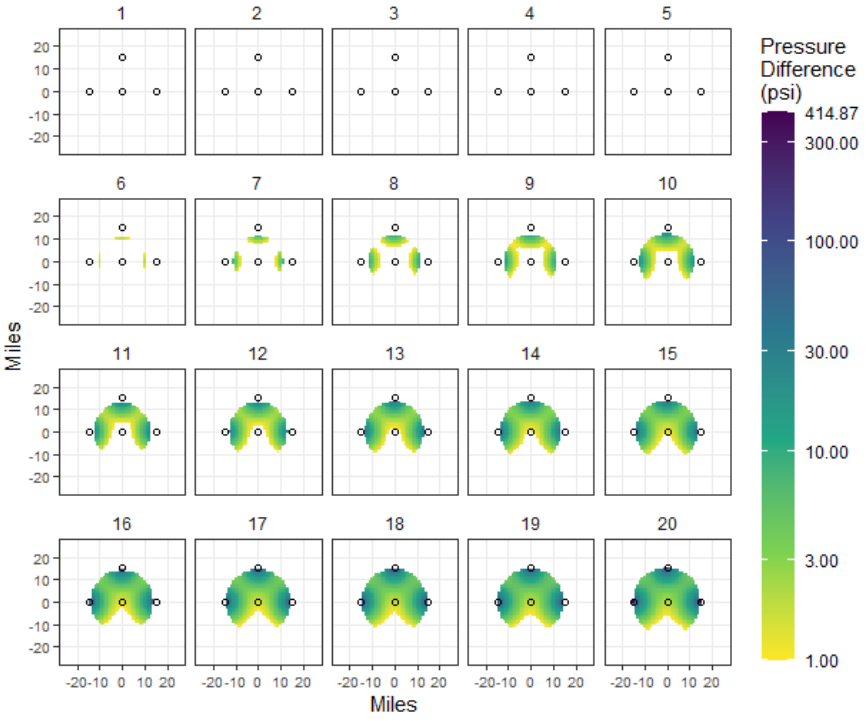

Figure C-138. Five-year delay, 1-Mtpa injection, 15-mi spacing.

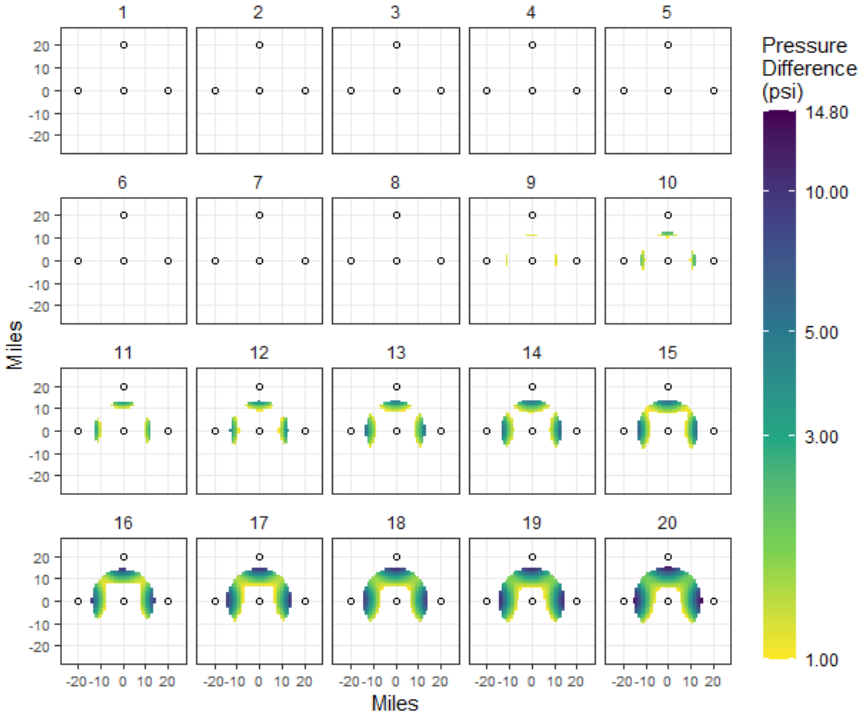

Figure C-139. Five-year delay, 1-Mtpa injection, 20-mi spacing.

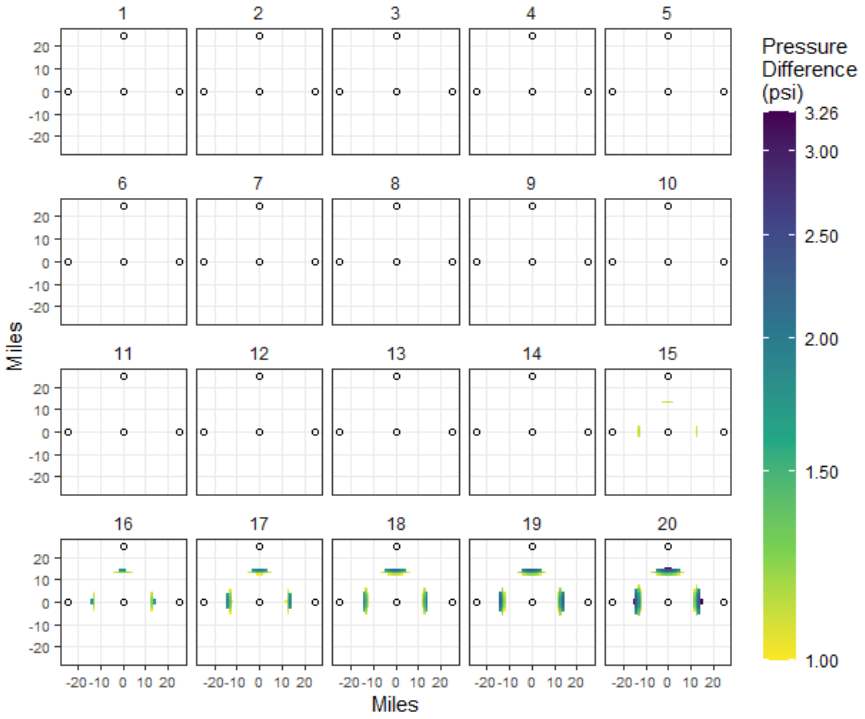

Figure C-140. Five-year delay, 1-Mtpa injection, 25-mi spacing.

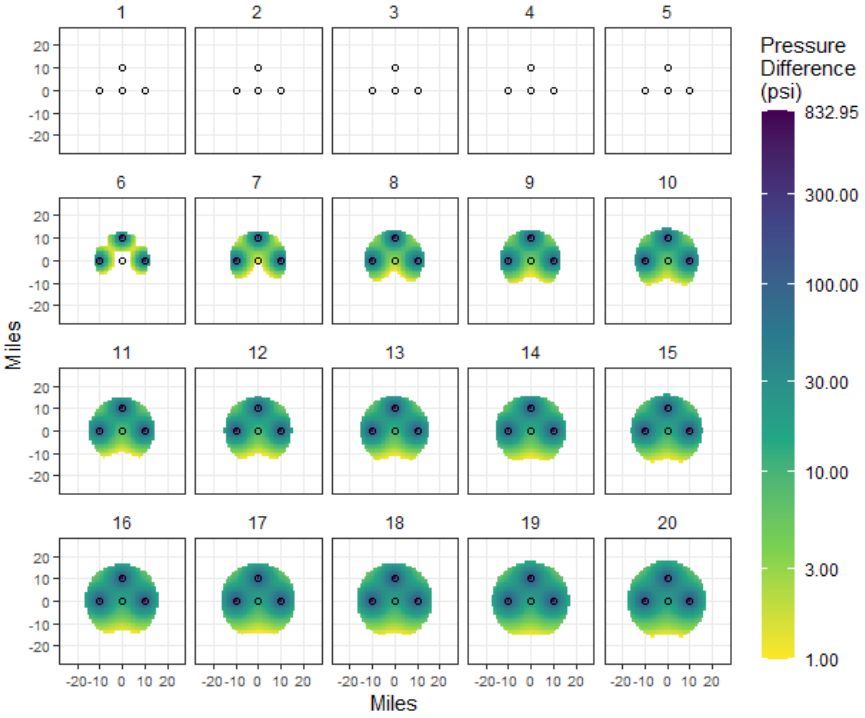

Figure C-141. Five-year delay, 2-Mtpa injection, 10-mi spacing.

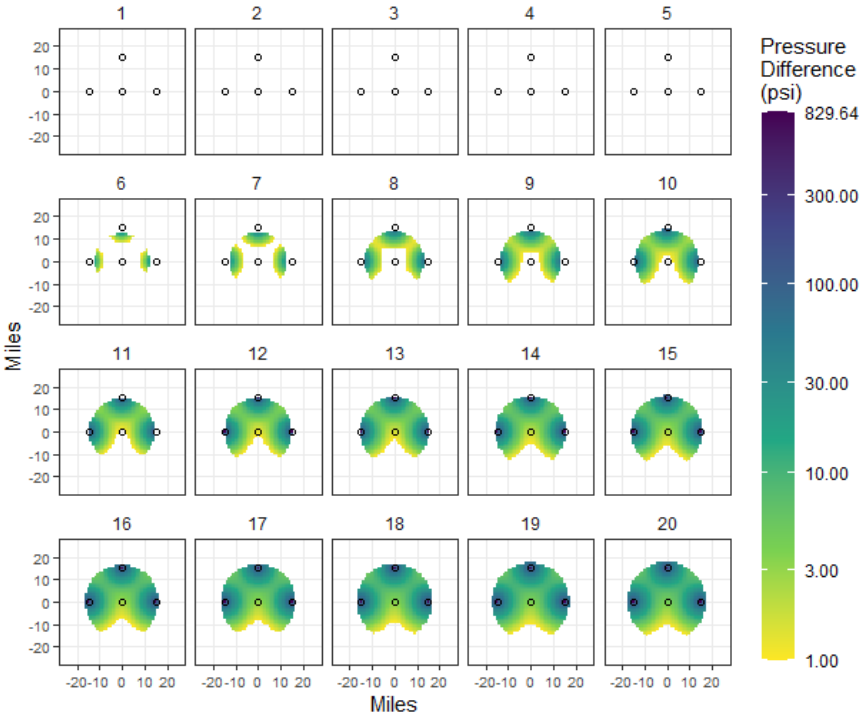

Figure C-142. Five-year delay, 2-Mtpa injection, 15-mi spacing.

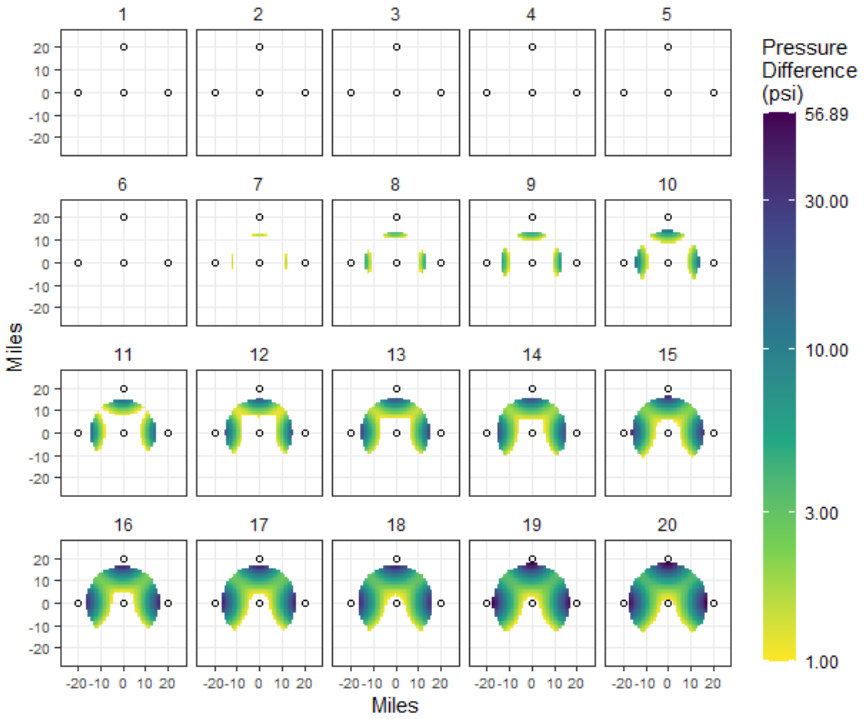

Figure C-143. Five-year delay, 2-Mtpa injection, 20-mi spacing.

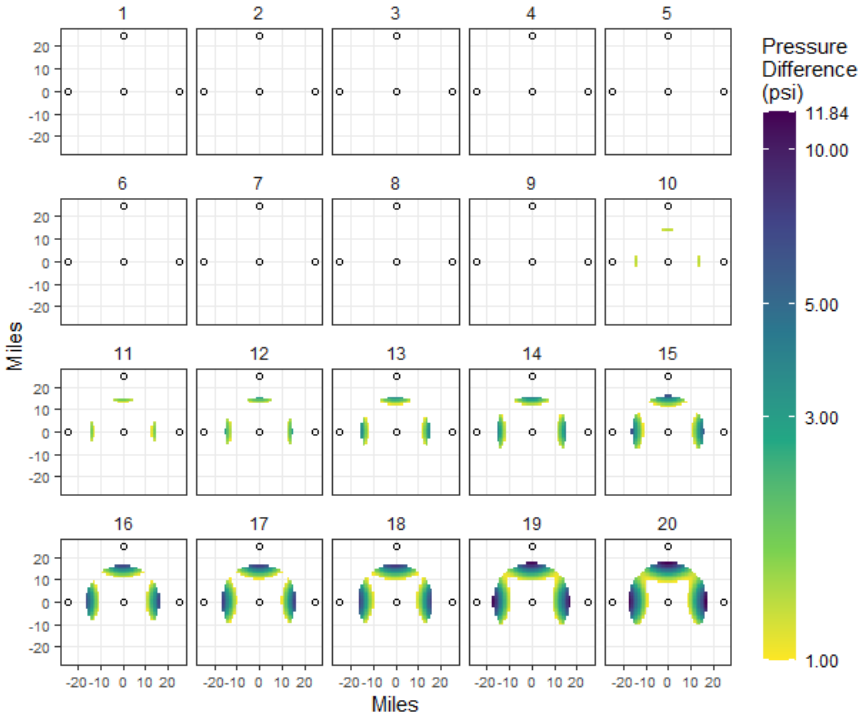

Figure C-144. Five-year delay, 2-Mtpa injection, 25-mi spacing.

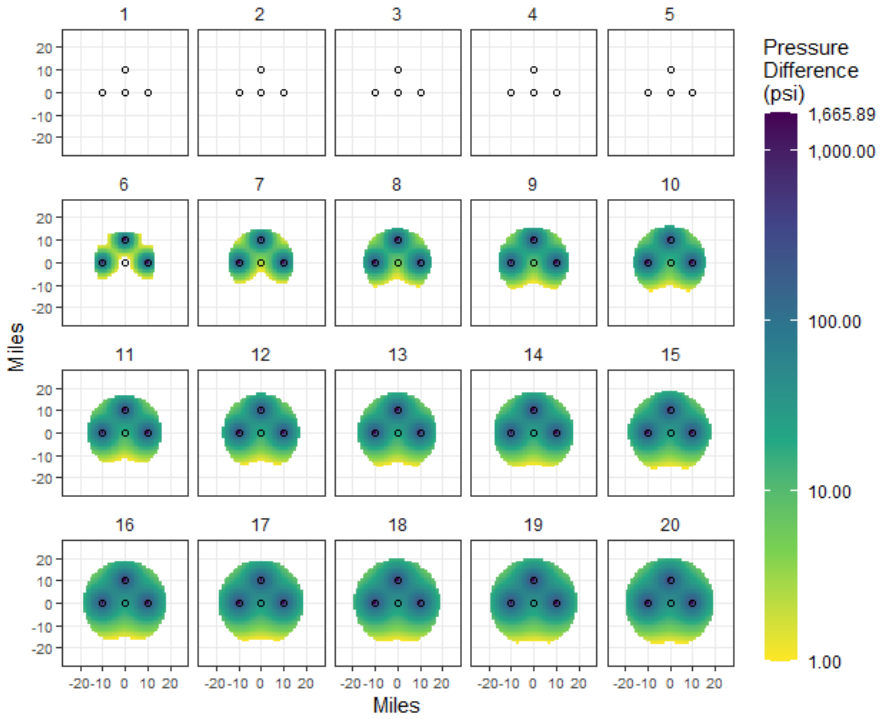

Figure C-145. Five-year delay, 4-Mtpa injection, 10-mi spacing.

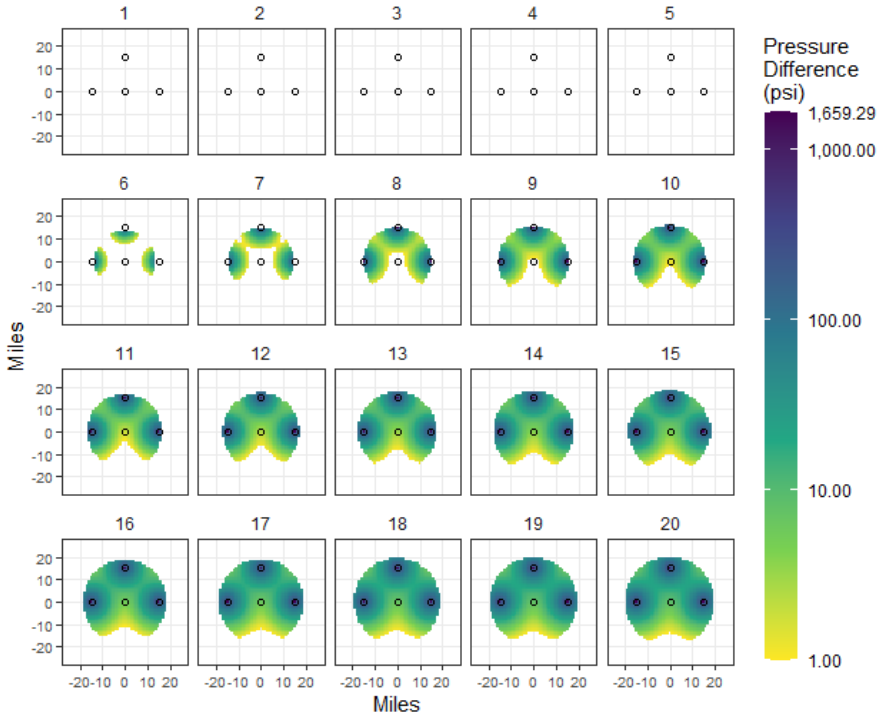

Figure C-146. Five-year delay, 4-Mtpa injection, 15-mi spacing.

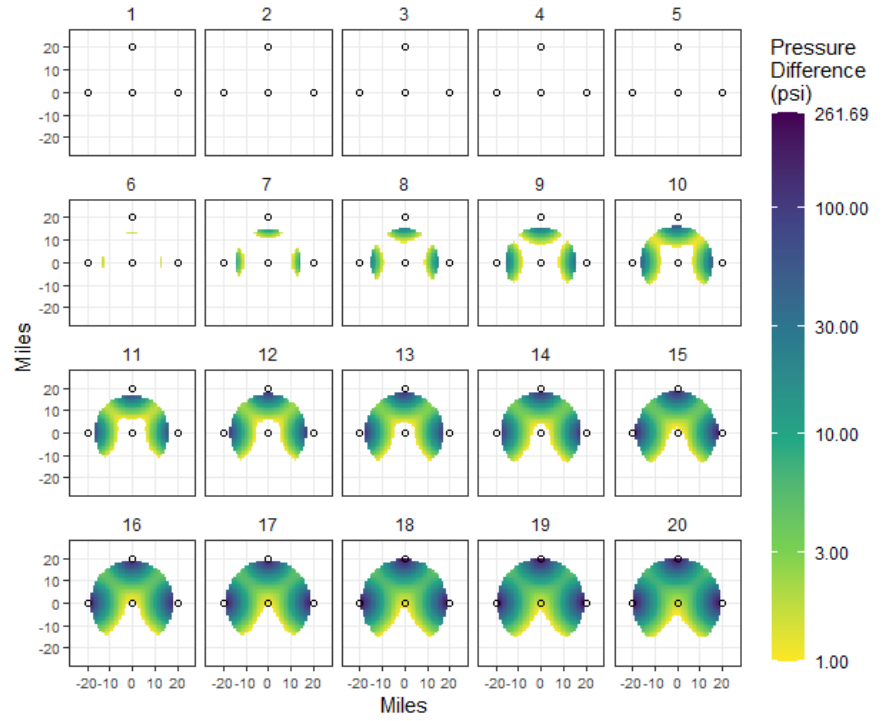

Figure C-147. Five-year delay, 4-Mtpa injection, 20-mi spacing.

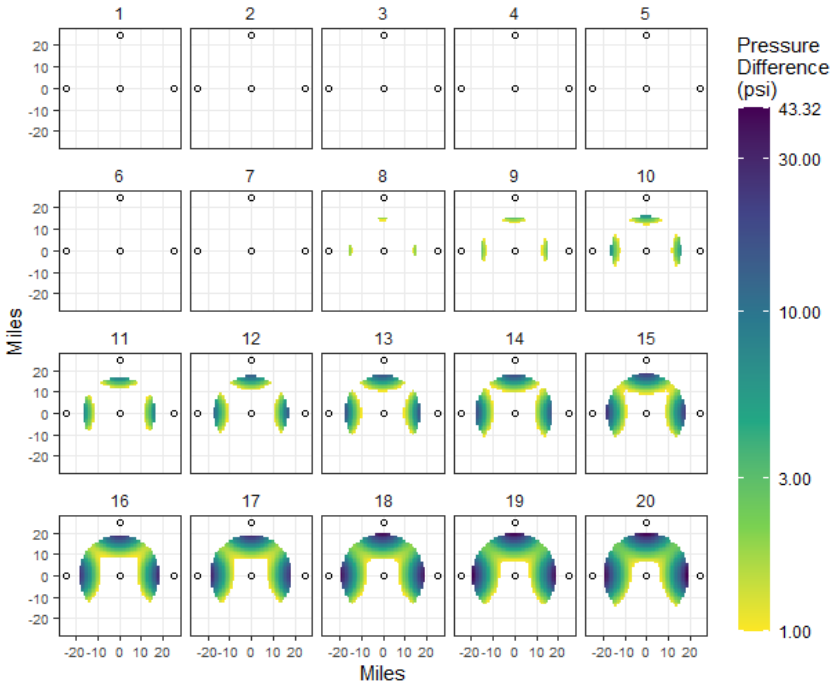

Figure C-148 Five-year delay, 4-Mtpa injection, 25-mi spacing.

SITES A, B, C, D, AND E

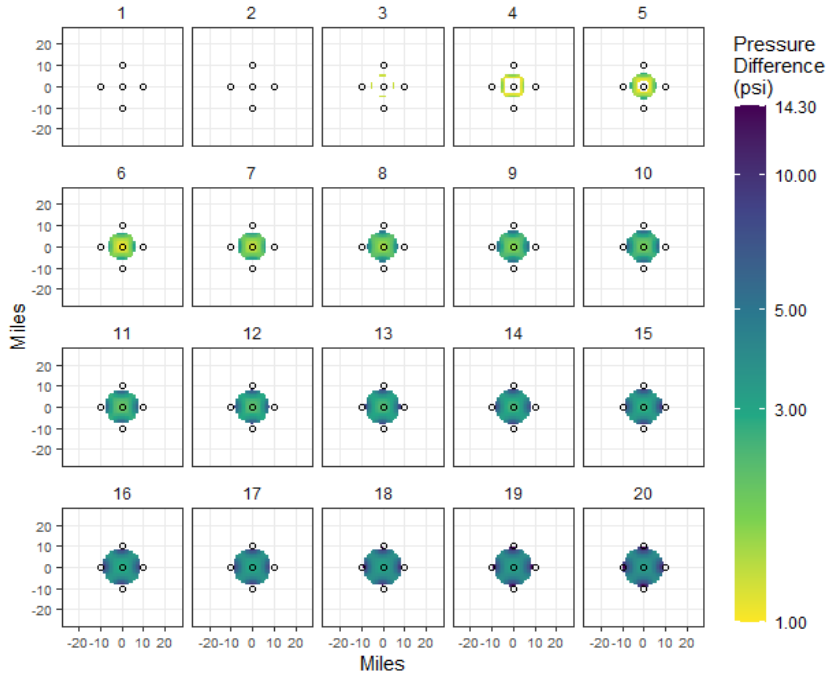

Figure C-149. Zero-year delay, 0.2-Mtpa injection, 10-mi spacing.

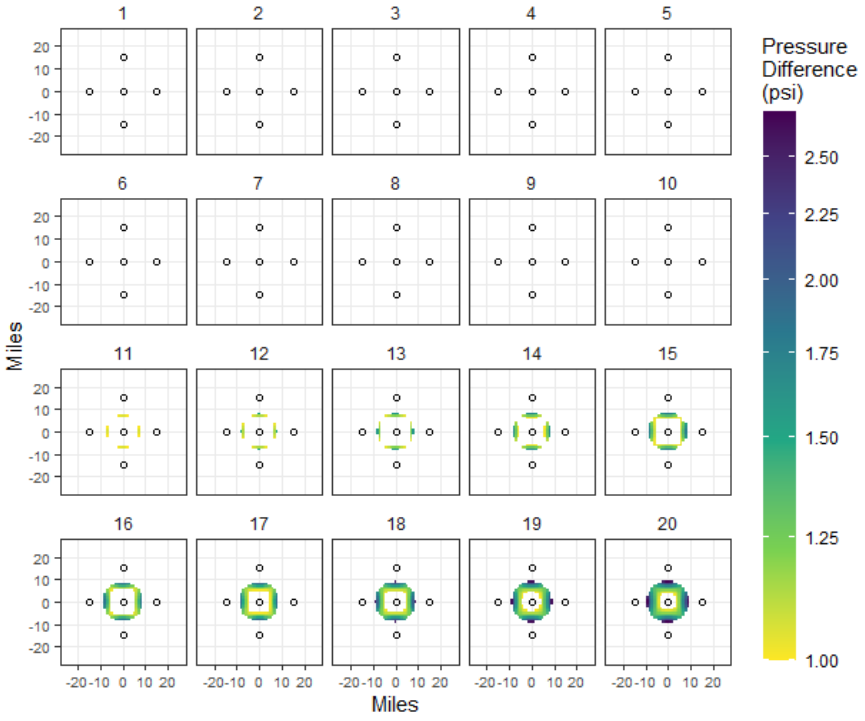

Figure C-150. Zero-year delay, 0.2-Mtpa injection, 15-mi spacing.

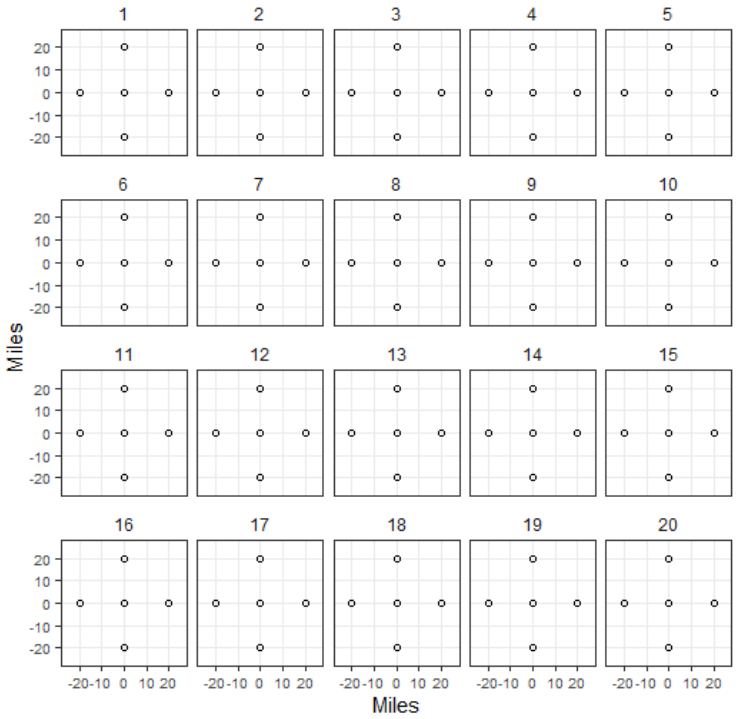

Figure C-151. Zero-year delay, 0.2-Mtpa injection, 20-mi spacing. All values less than 1 psi.

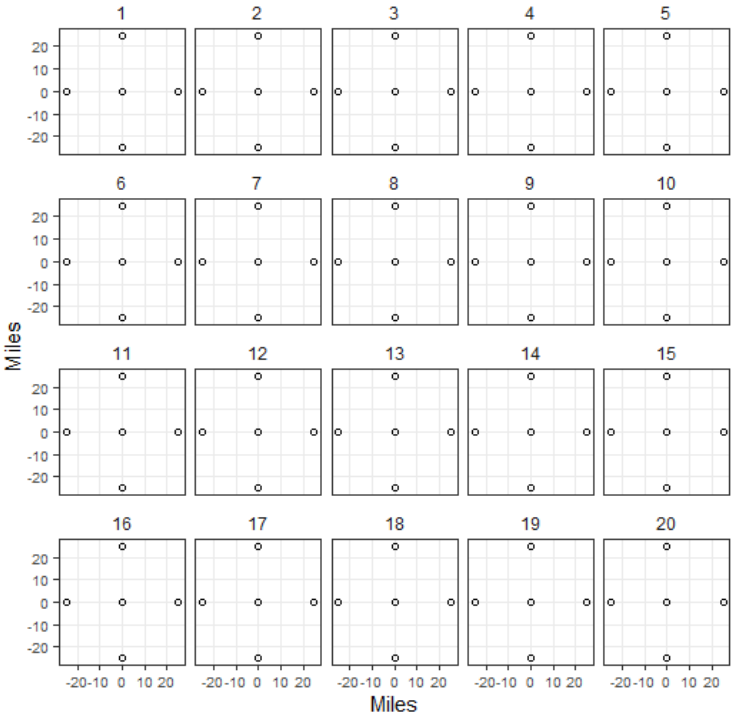

Figure C-152. Zero-year delay, 0.2-Mtpa injection, 25-mi spacing. All values less than 1 psi.

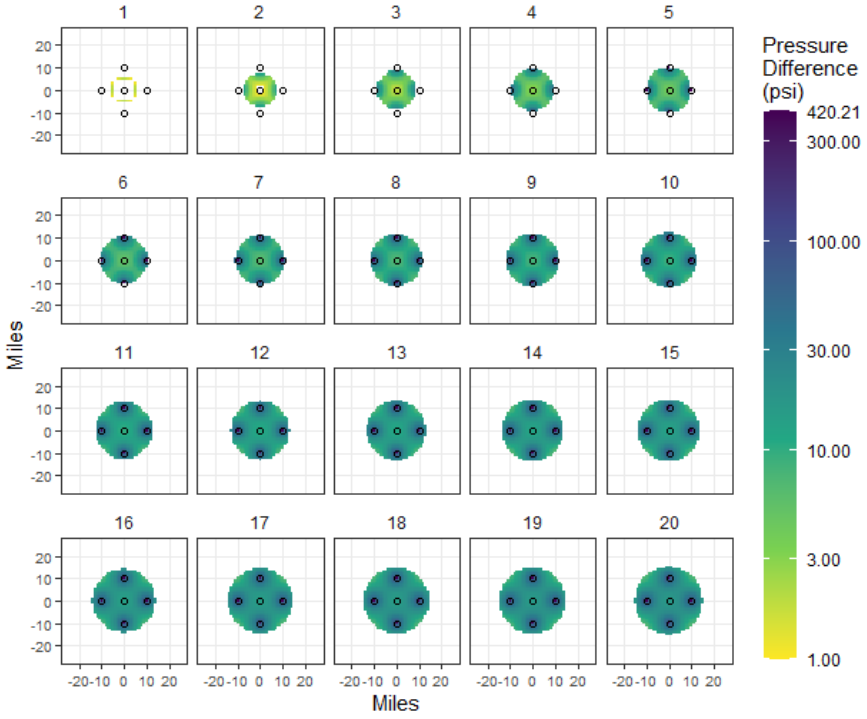

Figure C-153. Zero-year delay, 1-Mtpa injection, 10-mi spacing.

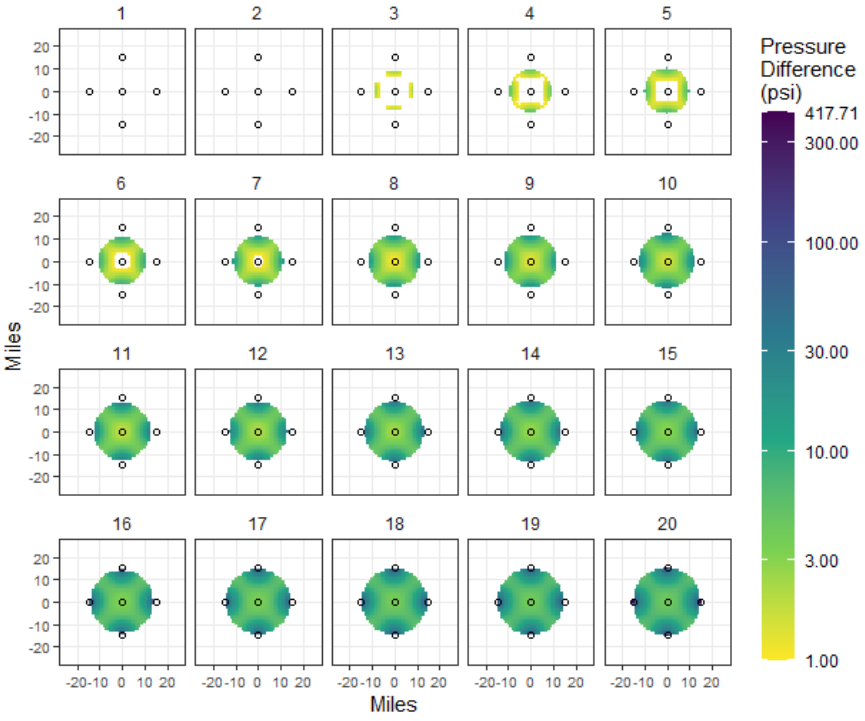

Figure C-154. Zero-year delay, 1-Mtpa injection, 15-mi spacing.

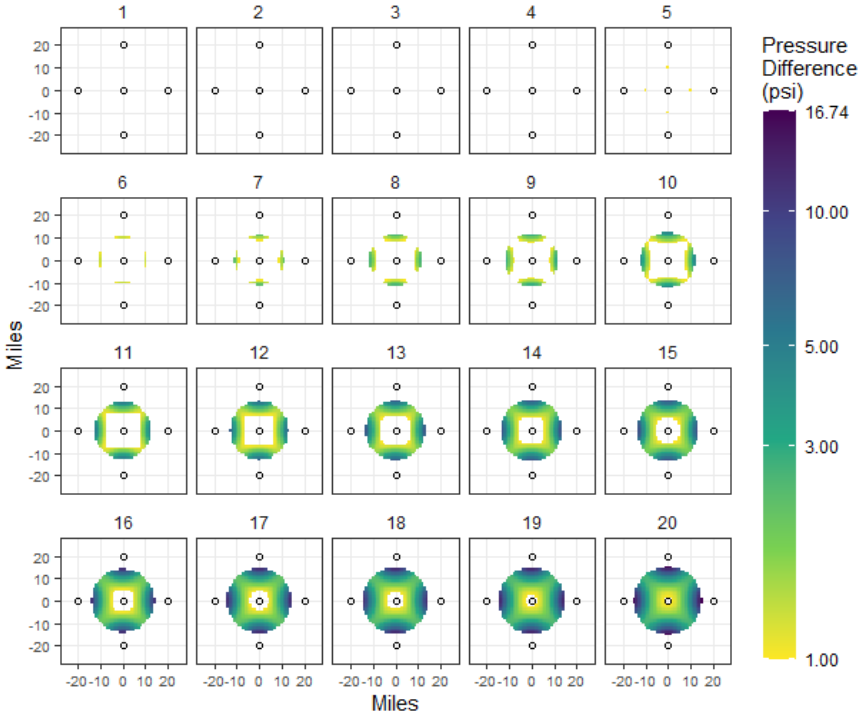

Figure C-155. Zero-year delay, 1-Mtpa injection, 20-mi spacing.

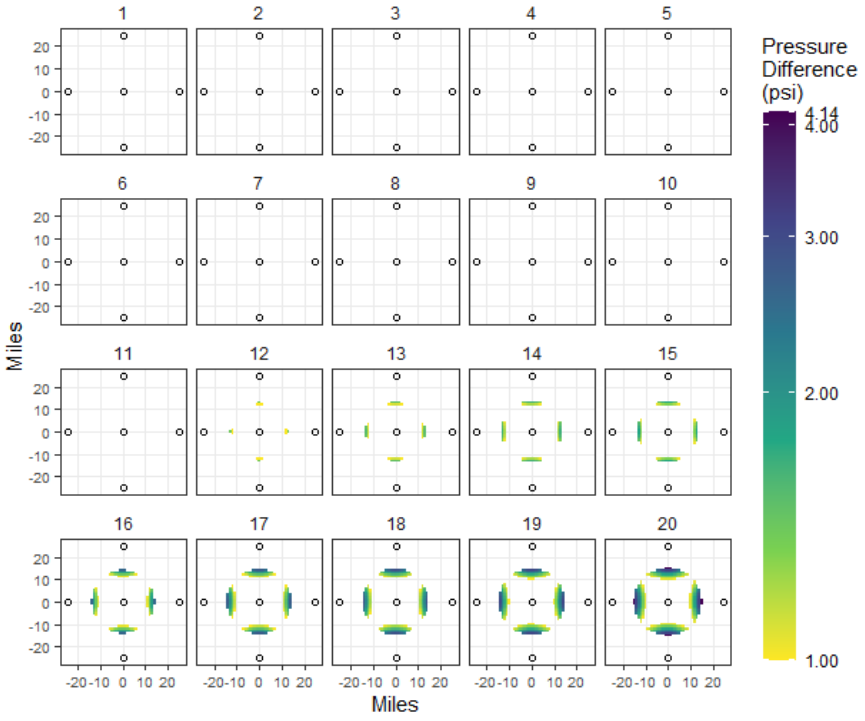

Figure C-156. Zero-year delay, 1-Mtpa injection, 25-mi spacing.

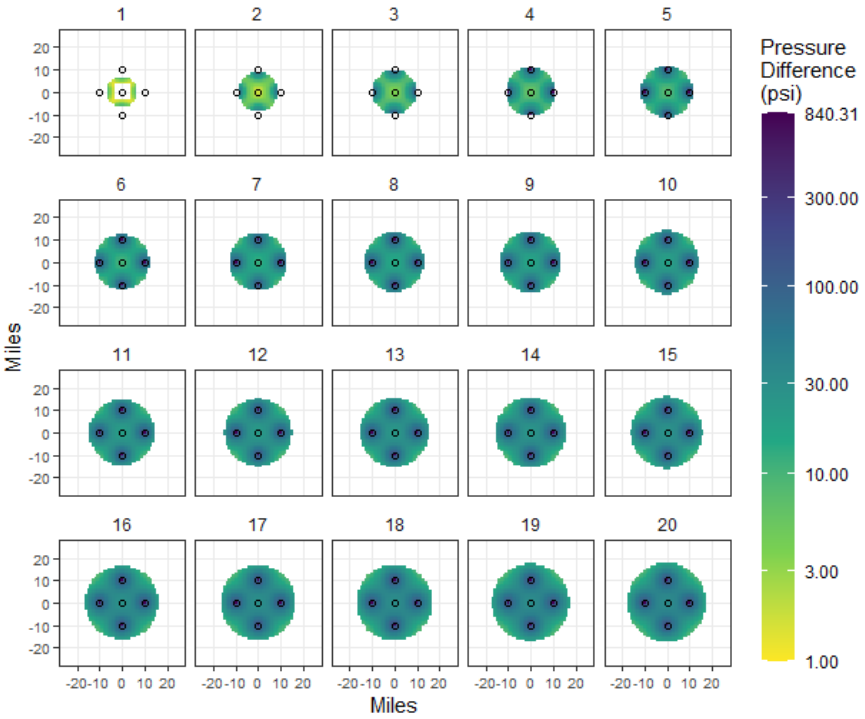

Figure C-157. Zero-year delay, 2-Mtpa injection, 10-mi spacing.

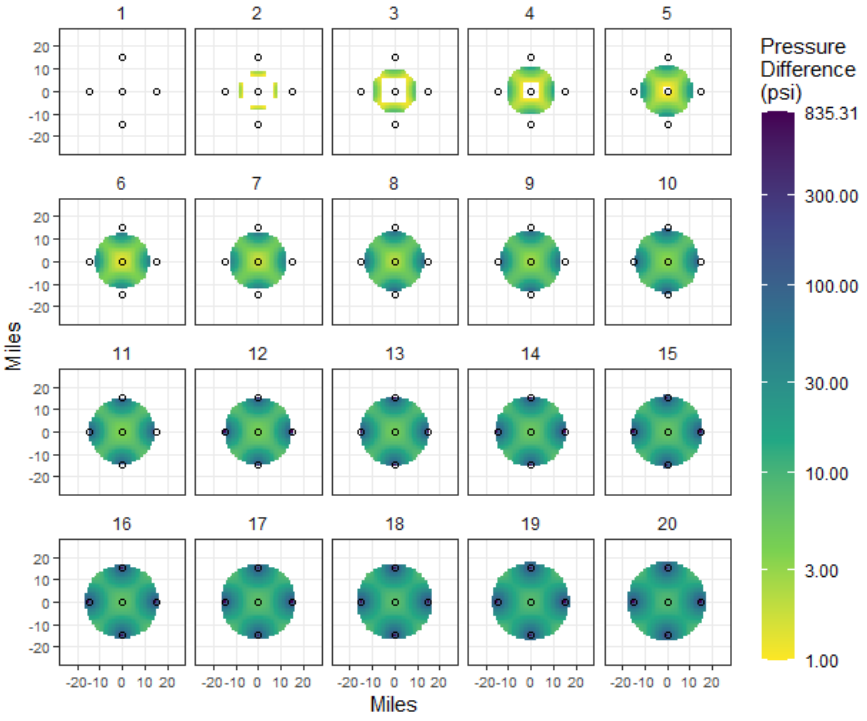

Figure C-158. Zero-year delay, 2-Mtpa injection, 15-mi spacing.

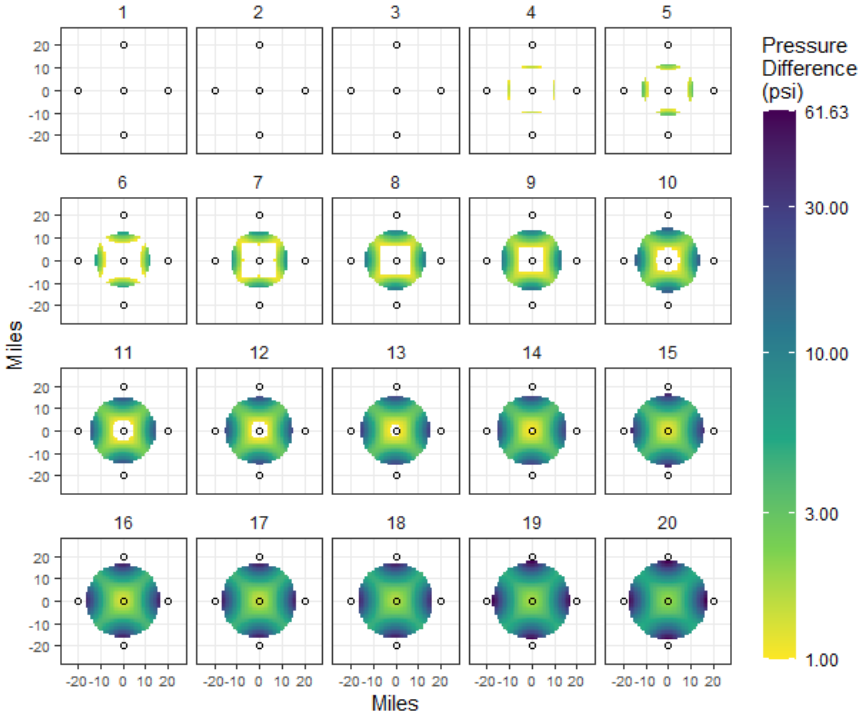

Figure C-159. Zero-year delay, 2-Mtpa injection, 20-mi spacing.

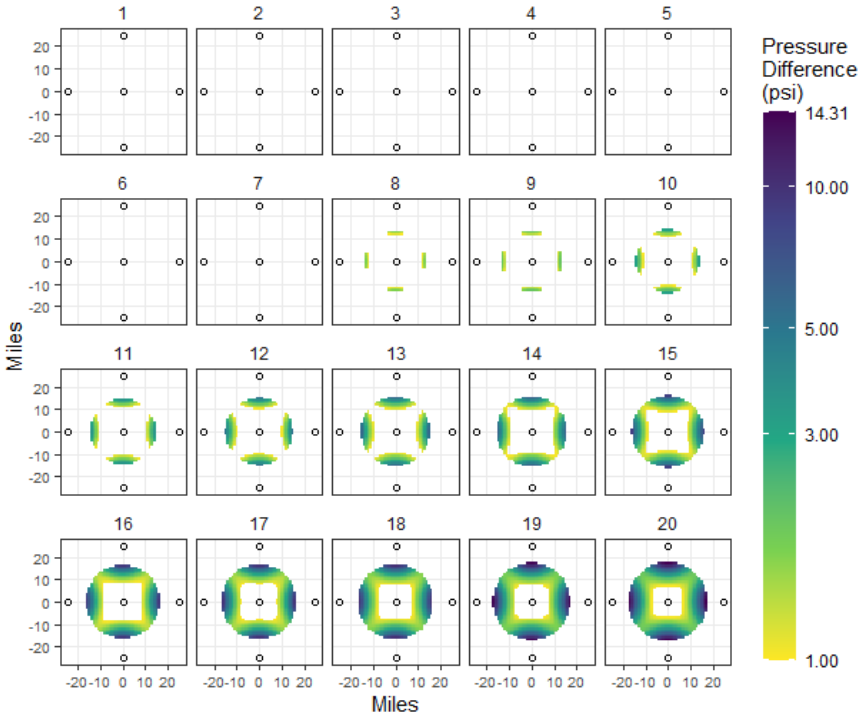

Figure C-160. Zero-year delay, 2-Mtpa injection, 25-mi spacing.

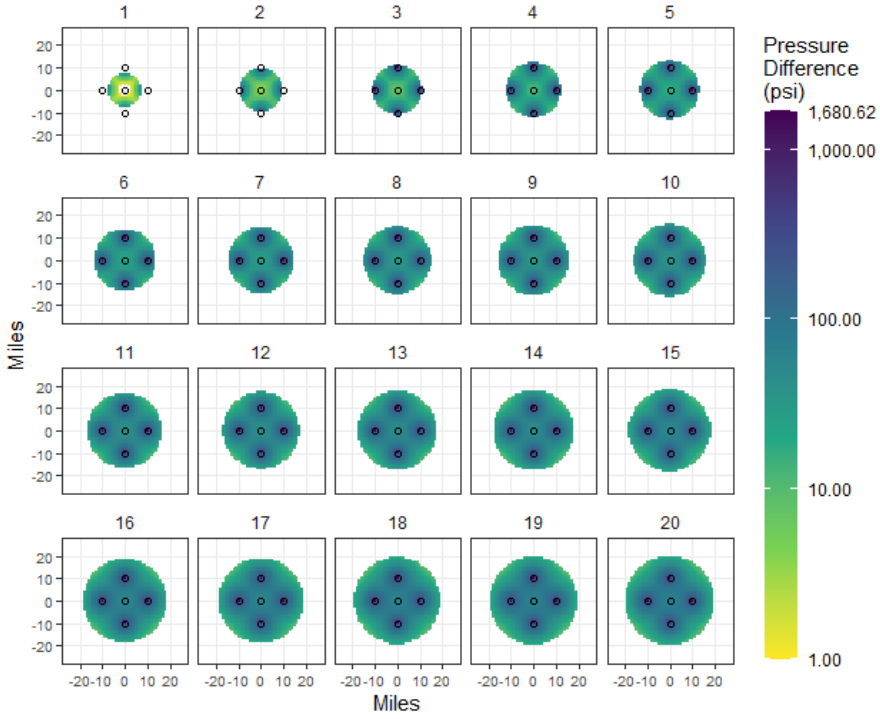

Figure C-161. Zero-year delay, 4-Mtpa injection, 10-mi spacing.

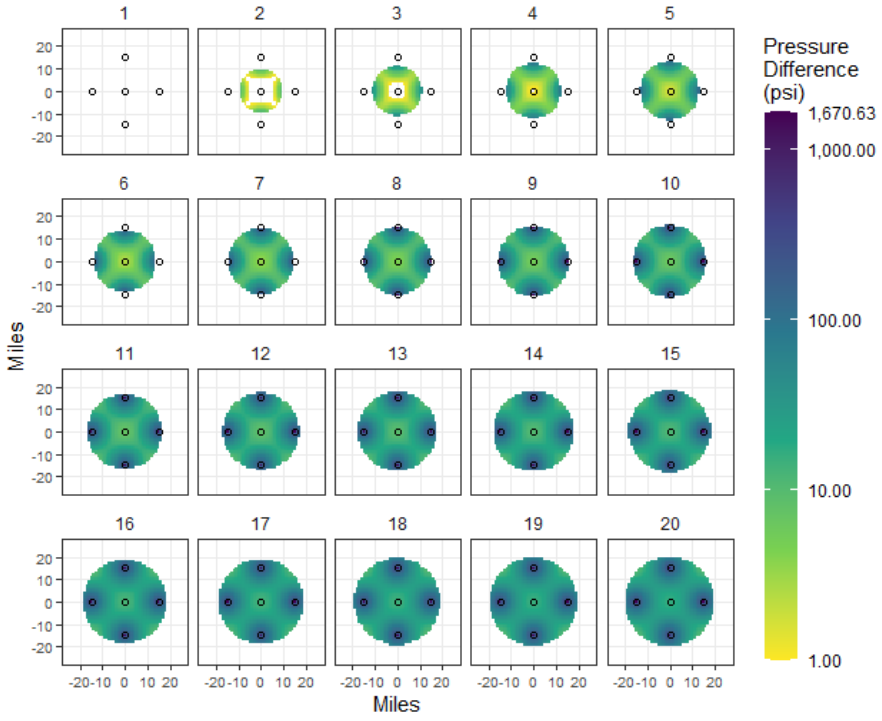

Figure C-162. Zero-year delay, 4-Mtpa injection, 15-mi spacing.

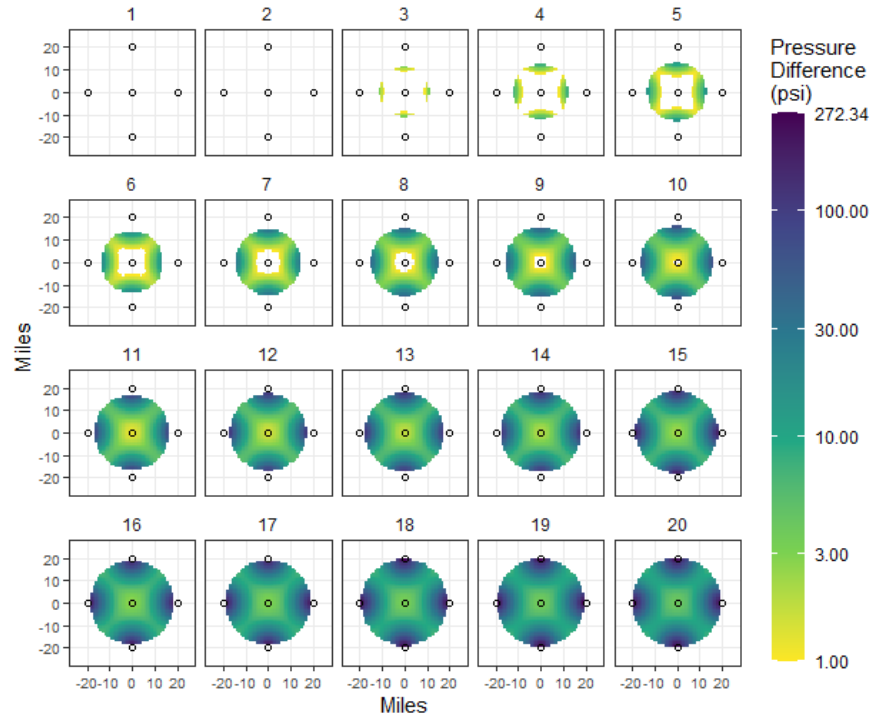

Figure C-163. Zero-year delay, 4-Mtpa injection, 20-mi spacing.

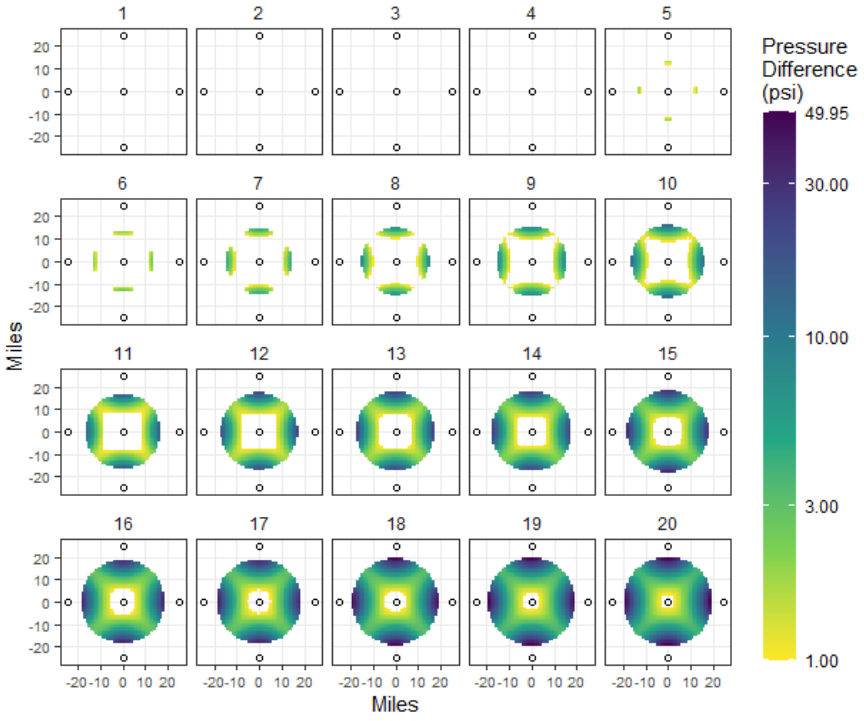

Figure C-164. Zero-year delay, 4-Mtpa injection, 25-mi spacing.

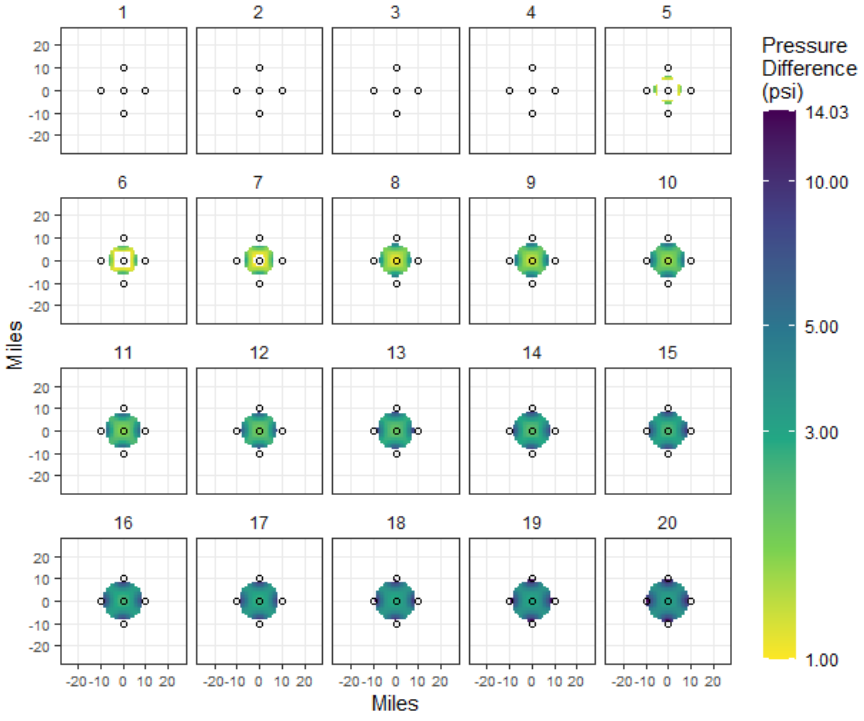

Figure C-165. Two-year delay, 0.2-Mtpa injection, 10-mi spacing.

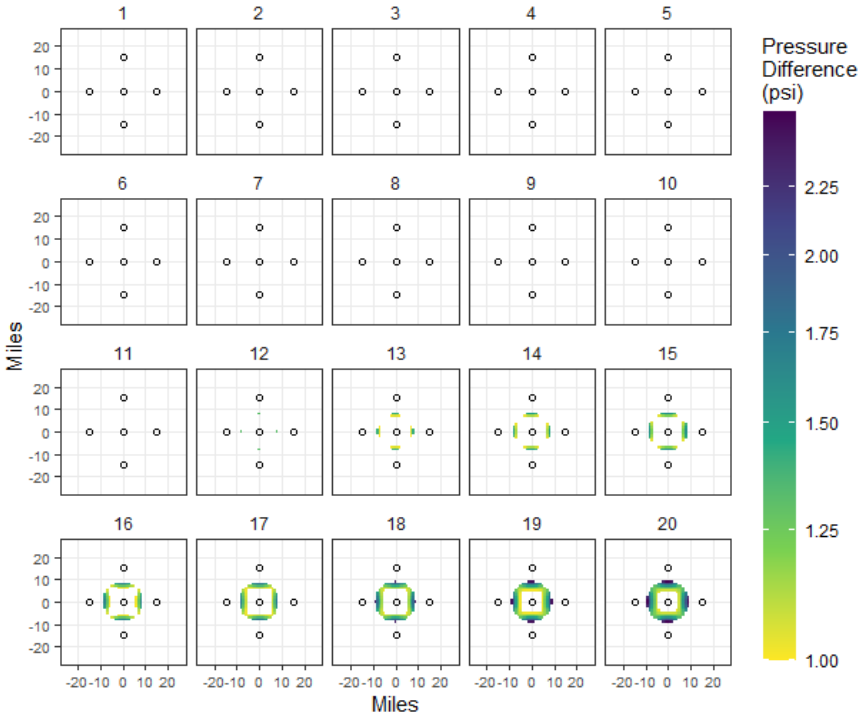

Figure C-166. Two-year delay, 0.2-Mtpa injection, 15-mi spacing.

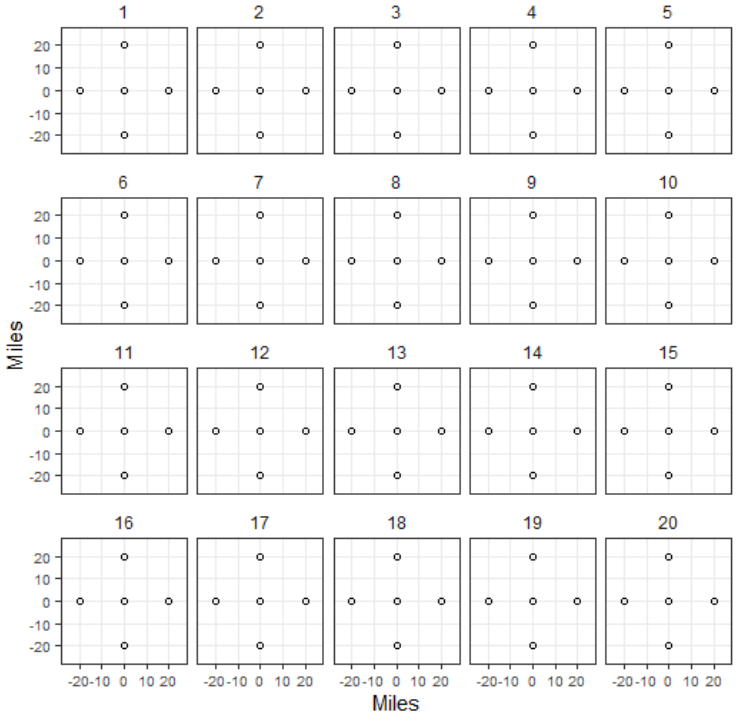

Figure C-167. Two-year delay, 0.2-Mtpa injection, 20-mi spacing. All values less than 1 psi.

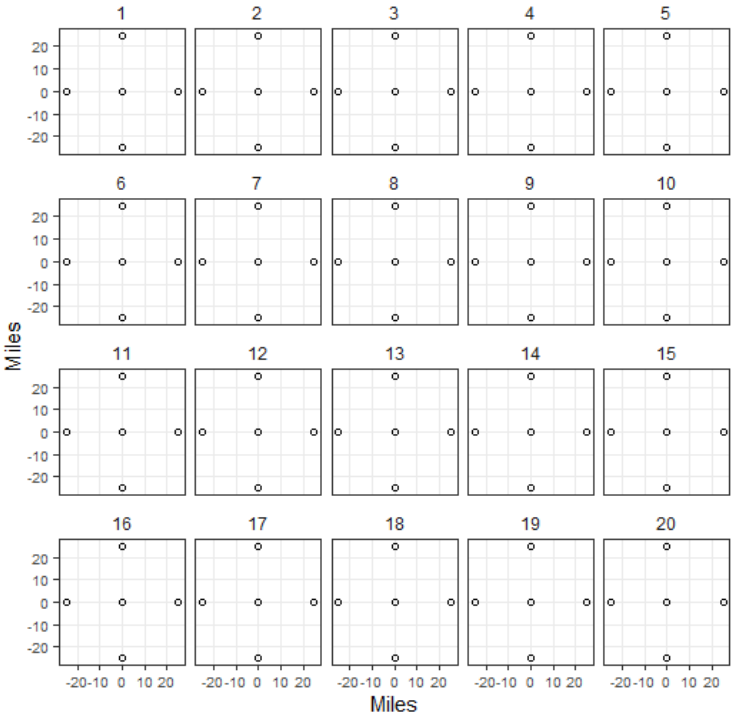

Figure C-168. Two-year delay, 0.2-Mtpa injection, 25-mi spacing. All values less than 1 psi.

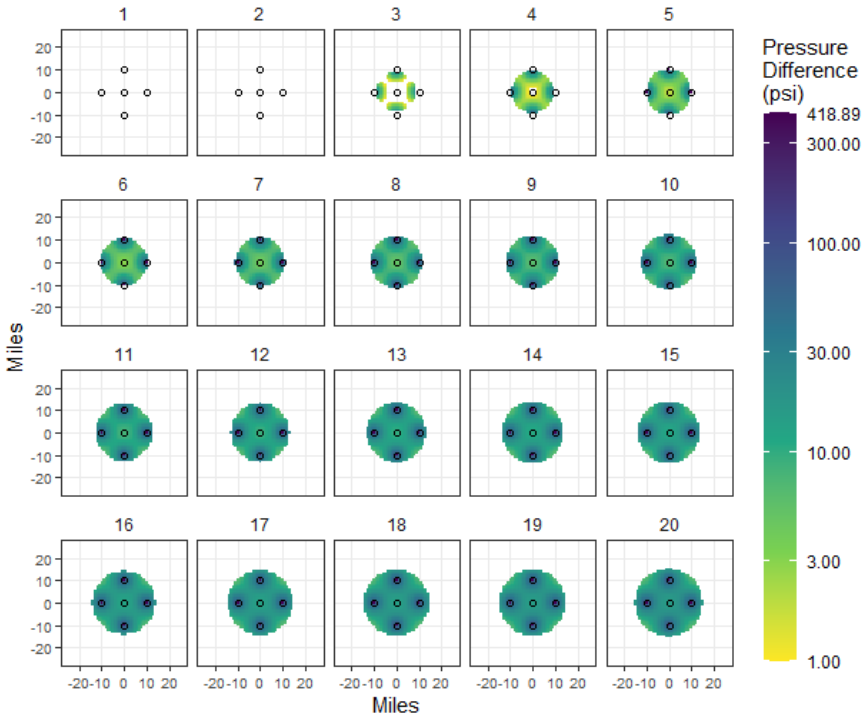

Figure C-169. Two-year delay, 1-Mtpa injection, 10-mi spacing.

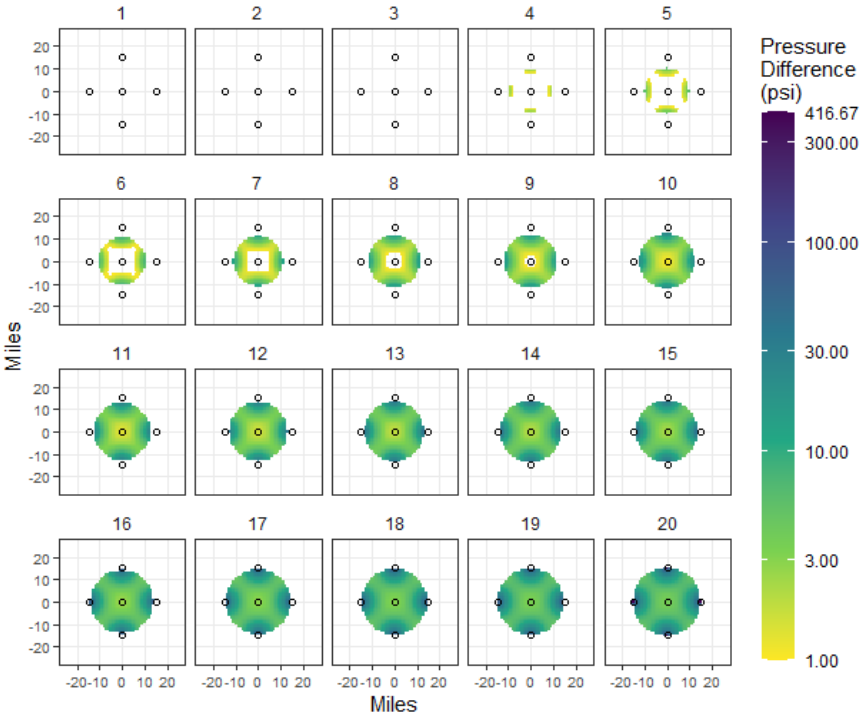

Figure C-170. Two-year delay, 1-Mtpa injection, 15-mi spacing.

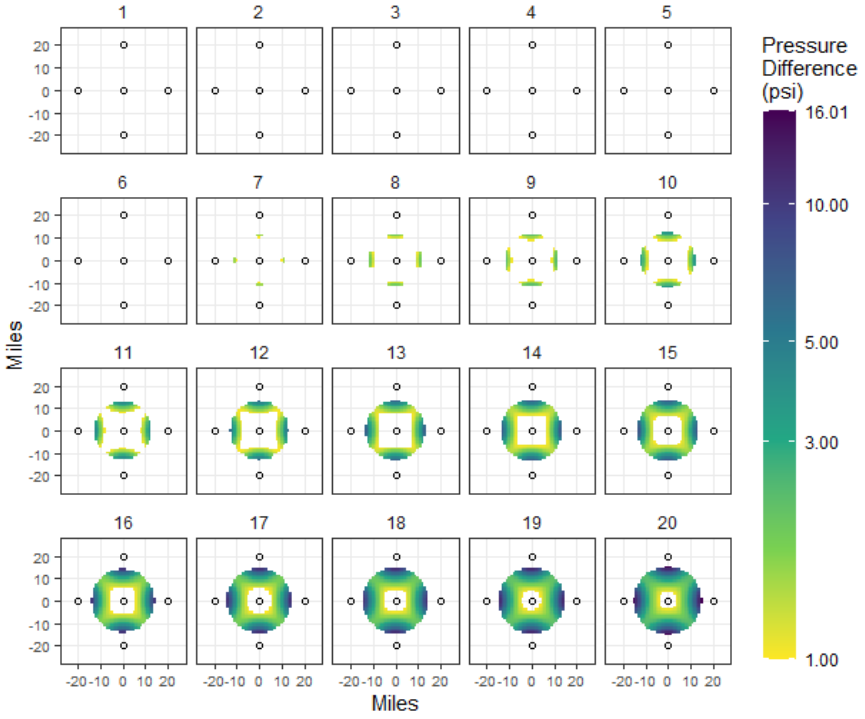

Figure C-171. Two-year delay, 1-Mtpa injection, 20-mi spacing.

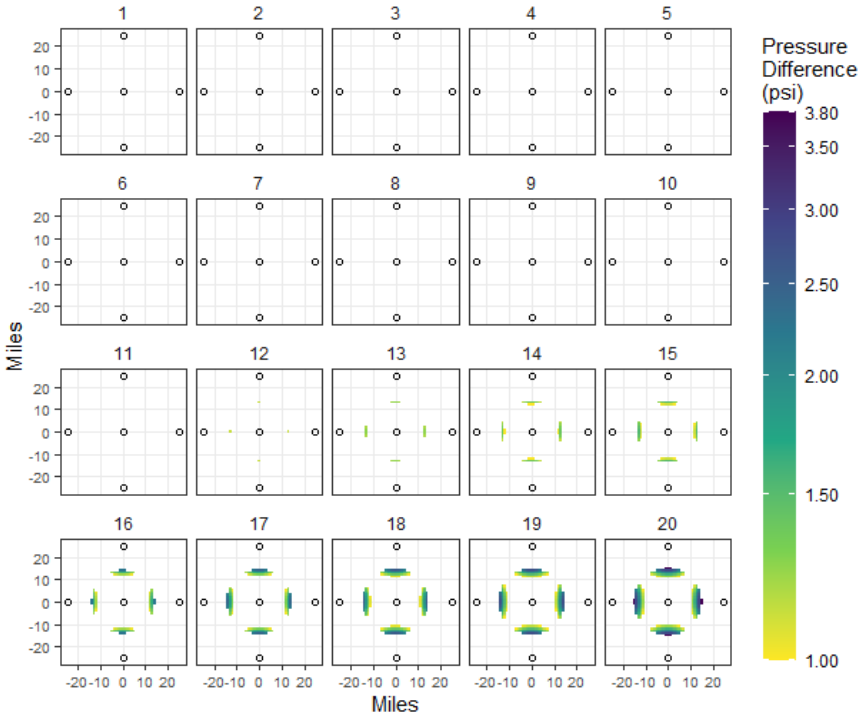

Figure C-172. Two-year delay, 1-Mtpa injection, 25-mi spacing.

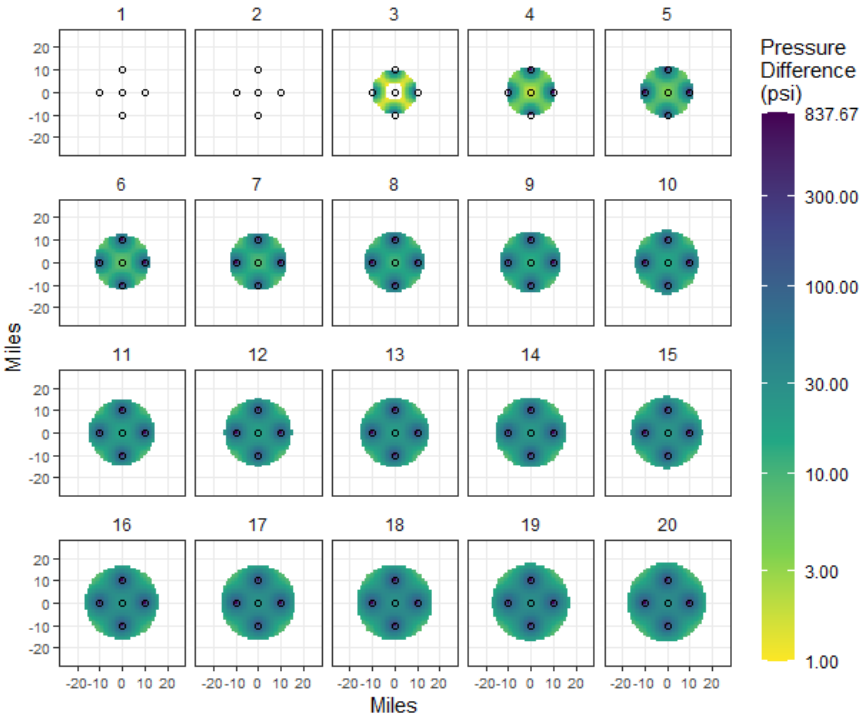

Figure C-173. Two-year delay, 2-Mtpa injection, 10-mi spacing.

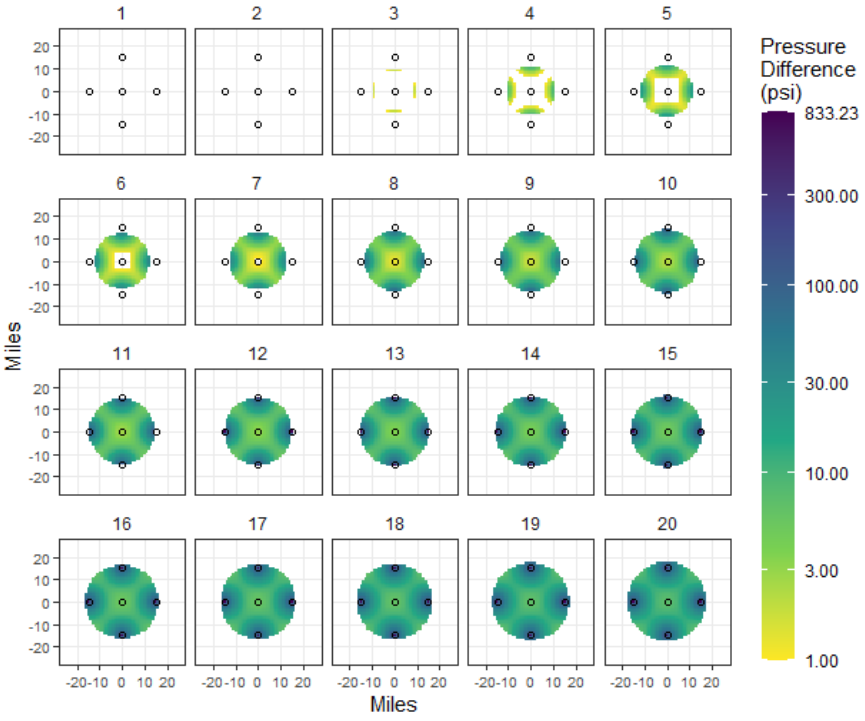

Figure C-174. Two-year delay, 2-Mtpa injection, 15-mi spacing.

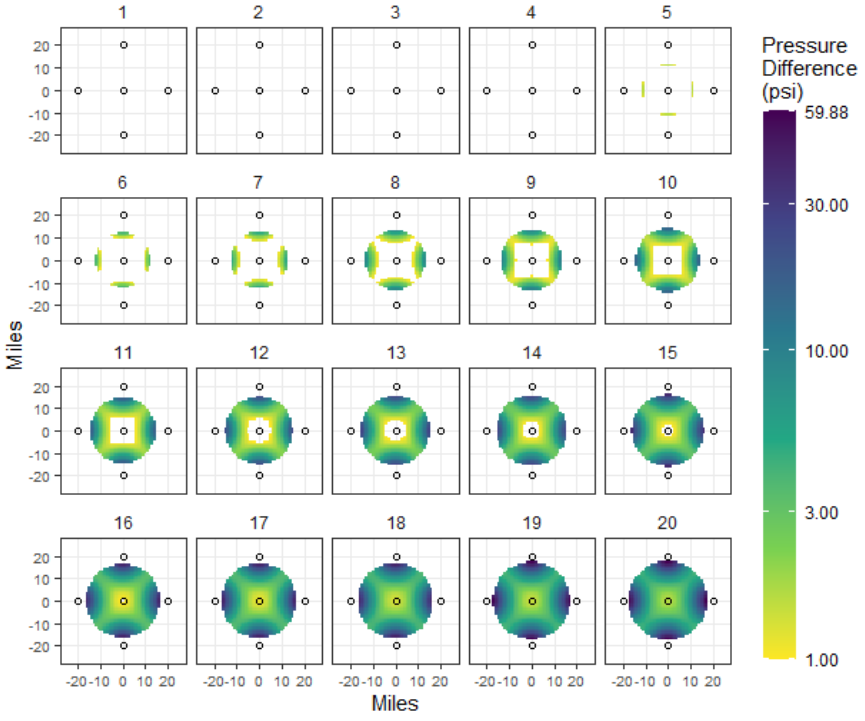

Figure C-175. Two-year delay, 2-Mtpa injection, 20-mi spacing.

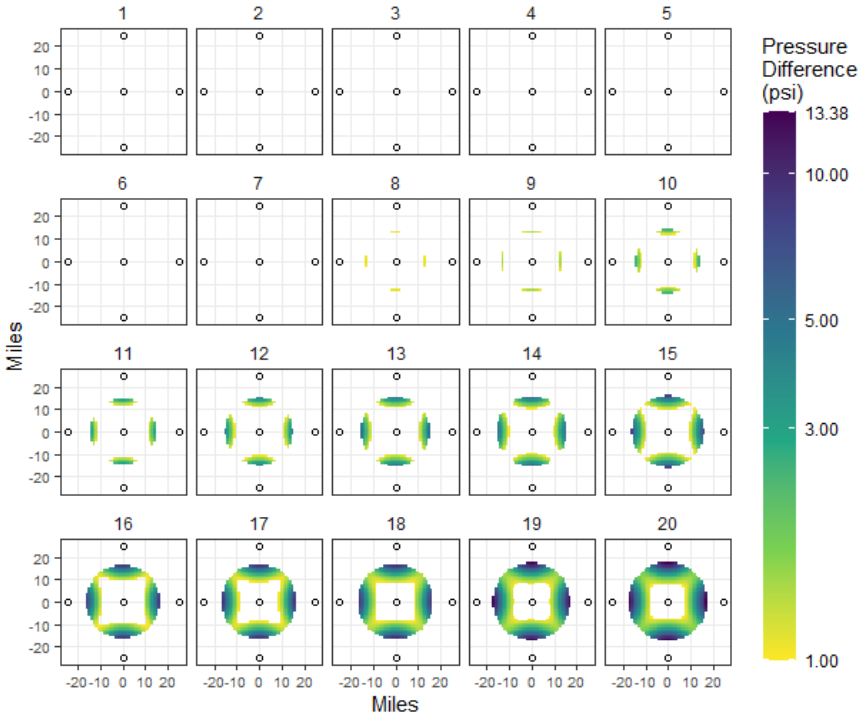

Figure C-176. Two-year delay, 2-Mtpa injection, 25-mi spacing.

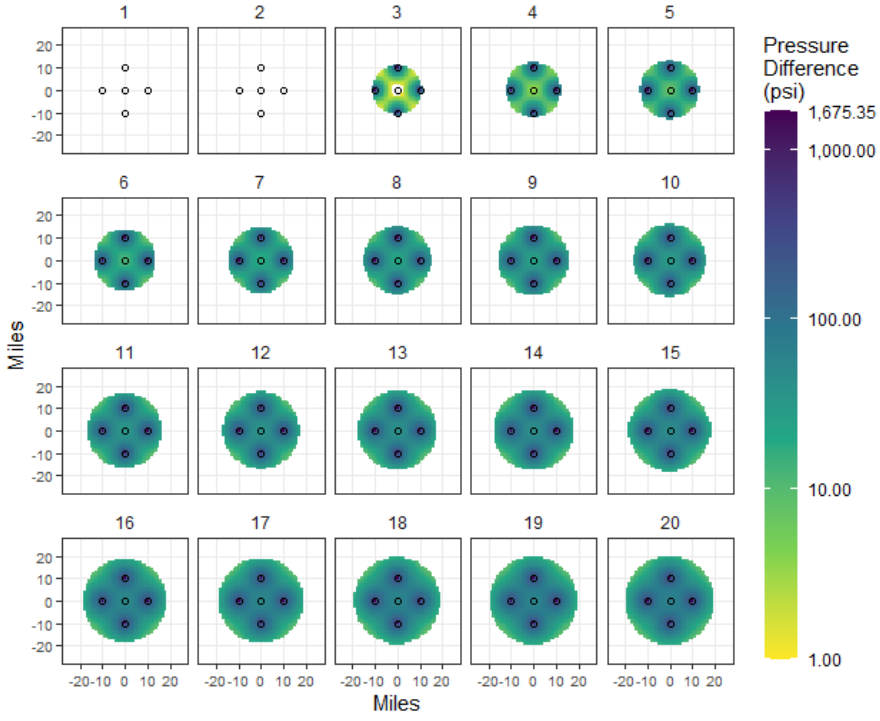

Figure C-177. Two-year delay, 4-Mtpa injection, 10-mi spacing.

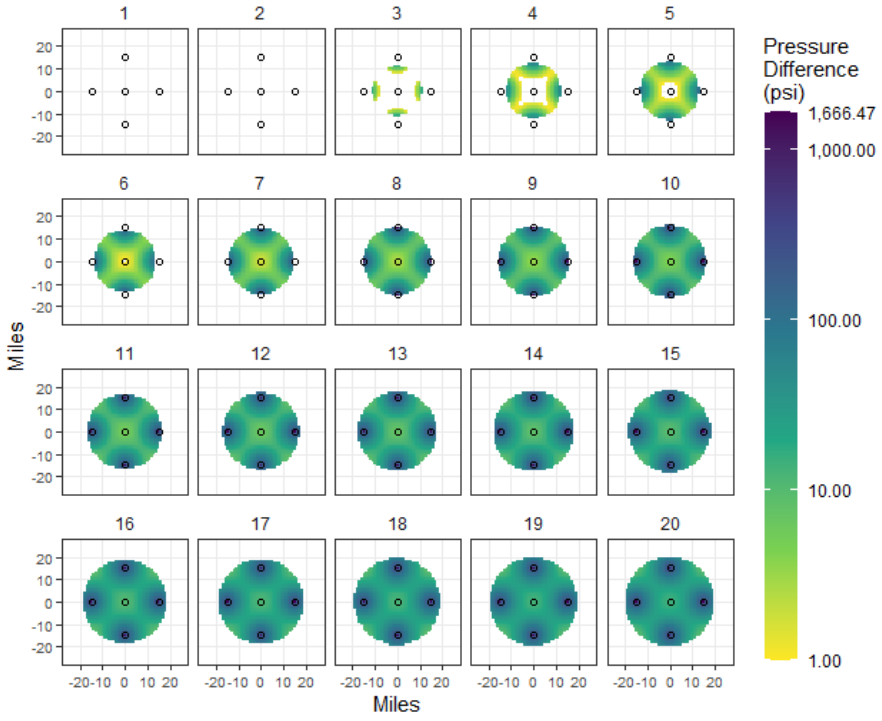

Figure C-178. Two-year delay, 4-Mtpa injection, 15-mi spacing.

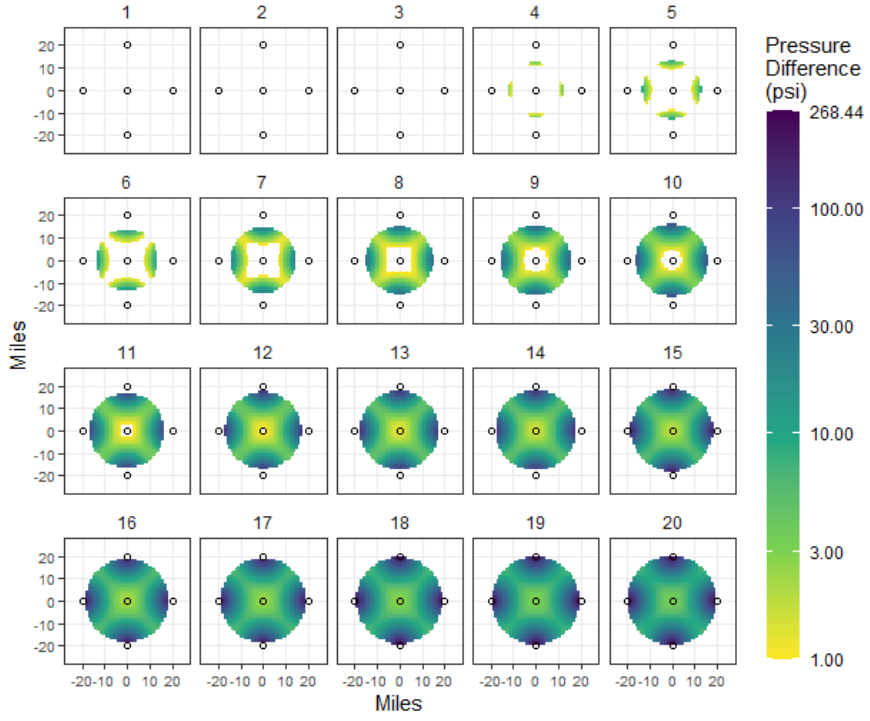

Figure C-179. Two-year delay, 4-Mtpa injection, 20-mi spacing.

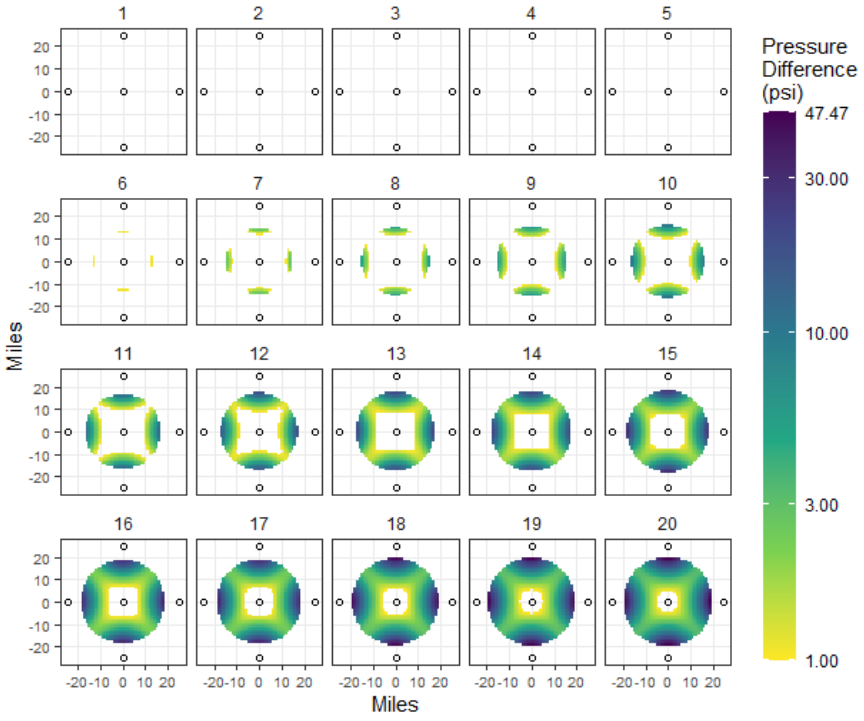

Figure C-180. Two-year delay, 4-Mtpa injection, 25-mi spacing.

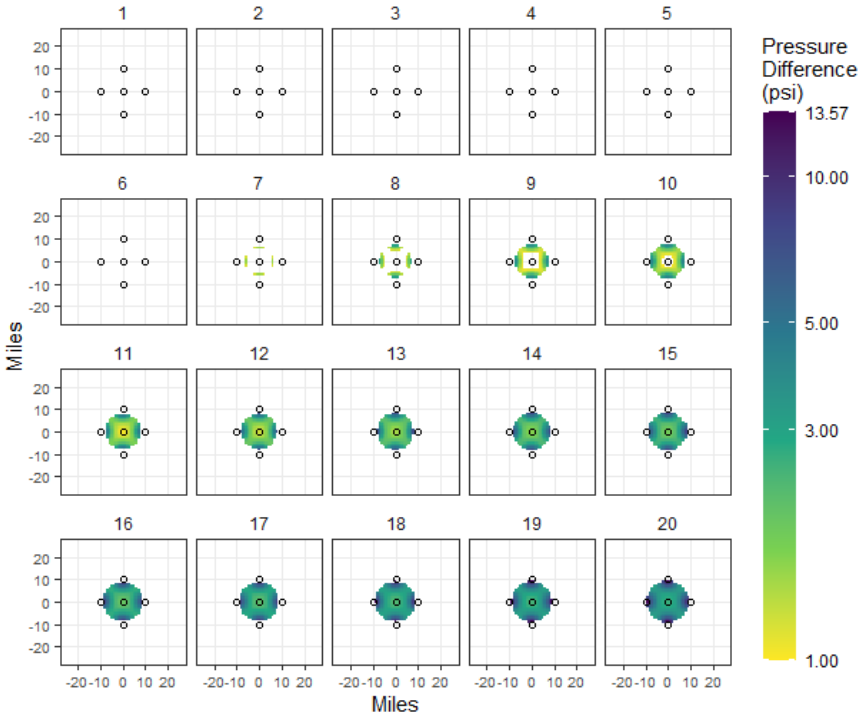

Figure C-181. Five-year delay, 0.2-Mtpa injection, 10-mi spacing.

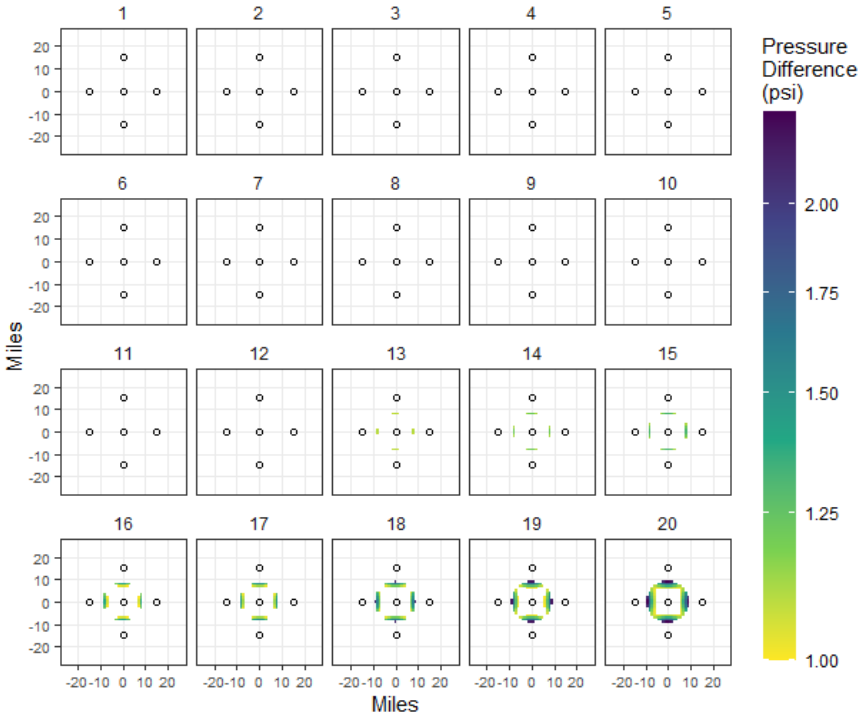

Figure C-182. Five-year delay, 0.2-Mtpa injection, 15-mi spacing.

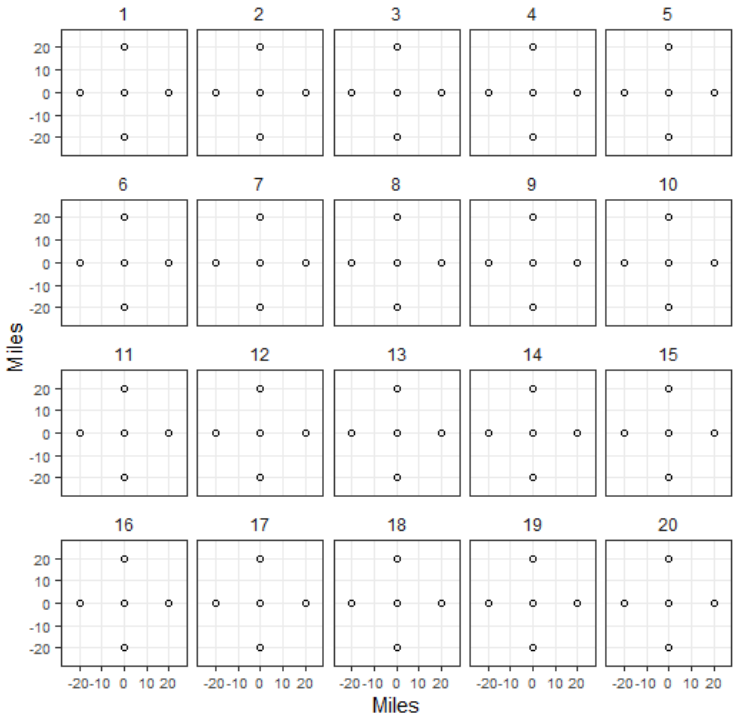

Figure C-183. Five-year delay, 0.2-Mtpa injection, 20-mi spacing. All values less than 1 psi.

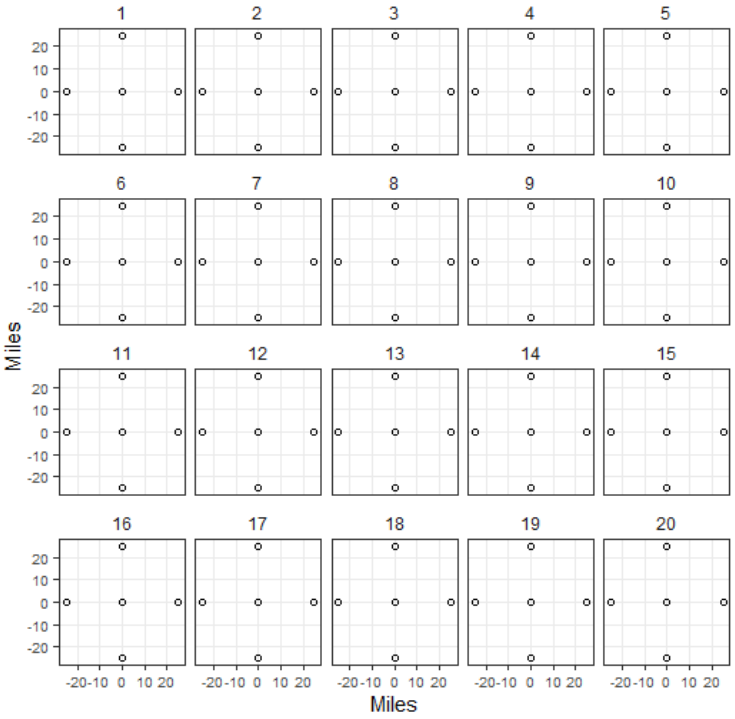

Figure C-184. Five-year delay, 0.2-Mtpa injection, 25-mi spacing. All values less than 1 psi.

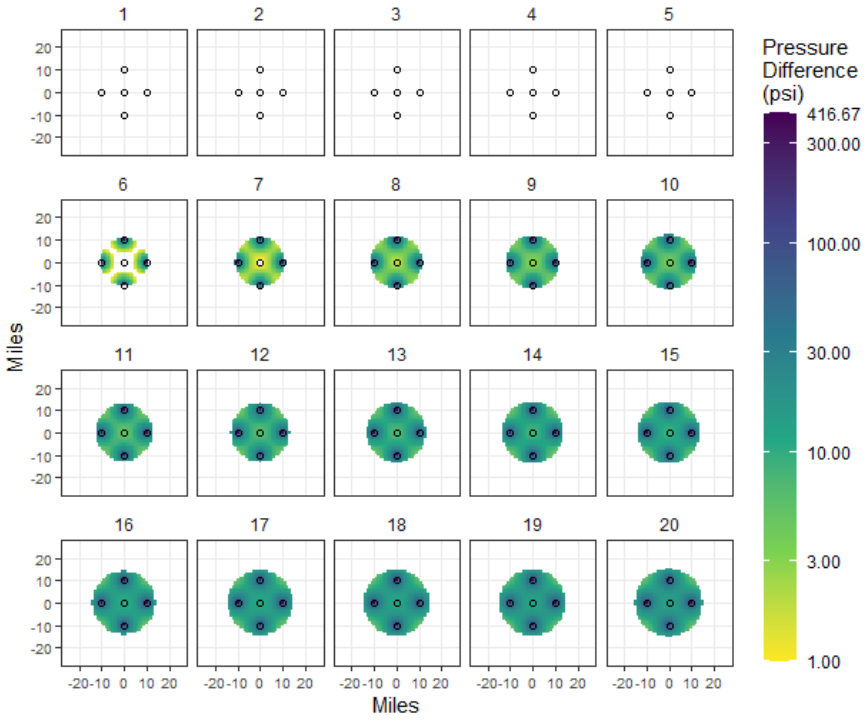

Figure C-185. Five-year delay, 1-Mtpa injection, 10-mi spacing.

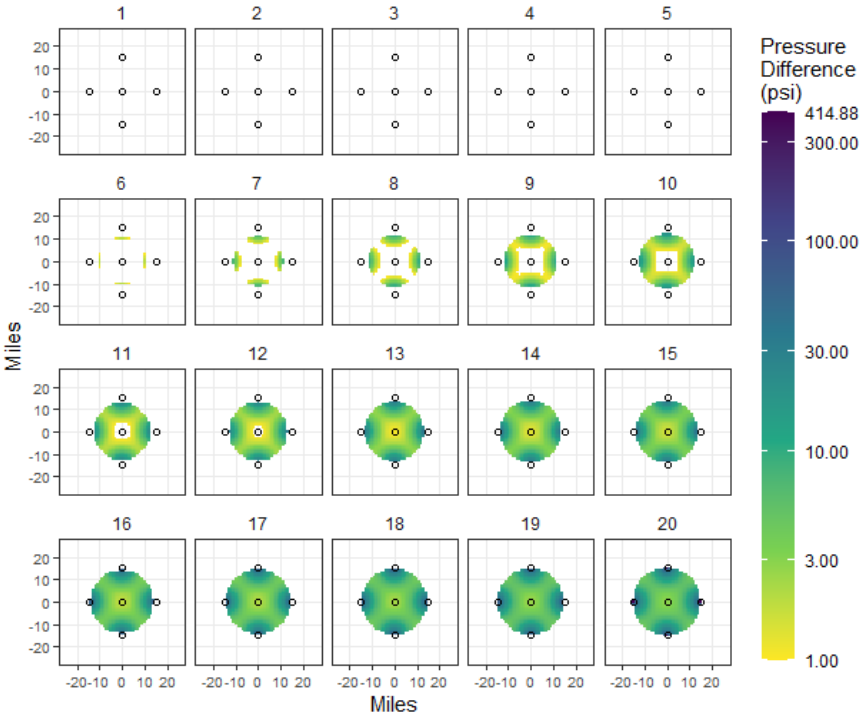

Figure C-186. Five-year delay, 1-Mtpa injection, 15-mi spacing.

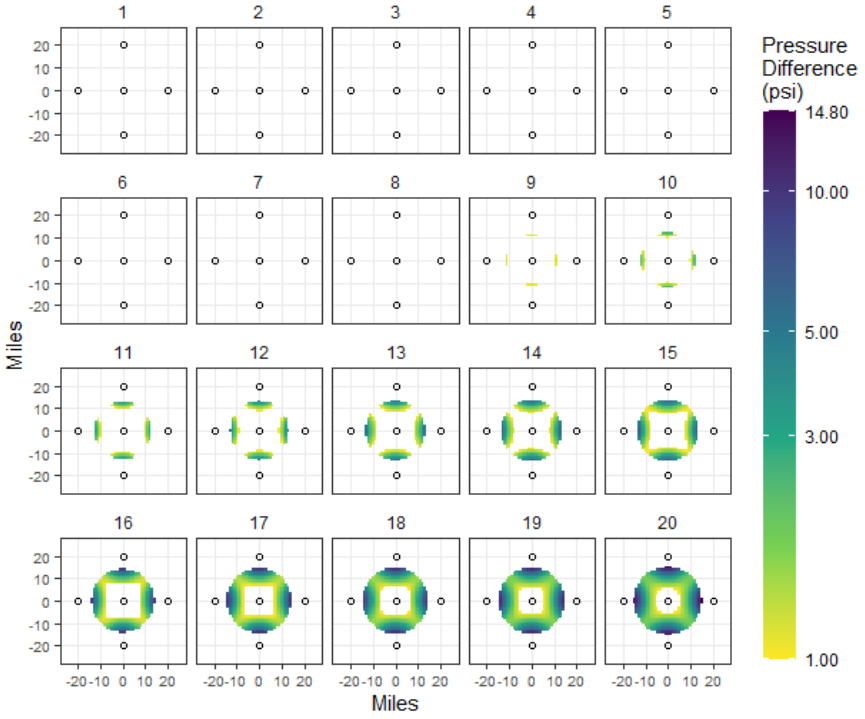

Figure C-187. Five-year delay, 1-Mtpa injection, 20-mi spacing.

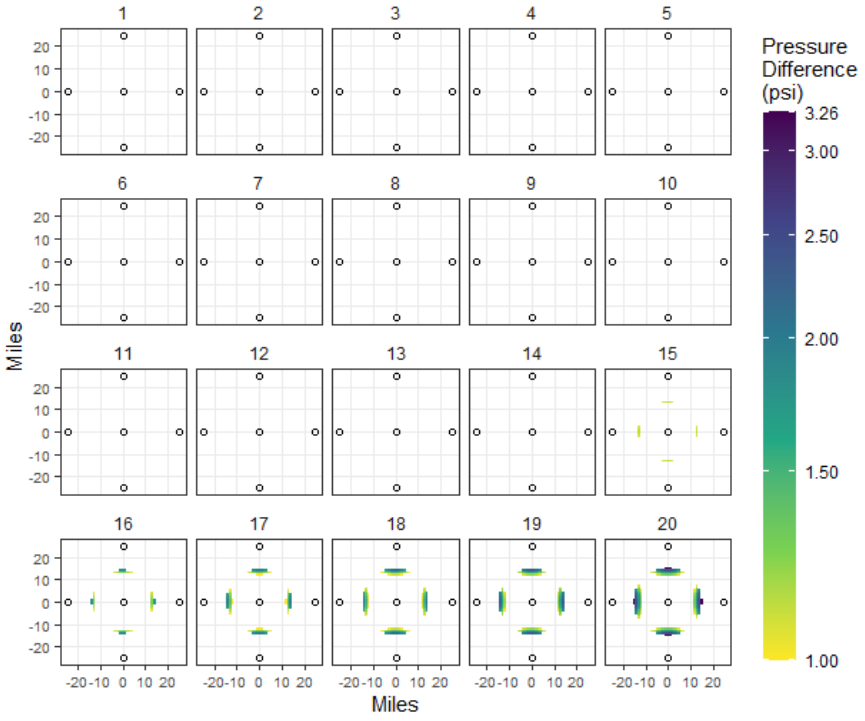

Figure C-188. Five-year delay, 1-Mtpa injection, 25-mi spacing.

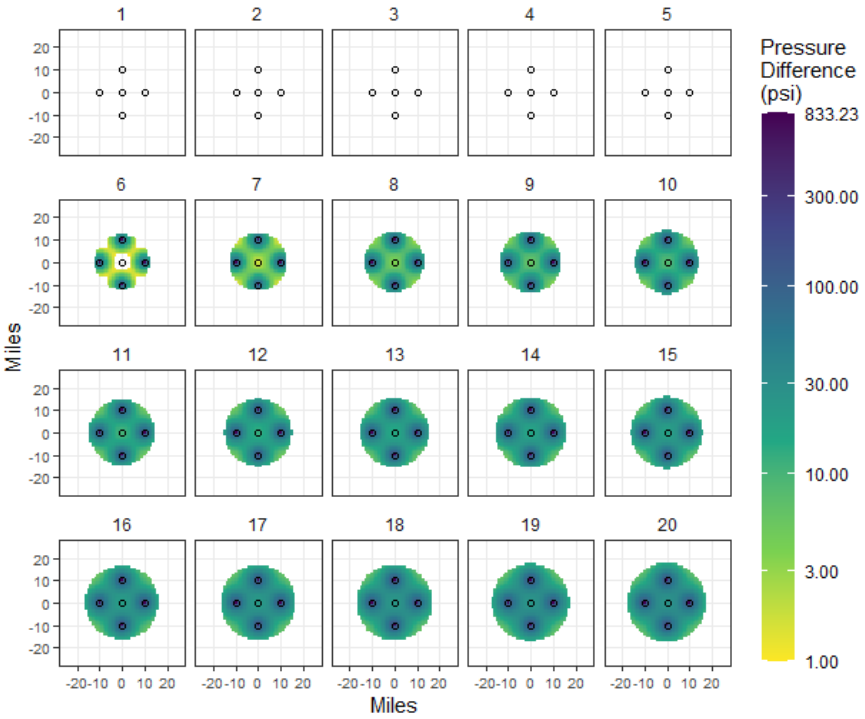

Figure C-189. Five-year delay, 2-Mtpa injection, 10-mi spacing.

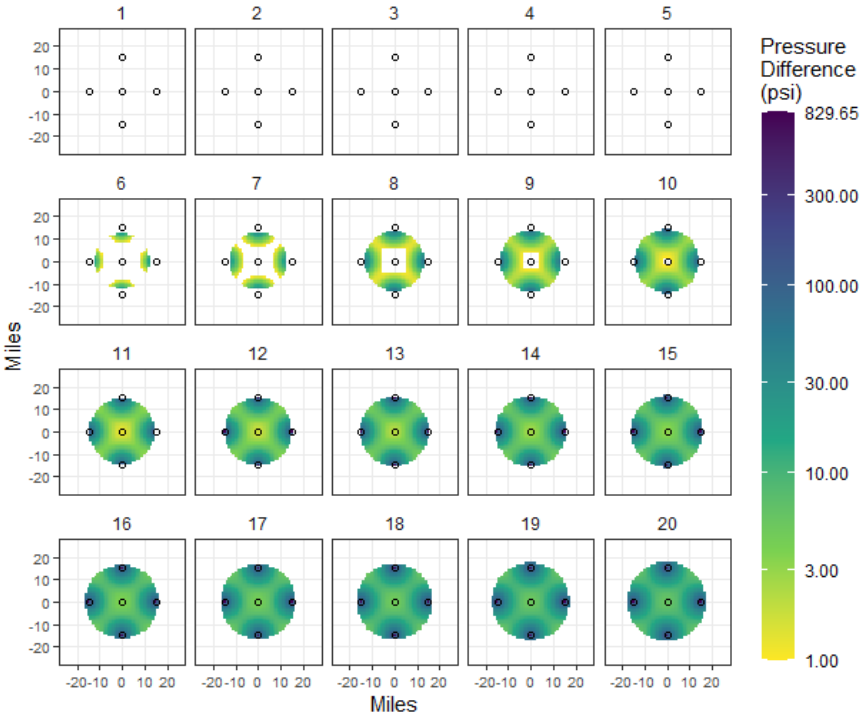

Figure C-190. Five-year delay, 2-Mtpa injection, 15-mi spacing.

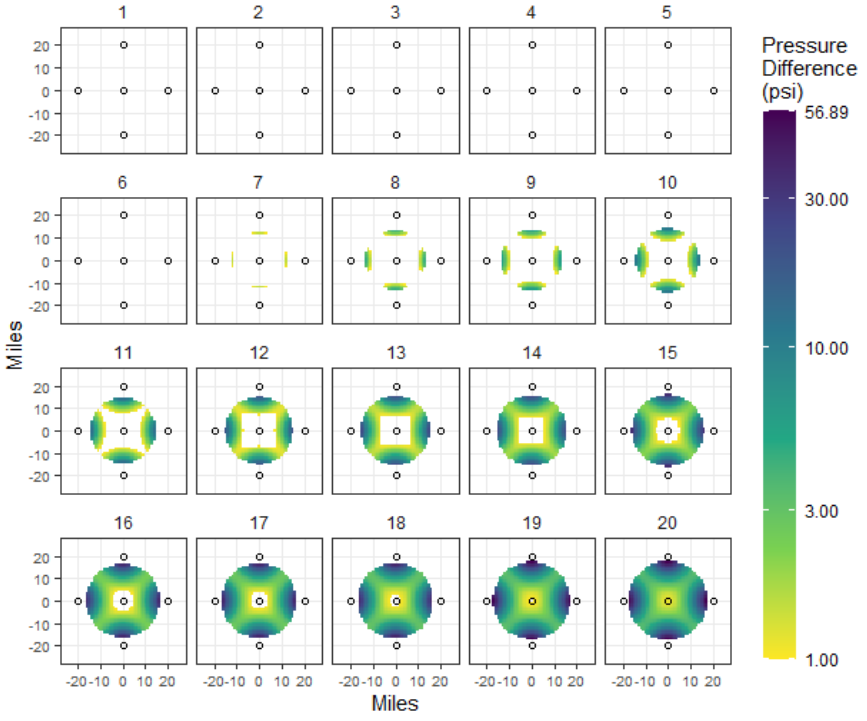

Figure C-191. Five-year delay, 2-Mtpa injection, 20-mi spacing.

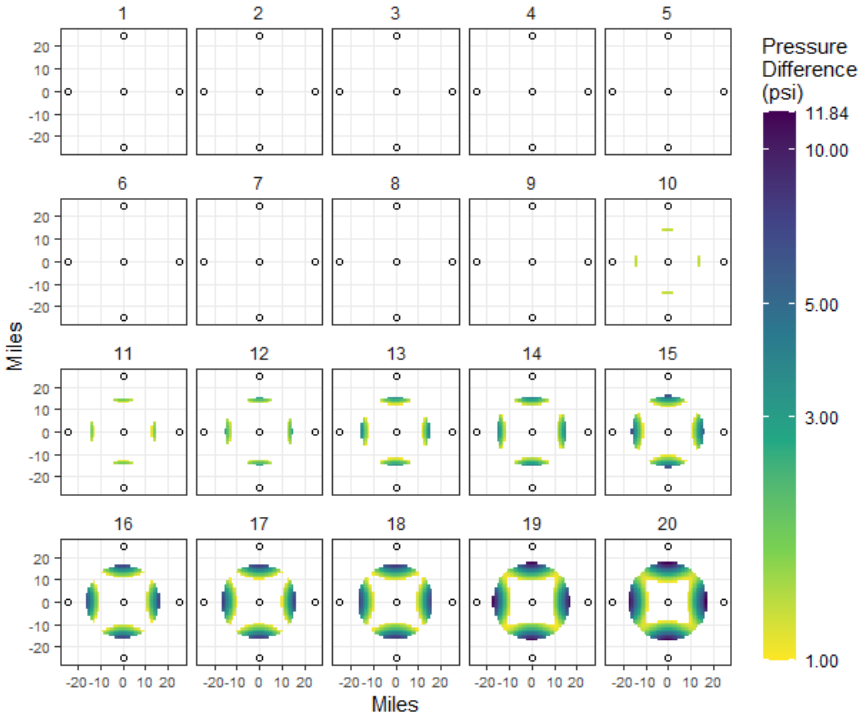

Figure C-192. Five-year delay, 2-Mtpa injection, 25-mi spacing.

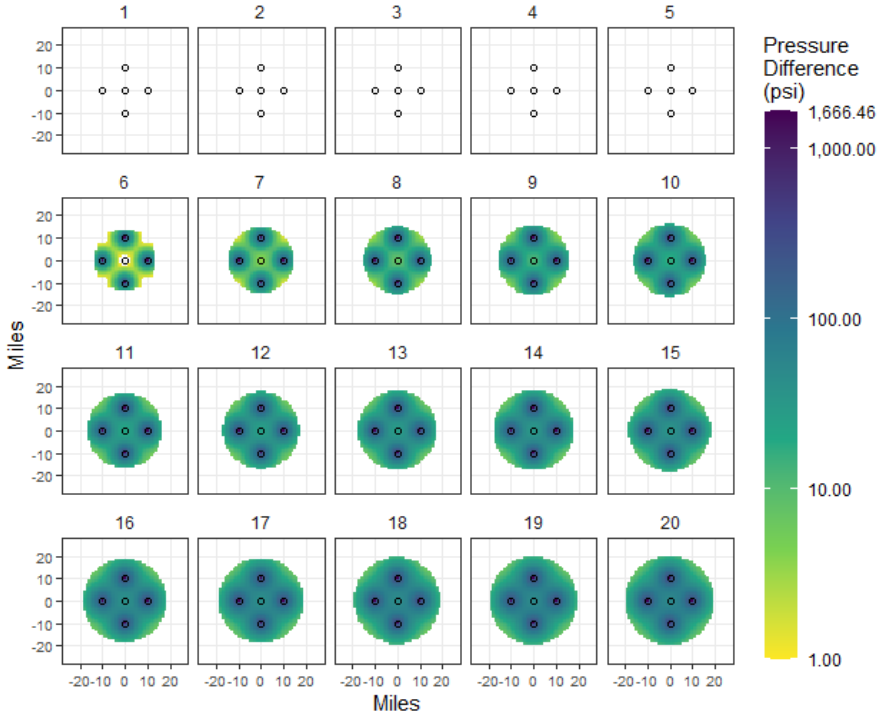

Figure C-193. Five-year delay, 4-Mtpa injection, 10-mi spacing.

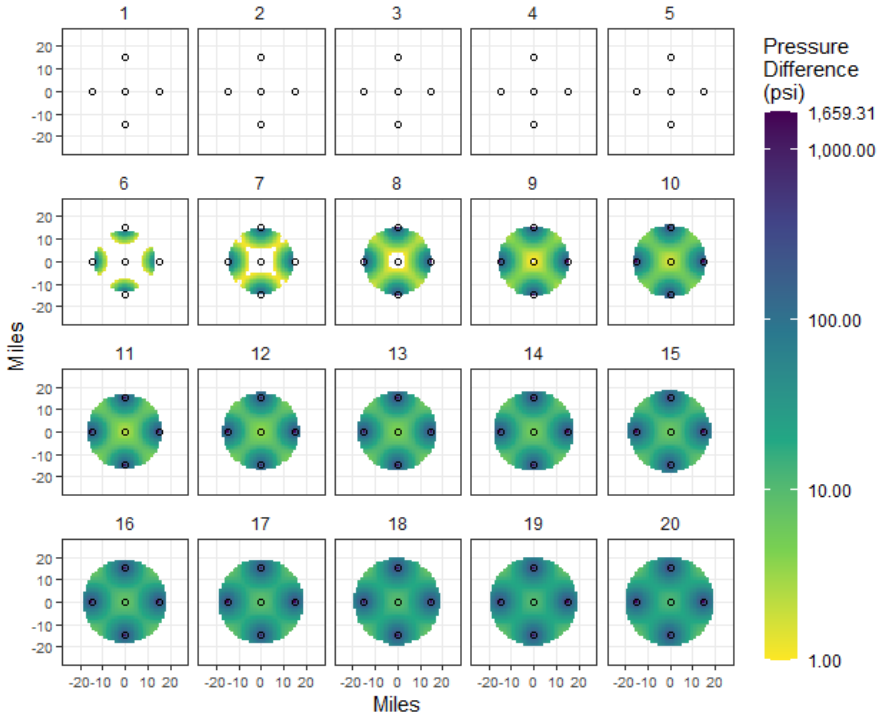

Figure C-194. Five-year delay, 4-Mtpa injection, 15-mi spacing.

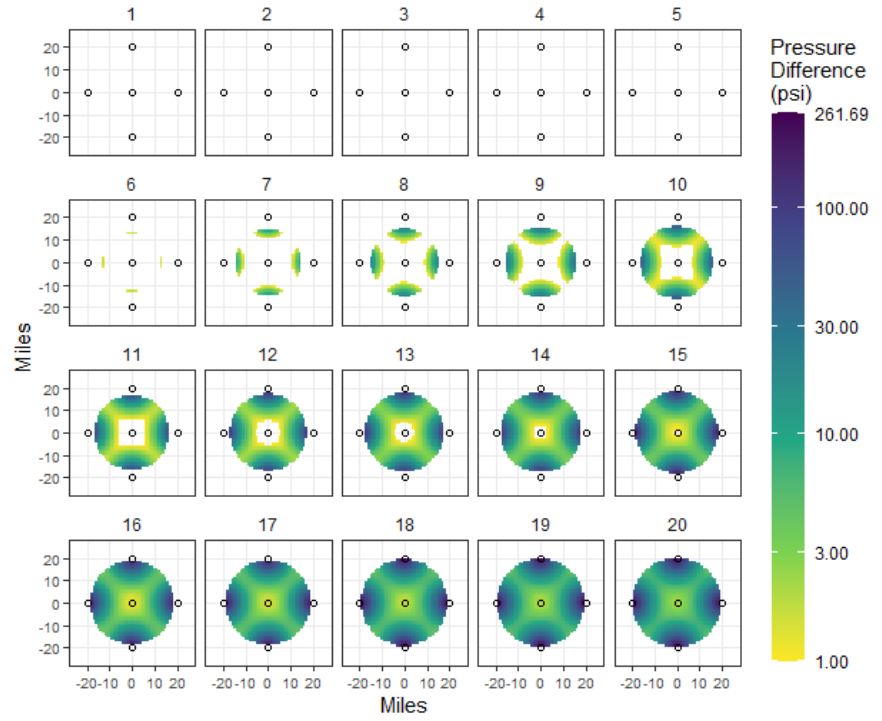

Figure C-195. Five-year delay, 4-Mtpa injection, 20-mi spacing.

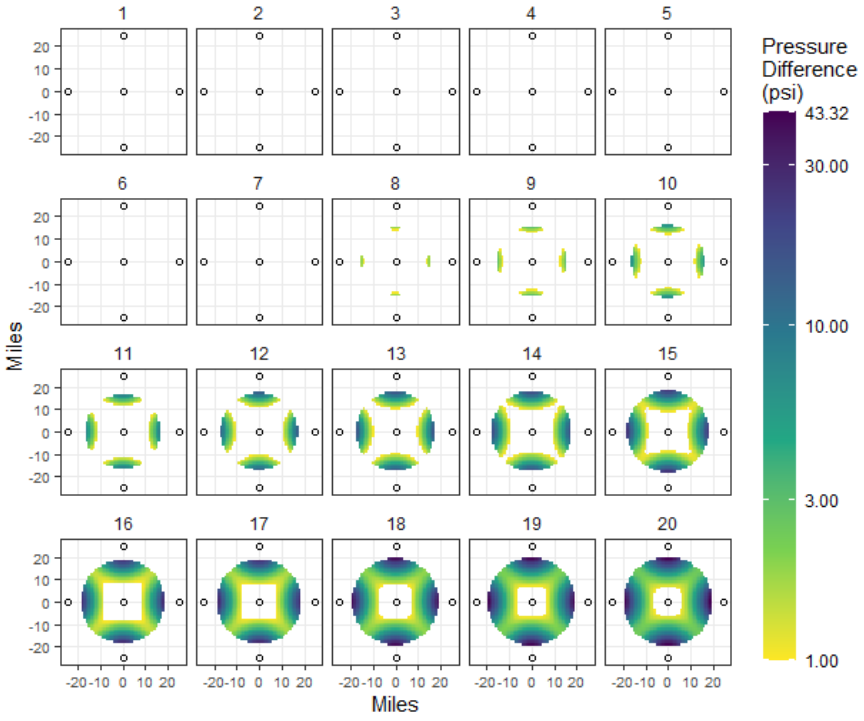

Figure C-196. Five-year delay, 4-Mtpa injection, 25-mi spacing.